STOL TECTICAL AIR CRAFT INVESTIGATION. VOLUME V. PART II. FLIGHT CONTROL TECHNOLOGY: PILOTED SIMULATION OF A MEDIUM STOL TRANSPORT WITH VECTORED THRUST/MECHANICAL FLAPS

James H. Vincent

Boeing Aerospace Company

Prepared for:

Air Force Flight Dynamics Laboratory

May 1973

AFFDL-TR-73-19
Volume V, Part II

AD 766643

STOL TACTICAL AIRCRAFT INVESTIGATION

Volume V, Part II

Flight Control Technology: Piloted Simulation of a Medium STOL Transport with Vectored Thrust/Mechanical Flaps

James H. Vincent

[redacted]

Technical Report AFFDL-TR-73-19 – Volume V, Part II

May, 1973

Air Force Flight Dynamics Laboratory
Air Force Systems Command
Wright-Patterson Air Force Base, Ohio 45433

Notice

When Government drawings, specifications, or other data are used for any purpose other than in connection with a definitely related Government procurement operation, the United States Government thereby incurs no responsibility nor any obligation whatsoever; and the fact that the Government may have formulated, furnished, or in any way supplied the said drawings, specifications, or other data, is not to be regarded by implication or otherwise as in any manner licensing the holder or any other person or corporation, or conveying any rights or permission to manufacture, use or sell any patented invention that may in any way be related thereto.

Copies of this report should not be returned unless return is required by security considerations, contractual obligations, or notice on a specific document.

AIR FORCE/56780/4 September 1973 — 150

Unclassified
Security Classification

DOCUMENT CONTROL DATA - R & D

(Security classification of title, body of abstract and indexing annotation must be entered when the overall report is classified)

1 ORIGINATING ACTIVITY (Corporate author) The Boeing Company Aerospace Group Seattle, Washington 98124	2a. REPORT SECURITY CLASSIFICATION Unclassified 2b. GROUP

3 REPORT TITLE
STOL TACTICAL AIRCRAFT INVESTIGATION, Volume V, Part 2
Flight Control Technology: Piloted Simulation of a Medium STOL Transport with Vectored Thrust/Mechanical Flaps

4 DESCRIPTIVE NOTES (Type of report and inclusive dates)
Final Technical Report - June 1971 through December 1972

5 AUTHOR(S) (First name, middle initial, last name)
James H. Vincent

6 REPORT DATE	7a. TOTAL NO. OF PAGES	7b. NO. OF REFS
	246	

8a. CONTRACT OR GRANT NO	9a. ORIGINATOR'S REPORT NUMBER(S)
F33615-71-C-1757 ✓ b PROJECT NO 643A c. d.	AFFDL-TR-73 - Vol. V, Part 2 9b. OTHER REPORT NO(S) (Any other numbers that may be assigned this report) Boeing Document D180-14412-2 ✓

10 DISTRIBUTION STATEMENT

11 SUPPLEMENTARY NOTES	12 SPONSORING MILITARY ACTIVITY
	Air Force Flight Dynamic Laboratory Air Force Systems Command Wright-Patterson Air Force Base, Ohio

13 ABSTRACT

Fixed base and piloted simulation studies were conducted to evaluate control systems for a STOL tactical transport equipped with vectored thrust. Unaugmented aircraft flying qualities were found to be unacceptable. However, an augmented control system configuration was found to give excellent flying qualities and satisfactory behavior following engine or control system component failure. The present flying qualities standard for STOL aircraft, MIL-F-83300, was reviewed and several changes are suggested.

DD FORM 1 NOV 68 1473

ia

Unclassified
Security Classification

14 KEY WORDS	LINK A		LINK B		LINK C	
	ROLE	WT	ROLE	WT	ROLE	WT
Mechanical Flap/Vectored Thrust						
STOL Aircraft						
Advanced Medium STOL Transport						
STOL Tactical Aircraft Investigation						
Piloted Simulation						
Flight Control System						
Control Law						
Control Mechanization						
Tracking Performance						
Touchdown Dispersions						
Handling Qualities						
STOL Flying Quality Specification						

*U.S.Government Printing Office: 1973 — 758-425/36

STOL TACTICAL AIRCRAFT INVESTIGATION

Volume V, Part II

Flight Control Technology: Piloted Simulation of a Medium STOL Transport with Vectored Thrust/Mechanical Flaps

James H. Vincent

FOREWORD

This report was prepared for the United States Air Force by The Boeing Company, Seattle, Washington, in partial fulfillment of Contract F33615-71-C-1757, Project No. 643A. It is one of eight related documents covering the results of investigations of vectored-thrust and jet-flap powered lift technology, under the STOL Tactical Aircraft Investigation (STAI) Program sponsored by the Air Force Flight Dynamics Laboratory, Air Force Systems Command, Wright-Patterson Air Force Base, Ohio. The relation of this report to the others of this series is indicated below:

AFFDL TR-73-19	STOL TACTICAL AIRCRAFT INVESTIGATION	
Vol. I	Configuration Definition: Medium STOL Transport with Vectored Thrust/Mechanical Flaps	
Vol. II Part I	Aerodynamic Technology: Design Compendium, Vectored Thrust/Mechanical Flaps	
Vol. II Part II	A Lifting Line Analysis Method for Jet-Flapped Wings	
Vol. III	Takeoff and Landing Performance Ground Rules for Powered Lift STOL Transport Aircraft	
Vol. IV	Analysis of Wind Tunnel Data, Vectored Thrust/Mechanical Flaps and Internally Blown Jet Flaps	
Vol. V Part I	Flight Control Technology: System Analysis and Trade Studies for a Medium STOL Trasnport with Vectored Thrust and Mechanical Flaps	
Vol. V Part II	Flight Control Technology: Piloted Simulation of a Medium STOL Transport with Vectored Thrust/Mechanical Flaps	THIS REPORT
Vol. VI	Air Cushion Landing System Study	

The work reported here was performed in the period June 1971 through December 1972 by the Sensors, Guidance, and Control Staff of the Research and Engineering Division and by the Tactical Airlift Program, Aeronautical and Information Systems Division, both of the Aerospace Group, The Boeing Company. Mr. Franklyn J. Davenport served as Program Manager.

The author wishes to express his gratitude to the following people, whose contributions were essential to the success of the STAI simulation program: Mr. Kenneth J. Crandall, Mr. William E. Gerken, Mr. Jerry L. Lee, Mr. Gary R. Letsinger, Mr. Harold S. Lewis, Mr. David J. Maund, and Mr. John R. Monk contributed to the definition of simulation mathematical models. The simulation programmers were Mr. Downey C. Cunningham and Mr. David G. Tubb of Boeing's Aerospace simulation group. The evaluation pilots were Mr. J. H. Armstrong, Mr. I. B. Decker, Jr., Mr. T. E. Edmonds, Mr. R. L. McPherson, and Mr. J. M. Swain of The Boeing Company and Lt. Col. A. K Davidson and Lt. Col. H. G. VanGieson, III of the United States Air Force. The author also wishes to thank Mr. C. T. Snyder of NASA Ames for his assistance to Boeing personnel during the moving base simulation test phase.

The Air Force Project Engineer for this investigation was Mr. Garland S. Oates, Air Force Flight Dynamics Laboratory, PTA, Wright-Patterson Air Force Base, Ohio.

This report was released within The Boeing Company as document D180-14412-2. It was submitted to the Air Force in December 1972.

This technical report has been reviewed and is approved.

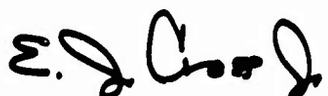

E. J. Cross, Jr., Lt. Col., USAF
Chief, Prototype Division
Air Force Flight Dynamics Laboratory

ABSTRACT

Fixed base and piloted simulation studies were conducted to evaluate control systems for a STOL tactical transport equipped with vectored thrust. Unaugmented aircraft flying qualities were found to be unacceptable. However, an augmented control system configuration was found to give excellent flying qualities and satisfactory behavior following engine or control system component failure. The present flying qualities standard for STOL aircraft, MIL-F-83300, was reviewed and several changes are suggested.

(vi blank)

TABLE OF CONTENTS

TABLE OF CONTENTS (Continued)

LIST OF ILLUSTRATIONS

LIST OF ILLUSTRATIONS (Continued)

LIST OF ILLUSTRATIONS (Continued)

LIST OF ILLUSTRATIONS (Continued)

LIST OF ILLUSTRATIONS (Continued)

LIST OF ILLUSTRATIONS (Continued)

LIST OF ILLUSTRATIONS (Continued)

(xvi Blank)

LIST OF TABLES

LIST OF TABLES (Continued)

LIST OF ABBREVIATIONS AND SYMBOLS

ABBREVIATIONS

ALB	α, Angle of Attack ∿ deg.
AMST	Advanced Medium STOL Transport
ARC	Ames Research Center
AX	a_x, Acceleration Along x Axis ∿ fps^2
AY	a_y, Acceleration Along y Axis ∿ fps^2
AZ	a_z, Acceleration Along z Axis ∿ fps^2
BETA	β, Sideslip Angle ∿ deg.
CAS	Control Augmentation System
CRT	Cathode Ray Tube
CTOL	Conventional Takeoff and Landing
DAIL	δ_a, Aileron Deflection Angle ∿ deg.
DCOL	δ_{COL}, Column Deflection ∿ inches
DLC	Direct Lift Control
DP	δ_{PED}, Pedal Deflection ∿ deg.
DR	δ_R, Rudder Deflection Angle ∿ deg.
DSIG	δ_σ, Vector Angle Deflection ∿ deg.
DSPL	$\delta_{SP_{LHW}}$, Left-Hand Wing Spoiler Deflection ∿ deg.
DSPR	$\delta_{SP_{RHW}}$, Right-Hand Wing Spoiler Deflection ∿ deg.
DTH	δ_{TH}, Throttle Lever Deflection Angle ∿ deg.
DW	δ_W, Wheel Deflection Angle ∿ deg.
FBW	Fly-By-Wire
FSAA	Flight Simulator for Advanced Aircraft
HD	$\dot{h}$, Altitude Rate ∿ fpm

LIST OF ABBREVIATIONS AND SYMBOLS (Continued)

ABBREVIATIONS

IFR	Instrument Flight Rules
LHW	Left-hand Wing
PDOT	$\dot{P}$, Roll Acceleration ∿ deg./sec.^{2}
PR	Pilot Rating
PSIGT	ψ_{GT}, Ground Track Angle ∿ deg.
QDOT	$\dot{Q}$, Pitch Acceleration ∿ deg./sec.^{2}
RDOT	$\dot{R}$, Yaw Acceleration ∿ deg./sec.^{2}
RHW	Right-hand Wing
RMS	Root Mean Square
SAS	Stability Augmentation System
STAI	STOL Tactical Aircraft Investigation
STOL	Short Takeoff and Landing
SX	s_x, x inertial position coordinate ∿ ft.
SY	s_y, y inertial position coordinate ∿ ft.
SYD	$\dot{s}_y$, inertial side velocity ∿ fps
TAT-ADP	Tactical Airlift Technology - Advanced Development Program
T/W	Thrust-to-Weight Ratio
VFR	Visual Flight Rules
VG	V_G, Ground Speed ∿ fps
VSI	Vertical Situation Indicator
VT	V_T, True Airspeed ∿ fps

LIST OF ABBREVIATIONS AND SYMBOLS (Continued)

SYMBOL	
a_x	Acceleration along x axis, $a_x = \frac{X_A + X_T}{m} \sim fps^2$
a_y	Acceleration along y axis, $a_y = \frac{Y_A + Y_T}{m} \sim fps^2$
a_z	Acceleration along z axis, $a_z = \frac{Z_A + Z_T}{m} \sim fps^2$
b_w	Wing span ~ ft.
$\bar{C}_w$	Wing mean aerodynamic chord ~ ft.
c.g.	Center of gravity
C_D	Drag coefficient
C_J	Thrust coefficient, $C_J = T_G/(.5\rho V_T^2 S_W)$
C_L	Lift coefficient
C_{ℓ}	Rolling moment coefficient
$C_{m_{cg}}$	Pitching moment coefficient about cg
$C_{n_{cg}}$	Yawing moment coefficient about cg
C_Y	Side force coefficient
C_μ	Momentum coefficient for boundary layer control
F	Controller force ~ lbs
h	Altitude ~ ft.
I_X	Body axis roll inertia ~ slug - ft^2
I_Y	Body axis pitch inertia ~ slug - ft^2
I_Z	Body axis yaw inertia ~ slug - ft^2
I_{XZ}	Body axes product of inertia ~ slug - ft^2
L	Rolling moment ~ ft-lbs
$L_{( )}$	Turbulence characteristic length ~ ft.
ℓ_H	Horizontal tail moment arm ~ ft.
M	Pitching moment ~ ft - lbs

SYMBOLS

m	Airplane mass, $m = W/32.2$ ~ slugs
m_a	Engine air mass flow rate ~ slug/sec
N	Yawing moment ~ ft-lbs
n_Z	Normal load factor
P	Roll rate (body axis unless noted otherwise) ~ deg/sec
Q	Pitch rate (body axis unless noted otherwise) ~ deg/sec
R	Yaw rate (body axis unless noted otherwise) ~ deg/sec
S_H	Horizontal tail area ~ ft^2
S_W	Wing area ~ ft^2
S_x	X inertial position coordinate ~ ft
S_y	Y inertial position coordinate ~ ft
S_z	Z inertial position coordinate, $S_z = -h$ ~ ft
σ	Stabilizer angle ~ deg
T_G	Gross thrust ~ lbs
T_R	Roll time constant ~ sec
T_2	Time to double amplitude ~ sec
t_{30}	Time to bank thirty degrees
u	Inertial velocity component along x axis ~ fps
u_A	Relative velocity component along x axis ~ fps
u_{SHEAR}	Shear strength ~ fps
u_W	Wind velocity component along x axis ~ fps
v	Inertial velocity component along y axis ~ fps
V	Total inertial velocity ~ fps

LIST OF ABBREVIATIONS AND SYMBOLS (Continued)

SYMBOLS

v_A	Relative velocity component along y axis ~ fps
V_{APP}	Approach airspeed
V_C	Climbout speed
V_E	Equivalent airspeed ~ knots
V_G	Ground speed ~ fps
V_{LO}	Liftoff speed
V_{MCG}	Ground minimum control speed
V_R	Rotation speed
V_S	Stall speed
V_T	True airspeed ~ fps
v_w	Wind velocity component along y axis ~ fps
V_1	Engine failure recognition speed
w	Inertial velocity component along z axis ~ fps; or airplane weight ~ lbs
w_A	Relative velocity component along z axis ~ fps
w_w	Wind velocity component along z axis ~ fps
X	External force component along x axis ~ lbs
Y	External force component along y axis ~ lbs
Z	External force component along z axis ~ lbs
$\dot{(\ )}$	$d(\ )/dt$
$\hat{(\ )}$	$(\ )\frac{b_w}{2V_T}$ or $(\ )\frac{\bar{c}_w}{2V_T}$

GREEK SYMBOLS

α	Angle of attack relative to x axis ~ deg
β	Sideslip angle ~ deg
γ	Flight path angle ~ deg

GREEK SYMBOLS

δ	Controller or control deflection angle ~ deg
ϵ	Downwash ~ deg
ϵ_{GS}	Glideslope error ~ dots [= .35° of ϵ_{GS}]
ϵ_{LOC}	Localizer error ~ dots [= .5° of ϵ_{LOC}]
ϵ_{V}	Airspeed error ~ fps
ζ	Damping ratio
θ	Pitch attitude ~ deg
ρ	Density of air ~ slug/ft^3
σ	Engine vector angle ~ deg; or RMS value of any variable
τ	Control system time constant ~ sec
$\Phi_{( )}$	Turbulence power spectral density ~ ft^2/sec
ϕ	Bank angle ~ deg
ψ	Airplane heading ~ deg
ψ_{GT}	Ground track angle ~ deg
ψ_{SHEAR}	Shear direction ~ deg
ψ_{1}	Heading change after 1 sec. ~ deg
ω	Frequency ~ rad/sec

SUBSCRIPTS

A	Aerodynamic force or moment
a	Aileron
C	Command
COL	Column
DLC	Direct lift control
e	Elevator

SUBSCRIPTS

LAT	Lateral Control
O	Initial value
P	Pilot
PED	Rudder pedal
PL	Power lever
R	Rudder
SA	Stability axes
SP	Spoiler
T	Thrust force or moment
TD	Touchdown
TH	Throttle
W	Wheel or wind component
σ	Thrust vector angle

SECTION I

INTRODUCTION

1.1 Background

The U.S. Air Force's need for modernization of its Tactical Airlift capability has led to establishment of the Tactical Airlift Technology Advanced Development Program (TAT-ADP), contributing to the technology base for development of an Advanced Medium STOL Transport (AMST).

The AMST must be capable of handling substantial payloads and using airfields considerably shorter than those required by large tactical transports now in the Air Force inventory. If this short field requirement is to be met without unduly compromising aircraft speed, economy, and ride quality, an advanced-technology powered-lift concept will be required.

The STOL Tactical Aircraft Investigation (STAI) was a major part of the TAT-ADP, and comprised studies of the aerodynamics and flight control technology of powered lift systems under consideration for use on the AMST. Under the STAI, The Boeing Company was awarded Contract No. F33615-71-C-1757 by the Air Force Flight Dynamics Laboratory to conduct investigations of the technology of the vectored-thrust powered lift concept. These investigations included:

(1) Aerodynamic analysis and wind tunnel testing

(2) Configuration studies

(3) Control systems technology studies

The unaugmented flying qualities of powered lift STOL transports in the landing approach condition are degraded by low dynamic pressure and severe aerodynamic cross-coupling between control axes. Precise control is needed if the short field capability attained by flying at low speed is not to be squandered in wide touchdown dispersion. Therefore, the control technology portion of the STAI was of as much importance as the aerodynamic and design studies.

1.2 Purpose of Piloted Simulation

The objective of the control technology study was the definition and validation of a control system for an AMST using the vectored thrust/mechanical flap powered lift concept. The control system was required to provide precise control throughout the flight envelope under normal and failure conditions. The selected control system was an end product of a trade study which considered:

- Performance
- Safety
- Vulnerability
- Redundancy
- Cost
- Weight
- Complexity
- Design Risk

Analytical methods alone are insufficient to assure that a control system design will function well. The varied reactions and capabilities of real human pilots are an essential ingredient, and can be introduced no other way short of actual flight test.

The purpose of the piloted simulation program was to evaluate performance characteristics and redundancy requirements of candidate control laws and mechanization concepts. Control system performance was measured in terms of pilot acceptance (i.e., pilot ratings and comments), pilot workload, tracking accuracy, and touchdown dispersions. Redundancy requirements evolved from evaluating various control system failure modes.

1.3 Summary of the Simulation Effort

Piloted simulation work consisted of 370 hours of fixed base and 54 hours of moving base (ARC-FSAA) simulator flying time. Five Boeing pilots and two Air Force pilots participated. As a group, these pilots have logged approximately forty thousand flight hours, of which ten thousand are engineering test time. Both military pilots logged combat time in C-130s in Viet Nam. The Boeing pilots flew the model 367-80 (BLC modification), the Augmentor Wing Buffalo, and simulations of upper surface blowing, vectored thrust, augmentor wing, and externally blown flap STOL configurations.

STAI piloted simulation tests include handling quality evaluations and an IFR approach/VFR landing task. The scope of the test matrix is summarized as follows:

(1) Seventeen longitudinal and fourteen lateral/directional control laws;

(2) Mechanical, stability augmentation, control augmentation, and fly-by-wire control system mechanizations;

(3) Hardover, loss of feedback, and passive control system failures; and

(4) Propulsion system failures.

1.4 Report Organization

Section II presents a description of the fixed and moving base simulations and a discussion of simulation test procedures. Simulation results are described and analyzed in Section III. A review of Mil-F-83300 criteria comprises Section IV. Section V includes the conclusions and recommendations drawn from the entire piloted simulation program. Appendix I contains biographies of each pilot who took part. The fixed and moving base simulations are compared in Appendix II. Appendix III defines simulation mathematical models and supporting data.

SECTION II

SIMULATION PROGRAM DESCRIPTION

2.1 Simulation Facilities

Both fixed and moving base simulators were used for the STAI simulation program. Boeing's fixed base simulator was used for both the conceptual control law and control mechanization investigations. NASA Ames' Flight Simulator for Advanced Aircraft (FSAA) was used to validate the selected control system.

The Boeing Visual Flight Simulator at the Boeing Space Center is a fixed-base, high fidelity visual simulator that has been in operation since June 1964. The equipment at this facility pertinent to this study was:

- One Xerox Data Systems 930 digital computer operating in conjunction with a Varian 622I digital computer.
- Two Boeing-designed and built precision six-degree-of-freedom carriage and gimbal systems for camera scanners. These carriages feature a digital servo system to enhance the overall system accuracy.
- A model landscape and drive system capable of handling models up to 12 by 88 feet.
- A TV camera equipped with a Photo Mechanisms optical probe to decrease the minimum simulated altitude.
- High-resolution closed circuit television systems.
- A hemispherical 30-foot-diameter projection screen.
- A cockpit with a CRT type VSI approach and landing display.

Figures 1 through 3 show Boeing's simulation laboratory and the STAI instrument layout and electronic vertical situation indicator.

The dynamic properties of the FSAA's motion system are presented in Table I. Aside from the obvious difference between the simulations (i.e., motion cues) there were other differences which could affect simulation results. A detailed comparison of fixed base and moving base simulators is presented in Appendix II.

2.2 Simulation Test Procedures

Candidate control laws and mechanization schemes were evaluated through a series of handling quality tests and an IFR approach/VFR landing task. Longitudinal and lateral-directional control systems

Figure 1: STOL TAI Simulation Cab and Visual Scene

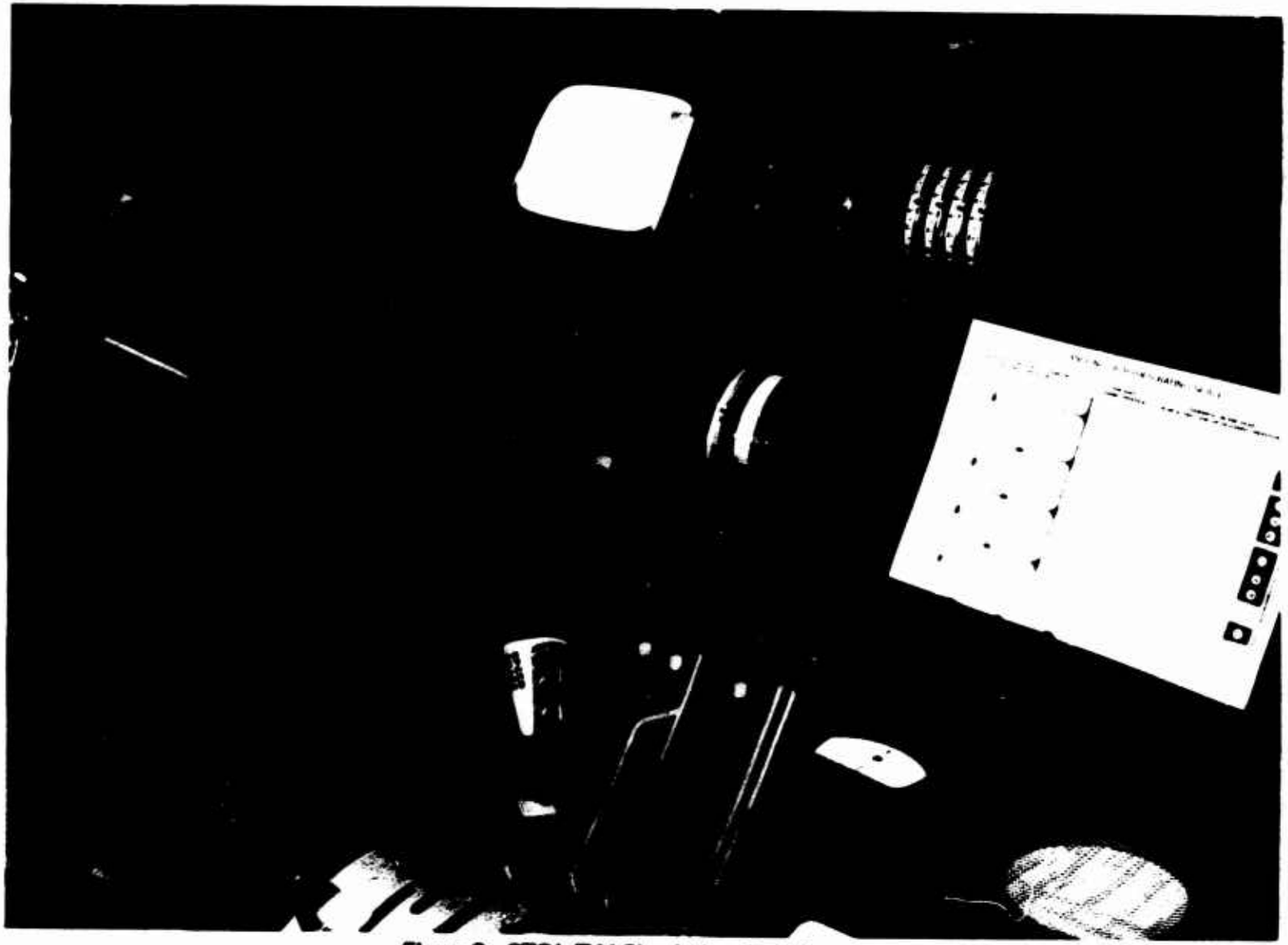

Figure 2: STOL TAI Simulation Cockpit

Figure 3: S/OL TAI CRT Vertical Situation Display

TABLE I

FLIGHT SIMULATOR FOR ADVANCED AIRCRAFT: DYNAMIC PROPERTIES

Motions Generated	Displacement	Acceleration	Velocity	Frequency @ 30° Phase Lag
Roll	±45° (±35)	4 Rad/Sec^2 (1.6)	1.77 Rad/Sec (0.5)	3.1 Hz
Pitch	±22½° (±18)	2 Rad/Sec^2 (1.6)	0.70 Rad/Sec (0.5)	1.5 Hz
Yaw	±30° (±24)	2 Rad/Sec^2 (1.6)	0.70 Rad/Sec (0.5)	1.7 Hz
Vertical	±5 Ft.(±3.9)	12 Ft/Sec^2	8.65 Ft/Sec (6.9)	2.2 Hz
Longitudinal	±4 Ft.(±2.8)	10 Ft/Sec^2	6.32 Ft/Sec (5.1)	1.8 Hz
Lateral	±50 Ft.(±40)	12 Ft/Sec^2	17.00 Ft/Sec (16.0)	1.0 Hz

NOTE: Quantities in parenthesis represent typical.

were evaluated separately. When a longitudinal control system was evaluated, the lateral-directional axes were augmented to minimize cross-axis effects. Conversely, the longitudinal axis was augmented when lateral-directional control systems were evaluated.

Each day, the pilots were given a brief description of the data required from the test and (if necessary) a general description of the airplane. They were then given a warm-up period in which to familiarize themselves with the simulation and the simulated airplane.

Pilot comments and ratings were recorded immediately after each evaluation task. The revised Cooper-Harper pilot rating scale was used, and it is presented by Table II for the reader's convenience. After each IFR approach/VFR landing task, a control system performance computer printout was taken. Figure 4 is an example of this printout which records quantitative data pertaining to pilot workload, control surface activity, tracking performance, and the touchdown state.

2.2.1 Handling Quality Tasks

The handling quality tasks were designed to provide specific stability and control information about candidate control systems. The decrab maneuver, and the landing phase of the "S" turn and energy management tests were flown under VFR conditions. All other handling quality evaluations were flown under IFR conditions. Except for the decrab test, all evaluations were flown in still air conditions. With the exception of the energy management task, the initial airspeed for handling quality evaluations was seventy-five knots. This was also the target landing speed for the IFR approach/VFR landing task. A seventy-five knot landing speed was selected at the beginning of the simulation studies since it provided a maneuver margin and power on speed margin of $\Delta n_z = .45g$ and $V/V_S = 1.2$, respectively.

The handling quality tasks are described below:

Longitudinal Handling Qualities

- Attitude Control: Increase pitch attitude by $\Delta\Theta = 5°$, stabilize, return to initial attitude. Keep airspeed constant. Repeat maneuver by reducing Θ by $\Delta\Theta = -5°$, stabilize, and return to initial attitude.

- Glide Slope Control: Steepen glide slope to -8° (and stabilize) from an initial -6° glide slope while keeping airspeed constant, then return to -6° glide slope. Repeat for glide slope changes to -4°.

- Altitude Control: From level flight, increase altitude by 200 ft. at 500 fpm. Stabilize airplane at new altitude, then return to initial altitude. Keep airspeed constant.

- Speed Control: Increase and decrease airspeed by 5 knots while tracking -6° glide slope.

TABLE II

COOPER-HARPER PILOT RATING SYSTEM

CONTROLLABLE Capable of being controlled or managed in context of mission, with available pilot attention.	**ACCEPTABLE** May have deficiencies which warrant improvement, but adequate for mission. Pilot compensation, if required to achieve acceptable performance, is feasible.	SATISFACTORY Meets all requirements and expectations; good enough without improvement. Clearly adequate for mission.	Excellent, highly desirable.	1
			Good, pleasant, well behaved.	2
			Fair. Some mildly unpleasant characteristics. Good enough for mission without improvement.	3
		UNSATISFACTORY Reluctantly acceptable. Deficiencies which warrant improvement. Performance adequate for mission with feasible pilot compensation.	Some minor but annoying deficiencies. Improvement is requested. Effect on performance is easily compensated for by pilot.	4
			Moderately objectionable deficiencies. Improvement is needed. Reasonable performance requires considerable pilot compensation.	5
			Very objectionable deficiencies. Major improvements are needed. Requires best available pilot compensation to achieve acceptable performance.	6
	UNACCEPTABLE Deficiencies which require improvement. Inadequate performance for mission even with maximum feasible pilot compensation.		Major deficiencies which require improvement for acceptance. Controllable. Performance inadequate for mission, or pilot compensation required for minimum acceptable performance in mission is too high.	7
			Controllable with difficulty. Requires substantial pilot skill and attention to retain control and continue mission.	8
			Marginally controllable in mission. Requires maximum available pilot skill and attention to retain control.	9
UNCONTROLLABLE Control will be lost during some portion of mission.			Uncontrollable in mission.	10

DATE 21:32 AUG 24.'72 FCS NO. = CP21 CR20 RUN NO. = 42

********** INITIAL CONDITION **********

W	= .1330E 06	ALTITUDE	= .1850E 04	GROUD TRACK	= .4500E 02
CG	= .3250E 00	LATERAL DISP.	= .1750E 04	SHEAR VELOCITY	= .3353E 02
VT	= .1453E 03	GROSS THRUST	= .5234E 05	SHEAR ANGLE	= -.4500E 02
GAMMA	= .0000E 00	VECTOR ANGLE	= .5619E 02	TURB. INTENSITY	= .5000E 01

********** RMS VALUES **********

(1) PILOT WORK LOAD

TOTAL					TRACKING			
DCOL	= .3862E 00	DTH	= .4629E-01	*	DCOL	= .3610E 00	DTH	= .4626E-01
DW	= .8016E 01	DSIG	= .8210E-01	*	DW	= .8375E 01	DSIG	= .8082E-01
DP	= .2942E-01			*	DP	= .2815E-01		

(2) CONTROL SURFACE ACTIVITY

DDLC	= .1053E 02	TG	= .5178E 05	DAIL	= .1160E 02	DR	= .1743E 01
DE	= .1794E 01	SIGMA	= .6834E 02	DSP	= .1059E 02		

(3) TRACKING PERFORMANCE

GLIDE SLOPE ERROR = .1699E 00 AIRSPEED ERROR = .7413E 01 GROUD TRACK ERROR = .4093E 00

********** TOUCHDOWN DATA **********

SX	= .2252E 03	SY	= -.6524E 01	PSIGT	= .8974E 02	VG	= .1365E 03
VT	= .1305E 03	HD	= -.5445E 01	SYD	= -.4099E 00		

********** MAXIMUMS **********

TOTAL							BELOW 300 FT.						
ALB	= .1369E 02	PDOT	= .1425E 02	DE	= .8545E 01	*	ALB	= .1369E 02	PDOT	= .8960E 01	DE	= .8545E 01
BETA	= .4031E 01	QDOT	= .5378E 01	DAIL	= .3000E 02	*	BETA	= .4031E 01	QDOT	= .4274E 01	DAIL	= .3000E 02
PHI	= .1296E 02	RDOT	= .2836E 01	DSPR	= .1425E 02	*	PHI	= .3494E 01	RDOT	= .2836E 01	DSPR	= .1269E 02
P	= .5851E 01	AX	= .4106E 01	DSPL	= .1524E 02	*	P	= .3304E 01	AX	= .4106E 01	DSPL	= .1339E 02
Q	= .2375E 01	AY	= .5352E 00	DR	= .5847E 01	*	Q	= .1790E 01	AY	= .4838E 00	DR	= .3729E 01
R	= .2788E 01	AZ	= .3583E 02	SIGMA	= .7989E 02	*	P	= .1284E 01	AZ	= .3569E 02	SIGMA	= .7904E 02
	SIGMA MINIMUM = .5668E 02					*		SIGMA MINIMUM = .6363E 02				

Figure 4: Control System Performance Data

- o Energy Management: (Validation Phase Only)
  - (a) High/Fast: Starting 2 dots above the glideslope and V_T = 85 knots, capture the glideslope and reduce the airspeed to V_T = 75 knots.
  - (b) Low/Slow: Starting 2 dots below glideslope and V_T = 65 knots, capture the glideslope and increase the airspeed to V_T = 75 knots.

Lateral-Directional Handling Qualities

- o Large Heading Changes: Change heading by 45 degrees while maintaining altitude. Repeat the maneuver for slow, nominal, and fast turn entries.

- o Small Heading Changes: Evaluate the ability to make small heading changes ($\Delta\Psi = \pm 2^{\circ}$).

- o Decrab Maneuver: Perform a decrab maneuver prior to touchdown in a 25 knot crosswind. Keep the wings level and minimize lateral drift.

- o "S" Turns: Trim the airplane on the correct glideslope but with a 100 ft. lateral offset. At an altitude of 100 ft., perform an "S" turn and land on the runway.

2.2.2 Performance Task

The IFR approach/VFR landing task was used to assess the performance of candidate control systems under typical STOL operational conditions. This task included the following control elements: localizer and glideslope capture, speed bleedoff, glideslope and localizer tracking, decrab, and land. These tasks are depicted by Figure 5. Pilots were asked not to flare the airplane. Instead, they were asked to transition to a vertical velocity less than six hundred feet per minute and aim for a landing at the touchdown point, which was located three hundred feet beyond the threshold. This landing approach task was made with random turbulence and a quartering tail wind shear. (See Figure 7 for wind shear profiles.) The turbulence level was set at three feet per second to increase the pilot's workload without masking control system characteristics. It was found that five feet per second and above turbulence levels made control system comparisons difficult (i.e., pilot ratings for simple and complex systems varied by approximately .5; therefore, pilot ratings were biased almost entirely on turbulence intensity.

Specific IFR approach/VFR landing piloting tasks are outlined below:

- Track initial heading at constant airspeed and altitude (V_T = 85 knots and h = 1850 ft.).
- Turn onto localizer beam, transition to 6° glideslope, and reduce airspeed to 75 knots.
- Track glideslope and localizer down to transition altitude (h = 60 ft.) at constant airspeed (V_T = 75 knots). IFR tracking should be continued as long as possible after breaking out from simulated ceiling (h ≈ 350 ft.).
- At transition altitude, reduce rate of descent to h < 600 FPM.
- Decrab and land airplane as close as possible to reference runway landing mark without flaring.

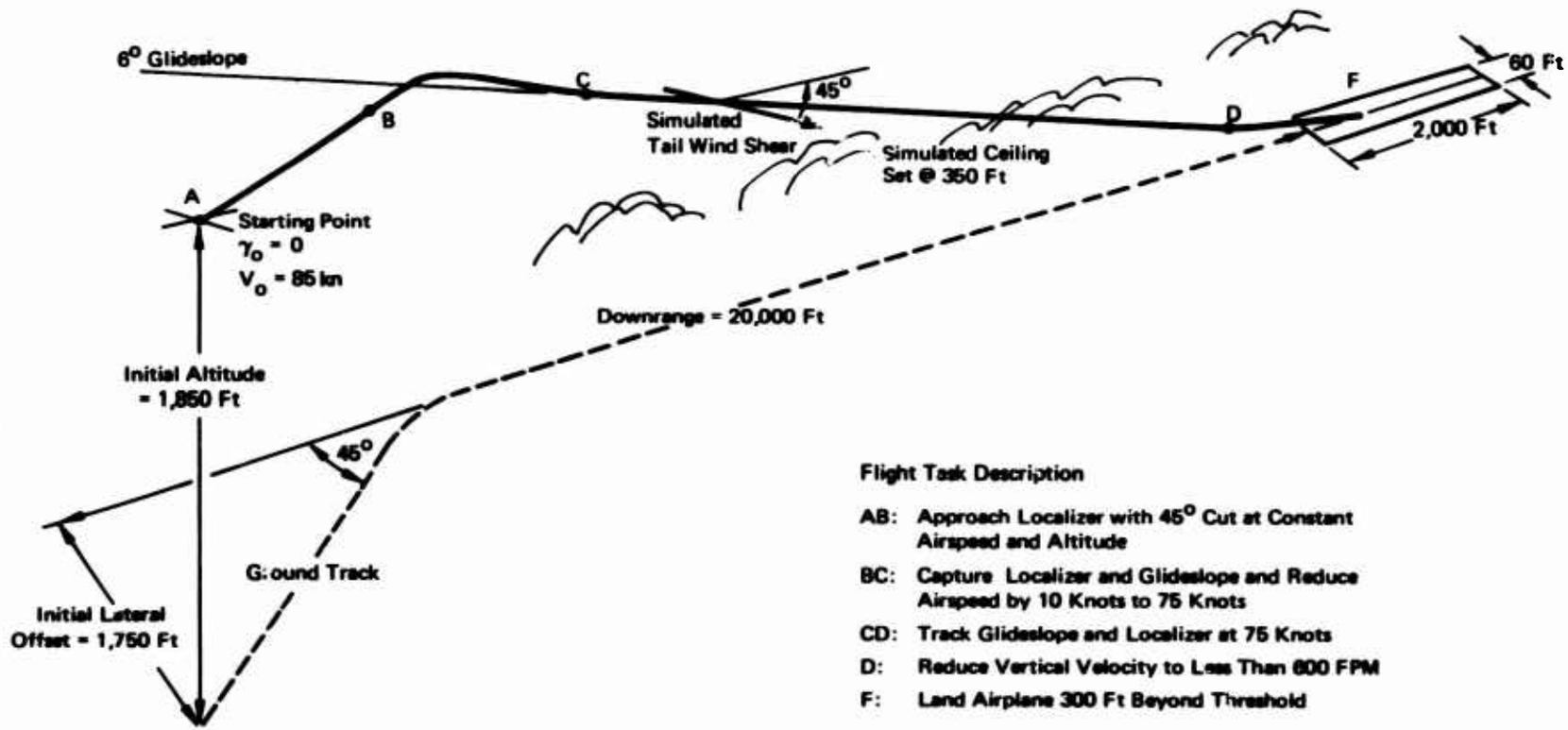

Figure 5: IFR Performance Task

SECTION III

SIMULATION RESULTS

3.1 General Considerations of STOL Flight

A review of pilot comments obtained in the STAI simulation study showed that several comments appear to be independent of control law configuration. These comments represent general flying quality considerations for the STOL landing approach. The STOL landing approach is characterized by low approach speeds (e.g., V_{APP} = 75 kn) and steep approach angles (e.g., γ_{APP} = -6°).

Pilots confirmed that they could use "conventional" techniques for controlling flight path angle and airspeed. The "conventional" technique implies that flight path angle is controlled with the column and that thrust vector angle is used for controlling airspeed. The other control technique often used for STOL approaches involves controlling airspeed with the control column and flight path angle with thrust magnitude. This control technique is often referred to as the "STOL" technique. The "STOL" technique is used only when speed control can be achieved by modulating drag (i.e., through angle of attack control). For a vectored thrust airplane, the "conventional" technique is preferred for the following reasons:

(1) With the thrust vector set at approximately 70°, changes in vector angle primarily produce axial acceleration, with a small change in normal acceleration.

(2) In the nominal approach condition and with the power set at 75% of maximum, the aerodynamic and propulsive normal acceleration capability is $\Delta n_{Z_{AERO}}$ (with DLC) = .45g and $\Delta n_{Z_{THRUST}}$ = .1g. With a single engine failure, $\Delta n_{Z_{THRUST}}$ = 0 if the thrust to weight ratio is maintained.

Boeing pilots learned that they could improve glideslope tracking performance in turbulence by closing a flight path angle inner loop, instead of using pitch attitude. The benefits resulting from this closure are proportional to turbulence intensity because pitch attitude is more sensitive than flight path angle to turbulence disturbances. Turbulence disturbances seem to affect pitch attitude directly through changes in angle of attack, since $\Delta\theta \approx \Delta\alpha$. On the other hand, the airplane dynamics attenuated the effects of turbulence on flight path angle. This was to be expected, since flight path angle is the ratio of $\dot{h}$ and V_G.

The data presented by Figure 6 analytically confirms the pilots' preference to using a flight path inner loop for glideslope tracking in turbulence. These data were generated by using "paper pilot" models which had either an attitude or a flight path inner loop and a glideslope outer loop. Inner loop gains were held constant and were optimized for each mode of control. These data resulted from computing

Note

1. Turbulence Intensity = 5 fps
2. Selected Longitudinal Control Law (CP21)
3. Paper Pilot
   (a) $\epsilon_{GS}, \theta_{\epsilon}$ or $\gamma_{\epsilon} \rightarrow \delta_{Col}$
   (b) Fixed Inner Loop Gain
   Variable Outer Loop Gain

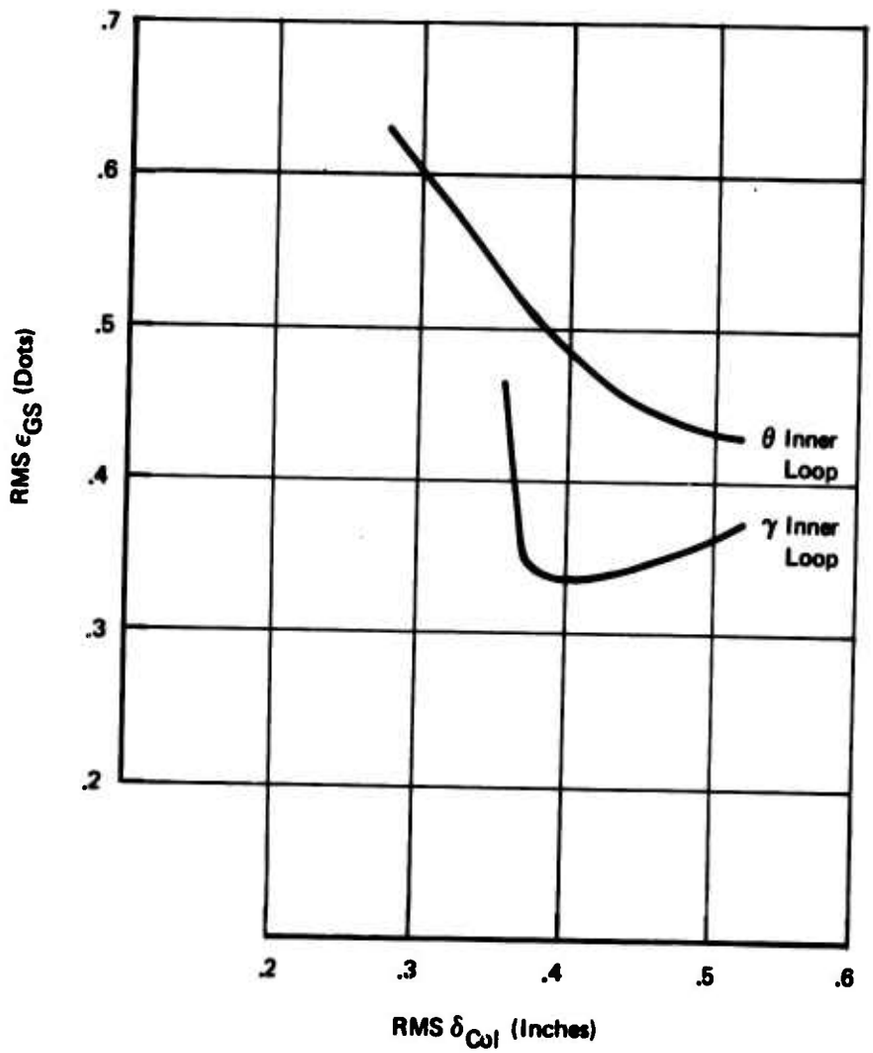

Figure 6: Effect of Inner Loop Closure on Glideslope Tracking Performance

root mean square values of glideslope error and pilot column activity as a function of the "pilot's" outer loop gain for a turbulence level of $\sigma_u = \sigma_w = 5$ fps.

Figure 7 illustrates another reason for using a flight path angle inner loop. These data show the effect of wind shears on flight path angle for CTOL and STOL approaches, if attitude and airspeed are held constant. It is apparent that if a pilot flies constant pitch attitude and airspeed for STOL approaches, landing dispersions will be larger.

The kinematic relationship between turn rate, airspeed, and bank angle dictates another operational consideration: Large bank angles are not required for turning flight at STOL approach speeds. Figure 8 defines this relationship for steady coordinated turns. Boeing pilots found that bank angles in excess of 22° could not be used for changing heading. The limiting bank angle was set by the pilot's ability to judge his roll out point. They also found that localizer tracking required constant attention, since small unattended bank angle errors quickly produced changes in heading.

Another kinematic property of turning flight is highlighted by Figure 9, which defines the relationship between elevator required for a steady turn as a function of bank angle and airspeed. This relationship is given by the following equation:

$$\delta_{e_{\substack{\text{steady}\\\text{turn}}}} = (\delta_e/g)\,\Delta n_z = \left(\frac{2W}{\rho S_w}\right)\left(\frac{MP-cg}{C_{m_{\delta_e}}}\right)\left(\frac{\sec\phi-1}{U_o^2}\right)$$

where:

ϕ = bank angle, deg

U_o = airspeed, fps

MP-cg = maneuver margin (MP is stick-fixed Maneuver Point based on turns)

$C_{m_{\delta_e}}$ = elevator effectiveness, 1/deg.

W = weight, lbs

ρ = air density, slug/ft^3

S_w = reference wing area, ft^2

These data show that more back stick pressure is required at constant bank angles as airspeed is reduced. However, these data also show that $\delta_{e_{\text{steady turn}}}$ is approximately proportional to turn rate. Thus, both CTOL and STOL aircraft should have similar trim characteristics for flight at a constant turn rate.

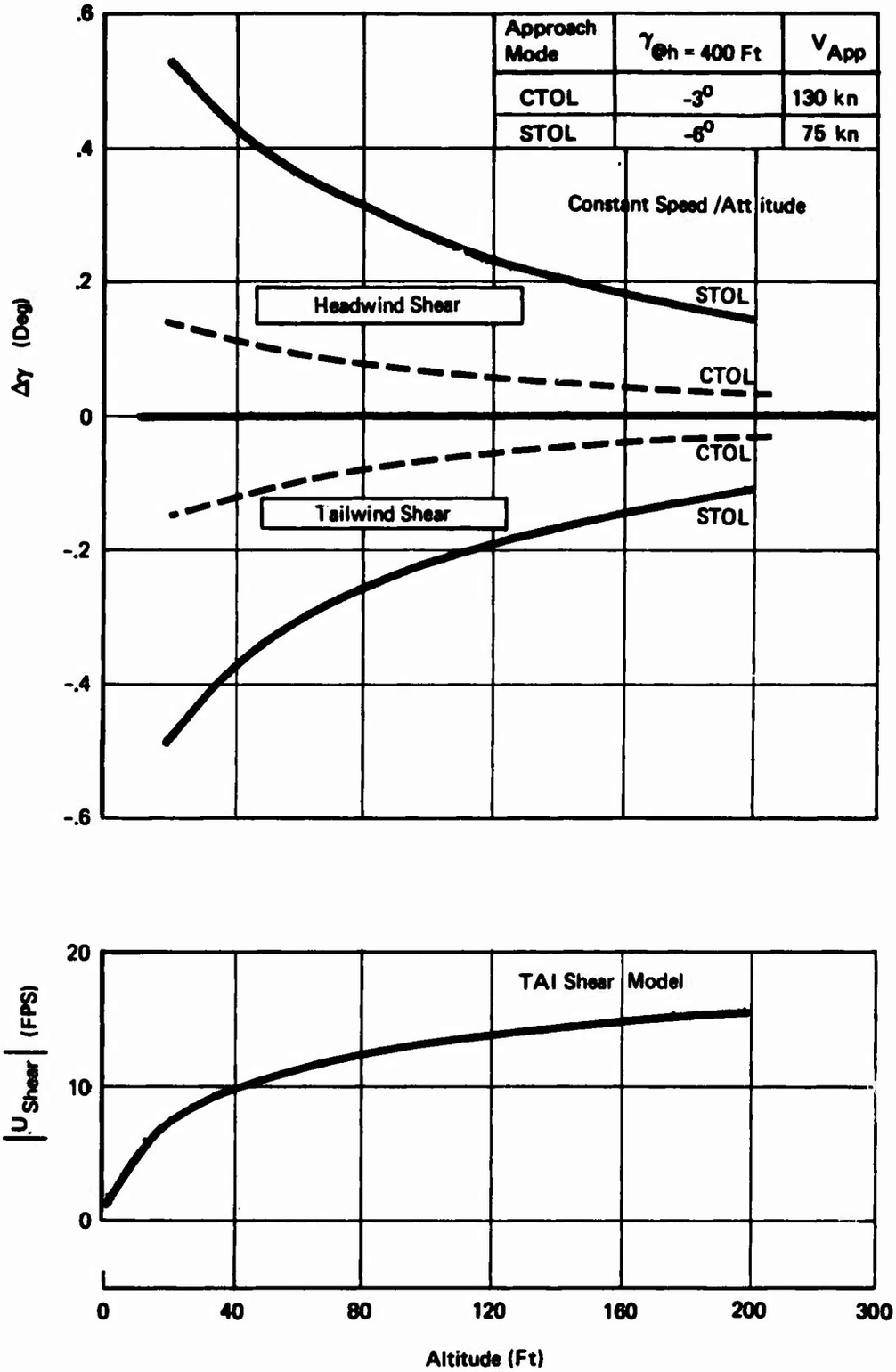

Figure 7 : Change in Flightpath Due to Windshear

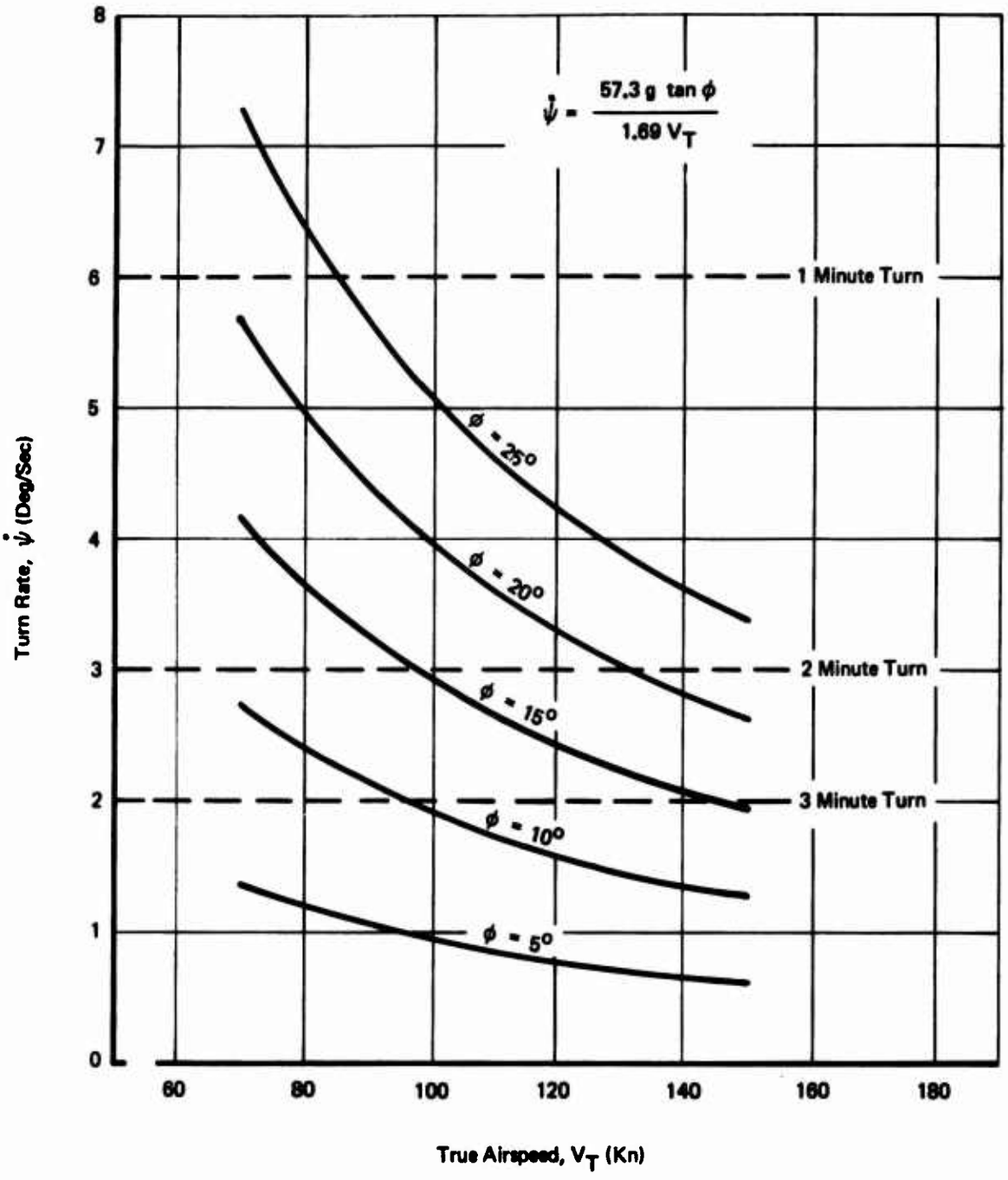

Figure 8: Effect of Bank Angle and Airspeed on Turn Rate

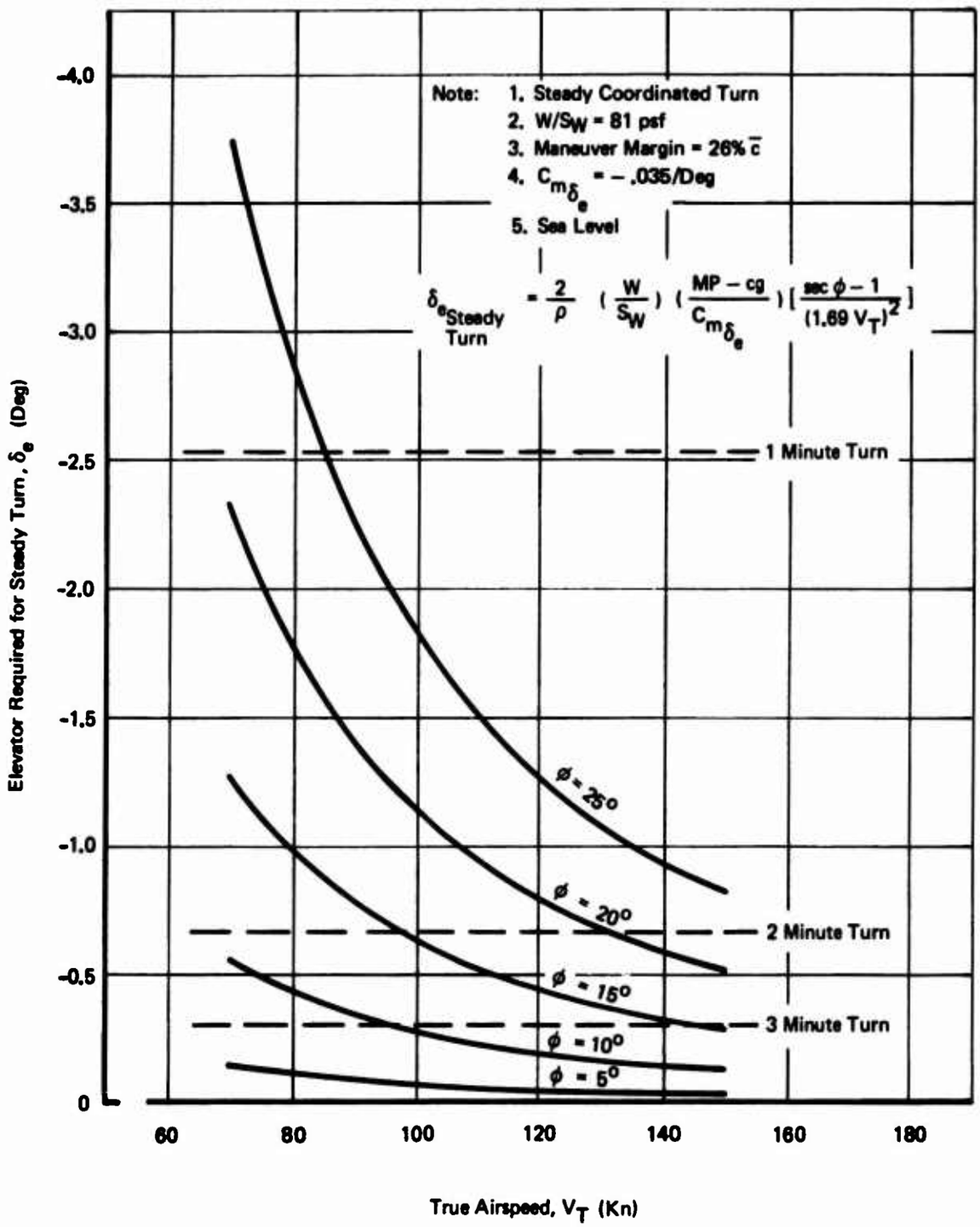

Figure 9: ***Effect of Bank Angle and Airspeed on Elevator Required for Steady Turn***

3.2 Analysis of Control Law Performance and Complexity

The relationship between control system performance and control law complexity is assessed in this section. Control system performance is measured in terms of pilot acceptance (i.e., pilot ratings and comments), pilot workload, tracking accuracy, and touchdown dispersions. Control law "complexity" as used in this section refers to the level of control/or stability augmentation.

Tables III and IV contain a brief description of each control law tested. In addition, appropriate simulation test phases are noted on these tables. The following convention has been used: C = conceptual control law phase, M = mechanization phase, and V = validation phase.

3.2.1 Control Law Evaluations: Pilot Ratings/Comments

Pilot ratings and comments for each longitudinal control law are presented in Table V. Ratings and comments for the lateral-directional control laws are given in Table VI. When a longitudinal control law was evaluated, the lateral/directional axes were augmented to minimize cross axis effects. Conversely, the longitudinal axis was augmented when lateral/directional control laws were evaluated. The control laws used for the non-evaluated control laws axis were SP02 and FR21.

The following conclusions pertaining to control system characteristics may be drawn from Tables V and VI:

- The flying qualities of the unaugmented airplane are unacceptable ($6.5 < PR < 9.5$).

- Satisfactory longitudinal flying qualities require that the longitudinal flight control system provide pitch damping, speed decoupling from column commands, and minimal glideslope deviations for speed commands. Figure 10 illustrates the differences in attitude control for a good control system (SP02), one with low pitch damping (AP01), and one that has excessive speed coupling (SP01). Pilots generally equated the requirement to "back check" their commands to low pitch damping. (This shows why pilot-in-the-loop dynamics must be considered in control system design.) Speed coupling increased the pilot's workload and generally made precision attitude and flight path control difficult.

- Satisfactory longitudinal flying qualities were achieved both with "attitude" and with "flight path" control laws. ("Attitude" control laws utilize Θ and Q feedback paths while the "flight path" systems used γ and $\dot{\gamma}$ paths.)

- Lateral-directional control systems that provide turn coordination, neutral spiral stability, and lateral damping are required for satisfactory flying qualities. (Note: Dutch roll damping was not a critical problem since $\zeta \simeq .2$ for the unaugmented airplane.) The requirement for lateral damping is analogous to the pitch

damping requirement described above. Figure 11 illustrates how a lack of turn coordination (SR20) makes precision control of bank angle and heading difficult.

- o "S" turns are more difficult for configurations which have adverse yaw. These configurations required larger lateral inputs for the "S" turn.

- o Dihedral effect (i.e., the ability to establish a roll rate with rudder inputs) does not appear to be a design consideration.

- o The addition of "stick steering" modes to the selected control system (CP20/CR20) improved its overall flying qualities by reducing pilot workload and by increasing the pilot's confidence to fly precision approaches. (The stick steering control system (AP07/AR20) was a rate command system that held pitch attitude when F_{COL} was less than three pounds, and bank angle ($|\emptyset|>10°$) or heading ($|\emptyset|<3°$) when F_w was less than two pounds.)

3.2.2 Control System and Powerplant Failure Evaluations: Pilot Ratings/Comments

During the control system mechanization and validation phases, elevator, spoiler, aileron and rudder hard-over failures were evaluated for various control systems. These failures were further subdivided into mechanical signal path failures (mechanical and control augmented mechanizations) and electrical signal path failures (control augmented and fly-by-wire mechanizations). Transient accelerations due to a failure and the resultant reduction in command and feedback path authorities are given by Table VII for all failures evaluated.

Table III: Longitudinal Control Law Description

CONFIGURATION NUMBER	COMMAND PATHS	FEEDBACK PATHS	TEST PHASE
MP01	$\delta_{COL} \rightarrow \delta_e$; $\delta_{\sigma_p} \rightarrow \delta_\sigma$		C
MP02	$\delta_{COL} \rightarrow \delta_e$, δ_{DLC}; $\delta_{\sigma_p} \rightarrow \delta_\sigma$		C, M
MP03	$\delta_{COL} \rightarrow \delta_e$, δ_{DLC}; $\delta_{\sigma_p} \rightarrow \delta_\sigma$, δ_e, δ_{DLC}		C
SP01	$\delta_{COL} \rightarrow \delta_e$, δ_{DLC}; $\delta_{\sigma_p} \rightarrow \delta_\sigma$	$\dot{\theta} \rightarrow \delta_e$, δ_{DLC}	C, M
SP02	$\delta_{COL} \rightarrow \delta_e$, δ_{DLC}; $\delta_{\sigma_p} \rightarrow \delta_\sigma$	$\dot{\theta} \rightarrow \delta_e$, δ_{DLC}; $\Delta\theta$, $\Delta V \rightarrow \delta_\sigma$	C
SP02A, CP21	$\delta_{COL} \rightarrow \delta_e$, δ_{DLC}; $\delta_{\sigma_p} \rightarrow \delta_\sigma$	$\dot{\theta} \rightarrow \delta_e$, δ_{DLC}; $\lvert\phi\rvert \rightarrow \delta_{DLC}$; $\Delta\theta$, $\Delta V \rightarrow \delta_\sigma$	M, V
SP03	$\delta_{COL} \rightarrow \delta_e$, δ_{DLC}; $\delta_{\sigma_p} \rightarrow \delta_\sigma$	$\dot{\theta} \rightarrow \delta_e$, δ_{DLC}; $\Delta\theta$, $\dot{\theta} \rightarrow \delta_\sigma$	C, M
SP04	$\delta_{COL} \rightarrow \delta_e$, δ_{DLC}; $\delta_{\sigma_p} \rightarrow \delta_\sigma$	$\dot{\theta} \rightarrow \delta_e$, δ_{DLC}; $\lvert\phi\rvert \rightarrow \delta_{DLC}$; $\Delta\theta$, $\Delta V \rightarrow \delta_\sigma$	M
SP05	$\delta_{COL} \rightarrow \delta_e$, δ_{DLC}; $\delta_{\sigma_p} \rightarrow \delta_\sigma$	$\dot{\theta} \rightarrow \delta_e$, δ_{DLC}; $\lvert\phi\rvert \rightarrow \delta_{DLC}$; $\Delta\theta$, ΔV, $\int\Delta V \rightarrow \delta_\sigma$	M
DP02	$\delta_{COL} \rightarrow \delta_e$, δ_{DLC}; $\delta_{\sigma_p} \rightarrow \delta_\sigma$	ΔV, $\dot{V} \rightarrow \delta_e$, δ_{DLC}; $\Delta\theta$, $\dot{\theta} \rightarrow \delta_\sigma$	C
DP03	$\delta_{COL} \rightarrow \delta_e$; $\delta_{\sigma_p} \rightarrow \delta_\sigma$	ΔV, $\dot{V}$, $\dot{\theta} \rightarrow \delta_e$; $\Delta\theta$, $\dot{\theta}$, $\Delta V \rightarrow \delta_\sigma$	C
DP05	$\delta_{COL} \rightarrow \delta_e$, δ_{DLC}; $\delta_{\sigma_p} \rightarrow \delta_\sigma$	$\dot{\gamma} \rightarrow \delta_e$, δ_{DLC}; $\Delta\gamma$, $\dot{\gamma}$, $\Delta V \rightarrow \delta_\sigma$	C

Table III: Longitudinal Control Law Description (Continued)

CONFIGURATION NUMBER	COMMAND PATHS	FEEDBACK PATHS	TEST PHASE
DP05A [2]	$\delta_{COL} \rightarrow \delta_e$, δ_{DLC}; $\delta_{\sigma_p} \rightarrow \delta_\sigma$	$\dot{\gamma}_{COMP} \rightarrow \delta_e$, δ_{DLC}; $\lvert\phi\rvert \rightarrow \delta_{DLC}$; $\Delta\gamma_{COMP}$, $\dot{\gamma}_{COMP}$, $\Delta V \rightarrow \delta_\sigma$	M
DP05B [3]	$\delta_{COL} \rightarrow \delta_e$, δ_{DLC}; $\delta_{\sigma_p} \rightarrow \delta_\sigma$	$\dot{\gamma}_{COMP} \rightarrow \delta_e$, δ_{DLC}; $\lvert\phi\rvert \rightarrow \delta_{DLC}$; $\Delta\gamma_{COMP}$, $\dot{\gamma}_{COMP}$, $\Delta V \rightarrow \delta_\sigma$	M
DP07 [3]	$\delta_{COL} \rightarrow \delta_e$, δ_{DLC}; $\delta_{\sigma_p} \rightarrow \delta_\sigma$	$\dot{\gamma}_{COMP} \rightarrow \delta_e$, δ_{DLC}; $\lvert\phi\rvert \rightarrow \delta_{DLC}$; $\Delta\gamma_{COMP}$, $\dot{\gamma}_{COMP}$, $\Delta V \rightarrow \delta_\sigma$	M
AP01	$\delta_{COL} \rightarrow \delta_e$ δ_{DLC}; $\delta_{\sigma_p} \rightarrow \delta_\sigma$	ΔV, $\dot{V} \rightarrow \delta_e$, δ_{DLC}; $\Delta\gamma$, $\dot{\gamma}$, $\Delta V \rightarrow \delta_\sigma$	C
AP02	$\delta_{COL} \rightarrow \delta_e$, δ_{DLC}; $\delta_{\sigma_p} \rightarrow \delta_\sigma$	ΔV, $\dot{V}$, $\dot{\gamma} \rightarrow \delta_e$, δ_{DLC}; $\Delta\gamma$, $\dot{\gamma}$, $\Delta V \rightarrow \delta_\sigma$	C
AP03	$\delta_{COL} \rightarrow \delta_e$, δ_{DLC}; $\delta_{\sigma_p} \rightarrow \delta_\sigma$	$\Delta\theta$, $\dot{\theta} \rightarrow \delta_e$, δ_{DLC}; $\Delta\theta$, $\Delta V \rightarrow \delta_\sigma$	C
AP05	$\delta_{COL} \rightarrow \delta_e$, δ_{DLC}; $\delta_{\sigma_p} \rightarrow \delta_\sigma$	$\Delta\gamma$, $\dot{\gamma} \rightarrow \delta_e$, δ_{DLC}; $\Delta\gamma$, $\dot{\gamma}$, $\Delta V \rightarrow \delta_\sigma$	C
AP07	$\delta_{COL} \rightarrow \delta_e$, δ_{DLC}; $\delta_{\sigma_p} \rightarrow \delta_\sigma$	$\dot{\theta}$, $\Delta\theta \rightarrow \delta_e$, δ_{DLC}; $\lvert\phi\rvert \rightarrow \delta_{DLC}$; $\Delta\theta$, $\Delta V \rightarrow \delta_\sigma$	V

[1] C: Conceptual control law phase; M: mechanization phase; V: validated

[2] γ_{COMP}, $\dot{\gamma}_{COMP}$ IS CALCULATED USING GROUND SPEED.

[3] γ_{COMP}, $\dot{\gamma}_{COMP}$ IS CALCULATED USING AIRSPEED.

Table IV: Lateral/Directional Control Law Description

CONFIGURATION NUMBER	COMMAND PATHS	FEEDBACK PATHS	TEST PHASE ①
MR0821	$\delta_W \rightarrow \delta_a$, δ_{SP}; $\delta_{PED} \rightarrow \delta_R$		C, M
SR0721	$\delta_W \rightarrow \delta_a$, δ_{SP}; $\delta_{PED} \rightarrow \delta_R$	R , P $\rightarrow \delta_a$, δ_{SP}	C
SR10	$\delta_W \rightarrow \delta_a$, δ_{SP}, δ_R; $\delta_{PED} \rightarrow \delta_R$	R,P$\rightarrow \delta_a$, δ_{SP}; R,P, $\phi \rightarrow \delta_R$	C
SR11	$\delta_W \rightarrow \delta_a$, δ_{SP}; $\delta_{PED} \rightarrow \delta_R$	R,P$\rightarrow \delta_a$, δ_{SP}; R,P$\rightarrow \delta_R$	C
DR141	$\delta_W \rightarrow \delta_a$, δ_{SP}; $\delta_{PED} \rightarrow \delta_R$, δ_a, δ_{SP}	R , P , ϕ, $A_Y \rightarrow \delta_a$, δ_{SP}, δ_R	C
DR142	$\delta_W \rightarrow \delta_a$, δ_{SP}; $\delta_{PED} \rightarrow \delta_R$, δ_a, δ_{SP}	R , P , ϕ, $A_Y \rightarrow \delta_a$, δ_{SP}, δ_R	C
AR142	$\delta_W \rightarrow \delta_a$, δ_{SP}; $\delta_{PED} \rightarrow \delta_R$, δ_a, δ_{SP}	R , P , ϕ, $A_Y \rightarrow \delta_a$, δ_{SP}, δ_R; $\psi \rightarrow \delta_a$, δ_{SP}	C
AR21	$\delta_W \rightarrow \delta_a$, δ_{SP}; $\delta_{PED} \rightarrow \delta_R$, δ_a, δ_{SP}	R , P , ϕ, $A_Y \rightarrow \delta_a$, δ_{SP}, δ_R; $\psi \rightarrow \delta_a$, δ_{SP}	C
SR20	$\delta_W \rightarrow \delta_a$, δ_{SP}, δ_R; $\delta_{PED} \rightarrow \delta_R$	R $\rightarrow \delta_a$, δ_{SP}; $\dot{\beta}_{SAS} \rightarrow \delta_R$	M
SR21	$\delta_W \rightarrow \delta_a$, δ_{SP}, δ_R; $\delta_{PED} \rightarrow \delta_R$	R , P $\rightarrow \delta_a$, δ_{SP}; $\dot{\beta}_{SAS} \rightarrow \delta_R$	M
CR20, FR20	$\delta_W \rightarrow \delta_a$, δ_{SP}, δ_R; $\delta_{PED} \rightarrow \delta_R$	R , P $\rightarrow \delta_a$, δ_{SP}; $\dot{\beta}_{SAS} \rightarrow \delta_R$	M, V
CR21, FR21	$\delta_W \rightarrow \delta_a$, δ_{SP}; $\delta_{PED} \rightarrow \delta_R$	R , P , ϕ, $A_Y \rightarrow \delta_a$, δ_{SP}, δ_R	M, V
AR20	$\delta_W \rightarrow \delta_a$, δ_{SP}, δ_R; $\delta_{PED} \rightarrow \delta_R$	R , P , ϕ, $\psi \rightarrow \delta_a$, δ_{SP}; $\dot{\beta}_{SAS} \rightarrow \delta_R$	V

NOTE: $\dot{\beta}_{SAS}$ IS A BLEND OF R_B, V, AND ϕ WHERE

$$\dot{\beta}_{SAS} \equiv \frac{1}{V_T} [- V_T R_B + g \phi] \sim \text{DEG./SEC.}$$

① C: Conceptual Control Law Phase; M: Mechanization Phase:
V: Validation Phase

TABLE V: PILOT RATING AND COMMENT SUMMARY - LONGITUDINAL CONTROL LAWS

CONFIGURATION NUMBER	PILOT	ATTITUDE CONTROL	FLIGHT PATH CONTROL	SPEED CONTROL	ALTITUDE CONTROL	OVERALL (HANDLING QUAL)	OVERALL (IFR TASK)	SUMMARY COMMENTS
MP01	(A)	4.0	5.0	5.0	---	6.0	---	Handling Quality o Pitch damping is low. o Flight path control is sloppy due to speed coupling.
MP02	(A)	3.0	3.5	4.5	5.0	4.5		Handling Quality o Pitch damping is low. o Response coupling between airspeed, attitude, and flight path made handling quality tasks difficult. IFR o Configuration is very objectionable because it lacks speed hold mode. Workload is high due to coupling between θ and V.
	(B)	3.0	3.0	3.0	3.0	3.0	7.0	
MP03	(A)	5.0	5.0	4.5	5.0	5.0	---	Handling Quality o Very poor configuration. o Pitch damping is low. o Coupling between θ and V is excessive.
SP01	(A)	2.5	3.5	3.5	3.5	3.5	4.0	Handling Quality o Workload increased slightly due to requirement for controlling airspeed
	(C)	3.0	2.0	2.5	3.0	2.0	3.0	
SP02 (CP21)	(A)	2.0	2.0	3.0	2.0	2.5	---	Handling Quality o Control of θ, γ, V is easy and precise. o Workload increases slightly when large pitch command rates are used. o Small amount of pitch retrim is required when changing θ. o Recovery from speed and altitude offsets is easy to perform. IFR o Glideslope tracking is precise. o Landings are consistent.
	(C)	2.0	2.0	3.0	2.5	2.5	---	
	(A)	1.5	1.5	---	2.0	1.5	2.5	
	(C)	2.0	2.0	---	2.5	2.0	2.5	
	(C)	2.0	High/Fast = 2.0 Low/Slow = 3.0			2.5	2.5	
	(A)	3.0	High/Fast = 2.0 Low/Slow			2.5	2.0	
	(B)	---	---	---	---	---	2.5	
	(B)	---	---	---	---	---	2.5 (aft cg)	
	(B)	---	---	---	---	---	2.0 (fwd cg)	
	(E)	---	High/Fast = 2.0 Low/Slow = 3.0				2.5	
	(E)	---	---	---	---	---	3.0 (aft cg)	
	(F)	---	---	---	---	---	3.0	
	(F)	---	---	---	---	---	3.0 (aft cg)	
	G						3.0	

NOTE: (1) All Flight Control Systems Were Tested at a Mid cg (.325 $\bar{c}$) Unless Noted Otherwise.

(2) cg_{AFT} at .40 $\bar{c}_w$

(3) cg_{FWD} at .25 $\bar{c}_w$

TABLE V: PILOT RATING AND COMMENT SUMMARY - LONGITUDINAL CONTROL LAWS (continued)

CONFIGURATION NUMBER	PILOT	ATTITUDE CONTROL	FLIGHT PATH CONTROL	SPEED CONTROL	ALTITUDE CONTROL	OVERALL (HANDLING QUAL)	OVERALL (IFR TASK)	SUMMARY COMMENTS
SP03	(A)	1.5	1.5	1.5	1.5	1.5	3.5	Handling Quality o θ and γ responses are similar to those for 727 and 737. IFR o Speed control is difficult. o Had tendency to overshoot flare.
	(B)	3.5	2.0	4.0	3.0	3.0		
	(C)	2.0	1.5	2.5	2.0	2.0	3.0	
SP04	(C)	2.0	2.0	3.0	3.0	2.5	3.0	Handling Quality o Longitudinal control is precise. o Damping is good, even when high command rates are used. o θ/δ_{col} is slightly low. IFR o Could maintain tight control of airspeed. o Workload increased due to coupling between longitudinal and lateral-directional axes.
	(A)	1.5	1.5	1.75	1.5	1.5	3.5	
SP05	(A)	1.5	1.5	2.0	1.5	1.5	3.0	Handling Quality o Longitudinal control is precise. o Speed control sensitivity is high. IFR o Flare characteristics seemed a bit sluggish. o Workload is low. o Glideslope tracking accuracy is very good.
	(C)	2.0	2.0	2.0	2.0	2.0	2.5	
DP02	(A)	3.5	4.0	4.0	2.0	4.0	---	Handling Quality o Pitch damping is low. o Speed stability is good.
DP03	(A)	4.0	4.5	5.0	3.0	4.0	---	Handling Quality o Pitch damping is low o Tendency to overcontrol speed and glideslope while making changes in airspeed. o It is difficult to stay on the glideslope while changing airspeed due to large θ/V coupling.

TABLE .. PILOT RATING AND COMMENT SUMMARY - LONGITUDINAL CONTROL LAWS (continued)

CONFIGURATION NUMBER	PILOT	ATTITUDE CONTROL	FLIGHT PATH CONTROL	SPEED CONTROL	ALTITUDE CONTROL	OVERALL (HANDLING QUAL)	OVERALL (IFR TASK)	SUMMARY COMMENTS
DPO5-A	(A) (C) (C)	1.75 3.5 2.0	1.5 3.0 2.0	1.5 4.5 ---	1.5 3.0 2.0	1.5 4.0 ---	--- --- 3.0	Handling Quality o Longitudinal control power and damping are good. IFR o Flight path control is not precise.
DPO5-B $\gamma_{\ell} = \frac{h}{V_T}$	(C)	---	---	---	---	---	4.0	IFR o Moderate pilot compensation required to stay on glideslope.
DPO7	(C)	3.0	3.0	---	2.5	---	3.0	Handling Quality o Longitudinal damping is low. o This system does not hold desired attitude. IFR o For the IFR task, DPO7 and DPO5 are similar.
APO1	(A)	4.0	4.0	3.0	3.5	3.5	---	Handling Quality o Pitch damping is low. o Airspeed control is good.
APO2	(A)	2.5	2.5	2.0	2.0	2.5	---	Handling Quality o Pitch damping is good. o Configuration could be improved by increasing $\dot{\theta}$, $\dot{\gamma}$ to δ_{col} sensitivity. o Airspeed control is good.
APO3	(A) (B)	3.0 3.0	3.5 3.5	3.0 2.0	3.5 2.0	3.0 3.0	---	o System is not satisfactory for making small attitude changes. o Stick forces are too high.
APO5	(A) (B)	1.5 2.0	1.5 2.5	1.5 3.0	1.5 2.0	1.5 2.5	--- ---	o Glideslope hold is weak. o Airplane is too stable; pilot would like to change θ more rapidly with less column.
APO7	(F)	---	---	---	---	---	2.0 (aft cg)	o Pilot's workload is low, even in turbulence. o The control system reduces the initial transient following an engine failure. o This control system increased the pilot's confidence to fly precision approaches.

TABLE VI: PILOT RATING AND COMMENT SUMMARY - LATERAL-DIRECTIONAL CONTROL LAWS

CONFIGURATION NUMBER	PILOT	LG. HEADING CONTROL	SM. HEADING CONTROL	DECRAB	"S" TURN	OVERALL (HANDLING QUAL)	OVERALL (IFR TASK)	SUMMARY COMMENTS
MR0821	(A) (B)	7.0	8.0	6.0	8.0	8.0	--- 9.0	Handling Quality o System is very poor. o Turn coordination is bad - can't coordinate turns with rudder. o Precision control isn't possible. IFR o Lateral-directional control is quite unsatisfactory. Heading response is lightly damped. Large heading reversal is objectionable.
SR0721	(A)	6.5	7.0	5.0	6.0	7.0	---	Handling Quality o Precision control is difficult due to excessive sideslip.
SR10	(A)	5.0	5.0	3.0	10.0	6.0	---	Handling Quality o Roll and yaw damping is low. o Turn coordination is poor.
SR11	(A) (C)	4.5 7.0	6.0 7.0	3.0 5.0	6.0 6.0	6.0 7.0	---	Handling Quality o Precise heading control requires considerable pilot compensation. o Lateral damping is low. o Turn coordination is poor.
SR20	(D) (A) (C)	4.0 5.0 ---	4.0 5.0 ---	4.5 3.0 ---	7.0 6.0 ---	7.0 5.5 ---	--- 5.0 4.0	Handling Quality o Lack of turn coordination showed up during rapid roll maneuvers. o Roll damping is low. o Slow and deliberate maneuvers are possible. IFR o The lateral-directional axes require moderate pilot compensation since the damping is low. o Excessive sideslip excursions were noticed.
SR21	(A) (D)	3.0 5.0	2.5 3.0	2.0 4.0	2.5 6.0	2.5 6.0	2.5 5.5	Handling Quality o Roll damping is high and the configuration exhibits a roll hold characteristic (neutral spiral stability). o It is difficult to exactly roll out onto commanded heading due to slight sideslip activity. o System is well damped directionally. o Only wheel inputs are required for the "S" turn.

TABLE VI: PILOT RATING AND COMMENT SUMMARY - LATERAL-DIRECTIONAL CONTROL LAWS (continued)

CONFIGURATION NUMBER	PILOT	LG. HEADING CONTROL	SM. HEADING CONTROL	DECRAB	"S" TURN	OVERALL (HANDLING QUAL)	OVERALL (IFR TASK)	SUMMARY COMMENTS
SR21 (Continued)								IFR o IFR task is fairly easy to handle for this configuration. The workload is low. NOTE: Pilot "D" had trouble "flying" this configuration because he lacked STOL simulation experience. For example, he used CTOL bank angles for the "S" turn and for making large heading changes.
DR141	(A)	3.5	6.0	2.0	2.5	2.5	---	Handling Quality o Turn coordination is good. o Roll damping is low.
DR142	(A)	2.0	1.5	2.0	1.5	2.0	---	Handling Quality o Roll damping and turn coordination are good. This configuration is easy to fly.
CR20	(A)	3.5	2.0	1.5	5.0	3.5	2.5	Handling Quality o Roll control is precise. o Turn coordination into the turn is good; small amount of bottom rudder is required to hold steading turn. o Small heading changes can be made with either the rudder or the aileron. o Rudder power is adequate for decrab maneuver. o Roll control power is adequate for demanding "S" turn task; however, the heading response is slightly sluggish. IFR o Localizer tracking and lateral alignment with the runway didn't present any problems.
(FR20)	(D)	2.0	3.0	3.0	3.0	2.5	6.0	
	(C)	3.0	2.5	3.0*	3.0	3.0	2.5	
	(A)	3.0	2.0	2.0	2.5	2.5	2.0	
	(E)	---	---	3.0	3.0	---	2.5	
	(F)	4.5	2.5	2.0	3.0	3.2	3.0	
	(B)	5.0	2.0	2.75	4.0	3.0	2.5	

*Pilot could only command 80% maximum directional control due to simulation error.

TABLE VI: PILOT RATING AND COMMENT SUMMARY - LATERAL-DIRECTIONAL CONTROL LAWS (continued)

CONFIGURATION NUMBER	PILOT	LG. HEADING CONTROL	SM. HEADING CONTROL	DECRAB	"S" TURN	OVERALL (HANDLING QUAL)	OVERALL (IFR TASK)	SUMMARY COMMENTS
CR21	(A)	2.0	1.5	1.5	2.5	2.0	2.5	Handling Quality
(FR21)	(D)	2.5	2.5	4.0	4.5	5.0	7.0	o Lateral control is precise due to good turn coordination.
	(C)	3.0	2.0(Aileron) 6.0(Rudder)	3.0*	2.5	3.0		o Small heading changes cannot be made with the rudder since the resulting sideslip produced heading oscillations.
	(A)	2.0	1.5(Aileron) 3.0(Rudder)	3.0	3.5	3.0	3.0	o "S" turn required less than 100% lateral control.
	(B)	---	---	---	---	---	6.0	IFR
	(F)	2.5	2 2.5	2.0	2.5	2.5	3.0	o Only small wheel corrections are required for tracking the localizer.
	(B)	4.0	2.0	2.5	3.0	3.0		o Turbulence seems to excite more sideslip with this configuration; thus, the localizer tracking workload is higher. Lateral accelerations at the pilot's station are noticeable for this configuration.
	(G)						3.0	o The Dutch roll $l\phi/\beta l$ ratio is abnormal; i.e., mostly sideslip with very little bank angle.
AR142	(A)	2.5	2.5	---	2.5	2.5	---	Handling Quality
								o Roll damping is good, but turn coordination requires improvement.
AR20	(F)	---	---	---	---	---	2.0	IFR
								o This control system is good for engine failures since it reduces the magnitude of the initial transient. This control system increased the pilot's confidence to fly precision approaches.
AR21	(C)	4.5	2.0	5.0	3.0	4.5	---	Handling Quality
								o Slight heading overshoot induced by sideslip.
								o Damping characteristics are excellent.
								o Rudder power is low for decrab maneuver.

*Pilot could only command 80% maximum directional control due to simulation error.

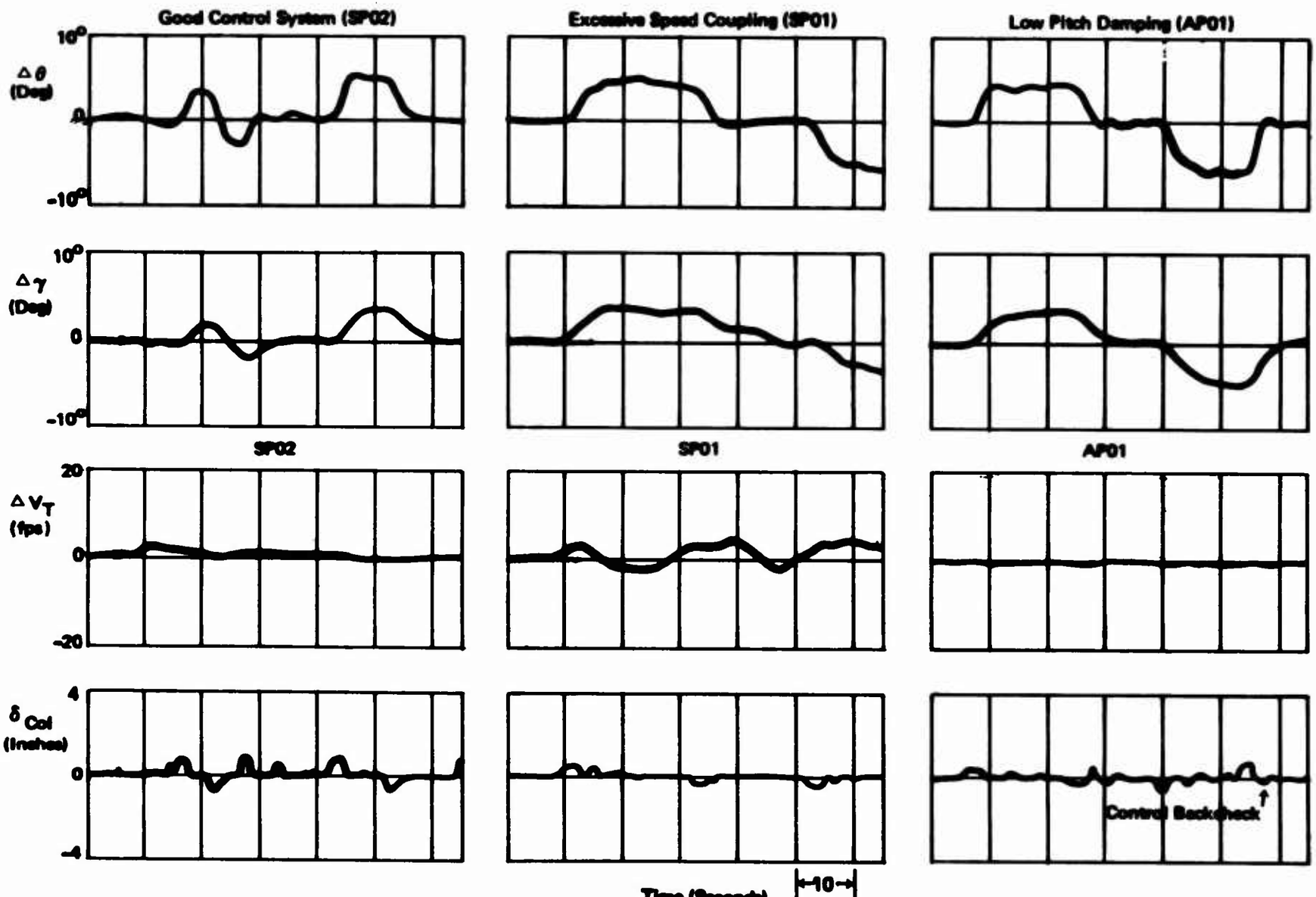

Figure 10: Examples of Pitch Attitude Control

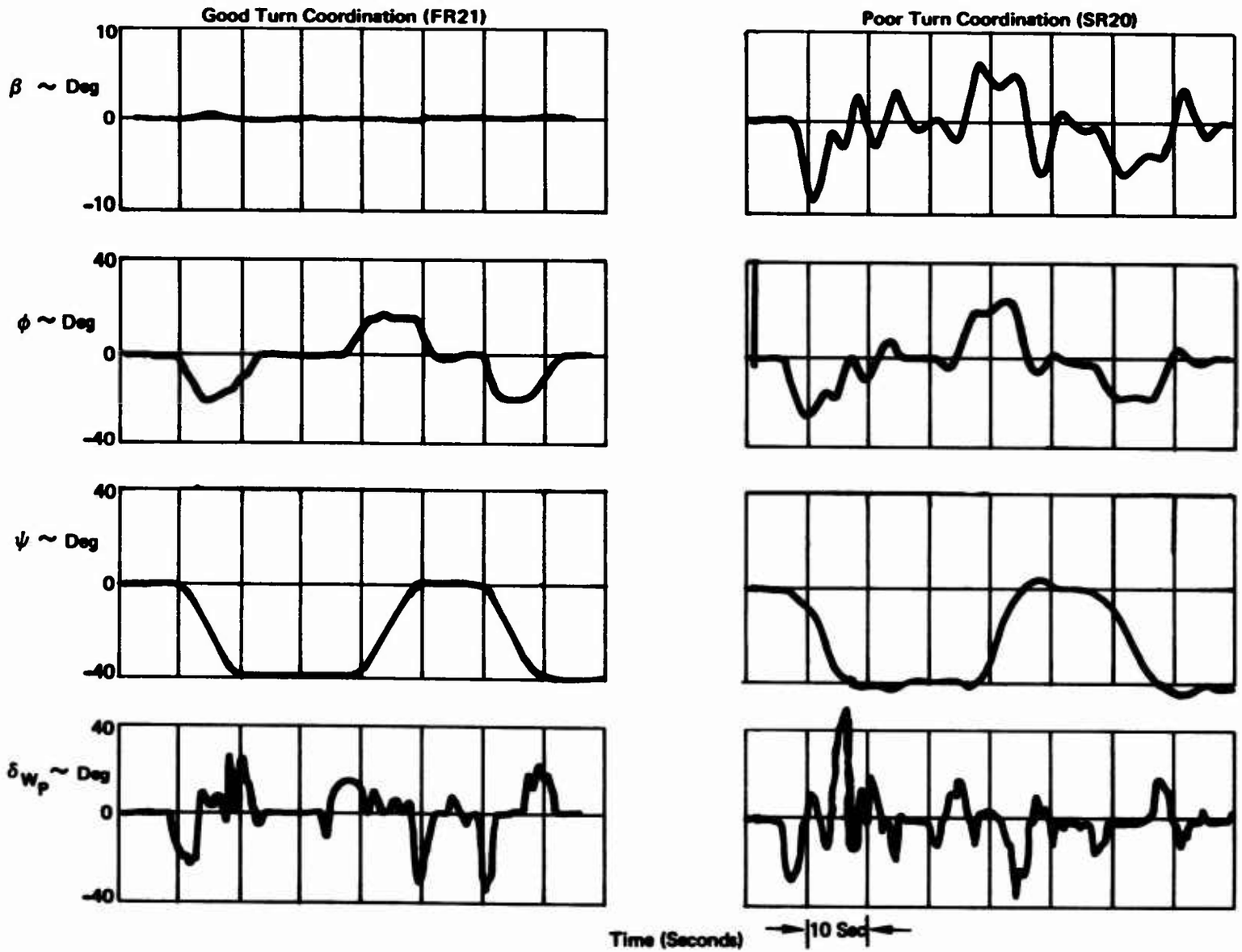

Figure 11 : Examples of Coordinated–Uncoordinated Turn Entries

Table VII: Transient Acceleration and Change in Control Authority Due to Control Sytem and Powerplant Failures

CONTROL SYSTEM	FAILURE TYPE	TRANSIENT ACCELERATION (% maximum control acc. for control system failures) [1]	POST FAILURE CONTROL PROPERTIES	
			Command Control Auth. (% max. control acc.) [1]	Augmentation Auth. (% of normal gain) [1]
Mechanical: MP02 MR0821	1. Engine-Out o Thrust set @ 75% max. o #4 engine o cg @ .325$\bar{c}$	$\dot{P}$ = .26 rad/sec^2 $\dot{Q}$ = .005 rad/sec^2 R = .05 rad/sec^2 A_x = -.58 fps^2 A_z = 3.04 fps^2		Not Applicable
	2. Locked Nozzle	None	75%	
	3. Control Sys (Mech) Elevator Aileron Spoiler Rudder	 32% 10% 11% 43%	 85% 90% 89% 78%	
Control/Stability Augmentation: SP03 CP21 SR21 CR20 CR21	1. Engine-Out	Same as Mechanical Sys.		
	2. Locked Nozzle	None	75%	75%
	3. Control Sys. (Mech Path) Elevator Aileron Rudder	 32% (62%) 10% (10%) 43% (63%)	 80% (63%) 100% (100%) 78%	 100% (100%) 100% (100%) 100% (100%)
	4. Control Sys. (Elec. Path) Elevator Aileron Spoiler Rudder	 7% (11%) 7% (10%) 23% (35%) 0%	 90% (88%) 100% (100%) 77% (65%) 100% (100%)	 67% (50%) 67% (50%) 100% (100%) 67% (50%)

Table VII: (Continued)

CONTROL SYSTEM	FAILURE TYPE	TRANSIENT ACCELERATION (% maximum control acc. for control system failures)	POST FAILURE CONTROL PROPERTIES Command Control Auth. (% maximum control acc)	Augmentation Auth. (% of normal gain)
Fly-By-Wire	1. Engine-Out	Same as Mechanical Sys.		
	2. Locked Nozzle	Same as CAS		
SP02A SP04 SP05 FR20 FR21	3. Control Sys. (Elect. Path) Elevator Aileron Spoiler Rudder	 39% 7% 23% 43%	 78% 93% 73% 78%	 67% 67% 100% 67%

[1] Control System CP21/CR20 was evaluated with both dual and triple (normal case) redundancy. Numbers in parenthesis are for the dual redundancy mechanization.

Control system and powerplant failures are analyzed subjectively in this report. Pilot ratings and comments from control system and powerplant failures are presented by Table VIII. The IFR approach/VFR landing task was used for these evaluations. Pilot rating and comments are given for both "normal" and "failure" state evaluations. Failure state pilot ratings represent a composite appraisal of all failures evaluated. Note that the normal state data presented in Table VIII are different from those presented by Tables V and VI. These normal state evaluations were made along with the failure evaluations so that the pilots could make a relative appraisal of failure effects.

The data presented by Table VIII are summarized briefly below. This summary comprises three topics: benefits due to control augmentation, control system failures, and engine failures.

Three augmentation properties simplified the pilot's failure recovery task: rate feedback, airspeed hold, and turn coordination. Rate feedback signals were beneficial for two reasons:

(1) They commanded control surface deflections which opposed the failure transient.

(2) They quickened the longitudinal and lateral responses. Thus the pilots had tighter control of the airplane.

Airspeed hold and turn coordination augmentation were beneficial since they greatly reduced the pilot's workload. With airspeed hold, pilots could make glideslope corrections without worrying about buildup of airspeed error. Turn coordination made precision heading control possible.

Figure 12 presents time-history traces of tracking performance, the airplane's state, pilot workload, and control surface activity for three IFR performance evaluations with a control system (CP21/CR20) which had pitch rate, roll rate, airspeed hold, and turn coordination augmentation. One approach was normal while the other two contained engine failures. The responses show the rudder, spoiler, and elevator control surface deflections which immediately follow the engine failure. Spoiler and elevator deflections were due to control system commands, since the pilot's column and wheel activity does not build-up until approximately five seconds after the failure occurs. Comparison of airspeed, vertical speed, and ground track responses illustrates the control benefits resulting from a control system which provides airspeed hold, turn coordination, and longitudinal and lateral damping.

Control system failures were not a problem for the pilots. Many times the pilots could not distinguish control system failure disturbances from those due to mild turbulence. Control system failures did not present a problem for the two reasons:

(1) Redundant signal paths and multiple control surfaces were utilized. Therefore accelerations resulting from a failure were minimized, and some control and/or augmentation was always kept.

(2) More importantly, the failure state did not change the pilot's mode of control. The pilots were not required to learn a separate flying technique for post failure flying.

Engine failures were more severe than control failures. Nevertheless, the pilots easily retained control of the airplane following an engine failure and usually completed the landing. Pilots detected an engine failure through the effect of the resulting lateral-directional imbalance on heading. The recovery from the engine failure therefore involved getting the airplane back onto the localizer. Corrections for glideslope deviation were usually small since the engine failure only changed load factor by $\Delta n_z = .1g$. If the pilot did not land, sufficient energy and control were available to complete a go-around successfully.

TABLE VIII: PILOT RATING AND COMMENT SUMMARY :

EVALUATION OF CONTROL SYSTEM AND POWERPLANT FAILURES

Note: Numbers in parenthesis following control system number indicate level of electrical redundancy.

CONTROL SYSTEM Long	Lat/Dir.	PILOT	NORMAL STATE (overall/long/ lat-dir)	FAILURE EVALUATION (overall/long/ lat-dir)	SUMMARY COMMENTS
MP02	SR21 (3)	A	5./5./3.5	5.5/-/-	Normal State o Longitudinal control characteristics are sluggish. o Workload was high because system doesn't have speed hold. Failures o Glideslope recovery following a failure was more difficult due to sluggish longitudinal response. o Elevator hardovers were always noticed. o Engine-out failure was hard to sort out, and the aircraft was minimally control-lable during and after the failures.
		C	4.75/-/-	6./-/-	
CP21 (3)	MR0821	A	7.0/3.5/7.0	7.0/-/-	Normal State o Lateral-directional flying qualities are very poor. o IFR flying is very difficult; VFR is easier. Failures o Difficult to separate failures from basic flying qualities. o Control system's performance is not adequate.
		C	6.0/3.0/6.0	7.5/-/-	

TABLE VIII: PILOT RATING AND COMMENT SUMMARY:

EVALUATION OF CONTROL SYSTEM AND POWERPLANT FAILURES (Continued)

Note: Numbers in parenthesis following control system number indicate level of electrical redundancy.

CONTROL SYSTEM Long	CONTROL SYSTEM Lat/Dir.	PILOT	NORMAL STATE (overall/long/ lat-dir)	FAILURE EVALUATION (overall/long/ lat-dir)	SUMMARY COMMENTS
SPO3 (3)	SR21 (3)	A B C	3.5/2.5/4.0 4.5/5.0/3.5 3.0/3.0/2.5	3.75/-/- 6/-/- 4.5/-/-	Normal State o Airspeed hold is not very tight. o Pitch damping is slightly low. o Directional control for decrab maneuver is good. o Configuration lacks turn coordination. Failure o The lack of airspeed hold degrades the system's failure characteristics. o Control system failures required only moderate pilot compensation. o Engine-out situations required extensive pilot compensation.
CP21 (3)	CR20 (3)	A B	2.5/2.0/3.0 ---	3.0/-/- 2.5/2.5/2.5	Normal State o Reasonable tracking and touchdown performance were attainable with this configuration. Failures o Failures were never severe enough to require a go-around. Failure performance was generally the same as baseline performance. The engine-out was easily recognizable.

TABLE VIII: PILOT RATING AND COMMENT SUMMARY:

EVALUATION OF CONTROL SYSTEM AND POWERPLANT FAILURES (Continued)

Note: Numbers in parenthesis following control system number indicate level of electrical redundancy.

CONTROL SYSTEM		PILOT	NORMAL STATE (overall/long/ lat-dir)	FAILURE EVALUATION (overall/long/ lat-dir)	SUMMARY COMMENTS
Long	Lat/Dir.				
CP21 (3)	CR21 (3)	A B	2.5/3./2.5 ---	2.5/-/- 3.5/3/3	Normal State o Lateral-directional configuration is very good; the workload is low. o Longitudinal system is satisfactory. Failures o Effects due to failures were minimal.
CP21 (2)	CR21 (2)	B	3/2.5/4.0	5/3/5	Normal State o The turn rate to bank angle ratio was high -- too sensitive. Failures o Lateral-directional oscillations due to failures were difficult to stabilize with the rudder.
SPO2A(3)	FR21 (3)	B G	3/3/3 ---	-/3/- 6/3.5/3.5	Normal State o Roll damping and response are good. o Pitch damping and response are good. o Speed response is rapid with little pitch attitude disturbance. Failures o Only noticeable failure was the engine-out (pilot G). o System was pretty good and was acceptable. o Elevator hardover caused small degradation in longitudinal control (pilot B).

TABLE VIII: PILOT RATING AND COMMENT SUMMARY:

EVALUATION OF CONTROL SYSTEM AND POWERPLANT FAILURES (Continued)

Note: Numbers in parenthesis following control system number indicate level of electrical redundancy.

CONTROL SYSTEM		PILOT	NORMAL STATE (overall/long/ lat-dir)	FAILURE EVALUATION (overall/long/ lat-dir)	SUMMARY COMMENTS
Long	Lat/Dir.				
SPO2A(3)	FR20 (3)	B	---	-/-/3.5	Failures o Lateral and directional control power are more than adequate for any failure situation evaluated. o Available thrust was more than adequate to perform an engine-out go-around.
		G	---	---	
SPO5(3)	FR21 (3)	B	---	-/4/-	Failures o Longitudinal response is more sluggish than that for SPO2A. o Dihedral effect is very low. A pilot used to using conventional engine-out recovery technique would probably crash during the first engine-out flight, unless he had proper engine-out preflight training (pilot G). o The EADI θ scaling is wrong for a STOL; it was bothersome because large θ changes affected the ability to track glideslope (pilot G).
		G	---	-/7/-	

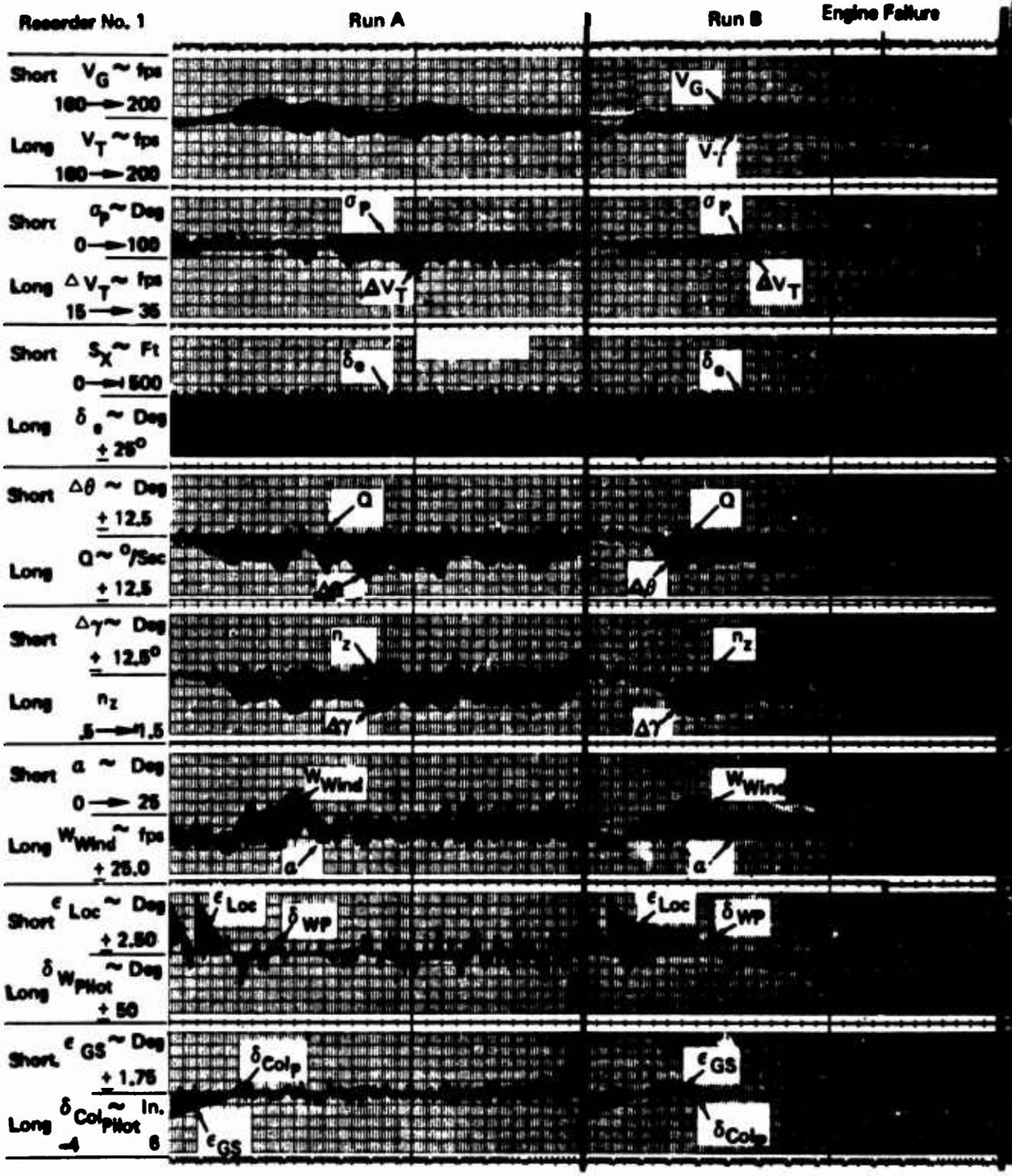

Note:

1. Scales Read from Bottom to Top; e.g.
   ΔV_T: 15 → 35
   σ_p: 0 → 100
2. Time Interval – 1 Sec.
3. Control System – CP21/CR 20
4. FSAA Simulation Data

A

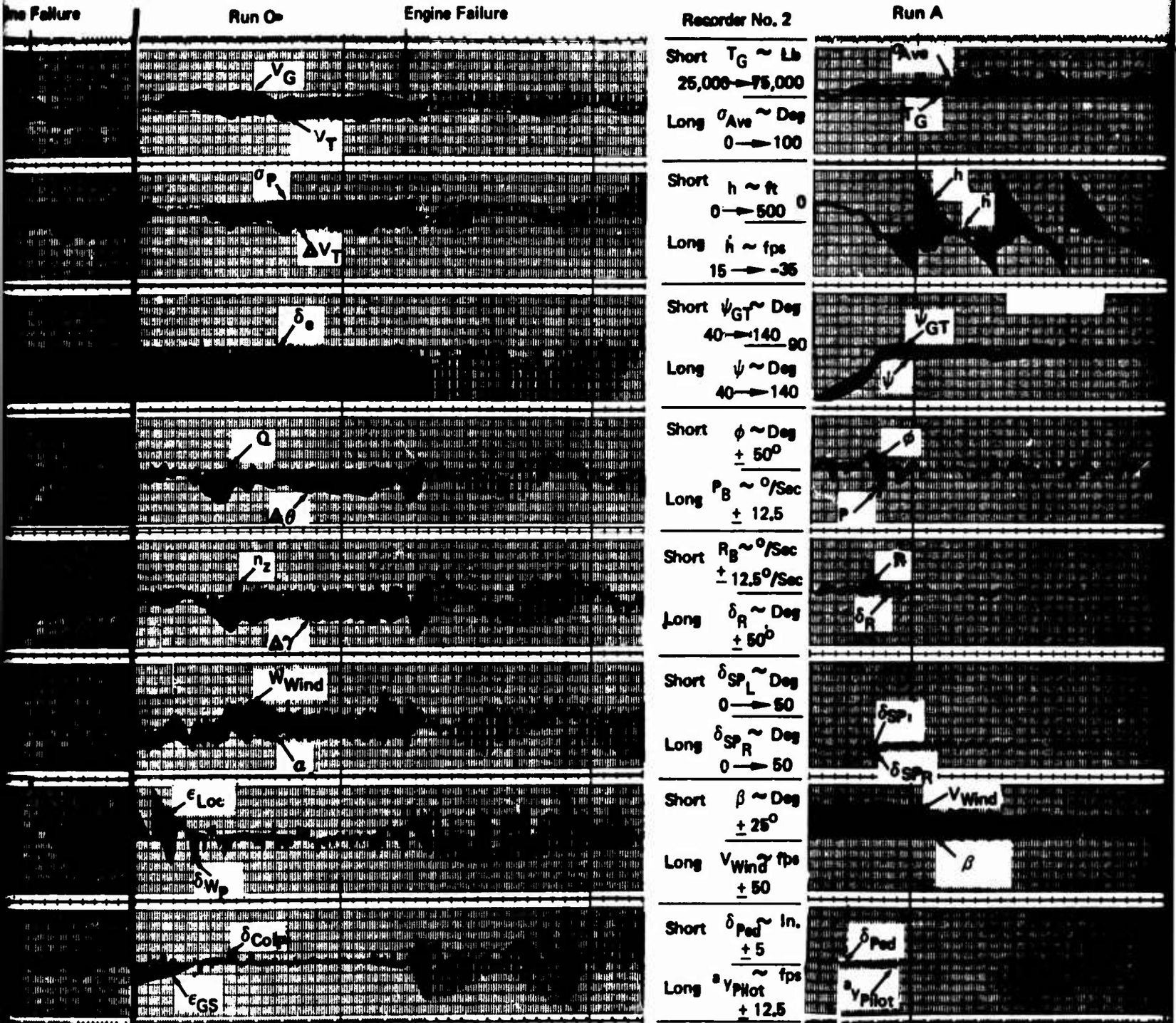
ine Failure
Run O
Engine Failure
Recorder No. 2
Run A
Short T_G ~ Lb
25,000 → 75,000
Long σ_{Ave} ~ Deg
0 → 100
Short h ~ ft
0 → 500
Long $\dot{h}$ ~ fps
15 → -35
Short ψ_{GT} ~ Deg
40 → 140
Long ψ ~ Deg
40 → 140
Short ϕ ~ Deg
± 50°
Long P_B ~ °/Sec
± 12.5
Short R_B ~ °/Sec
± 12.5°/Sec
Long δ_R ~ Deg
± 50°
Short δ_{SP_L} ~ Deg
0 → 50
Long δ_{SP_R} ~ Deg
0 → 50
Short β ~ Deg
± 25°
Long V_{Wind} ~ fps
± 50
Short δ_{Ped} ~ In.
± 5
Long $a_{V_{Pilot}}$ ~ fps
± 12.5
V_G
V_T
σ_P
ΔV_T
δ_e
Q
$\Delta\theta$
n_z
$\Delta\gamma$
W_{Wind}
α
ϵ_{Loc}
δ_{W_P}
δ_{Col}
ϵ_{GS}
σ_{Ave}
T_G
h
$\dot{h}$
ψ_{GT}
ψ
ϕ
P
R
δ_R
δ_{SP_L}
δ_{SP_R}
V_{Wind}
β
δ_{Ped}
$a_{V_{Pilot}}$

B

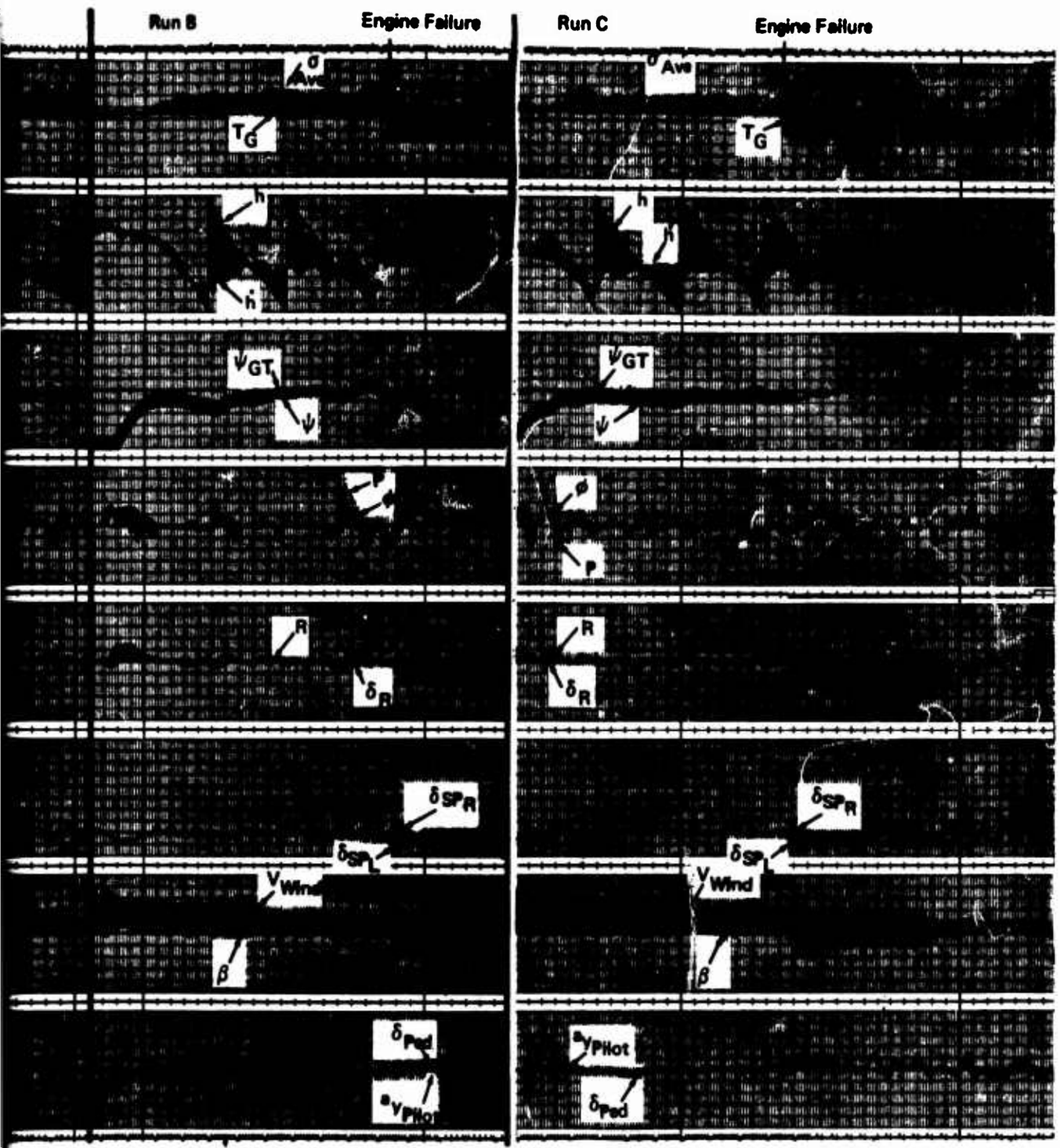

Figure 12: IFR Approach / VFR Landing Task — With and Without Engine Failure

3.2.3 Control Law Comparison: Quantitative Performance Data

Quantitative control system performance data were computed and printed (see Figure 4) for each IFR approach. Both simulations had data analysis routines which calculated root mean square (rms) values and stored the airplane's touchdown state. From these printouts, quantitative measurements of pilot workload, control surface activity, tracking accuracy, and landing touchdown data were obtained.

These data were taken to provide an objective measurement of control system performance in addition to pilot ratings and comments, which are subjective. The relationship between the quantitative perforance data and pilot ratings is discussed in Section 3.2.4.

The STAI simulation test matrix included evaluations of many control laws and control mechanization concepts. Because of the test matrix size, the number of evaluation "flights" per control law or control mechanization was small. Additionally, not all control systems were evaluated by all pilots. Thus, care must be taken in comparing the performance data since they are from small samples. Furthermore, apparent differences between control systems could possibly be attributed to piloting technique.

A statistical analysis approach was taken to determine if differences between small sample means and standard deviations are statistically significant. This analysis logic is depicted by the flow chart presented by Figure 13. The various tests shown by this figure are described by Reference 1. When the sample standard deviation (square root of the sample variance) provided the best measure of the parameter behind investigated, the "F" test was used to check for significant differences between the two deviations. (An example of this type of comparison is the use of touchdown dispersion standard deviation as a measure of repeatability in landing performance.) In cases where the mean was a better indicator of performance (e.g., glide-slope tracking), the "F" and "Student t" tests or the "F" AND "θ" test were used to check for significant differences between means. The "Student t" test was used when the variances from both groups were from the same population. The "θ" test was employed when the variances were not from the same population. The confidence level was set at 5% for each of these tests. Each uses the "null hypothesis."

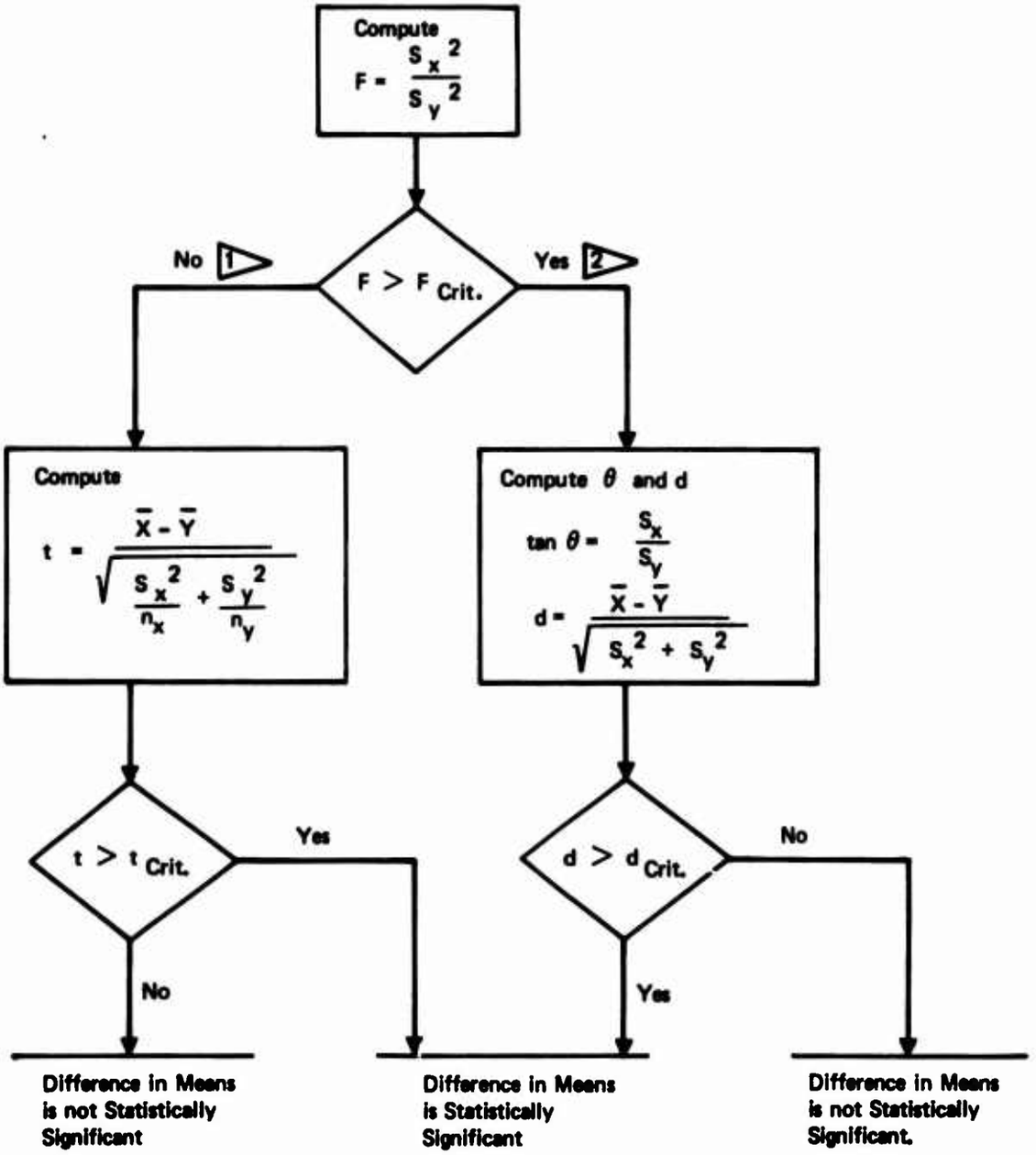

Notes:

$\bar{X}$ and $\bar{Y}$ are Sample Means of Samples X and Y Respectively

S_x^2 and S_y^2 are Sample Variances of Samples X and Y Respectively

$F_{Crit.}$, $t_{Crit.}$, and $d_{Crit.}$ are Obtained from Tables and are Dependent upon $n_x - 1$ and $n_y - 1$

1 Variances are from Same Population

2 Variances are from Different Populations.

Figure 13: Comparison of Sample Means

Longitudinal performance data for a spectrum of longitudinal control laws is presented by Figure 14. Figure 15 shows performance data for a group of pilots flying the same control system. The pilot technique comparison is included since these data aid the interpretation of control system effects. The statistical analysis procedure described above was used to compare five data sets. The results of this evaluation are presented by Table IX. Significant differences between longitudinal control system characteristics are summarized briefly below:

- SP03 vs MP02

  1. Glideslope tracking was more consistent with SP03.

  2. Speed errors were reduced with SP03.

  3. Column activity was different for both systems. This reflected differences in piloting techniques, rather than a control system effect.

- SP02 vs SP03

  1. Glideslope tracking was more consistent with SP03. Because both control systems were from different populations, the difference between glideslope error means was not significant.

  2. Suppression of speed errors was more consistent with SP02.

  3. Pilots had better control of the touchdown point with SP02.

- DP05 vs SP02

  1. The flight path system (DP05) was superior in minimizing glideslope tracking error and for maintaining speed with less controller activity.

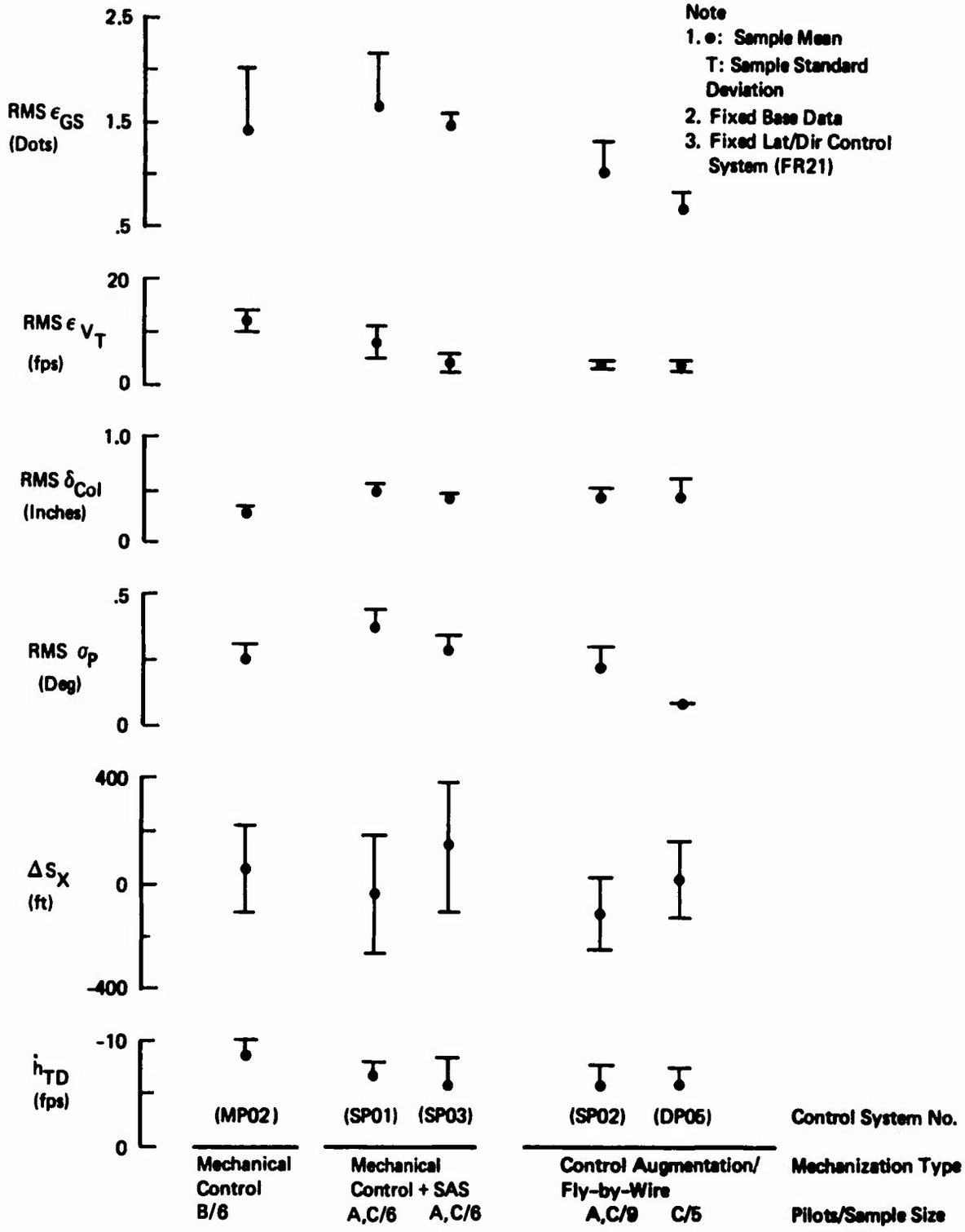

Figure 14: Longitudinal Performance Summary : Effect of Control Law

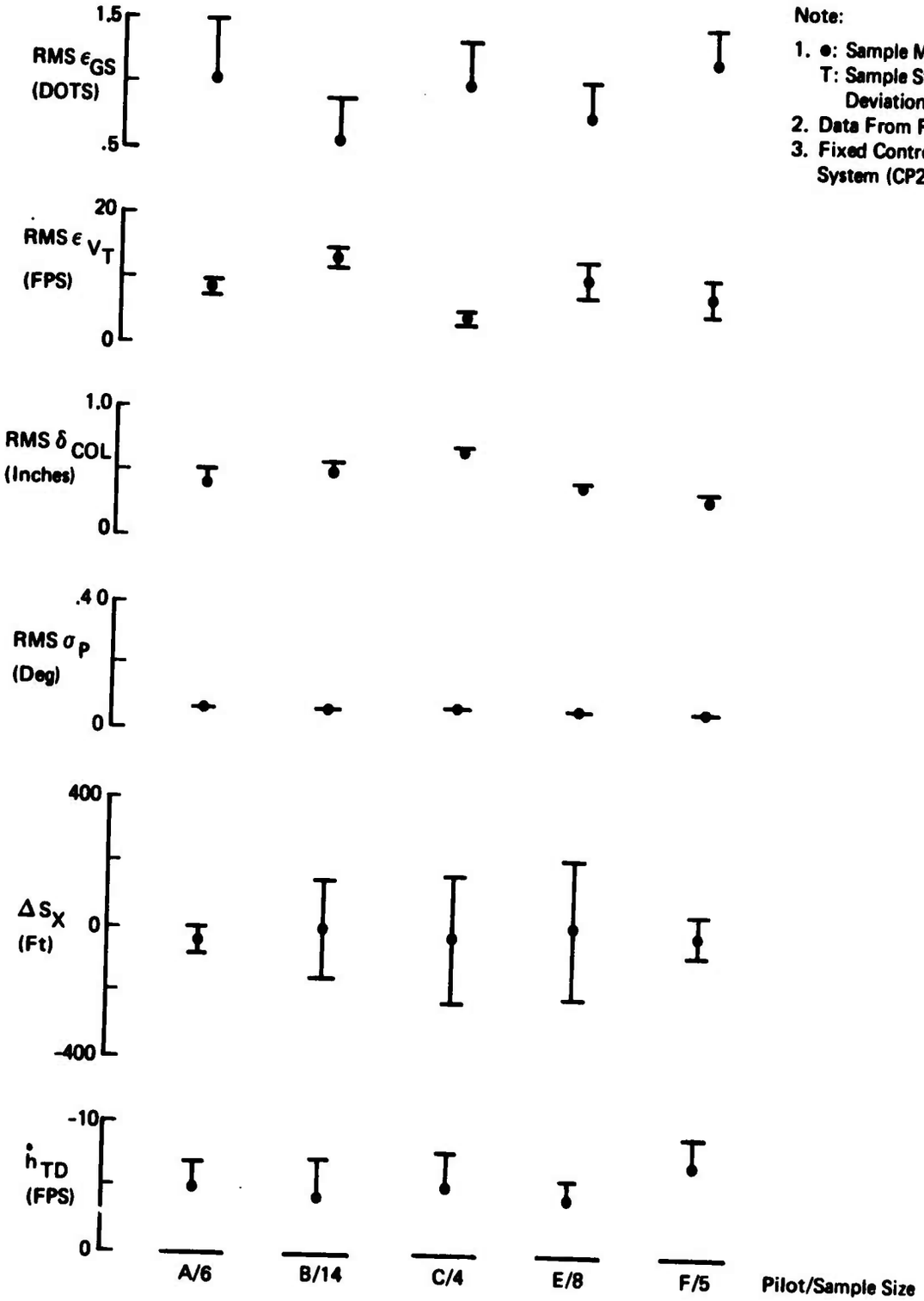

Figure 15: Variation in Longitudinal Performance Data Due to Pilot Technique

TABLE IX

COMPARISON OF LONGITUDINAL PERFORMANCE DATA

CONTROL SYSTEMS	PILOTS	PARAMETER					
		ϵ_{GS}	ϵ_{VT}	$\delta_{Col.}$	$\delta\sigma_{p}$	ΔS_{x}	h_{TD}
		1 2	1 2	1 2	1 2	1 2	1 2
MPO2 vs SPO3	B A,C	S N	N S	N S	N N	N N	N N
SPO3 vs SPO2	A,C A,C	S N	S N	N N	N N	N S	N N
SPO2 vs DPO5	A,C C	N S	N N	N N	S N	N N	N N
CP21	A vs B	N S	N S	N S	N N	S N	N N
CP21	A vs C	N N	N S	N S	N N	S N	N N

1 This column reflects the existence of significant (S) or nonsignificant (N) variation in the variance of the two compared systems or pilots. Variance is a measure of the parameter consistency.

2 This column reflects the existence of significant (S) or nonsignificant (N) variation in the sample means. The mean is a measure of a parameter's average value.

Lateral-directional performance data for a spectrum of control laws is given in Figure 16. Figure 17 shows the performance of a group of pilots for the same control law. The statistical analysis procedure described above was used to compare five data sets. The results of this evaluation are presented by Table X. Significant differences between lateral-directional control system characteristics were:

- SR20 vs MR0821
  1. Localizer tracking is more consistent with SR20. This improvement in tracking performance is even more significant when the comparative pilot data are considered. These data indicate that pilot B could track better than either pilots A or G.
  2. The pilot's workload (i.e., rms $\overline{\delta}_W$ and $\overline{\delta}_{PED}$) is greatly reduced by SR20.
- SR21 vs SR20
  1. Tracking performance is more consistent with SR20.
  2. Wheel activity is lower with SR21.
  3. Pedal activity is more consistent with SR20.
  4. Pilots have better control of the lateral touchdown point with SR21.
- CR21 vs CR20
  1. These control systems are statistically similar in all respects.

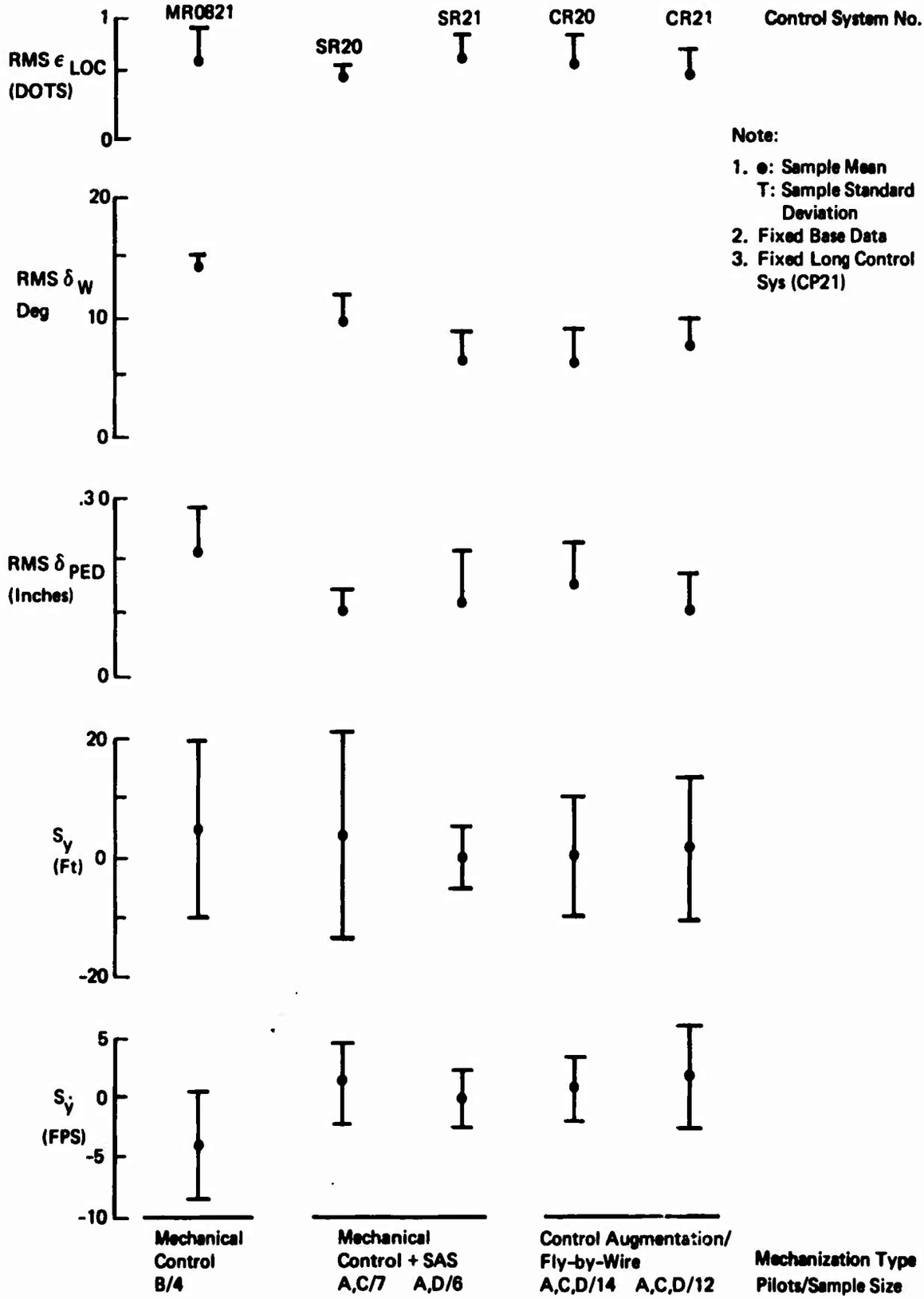

Figure 16: Lateral-Directional Performance Summary: Effect of Control Law

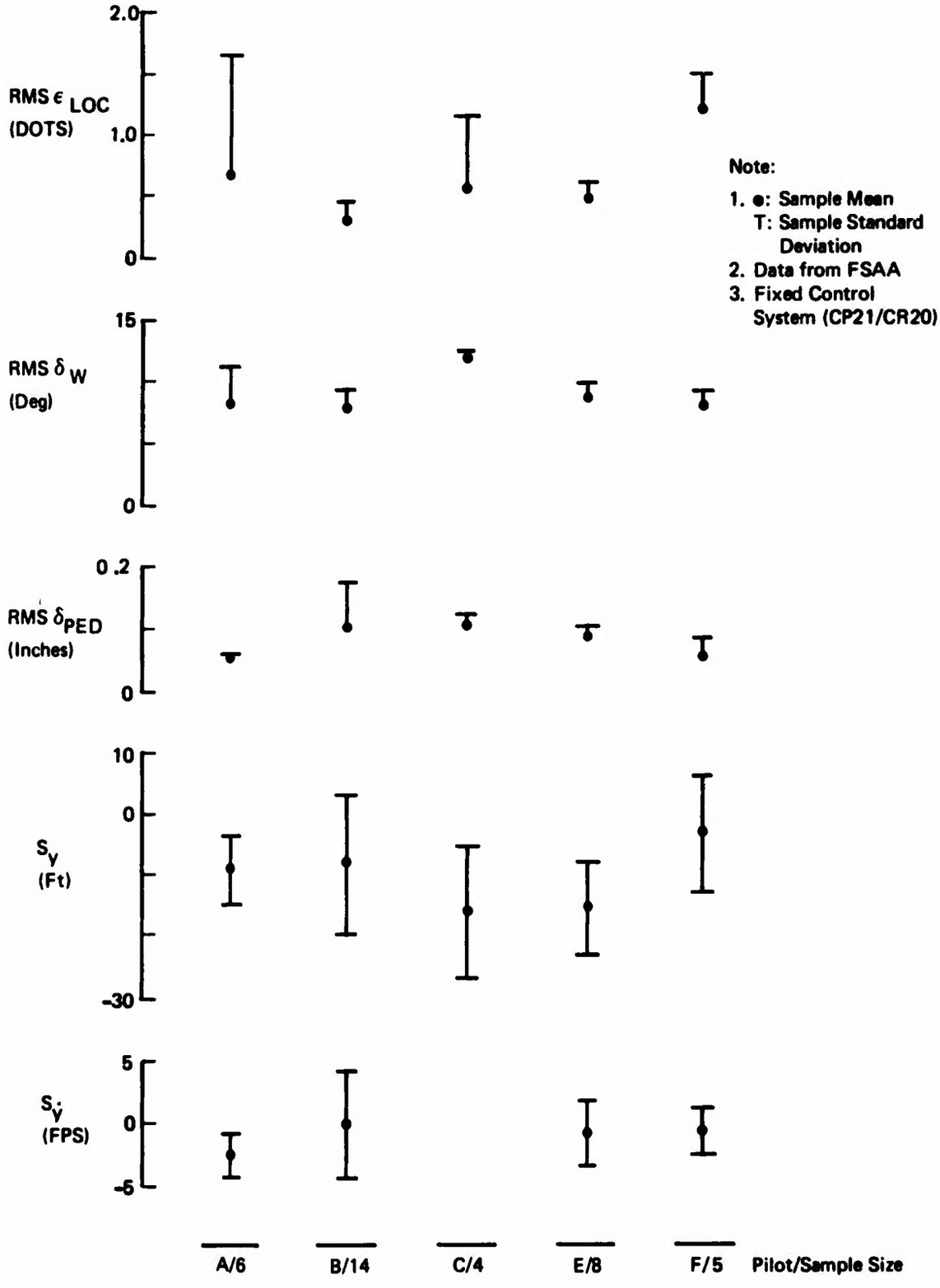

Figure 17 : Variation in Lateral-Directional Performance Data Due to Pilot Technique

TABLE X

COMPARISON OF LATERAL/DIRECTIONAL PERFORMANCE DATA

CONTROL SYSTEM	PILOTS	PARAMETER				
		ϵ_{LOC} ①②	δ_W ①②	δ_{PED} ①②	S_y ①②	$\dot{S}_y$ ①②
MRO821 vs SR20	B vs A,C	S N	N S	N S	N N	N N
SR20 vs SR21	A,C vs A,D	S N	N S	S N	S N	N N
SR21 vs CR20	A,D vs A,C,D	N N	N N	N N	N N	N N
CR20 vs CR21	A,C,D vs A,C,D	N N	N N	N N	N N	N N
CR21	A vs B	S N	S N	S N	N N	S N
CR21	A vs C	N N	S N	N S	N S	- -

① This column reflects the existence of significant (S) or nonsignificant (N) difference in the variance of the two compared systems or pilots. Variance is a measure of the parameter consistency.

② This column reflects the existence of significant (S) or nonsignificant (N) difference in the sample means. The sample mean is a measure of the average value of the parameter.

3.2.4 Pilot Rating/Quantitative Performance Data Comparison

This sub-section presents an analysis of pilot ratings in terms of the quantitative performance parameters discussed in Section 3.2.3. The purpose of this analysis is to define the relative importance that pilots place on tracking performance, touchdown disperions and workload. In addition, this analysis should underscore salient conclusions drawn from both the subjective (pilot ratings) and quantitative performance data sets. Pilot ratings used in this analysis are from the IFR approach/VFR landing task.

Linear regression analysis techniques were used to determine a mathematical relationship between pilot rating and the quantitative performance data. Statistical tests were used to determine the "goodness" of the regression and the significance of each variable and the regression. The following statistical figures of merit were used to judge candidate relationships. The level of confidence for the correlation was set at 95%. The "t" test was used to determine the significance of each variable of the linear regression equation, and the "F" test was used for checking the significance of the regression. Both of these tests use the "null hypothesis" with the confidence level set at 5% for each test.

Longitudinal and lateral-directional control tasks were treated separately. The following equations define the linear models that best related pilot ratings to the quantitative parameters for longitudinal and lateral-directional control.

$$PR_{LONG} = .89 + 1.70\left(\frac{\bar{\epsilon}_{GS_{RMS}}}{\bar{\delta}_{COL_{RMS}}}\right) + .105\ \bar{\epsilon}_{V_T}$$

$$PR_{LAT\text{-}DIR} = -.81 + 18.38\left(\frac{\bar{\epsilon}_{LOC_{RMS}}}{\bar{\delta}_{W_{RMS}}}\right) + .094\ S_{S_Y} + 29.39\ \bar{\delta}ped_{RMS}$$

where

$\bar{\epsilon}_{GS_{RMS}}$ = mean of root mean square glideslope error, dots

$\bar{\epsilon}_{LOC_{RMS}}$ = mean of root mean square localizer error, dots

$\bar{\epsilon}_{V_{T_{RMS}}}$ = mean of root mean square airspeed error, fps

$\bar{\delta}_{COL_{RMS}}$ = mean of root mean square column, inches

$\bar{\delta}_{W_{RMS}}$ = mean of root mean square wheel, degrees

$\bar{\delta}_{PED_{RMS}}$ = mean of root mean square pedal, inches

S_{S_Y} = standard deviation of lateral offset at touchdown, feet

These equations point out the importance which pilots placed on tracking accuracy and the penalty associated with unwanted motion (i.e., airspeed error and sideslip). Airspeed error rather than vector angle control activity turned out to be more significant to the pilots. Pedal activity indicated lack of turn coordination.

The correlation between $\overline{\delta}_{COL}$ and PR_{LONG} and $\overline{\delta}_{W}$ and $PR_{LAT/DIR}$ was insignificant. These workload terms did not become significant until they were used in ratio form as shown by the above equations.

With the exception of lateral offset at touchdown, touchdown errors did not correlate with pilot ratings. Since simulation runs terminated at touchdown, pilots were given no indication of whether longitudinal dispersion or ground track error could have produced an unsuccessful landing. On the other hand, lateral offsets at touchdown were important since a pilot could judge whether he landed on or off the runway. The standard deviation of the lateral offset was used since it reflects the repeatability of landing on the runway.

The pilot rating equations were used to calculate ratings for the control systems which were used for the linear regression analysis. A comparison of calculated and actual pilot ratings is presented by Figures 18 and 19 of longitudinal and lateral-directional control, respectively. These figures show that the pilot rating equations can generally reproduce actual ratings to within $\Delta PR = .5$. Points falling outside the envelope of $\Delta PR \pm .5$ reflect three shortcomings of this linear regression analysis:

- Pilot compensation was not accounted for since it was not measured. This parameter does not lend itself to direct measurement. Lightly damped control systems probably required lead compensation. For these systems, computed pilot ratings are low.

- Cross-axis effects were neglected since longitudinal and lateral/directional control were analyzed separately. If there are any cross-axis effects, they would probably be most pronounced for poorer control systems. This could be overcome by using a six degree of freedom regression model. This was not considered for this study since the linear regression program which was used for this analysis was limited to five variables.

- The regression coefficients are linear weighting factors that best match a group of data for several pilots. Since each pilot has his own ideas on what represents good flying qualities, the linear regression model cannot account for individual pilot differences.

Note:

1. Sample Properties:
   (a) 5 Pilots
   (b) 10 Control Systems } 26 Samples
   (c) Flagged Data Points = 2 PRs (s)

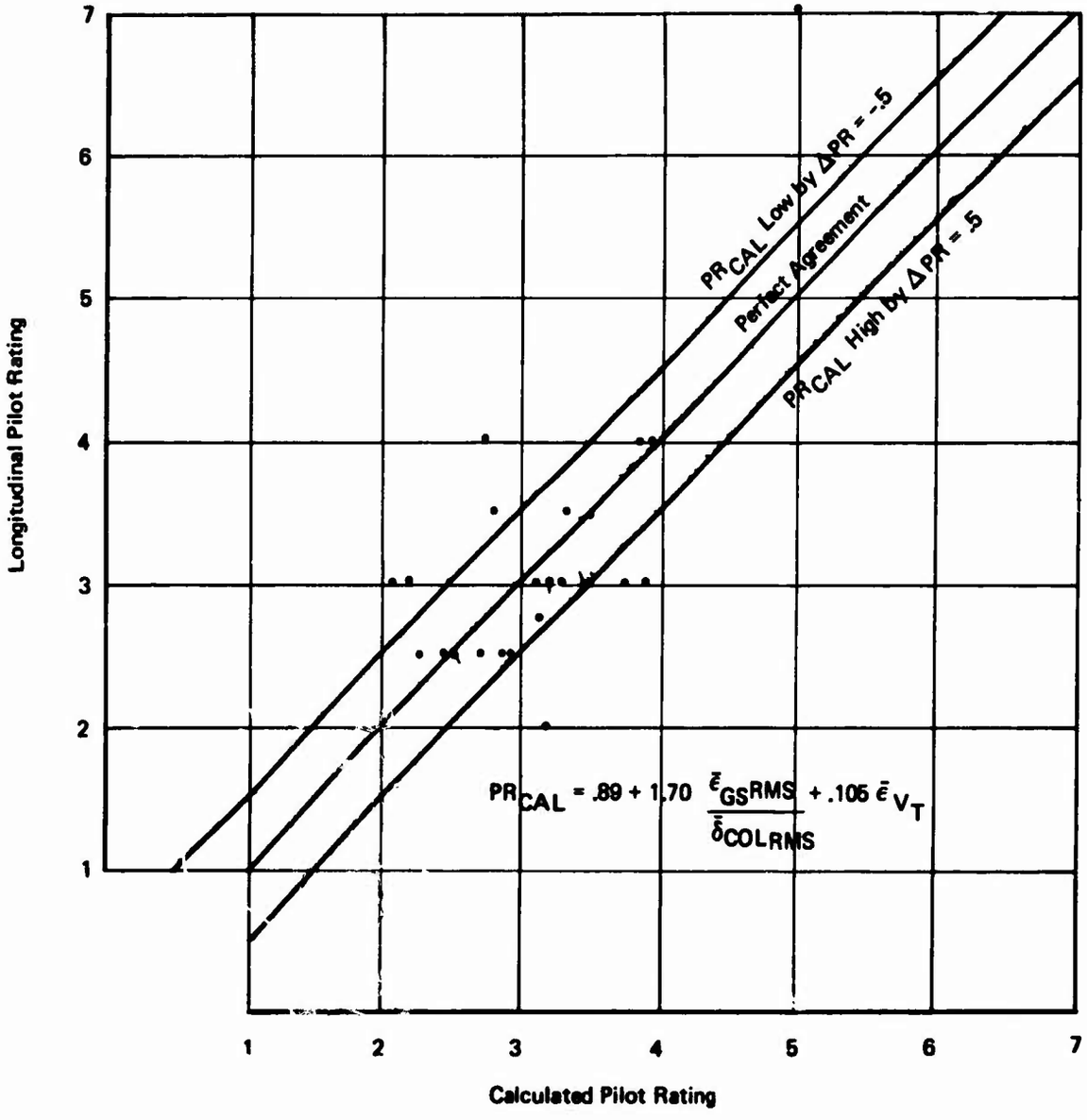

Figure 18 : Analysis of Longitudinal Pilot Rating

Note:

1. Sample Properties:
   (a) 6 Pilots
   (b) 5 Control Systems } 18 Samples
   (c) Flagged Data Points = 2 PRs (◦)

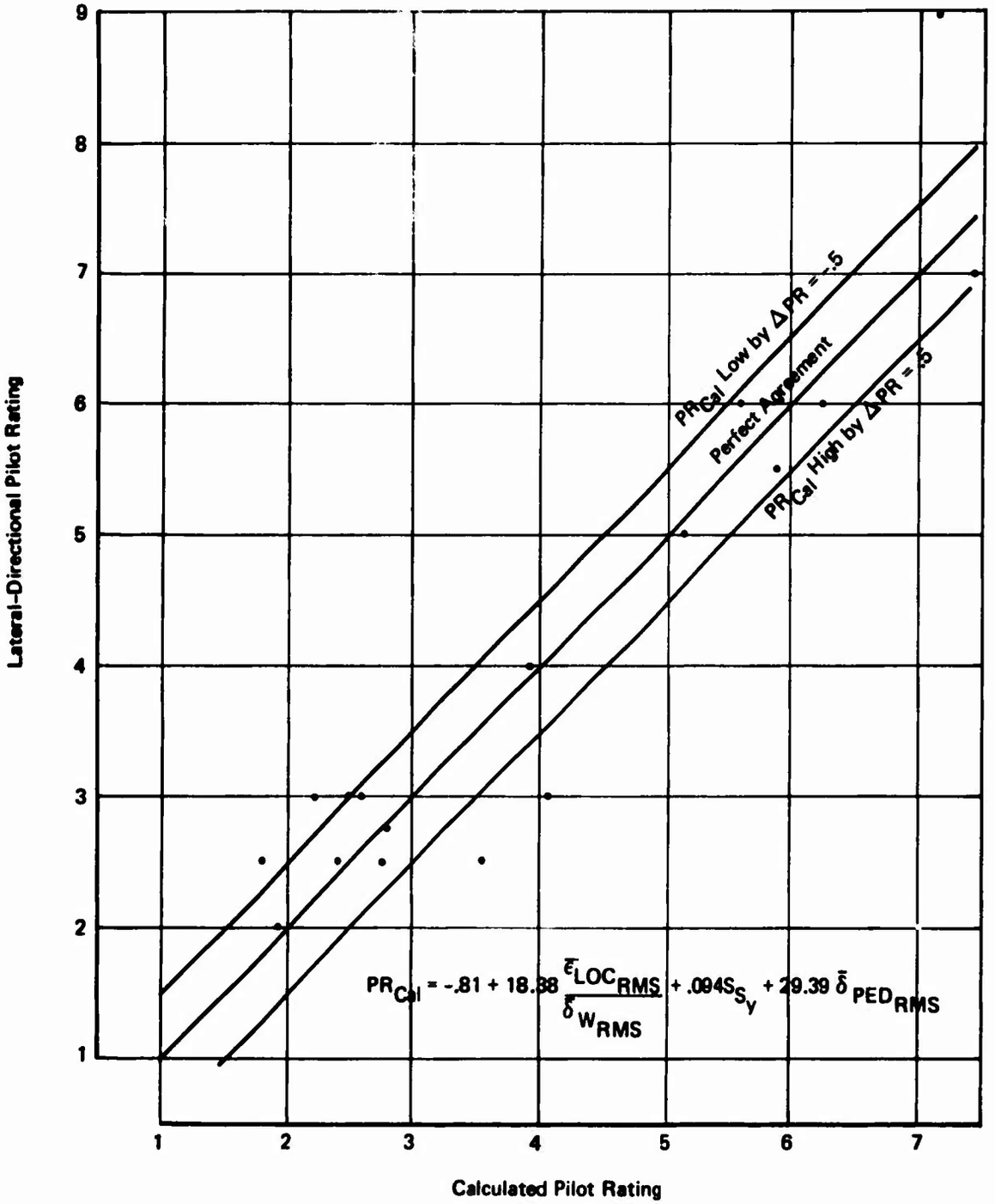

Figure 19 : Analysis of Lateral -Directional Pilot Rating

3.3 Description of Selected Control Systems' Flying Qualities

The selected flight control system was the end product of the STOL STAI flight control system trade study. The longitudinal and lateral-directional control laws (referred to as CP21/CR20) of the selected control system are depicted by the block diagrams presented in Figures 20 and 21. CP21/CR20 is a control augmented system which provides:

(1) Increased longitudinal and lateral damping,

(2) Airspeed hold,

(3) Turn coordination, and

(4) Neutral spiral stability.

Validation of CP21/CR20's STOL flying qualities included piloted simulation evaluations and a comparison of its flying qualities to the requirements defined by MIL-F-83300.

The selected control system was evaluated on both the fixed and moving base simulators. Pilots A, B, C, E, and F participated in the tests. The airplane's flying qualities were evaluated for three different center of gravity locations, with random turbulence and wind shears, and at airspeeds ranging from sixty-five to eighty-five knots.

The flying qualities of the vectored thrust AMST with CP21/CR20 are satisfactory (i.e., 2< PR< 3). Specific pilot ratings and comments for this control system may be found in Tables V, VI, and VIII. These pilot ratings and comments include handling quality and IFR approach/VFR landing evaluations. The IFR/VFR data include control system failure and engine-out evaluations.

Landing-approach flying qualities of the vectored thrust AMST with CP21/CR20 generally comply with Level 1 criteria defined by paragraphs 3.3 through 3.8 of MIL-F-83300. Controller force characteristics are summarized by the table below. Figures 22 through 28 depict trim properties, characteristics roots, typical longitudinal and lateral-directional responses, and control power characteristics of the vectored thrust airplane as simulated for the control system validation phase. Pertinent MIL-F-83300 paragraph numbers are noted on these figures.

Table XI: Controller Force Characteristics Summary

Controller	Breakout Force∿Lbs.	Force Gradient	Maximum Force∿Lbs.
Column	3.0	3 Lbs/In.	21.0
Thrust Vector	1.0	---	--
Throttles	1.0	---	--
Wheel	2.0	.25 Lbs/Deg.	17.0
Pedals	7.0	20 Lbs/In.	63.0

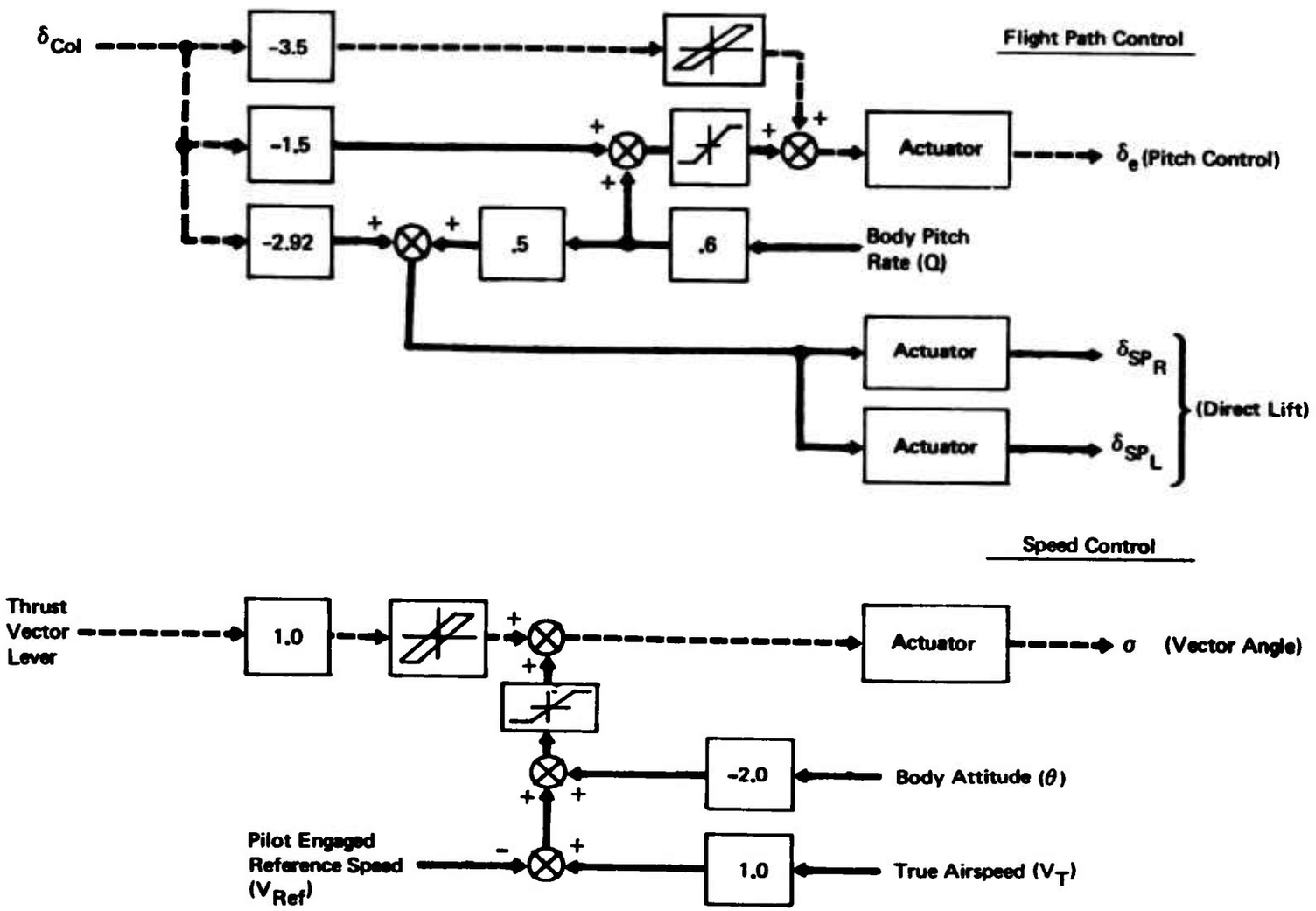

Figure 20: Selected Longitudinal System (CP21)

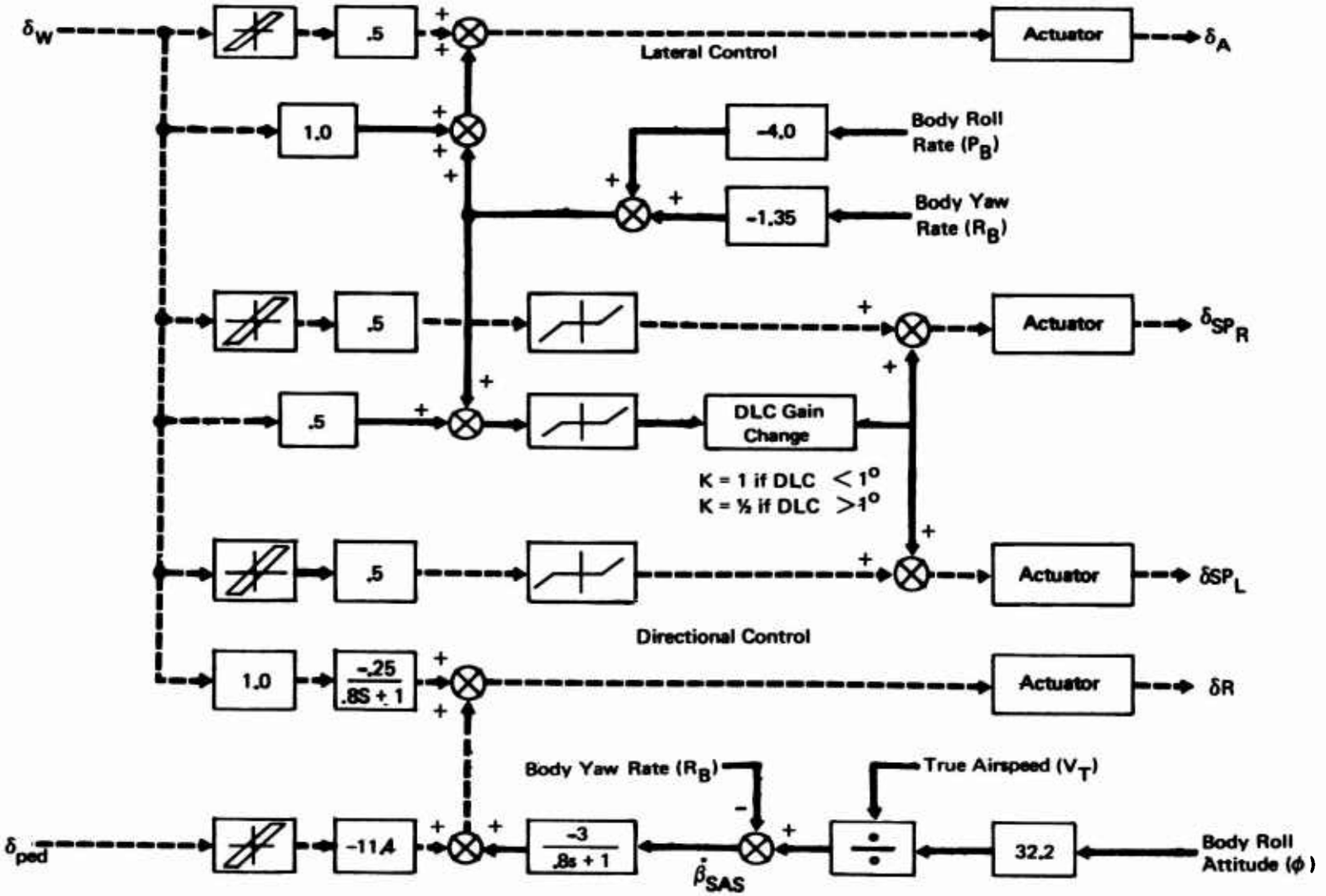

Figure 21 : Selected Lateral/Directional System (CR20)

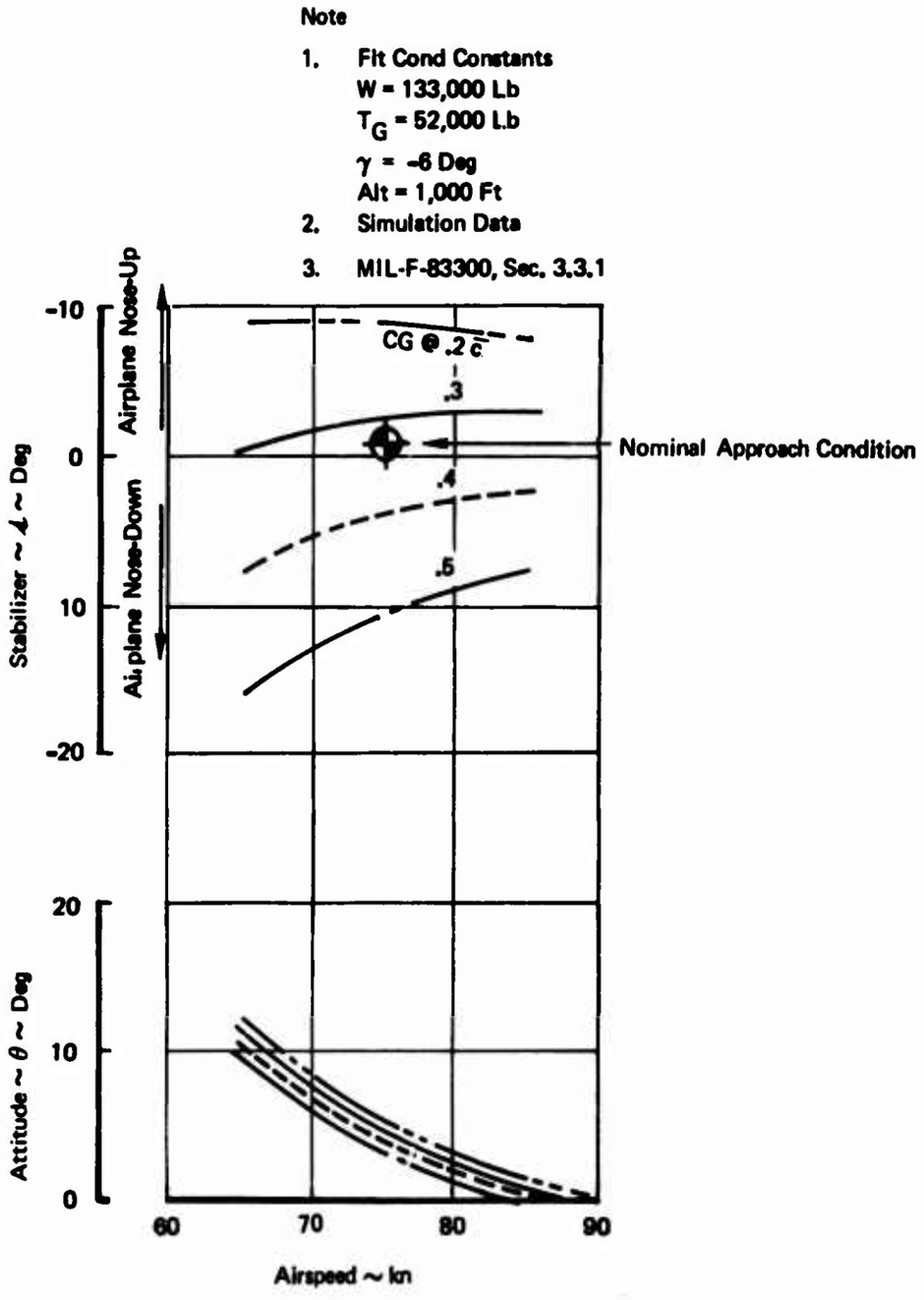

Figure 22: Longitudinal Trim

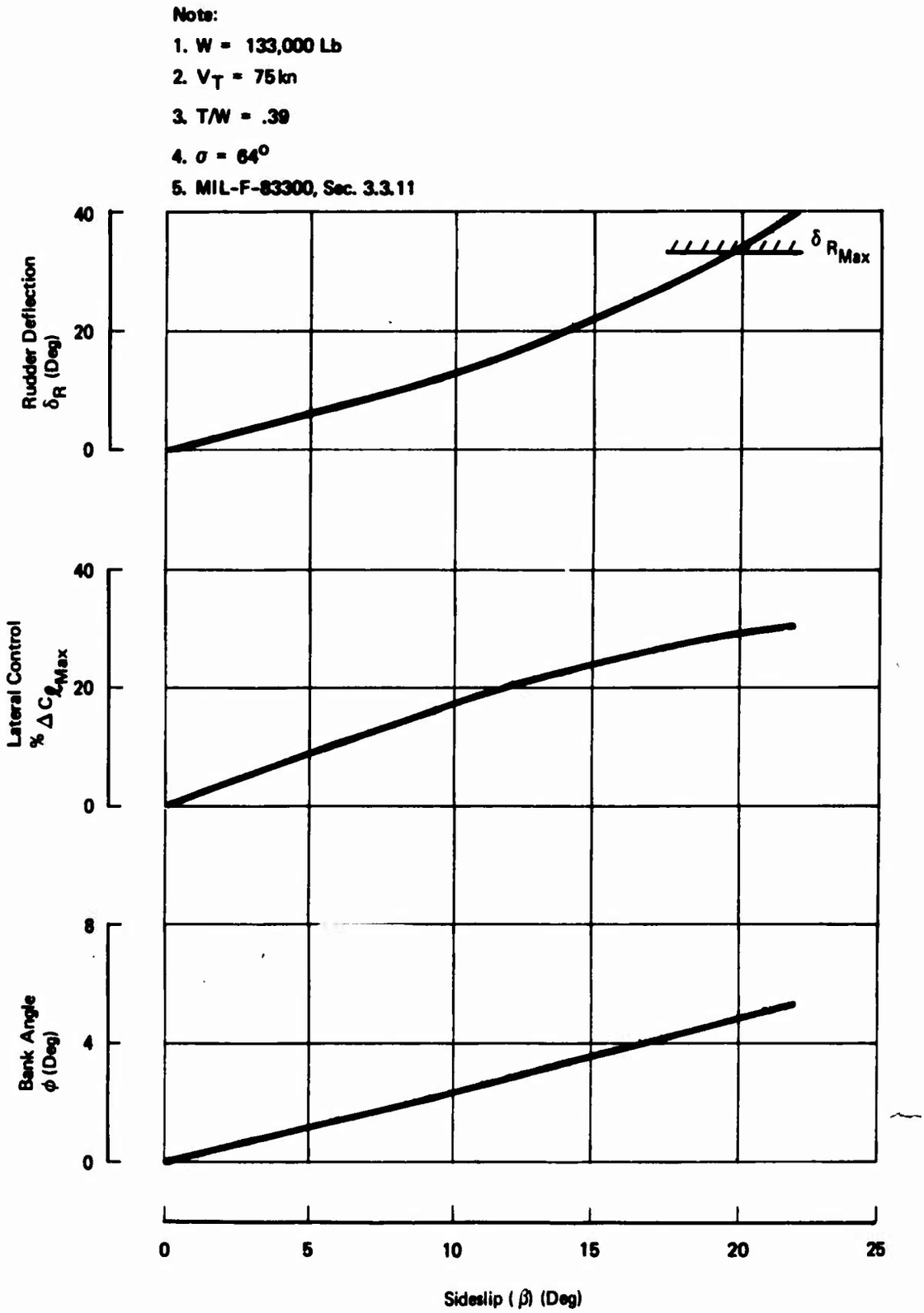

Figure 23: Lateral Directional Trim

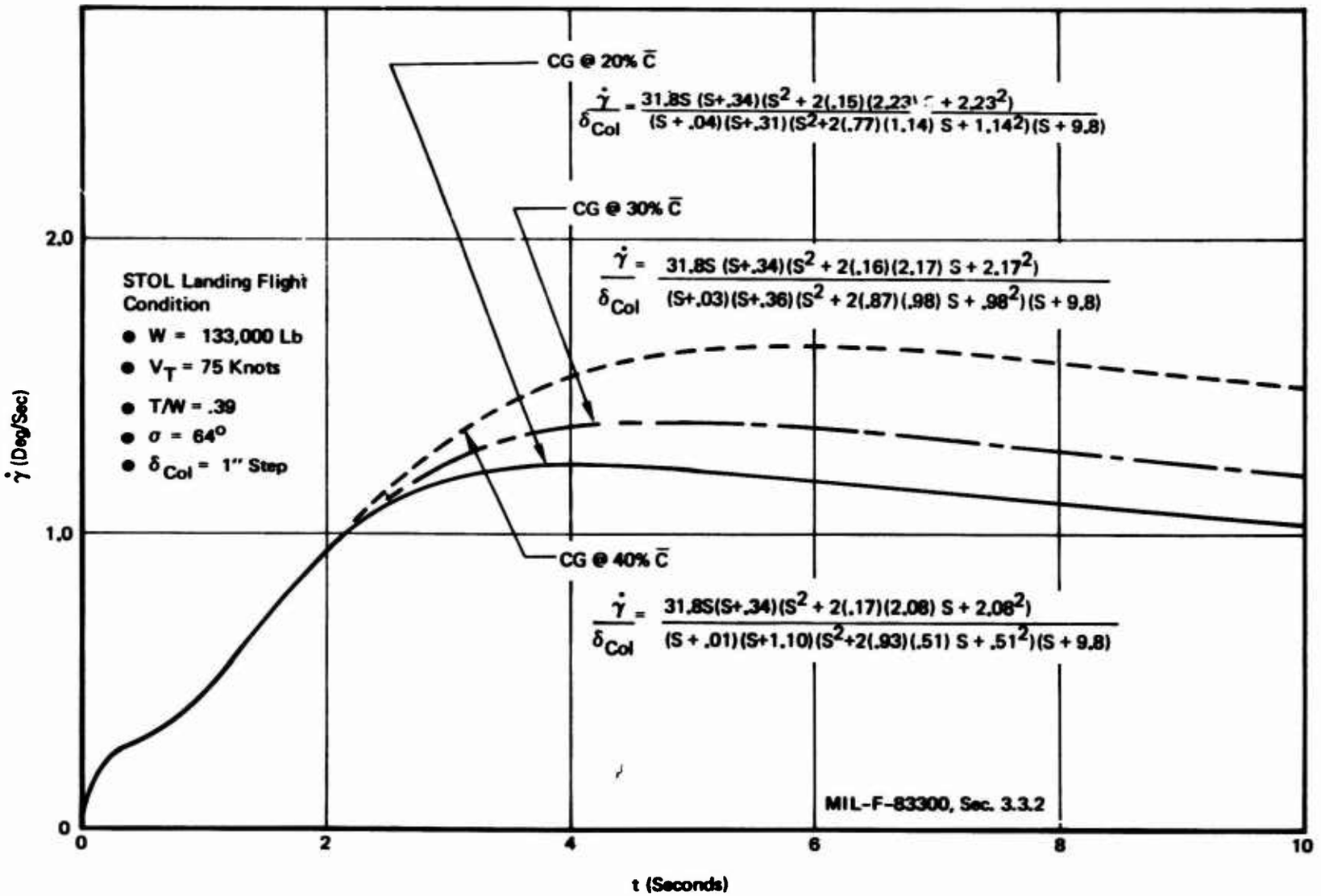

Figure 24: Effect of CG Position on the Longitudinal Dynamic Response

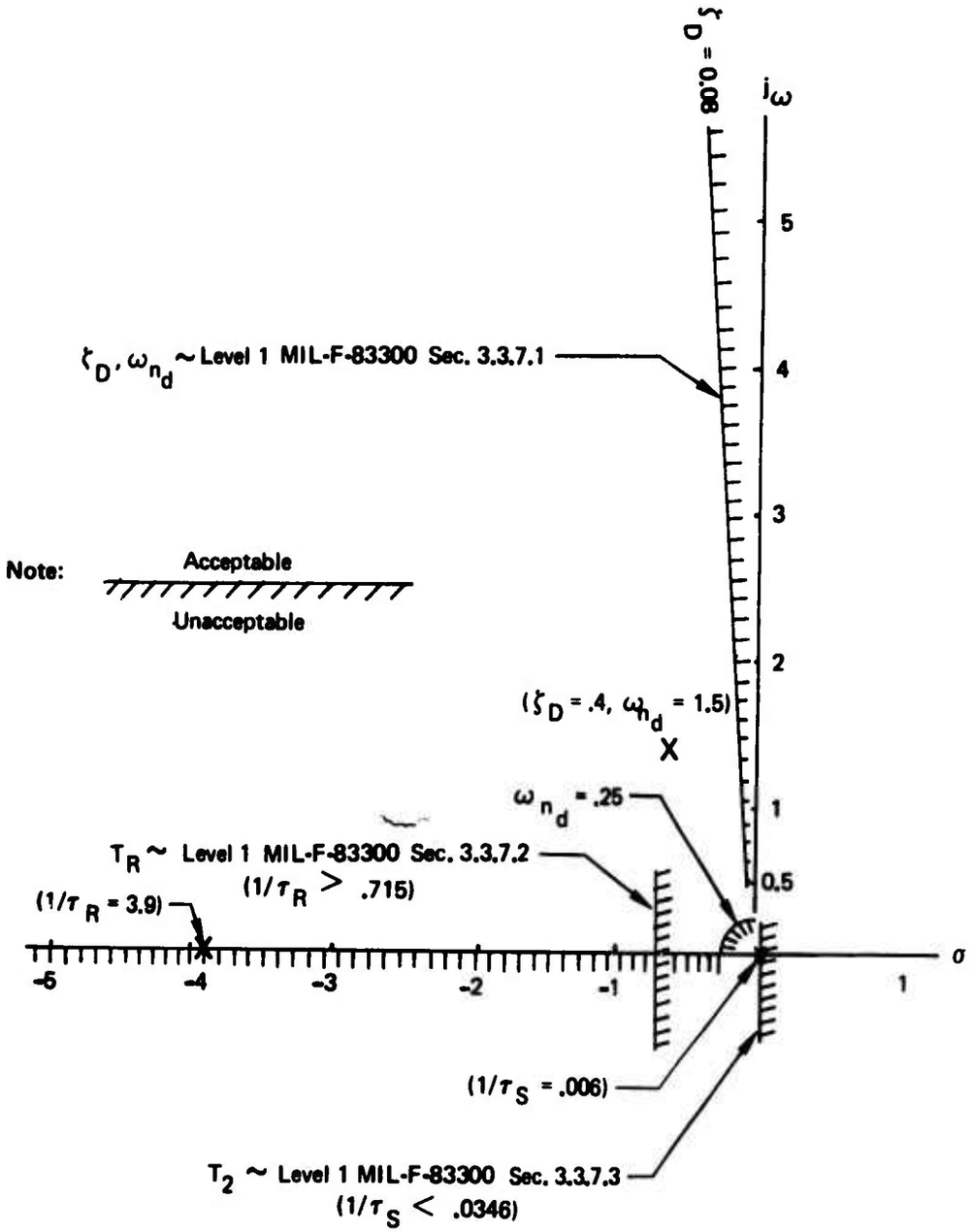

STOL TAI Landing Flight Condition

- W = 133,000 Lb
- V_T = 75 kn
- T/W = .39, $\sigma = 64^o$

Figure 25: Stability of Lateral Directional Roots

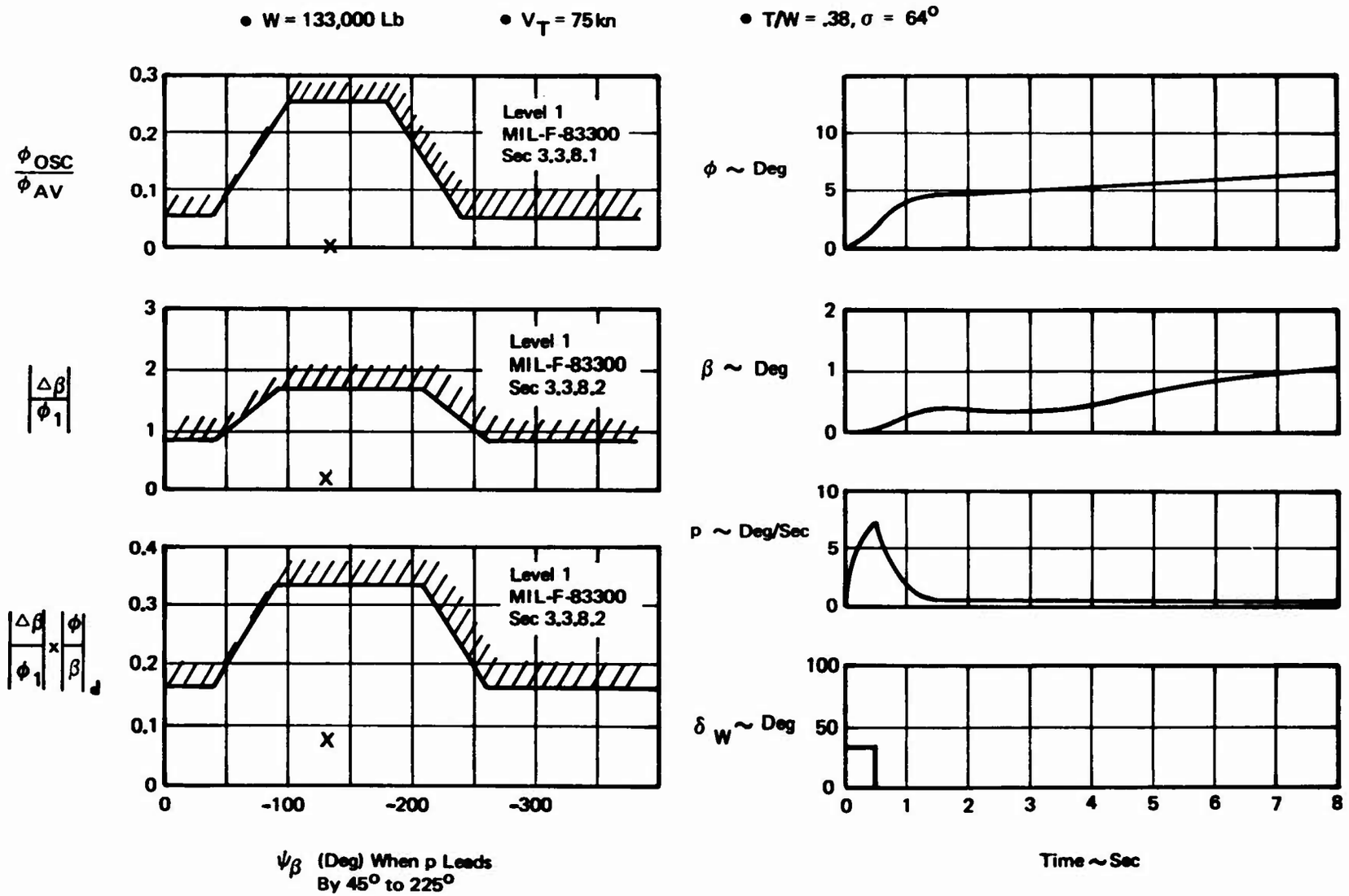

Figure 26: Roll/Sideslip Coupling for Roll Control

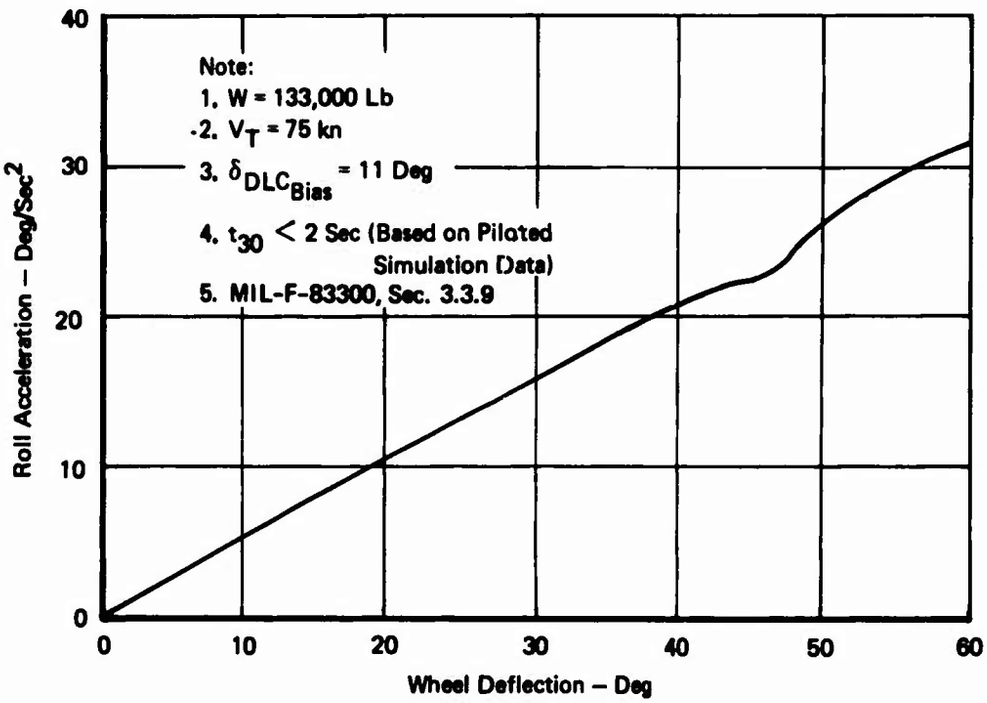

Figure 27 : Lateral Control Power Summary

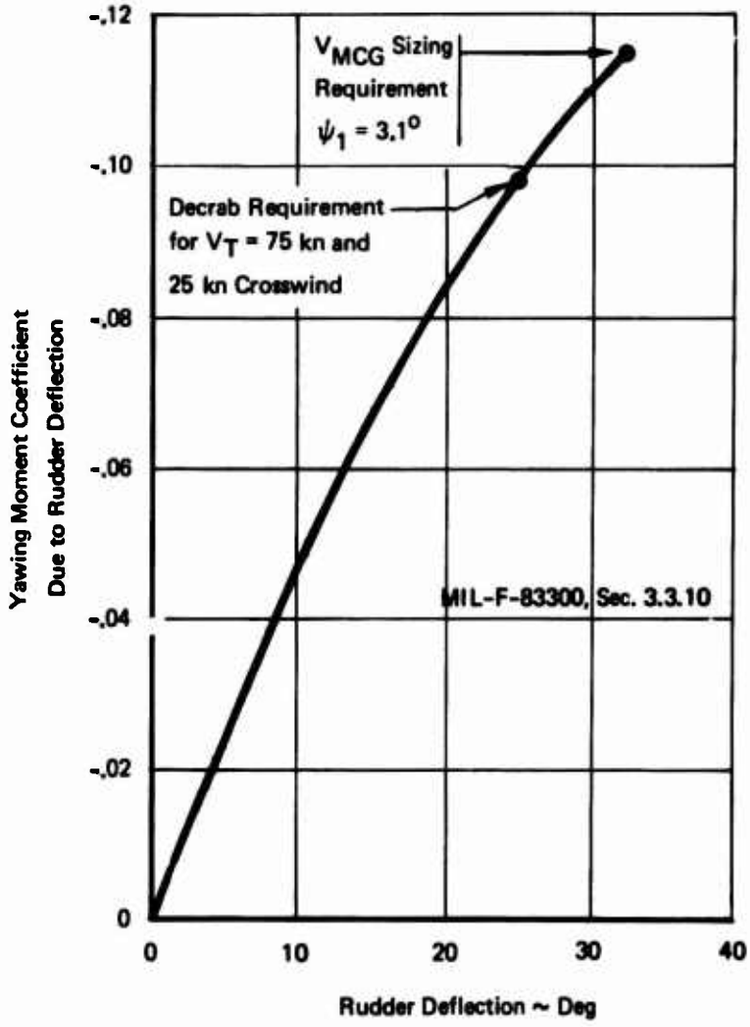

Figure 28 : Directional Control Power Summary

SECTION IV

DISCUSSION OF MIL-F-83300 FLYING QUALITY CRITERIA

4.1 General

The analysis of STAI simulation results has provided an opportunity to review MIL-F-83300 criteria as they apply to a powered lift STOL airplane with full control augmentation. Several portions of the specification were found to be invalid for one of the following reasons:

- o They allowed unsatisfactory flying qualities even though the specification is met.
- o They were overly restrictive in that they required airplane and control system features which were not necessary for good flying qualities.
- o They imposed operational requirements which were not relevant to STOL landing approaches.

Each of these items is discussed in detail below. The discussion is limited to Level 1 criteria since most of the simulation time dealt with evaluations of augmented control systems. MIL-F-83300 paragraphs are included for the reader's convenience.

4.2 Criteria Review

4.2.1 Longitudinal Dynamic Response

Longitudinal dynamic response (Para. 3.3.2). "The following requirements shall apply to the dynamic response of the aircraft with the pitch control free and with it fixed. These requirements apply following a disturbance in smooth air, and following abrupt pitch control inputs in each direction, for responses of any magnitude that might be experienced in operational use. If the oscillations are nonlinear with amplitude, the requirements shall apply to each cycle of the oscillation.

Level 1: The response of the aircraft shall not be divergent (i.e., all roots of the longitudinal characteristic equation of the aircraft shall be stable). In addition, the undamped natural frequency, ω_n, and damping ratio, ζ, of the second-order pair of roots (real or complex) that primarily determine the short-term response of angle of attack following an abrupt pitch control input shall meet the Level 1 requirements of Figure 1 (Page 19 of MIL-F-83300)."

These requirements are based on the assumption that the dominant mode is second order. This is not necessarily valid since augmented vehicles can be characterized by lower or higher order responses due to additional modes, pole/zero cancellation, or minimum residues due to pole/zero proximity.

The data shown by Figure 24 with the c.g. at 40%$\bar{c}$ is a case in point. The characteristic equation for this response is cubic. The response does not meet Level 1 criteria since the natural frequency of the complex roots is less than $\omega_{MIN} = \sqrt{.15 n_{z_\alpha}}$. Nevertheless, pilots gave this configuration a satisfactory pilot rating. This is a direct result of the small contribution of these complex roots to the total response.

For powered lift aircraft that use direct lift control, the load factor response is not directly related to the angle of attack response. Thus, rate of change of flight path ($\dot{\gamma}$) should be used to describe the short-term longitudinal response, instead of angle of attack as specified by Paragraph 3.3.2.

4.2.2 Roll Sideslip Coupling

Roll-sideslip coupling (Para. 3.3.8). "The requirements on roll-sideslip coupling are stated in terms of allowable bank angle oscillations, sideslip excursions, roll control forces and yaw control forces that occur during specified rolling and turning maneuvers. The requirements of 3.3.8.1 and 3.3.8.2 apply for both right and left roll control commands of all magnitudes up to the magnitude required to meet the roll performance requirements of 3.3.9, unless otherwise stated."

Bank angle oscillations (Para. 3.3.8.1). "The value of the parameter ϕ_{OSC}/ϕ_{AV} following a yaw-control-free impulse roll control command shall be within the limits specified in Figure 3 (Page 23, MIL-F-83300) for Levels 1 and 2. The impulse shall be as abrupt as practical within the strength limits of the pilot and the rate limits of the roll control system. For Levels 1 and 2, ϕ_{AV} shall always be in the direction of the roll control command."

Sideslip excursions (Para. 3.3.8.2). "The amount of sideslip resulting from abrupt roll control commands shall not be excessible or require complicated or objectionable rudder coordination. For Flight Phase Categories A and C, the ratio of the maximum change in sideslip angle to the initial peak magnitude in roll response, $|\Delta\beta/\phi_1|$, for an abrupt roll control pulse command shall not exceed the limit specified in Figure 4 (Page 24, MIL-F-83300). In addition, $|\Delta\beta/\phi_1| \times |\phi/\beta|_d$ shall not exceed the limit specified in Figure 5 (Page 4, MIL-F-83300)."

Turn coordination (Para. 3.3.8.4). "It shall be possible to maintain steady constant-altitude coordinated turns in either direction, using bank angles up to either that required to produce a turn rate of 10 degrees per second or a bank angle of 60 degrees for Class IV aircraft, 45 degrees for Class I and Class II aircraft, or 30 degrees for Class III aircraft. Yaw control forces shall not exceed 40 pounds and roll control forces shall not exceed five pounds. This requirement applies to Level 1, with the aircraft trimmed for zero-bank-angle straight flight."

The purpose of these paragraphs is to insure good turn coordination. The emphasis that these paragraphs place on good turn coordination is well supported by the STAI simulation experience with several different lateral-directional control laws (see Section 3.2). However, STAI simulation and analytical results indicate that the Level 1 boundaries for $\emptyset OSC/\emptyset AV$, $|\Delta\beta/\emptyset_1|$, and $|\Delta\beta/\emptyset_1| \times 1\emptyset/\beta|_d$, as defined above, do not guarantee satisfactory turn coordination. A comparison of Paragraph 3.3.8 Level 1 boundaries with candidate control law characteristics is presented by Figures 30 through 32. It is important to note that all of these control systems surpass Level 1 dutch roll, roll mode, and spiral mode criteria of MIL-F-83300.

The turn rate and bank angle limits of Paragraph 3.3.8.4 seem excessive. It is stated that it should be possible to maintain coordinated turns using bank angles either up to that required to produce a turn rate of $\dot{\psi}$= 10 deg/sec or up to $\emptyset$ = 45° for Class II aircraft. A turn rate of $\dot{\psi}$= 10 deg/sec seems to be completely unrealistic for STOL transports. Boeing pilots found that they could not use turn rates faster than $\dot{\psi} \approx$ 5 deg/sec (i.e., $\emptyset \approx 19°$ @ 75 knots) because at higher rates they were then unable to precisely judge the roll-out point for the new heading.

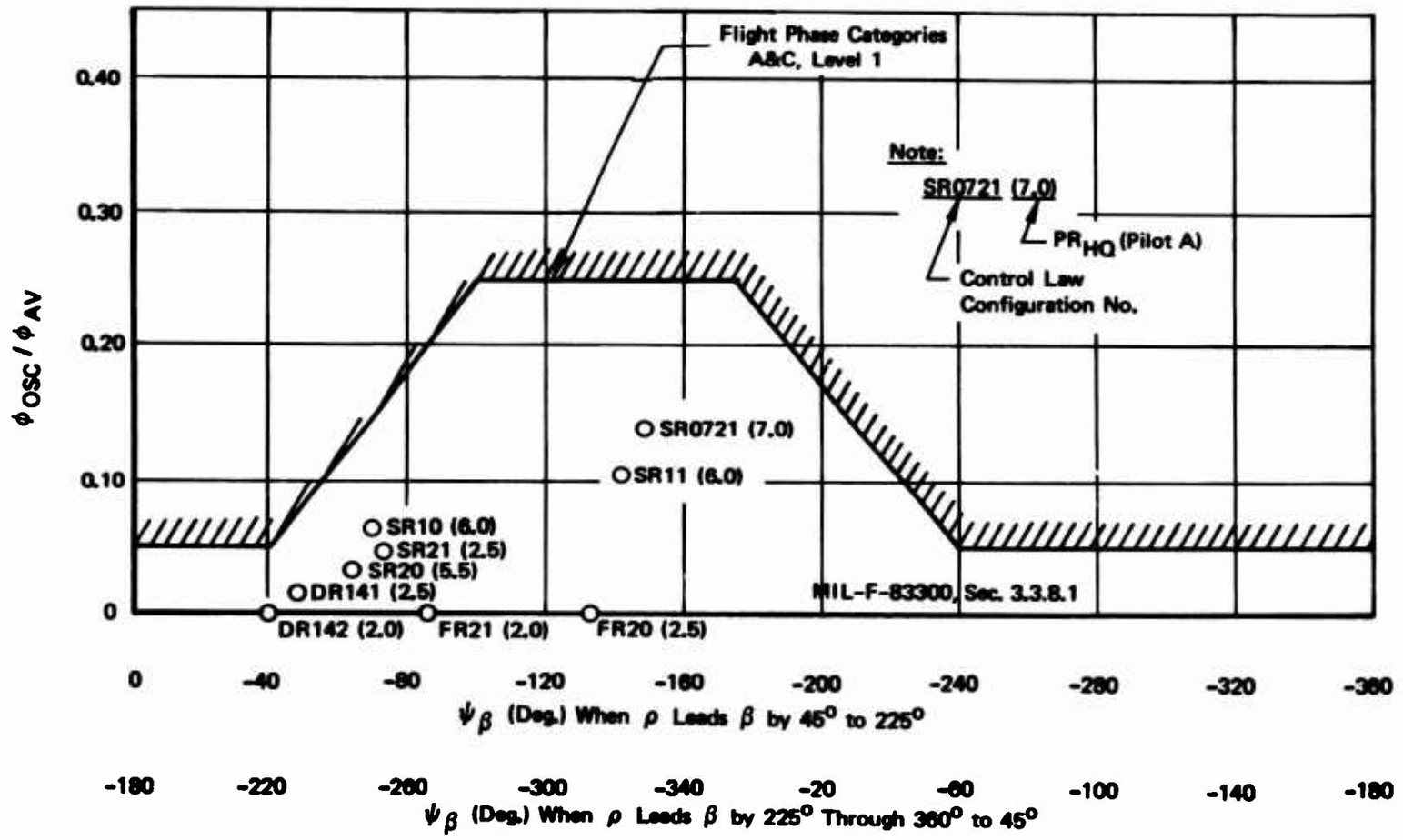

Figure 30: Bank Angle Oscillations

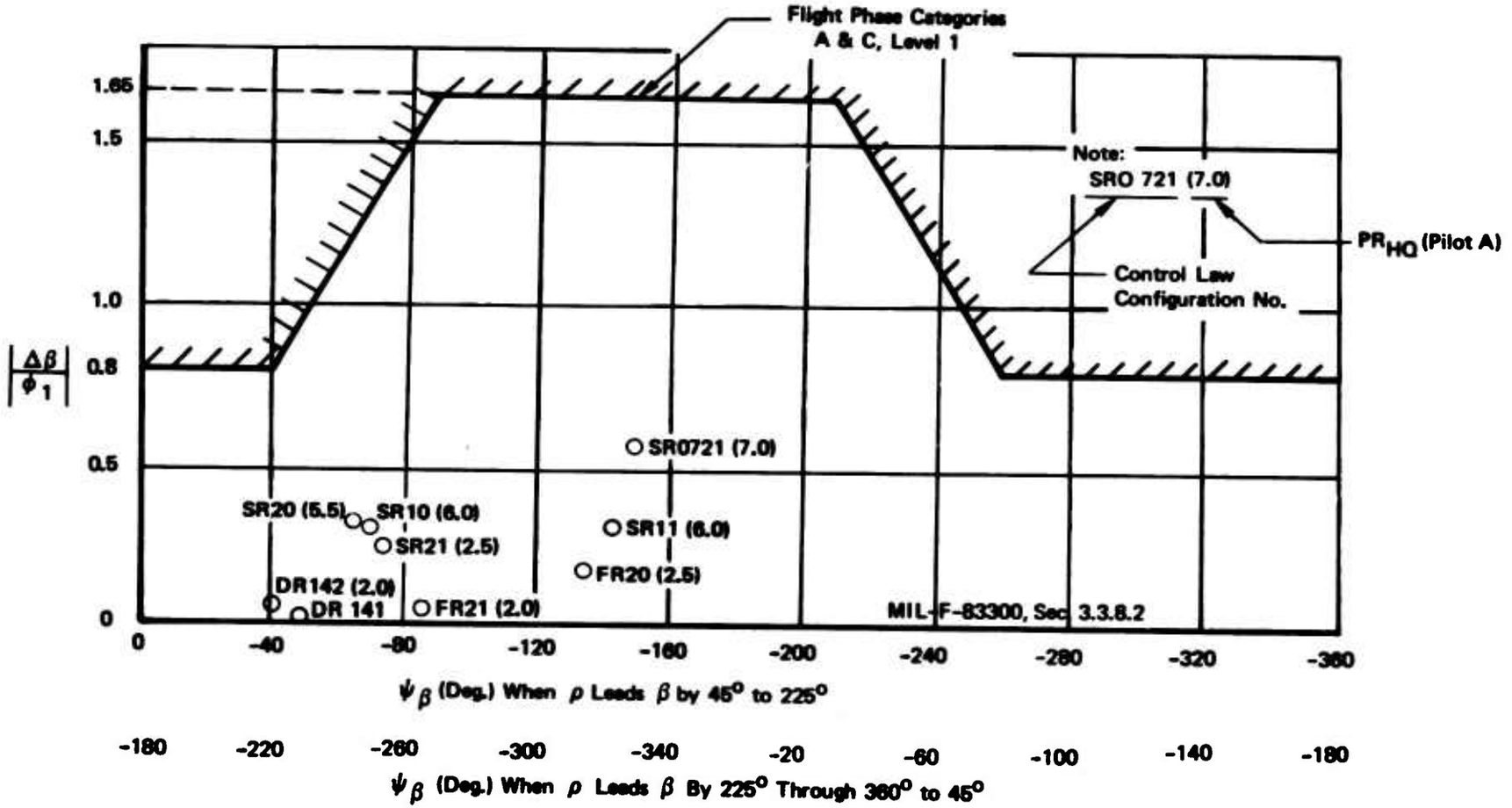

Figure 31: Sideslip Excursions: $|\Delta \beta / \phi_1|$

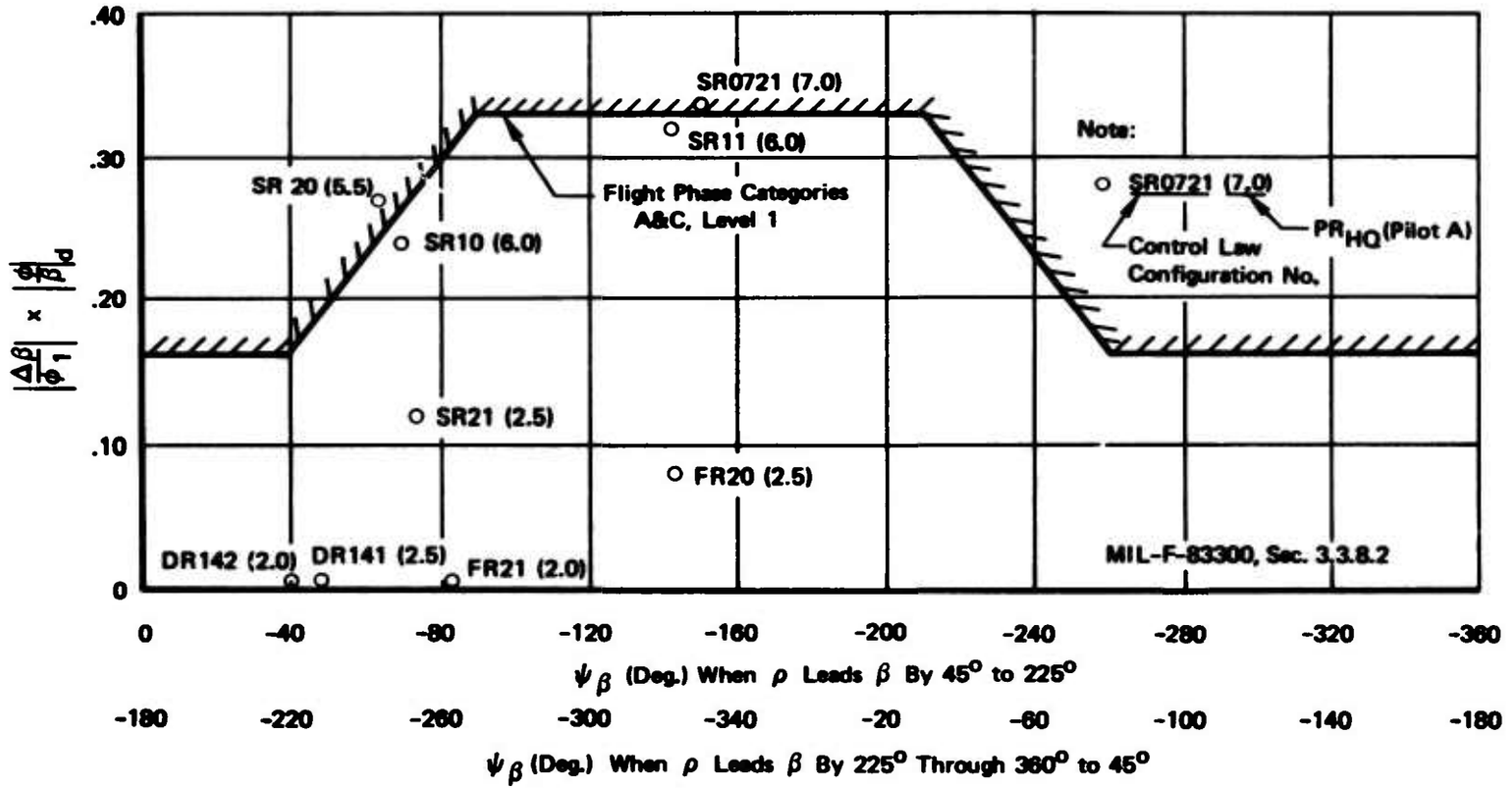

Figure 32: Sideslip Excursions: $|\Delta\beta/\phi_1|x|\phi/\beta|d$

4.2.3 Directional Response to Yaw Control Input

Directional response to yaw control input (Para. 3.3.10.1). "The yaw attitude change within the first second following an abrupt step displacement of the yaw control shall not be less than:

Level 1: 6.0 degrees

This requirement applies with all other cockpit controls fixed."

This paragraph defines the required directional control power in terms of the change in heading after one section (ψ_1) following a step rudder command. The Level 1 requirement of $\psi_1 = 6°$ was not met by the simulated vectored thrust airplane. The directional response for the selected lateral-directional control law is $\psi_1 = 3.1°$. The rudder for this configuration was sized for engine out control during the takeoff ground run. Engine out control was more demanding than the decrab maneuver. Approximately 85 percent of the total directional control power was required to decrab from a 25 knot crosswind when the approach speed was 75 knots, (see Figure 28). Since the simulated airplane received good pilot ratings (see comments for CP21/CR20 in Table VIII) with yaw control power substantially below the MIL-F-83300 requirement, it appears that the specification is excessive.

4.2.4 Review Conclusions

MIL-F-83300 control power criteria are defined in terms of attaining a specific displacement within a specified time period. These criteria do not reflect operational considerations, and therefore do not necessarily ensure a safe vehicle. Control power criteria should define the control capability which an aircraft must have in order to complete the intended mission safely. Operational criteria should be in terms of trim, stabilization, and maneuver requirements. Since these requirements are dependent on an airplane's size, configuration, and intended mission, airplane designers can balance them to minimize the total control power requirement without sacrificing vehicle safety. Since operational control power requirements are an integral part of the "control configured vehicle" design process, flying quality specifications should use operational control power criteria.

The formats used by MIL-F-83300 to specify dynamic response criteria for the longitudinal and lateral-directional axes are inconsistent. Furthermore, these criteria are not task oriented. It is suggested that MIL-F-83300 could be strengthened by using task oriented criteria which utilize a common format. Dynamic response criteria could be defined for flight path, speed, bank angle, and sideslip control and turbulence suppression. One format that could be used would specify control sensitivity, responsiveness, damping, and modal coupling characteristics. If these criteria were specified in the frequency domain, these requirements could be stated in terms of the primary response's low frequency gain, bandwidth, high frequency resonant peak, and modal coupling and turbulence sensitivity boundaries.

SECTION V

CONCLUSIONS AND RECOMMENDATIONS

5.1 Conclusions

(1) The flying qualities of the unaugmented airplane are unacceptable (6.5< PR< 9.5).

(2) Satisfactory longitudinal flying qualities (PR< 3.5) were achieved with control systems that provide pitch damping, speed decoupling from column commands, and minimal glideslope deviations for speed commands.

(3) Lateral-directional control systems that provide turn coordination, neutral spiral stability, and lateral damping are required for satisfactory lateral-directional flying qualities.

(4) For approach speeds less than 85 knots, bank angles larger than approximately 20 degrees could not be used for normal maneuvering because of excessive turn rates associated with larger angles.

(5) Pilots require some form of flight path information such as flight path angle in order to make precision STOL approaches in turbulence.

(6) Both the Boeing fixed base and the NASA moving base simulations gave comparable results. Quantitative data from each simulation were statistically similar and Cooper-Harper pilot ratings for the selected control system were within a spread of 2< PR< 3.

(7) Several portions of MIL-F-83300, Flying Qualities of Piloted V/STOL Aircraft (dealing with longitudinal equilibrium, longitudinal dynamic response, roll-sideslip coupling, and directional response to yaw control) may allow unsatisfactory flying qualities, are possibly overly restrictive, or might impose irrelevant operational requirements.

5.2 Recommendations

It is recommended that further STOL simulation investigations consider the following:

(1) The effect of landing disperions and ground handling technique on landing field length. The following aspects should be assessed:

   (a) The effect of control augmentation systems on reducing touchdown dispersions.

   (b) The effect of high touchdown sink rates and lateral velocities on landing gear design philosophy.

(c) The effect of automatic spoiler deployment, automatic braking devices, and reverse thrust operation on stopping distance.

(2) Takeoff performance and operational criteria (e.g., the dynamic relationship between V_{MCG}, V_1, V_R, V_{LO} and V_C) for powered lift STOL aircraft.

(3) The improvement in tracking performance and control of safety margins resulting from utilization of a modern CRT vertical situation indicator.

APPENDIX I

EVALUATION PILOT BIOGRAPHIES

Pilot A

Pilot A holds a B.S. degree in Aeronautical Engineering from Oregon State University. He has a total of 8800 flight hours of which 4200 are engineering flight hours in military and commercial jet aircraft. After four years of military flying with the Air Force during World War II, he flew for three years as an aeronautical research pilot with NASA. Pilot A has been flying as an engineering test pilot for The Boeing Company for the last twenty-one years. He has flown approximately 200 hours of STOL simulation evaluating externally blown flaps, vectored thrust, upper surface blowing and augmentor wing configurations. Pilot A is now Boeing's AMST project pilot.

Pilot B

Pilot B holds a B.S. degree in Aeronautical Engineering from the University of Wichita. He served 5 years in the Air Force as a transport pilot and is a graduate of the Air Force Test Pilot School. He has a total of 6300 hours of which approximately 400 are engineering flight hours. Total commercial transport time is 2600 hours and total military flight time is 3254 hours. Total STOL simulator time is approximately 90 hours. He has been employed by The Boeing Company for the past eight years.

Pilot C

Pilot C graduated for Washington State University in 1958 with a B.A. degree. He has a total of 3700 flight hours of which 1800 are production flight test hours and 290 are engineering or experimental flight hours. He spent eight years on active duty with the Air Force as a tanker pilot in SAC. He has participated as handling qualities evaluation pilot on 747, 737, SST, Boeing/Aeritalia, and TAI programs. His total STOL simulation experience is 84 hours. He has been employed by The Boeing Company for six years.

Pilot D

Pilot D graduated from Washington State University with a B.S. in Mechanical Engineering. He started with The Boeing Company as a flight test engineer and then took military leave to fly with the Air Force for five years. He returned to Boeing in 1965. He has a total of 3650 flight hours of which 2250 are commercial transport time, 1300 in military time, 435 in experimental, and 25 in STOL simulator time. He has been flying for The Boeing Company for the past seven years.

Pilot E

Pilot E is a Lt. Colonel in the United States Air Force. Total flying time is 6000 hours covering an eighteen year period. Pilot E served as command pilot for C-130A, B, E. Currently, he is the Tactical Aircraft STOL Project Officer at TAC Headquarters, Langley AFB, Va.

Pilot F

Pilot F is a Lt. Colonel in the United States Air Force. He holds a B.S. degree in Mechanical Engineering from Oregon State University and an M.S. degree in R&D Systems Management from the University of Southern California. Total flying time is 6000 hours of which 4500 hours are C-130A & E time. Pilot F has extensive SEA combat experience in STOL landing and air drop operations including the Khe Sanh siege. He has served as squadron instructor pilot, flight commander, squadron chief pilot, and wing flight examiner. He is now serving as staff officer for AMST studies and analysis in USAF headquarters.

Pilot G

Pilot G holds a B.S. degree in Aeronautical Engineering from the University of Kansas. He is a graduate of the USAF Test Pilot School. He has a total of 6000 flight hours of which 4500 are from engineering test flying. Four years of flying experience were acquired as a military fighter pilot and instrument instructor. He has participated in the testing of all Boeing models since B-52. He conducted initial flights on the STOL model 367-80, Buffalo, and 720B. He has been employed by The Boeing Company for 16 years.

APPENDIX II

COMPARISON OF FIXED AND MOVING BASE SIMULATIONS

The STAI simulation program has provided an opportunity to compare fixed and moving base simulators. Boeing ASG's Flight Simulator (fixed base) and ARC's Flight Simulator for Advanced Aircraft (moving base) were used for the STAI program. Both simulations used the mathematical models described in Appendix III. Aside from the obvious difference between the simulations (i.e., motion), there are other differences which could influence the fixed versus moving base comparison. These differences are summarized in Table XII. This discussion includes pilot comments and a statistical comparison of quantitative flying quality data.

Pilots, who participated in the moving base evaluations, generally felt that motion cues increased the realism of simulated flight. The motion cues seemed to be beneficial for recognition of an engine failure, but they did not help the pilot in controlling the failure. The motion cues pointed out shortcomings of a lateral-directional control system which had gone undetected during fixed base evaluations.

Boeing pilots discovered that they could greatly improve their glideslope tracking performance (in turbulence) by using a flight path inner loop (see Section 3.1). The CRT VSI, which was used for the fixed base simulation, has a prominent flight path presentation as is illustrated by Figure 3. The electro-mechanical VSI, which was used on the FSAA, had a makeshift flight path presentation which utilized the flight path command bar. The pilots commented that they could not obtain usable flight path information from this instrument. The flight path bar sat at the bottom of the "ball" for normal six degree approaches. In this position, the parallax was excessive. This lack of flight path information was the biggest deficiency of the moving base simulation.

The FSAA's Redifon color video presentation was liked by all pilots. One Boeing pilot commented that it was easier for him to judge the flare altitude on the FSAA simulator. This is a strong recommendation for color video since the FSAA landing model is scaled at 1:600, while its black and white counterpart was scaled at 1:150.

The fixed and moving base simulations are also compared by using quantitative performance data (Figure 33) from each simulation. The statistical analysis procedure discussed in Section 3.2.3 was used to determine areas of statistical difference. The results of this analysis (Table XIII) show that the performance data from both simulations are statistically similar. Since tracking performance is similar for each simulation, it appears that motion cues helped the pilots to improve their tracking performance. This conclusion is based on the assumption that pilots could achieve better tracking performance from the CRT vertical situation indicator, which was used on the fixed base simulator.

Table XII: *Comparison of Fixed and Moving Base Simulations*

ITEM	BOEING (KENT)	NASA FSAA (AMES)
1. Motion Cue	No	Yes
2. Controller (Longitudinal and Lateral)	"Brolley handles"	Stick
3. Instruments		
o VSI	CRT Electronic Attitude Director Indicator	Electro-mechanical
o Airspeed	ΔV = 2Kn/Calibration	ΔV = 5Kn/Calibration
o Localizer transmitter location	10,000' beyond runway threshold	2000' beyond runway threshold
4. Visual Display	Black and White	Color
5. Field-of-View	60° horizontally 45° vertically	46° horizontally 38° vertically
6. Terrain Model Scale		
o Approach	1:640	1:600
o Landing	1:150	1:600
7. Terrain Type	Jungle Surroundings with austere landing strip	Commercial STOL port Adjacent to CTOL runway
8. Runway Width (Full Scale)	60'	150'
9. Audio Cues	Tire squeal at touchdown	Engine noise

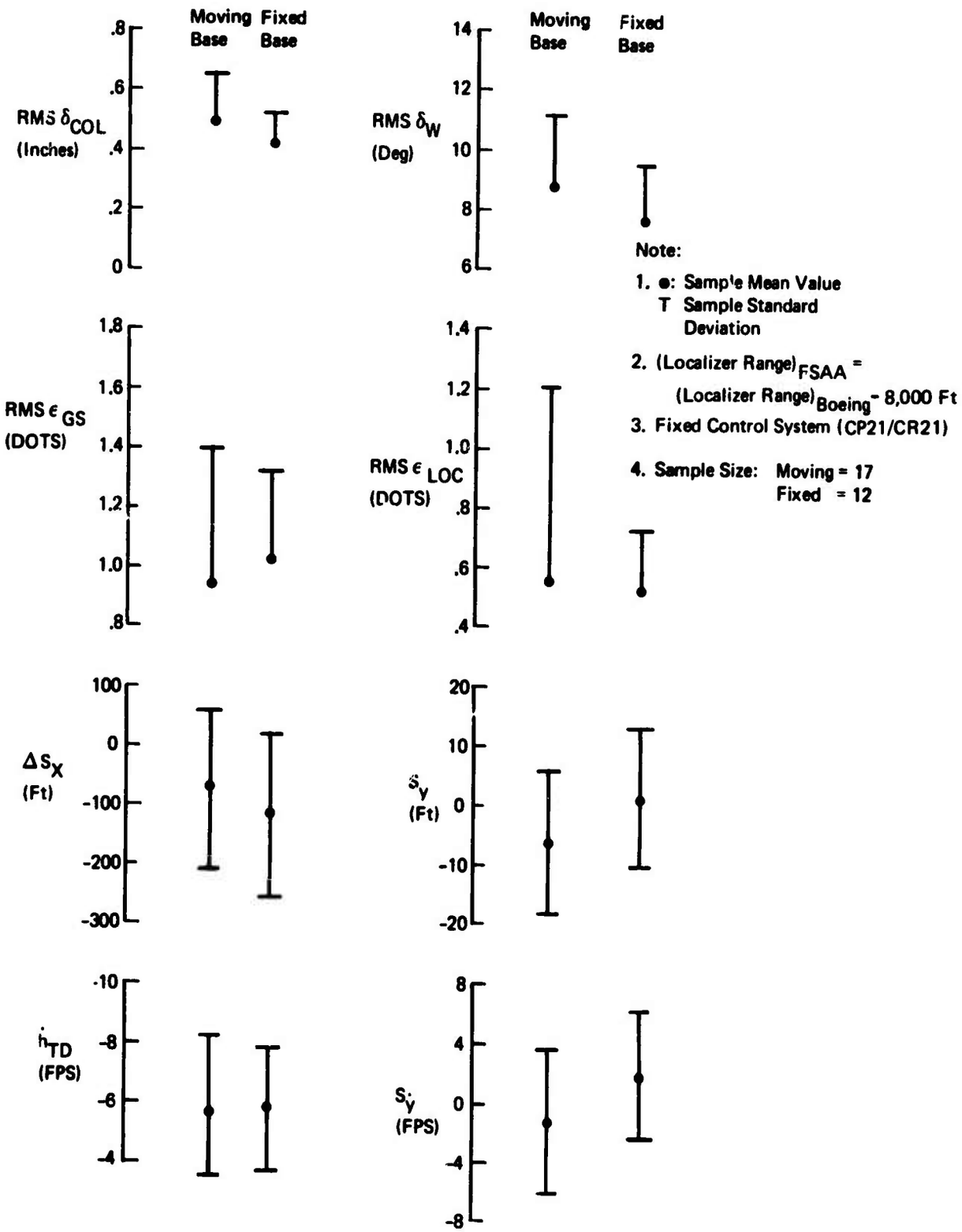

Figure 33: Comparison of Moving and Fixed Base Simulation Results

Table XIII: *Comparison of Fixed and Moving Base Performance Data*

Simulator	Pilots	PARAMETER							
		$\delta_{col.}$	$\epsilon_{G.S.}$	ΔS_x	$\dot{h}_{TD}$	δ_w	$\epsilon_{Loc.}$	S_y	$S_{\dot{y}}$
		(1) (2)	(1) (2)	(1) (2)	(1) (2)	(1) (2)	(1) (2)	(1) (2)	(1) (2)
Fixed vs moving Base	A,B,C A,B,C E and F	N N	N N	N N	N N	N N	N N	N N	N N

Notes: Control system CP21/CR21 was used for all comparisons.

(1) Significant (S) or nonsignificant (N) differences exist in the parameter variance.

(2) Significant (S) or nonsignificant (N) differences exist in the parameter means.

APPENDIX III

SIMULATION MATHEMATICAL MODELS AND DATA

SECTION III.1

INTRODUCTION

III.1.1 General

Appendix III defines the simulation used for flight control technology portions of the STOL Tactical Aircraft Investigation. This description includes a discussion of the following topics: simulation operational requirements, the equations of motion, and component mathematical models. These mathematical models describe the aerodynamic characteristics, propulsion system, flight control system, and atmospheric disturbances. Mass and geometry properties of the STOL TAI simulation baseline (model 953-801) are also included in this Appendix. Figure 34 illustrates major elements of the STOL TAI flight simulation. Number in the boxes indicate the appendix section in which that simulation module is described.

III.1.2 Airplane Description

Figure 35 illustrates the simulation baseline configuration. The reference geometry is also called out by Figure 35.

Since the airplane is assumed to be a rigid body, the inertial motion of the center-of-gravity describes the airplane's kinematics. Figure 36 defines the pilot's location relative to the center of gravity and the altitude of the landing gear (h_{MG} and h_{NG}) in terms of h_{cg} and θ. The altitude signal for the television servo is h_{EYE}. The radio altimeter and the barometric altimeter are driven by h_{MG}. When h_{MG} is zero, the airplane is on the ground and the simulator test pilot should get an audio tire squeal signal.

The pitching, rolling, and yawing moment arms for each of the four engines are defined by Figure 37. Moment arms for both the inlet ram force and gross thrust are specified. Numerical values for the 953-801's engine moment arms are defined by Table XIV.

The variation in the airplane's inertias with gross weight is presented by Figure 38.

III.1.3 Equations of Motion, Sign Conventions, Axis Definitions

The airplane equations of motion and the input requirements for the aerodynamic, propulsion, and atmospheric disturbance models are presented by Figure 39. The airplane is initially trimmed by specifying values for the following: V_{T_o}, W, c.g., δ_{TH_o}, S_{x_o}, S_{y_o}, h_o, $u_{shear\ @\ 50'}$ γ_o and Ψ_{GT}. The airplane's heading is determined such that $\phi_o=\beta_o=0$.

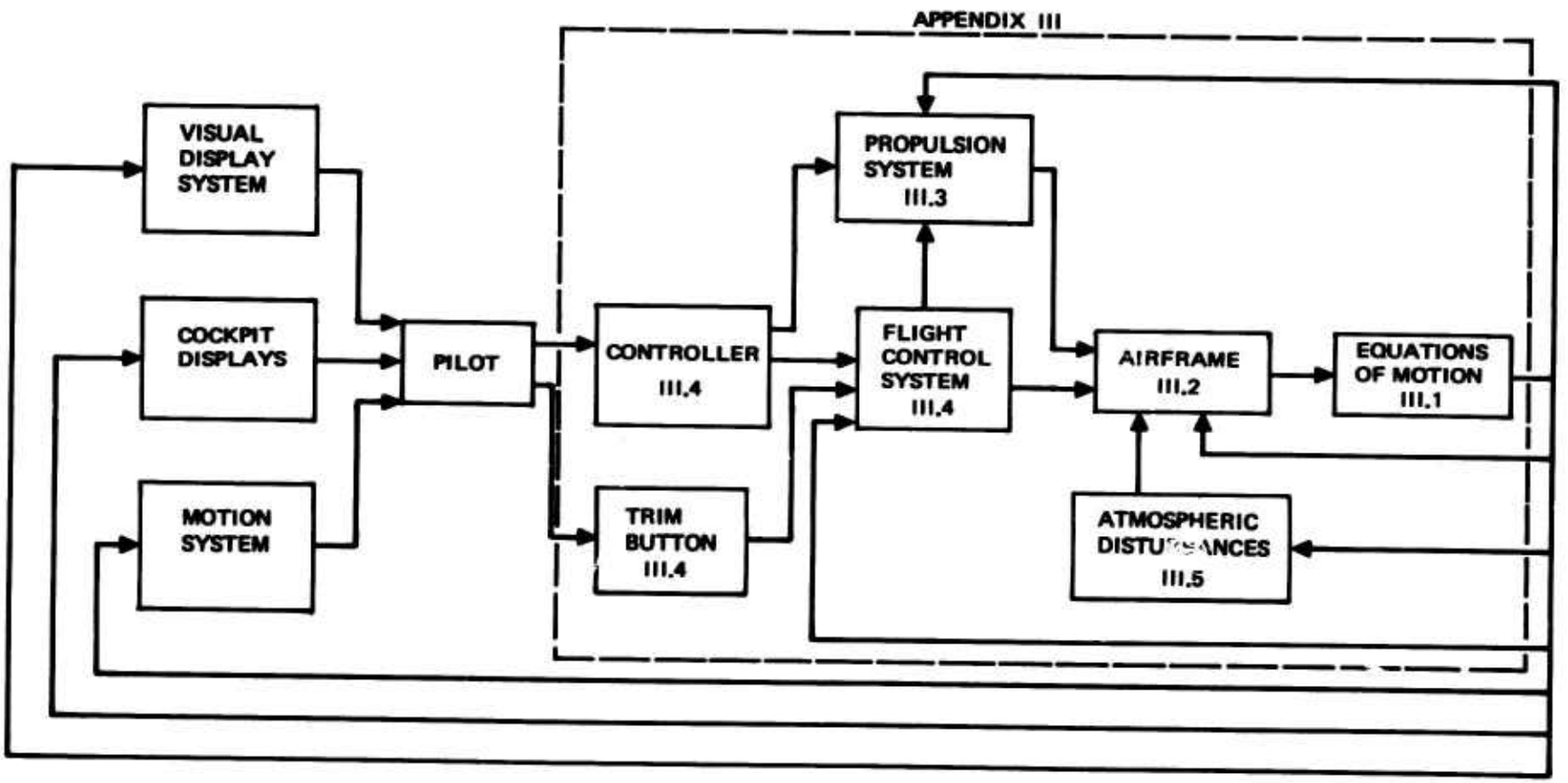

Figure 34: Flight Simulation Block Diagram

Reference Geometry

S_W = 1,840 Ft^2

b_W = 114.5 Ft

$\bar{C}_W$ = 16.7 Ft

S_H = 442.6 Ft^2

ℓ_H = 64 Ft

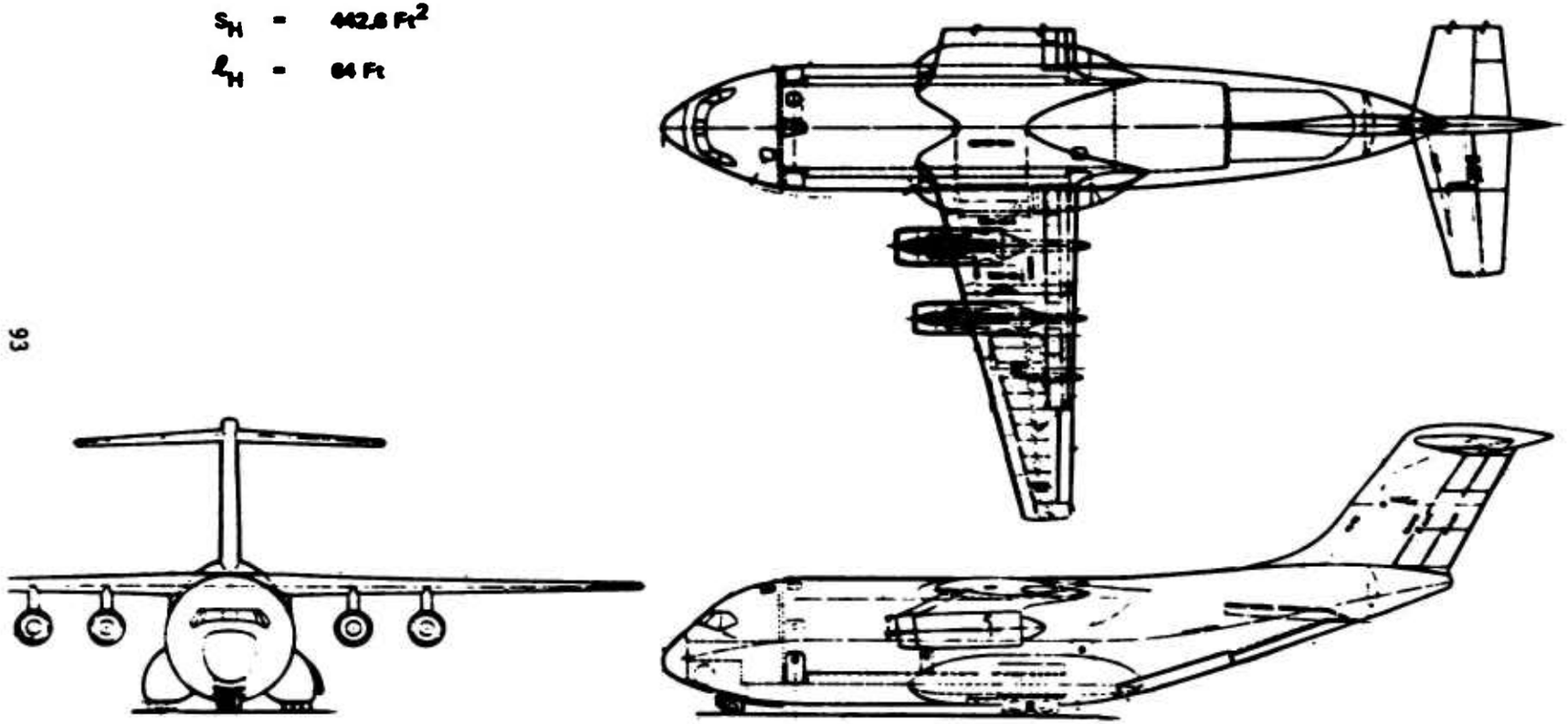

Figure 35: General Arrangement STOL Tactical Transport Model 953-801

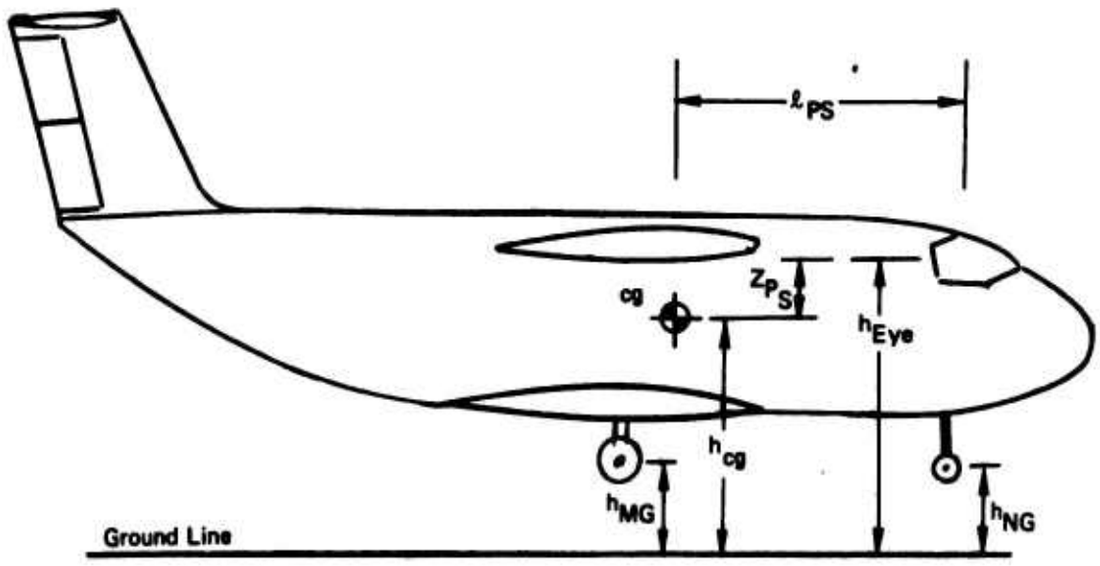

$$h_{Eye} = h_{cg} + 37.5 \sin \ominus$$

$$h_{MG} = h_{cg} - 13.33 - 5.5 \sin \ominus \qquad (h_{MG} > 0)$$

$$h_{NG} = h_{cg} - 13.33 + 36.0 \sin \ominus \qquad (h_{NG} > 0)$$

$$\ell_{PS} = 37.5 + 15.7 \, (cg - .25)$$

$$Z_{PS} = 0$$

Figure 36: Altitude and Pilot Station Geometry

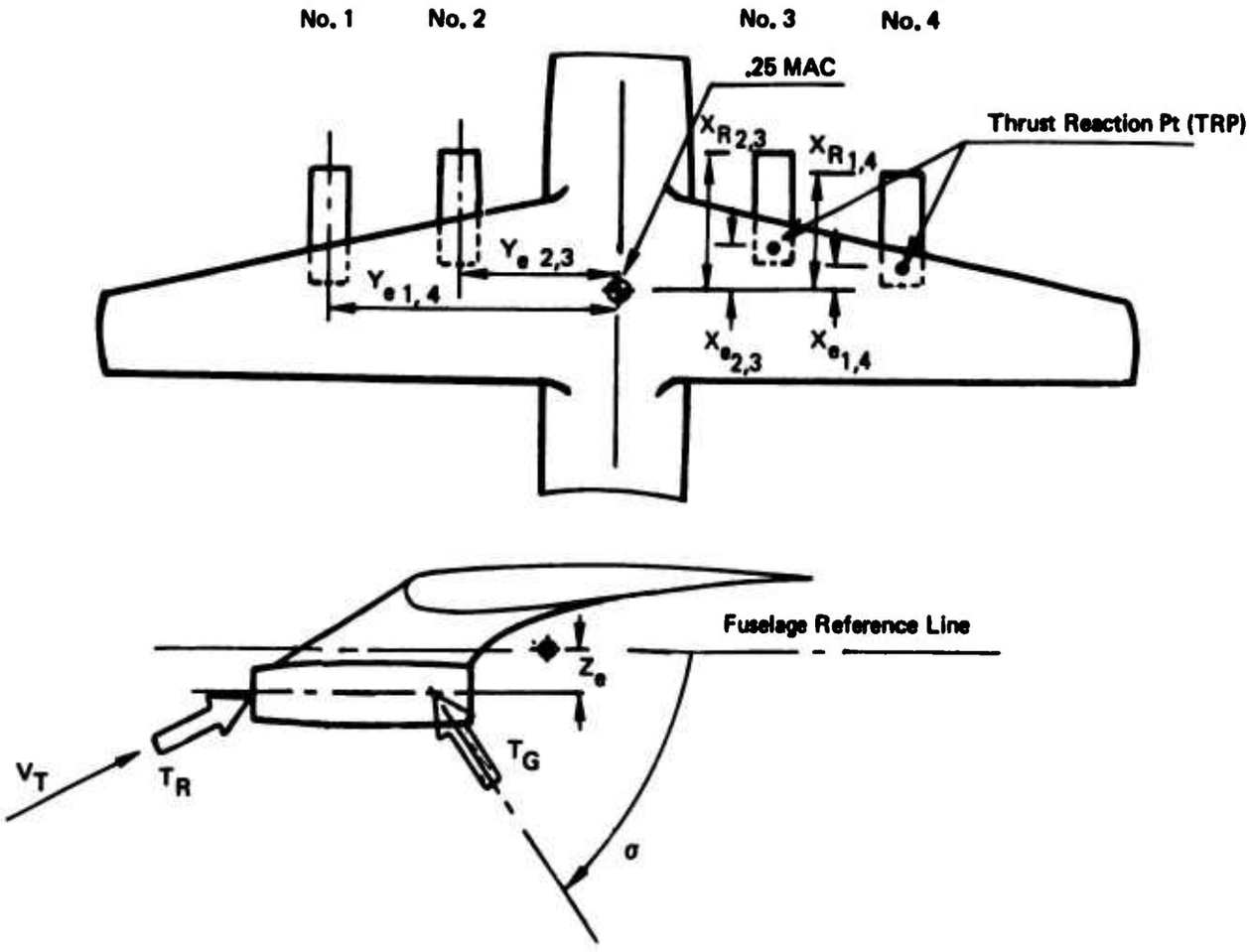

Thurst Moment Arm Sense

- $X_{e_i} > 0$ For TRP Fwd of .25 MAC
- $Y_{e_{1,2}} > 0$; $Y_{e_{3,4}} < 0$
- $Z_{e_i} > 0$ For TRP Below CG
- $X_{R_i} > 0$ For Inlet Fwd of .25 MAC

Figure 37: Vectored Thrust Geometry

TABLE XIV: ENGINE MOMENT ARMS

- Longitudinal Arms

$X_{e_{1,4}}$ = - .25 ft.

$X_{e_{2,3}}$ = 2.0 ft.

$X_{R_{1,4}}$ = 10.42 ft.

$X_{R_{2,3}}$ = 12.67 ft.

- Lateral Arms

Y_{e_1} = 27.33 ft.

Y_{e_2} = 17.17 ft.

Y_{e_3} = -17.17 ft.

Y_{e_4} = - 27.33 ft.

- Vertical Arms

$Z_{e_{1-4}}$ = 1.17 ft.

$Z_{R_{1-4}}$ = 1.75 ft.

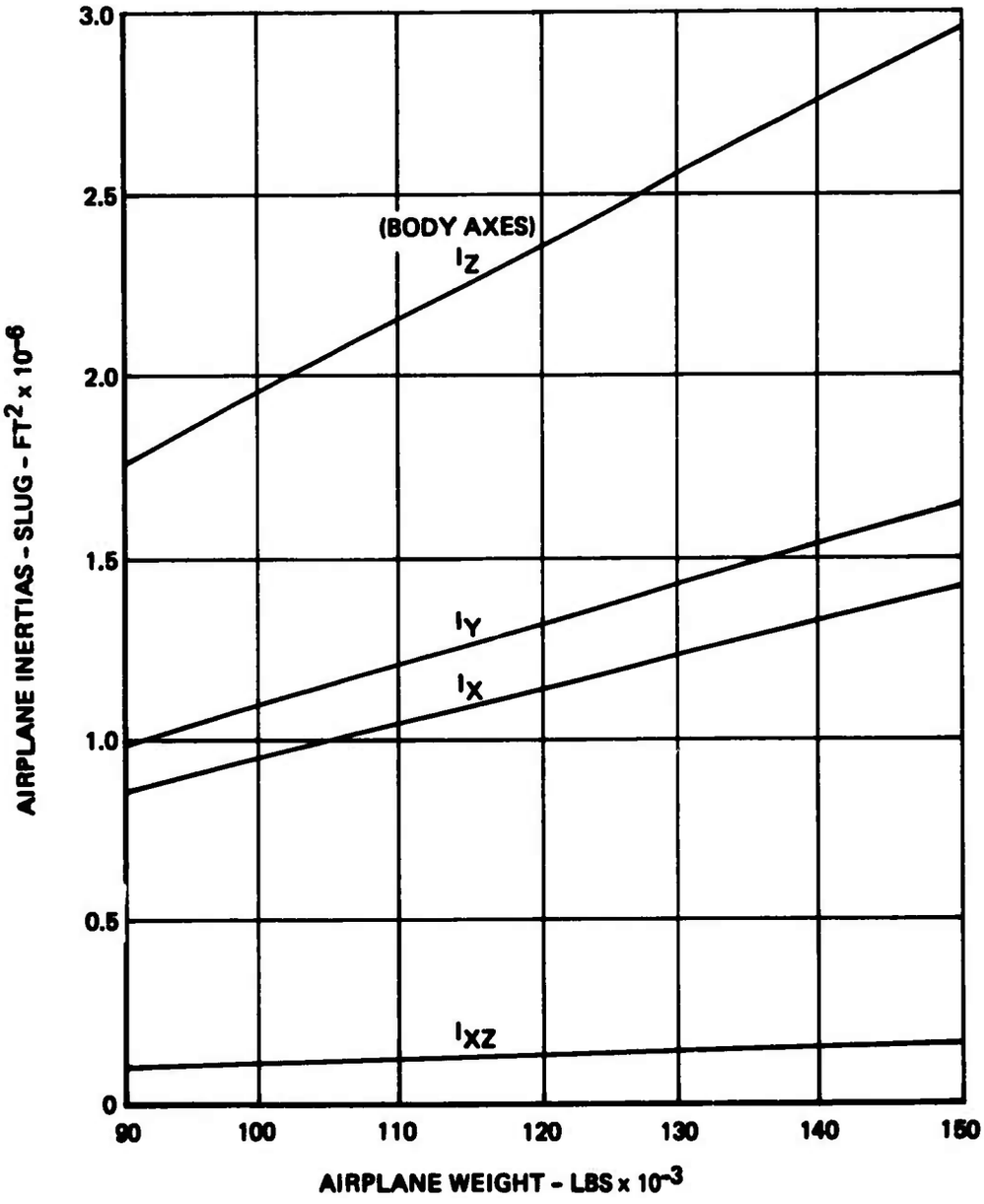

Figure 38: Airplane Inertias

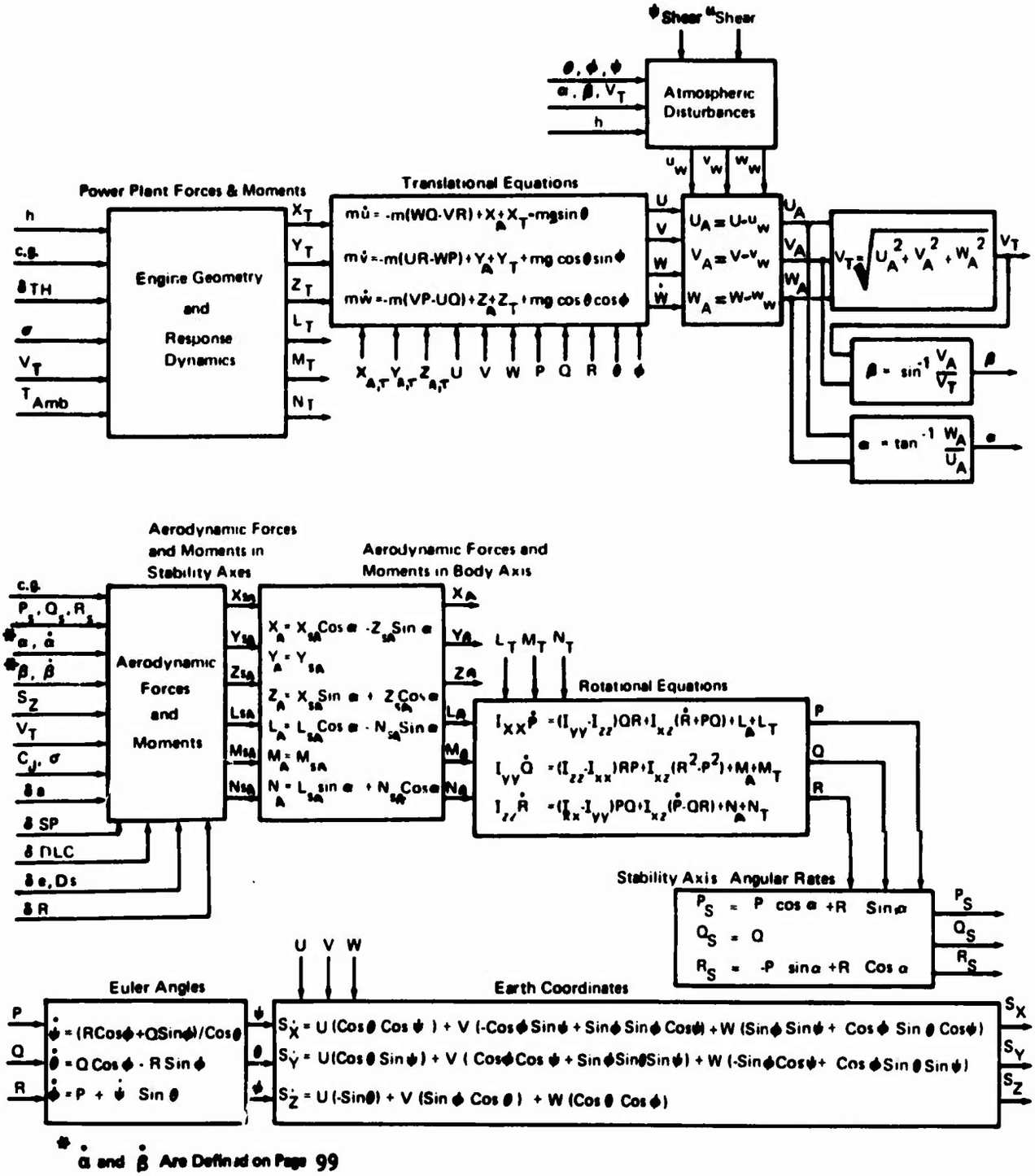

Figure 39: Equations of Motion

The following equation can be used to calculate Ψ_o:

$$\sin\Psi_o - \cos\Psi_o \tan\Psi_{GT} = \frac{U_{SHEAR}}{V_{T_o}\cos\gamma_o}\left[\sin\Psi_{SHEAR} - \cos\Psi_{SHEAR}\tan\Psi_{GT}\right]$$

Figure 40 defines the axes systems that are used throughout this report. The sign convention for body axes forces and velocities are specified by Figure 41. Figure 42 presents the sign convention for control surface deflections and Euler Angles. Figure 43 graphically illustrates the inertial position of the airplane relative to the runway. Since the $\dot{\alpha}$ and β stability derivatives are a quasi-steady representation of an unsteady flow phenomenon, the expressions for $\dot{\alpha}$ and β should not include turbulence velocities. $\dot{\alpha}$ and β are defined by the following equations: (The unsubscripted velocities and acceleration terms are inertial velocities and accelerations, and the subscripted terms are body axes shear velocities.)

$$\dot{\alpha} = \frac{(u-u_{SB})\dot{w} - (w-w_{SB})\dot{u}}{(u-u_{SB})^2} \sim \text{RAD/SEC}$$

$$\dot{\beta} = \frac{\dot{v}}{V_{T'}} - \frac{(v-v_{SB})\dot{V}_{T'}}{V_{T'}^2} \sim \text{RAD/SEC}$$

WHERE

$$V_{T'} = \left[(u-u_{SB})^2 + (v-v_{SB})^2 + (w-w_{SB})^2\right]^{1/2}$$

$$\dot{V}_{T'} \doteq \frac{(u-u_{SB})\dot{u} + (v-v_{SB})\dot{v} + (w-w_{SB})\dot{w}}{V_{T'}}$$

III.1.4 Data Handling

Simulation data fit into one of two categories: tabulated data, or time histories.

Figure 44 defines the "current status hold print." The information contained by the parentheses defines the "hold print" symbology; thus, it is not included on the computer hold print. Control system performance data are specified by Figure 45. A third hold print specified feedback and feedforward transfer function gains, interconnect gains, actuator rate limits, control surface deflection limits, redundancy and failure annunciation, and the flight control system identification number (see Figure 46).

Any variable recorded on the "current status hold print" may be recorded on the strip charts.

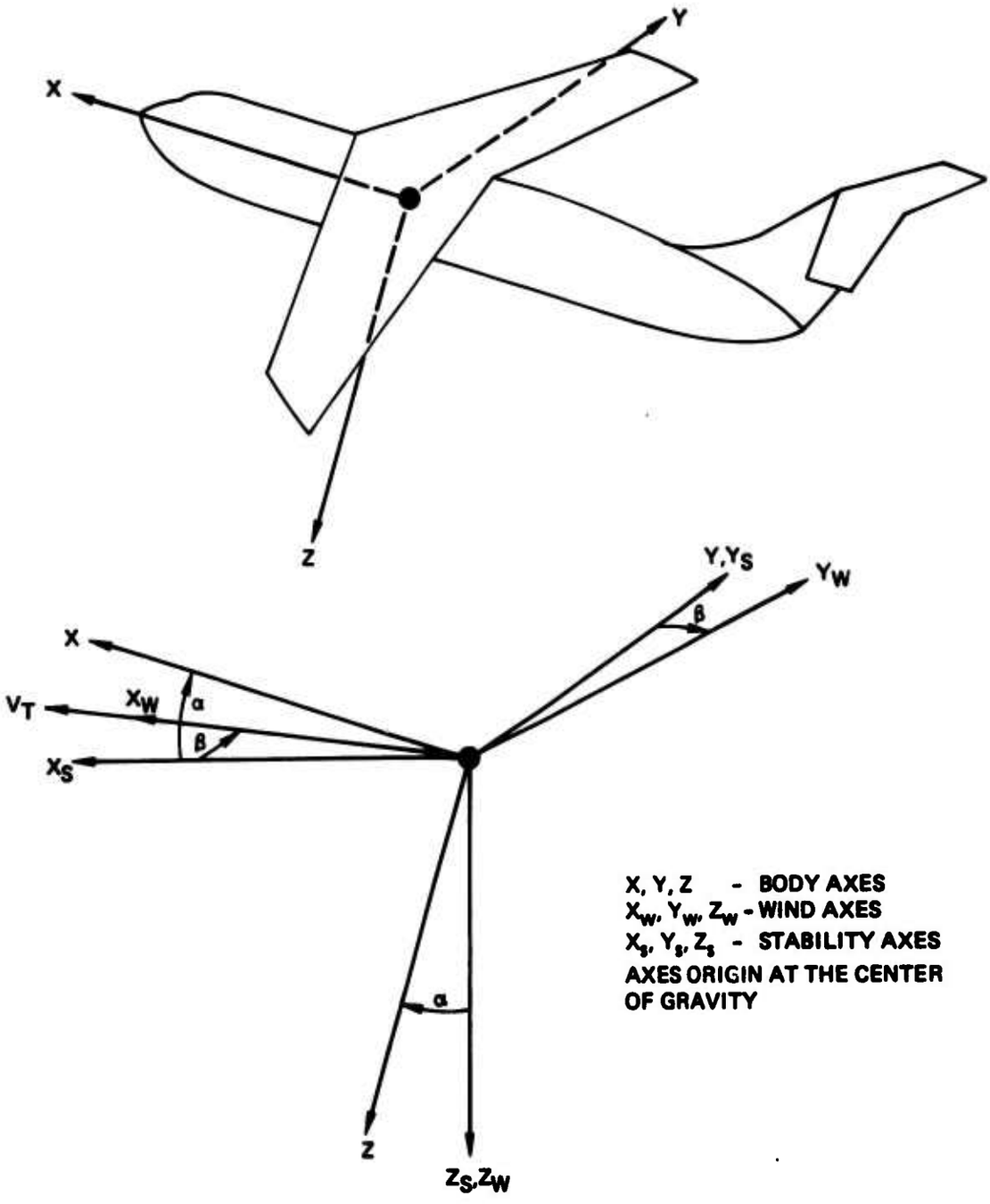

Figure 40: Axes Systems

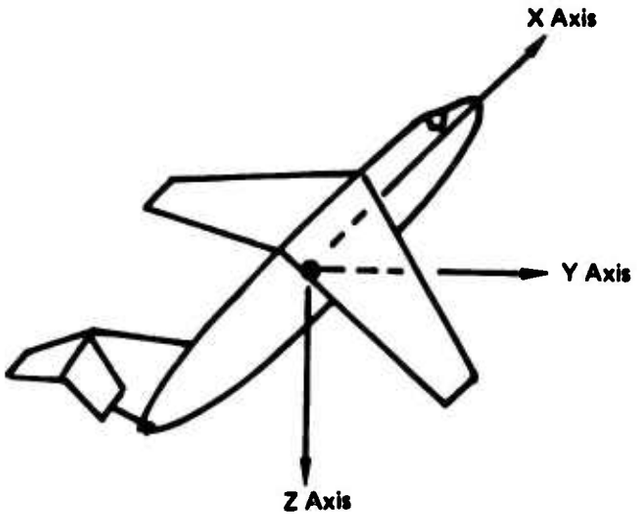

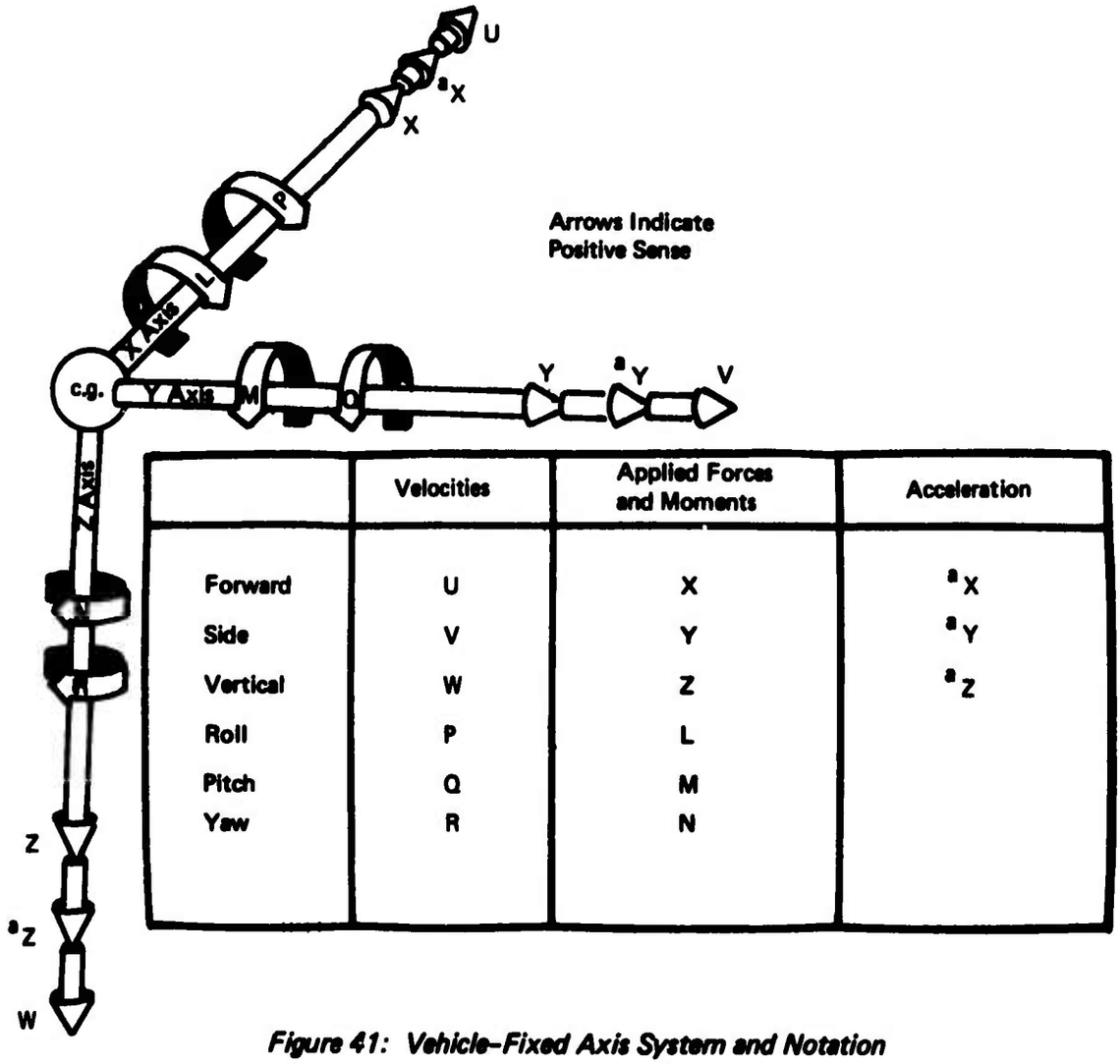

	Velocities	Applied Forces and Moments	Acceleration
Forward	U	X	a_X
Side	V	Y	a_Y
Vertical	W	Z	a_Z
Roll	P	L	
Pitch	Q	M	
Yaw	R	N	

Figure 41: Vehicle-Fixed Axis System and Notation

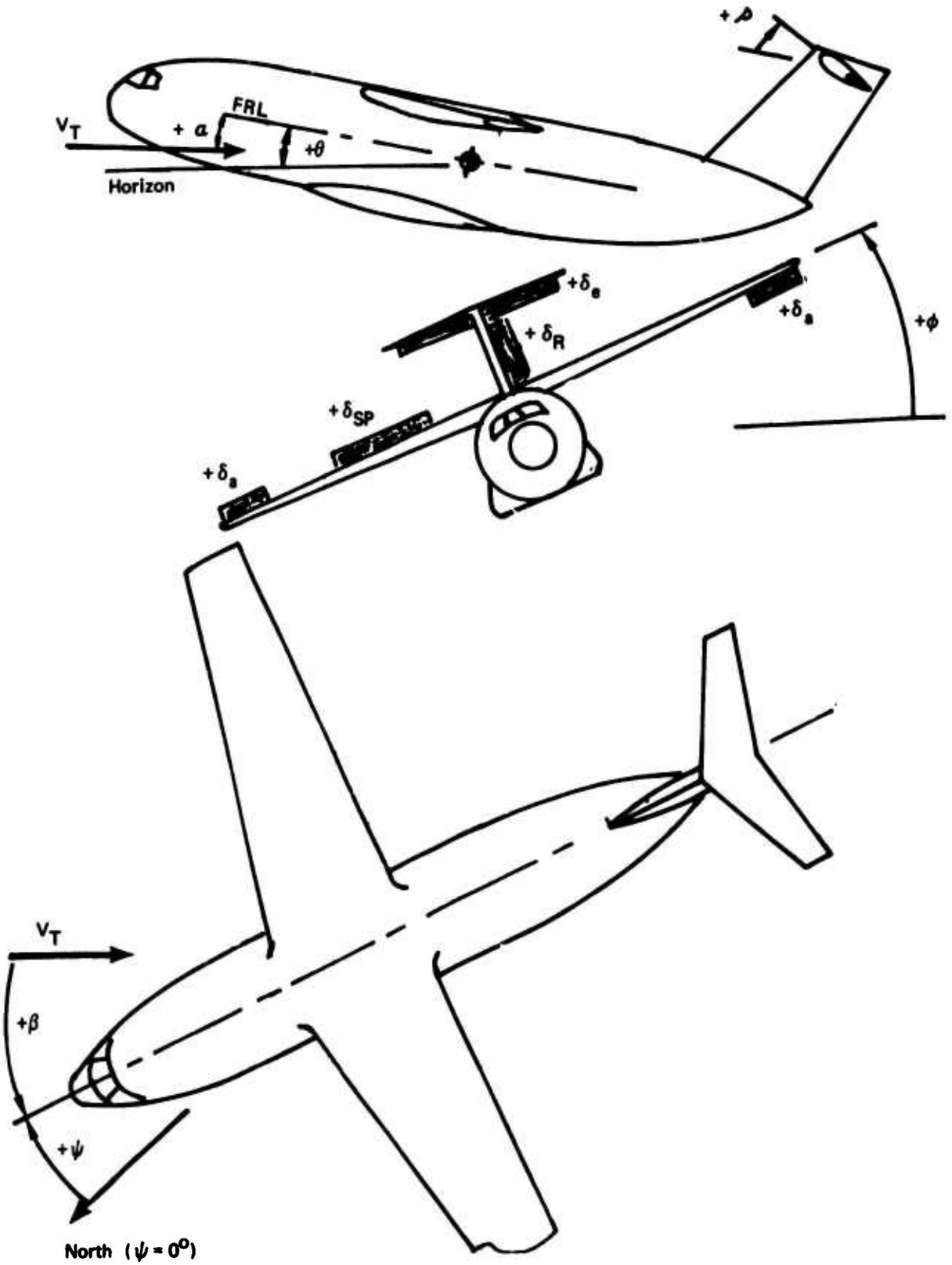

Figure 42: Control Surface and Euler Angle Sign Convention

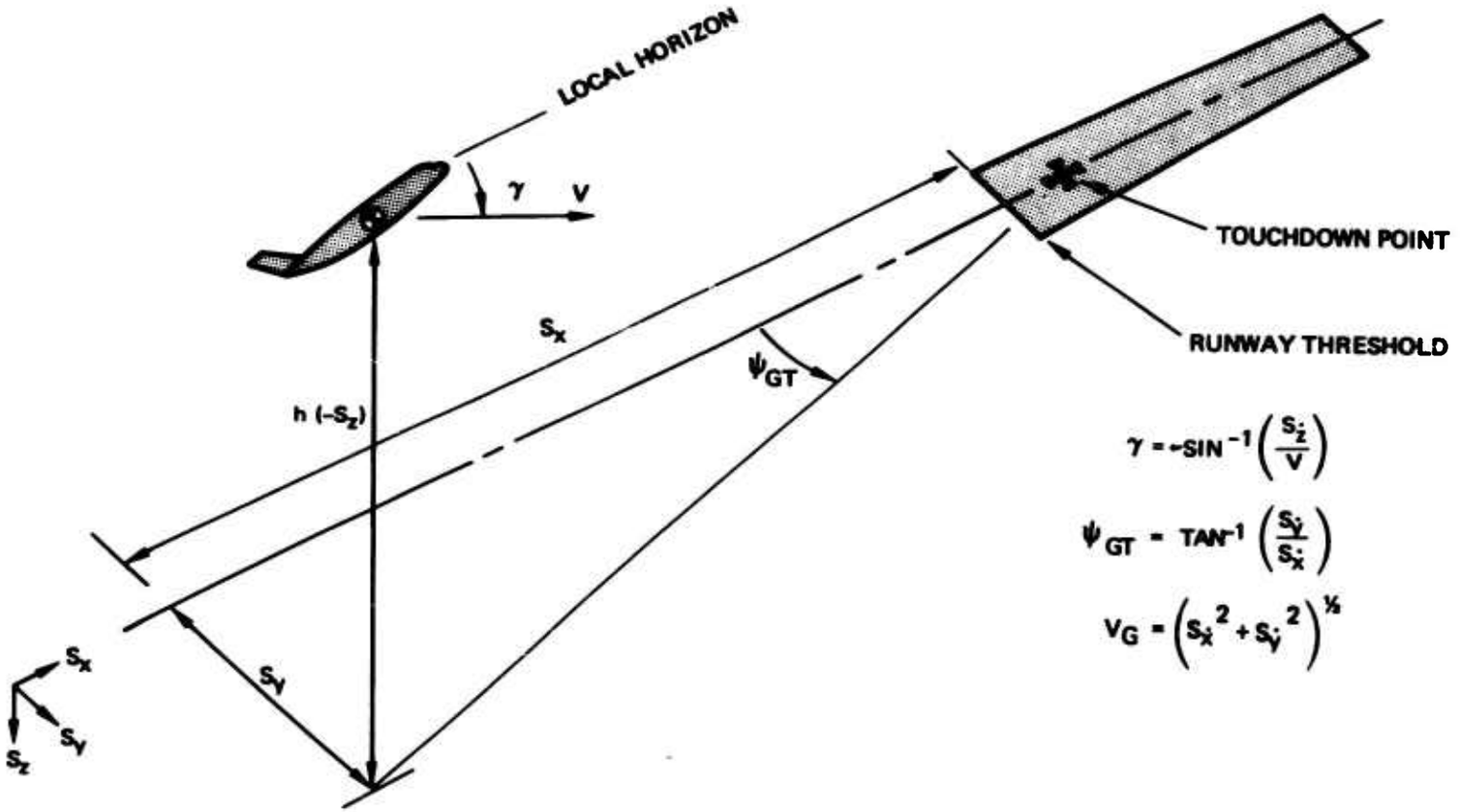

Figure 43: Airplane Inertial Position Description

STOL TAI Date = Elapsed Time = (secs)

CONSTANTS

W =	cg =	IX =	IY =	IZ =	IXZ =

ATMOSPHERIC

Q = ($.5\rho V_T^2$)	RHO = (ρ)	USHEAR = (U_{SHEAR})	PSIW = (Ψ_{SHEAR})		

AERO COEFF

CLIFT = (C_L)	CD = (C_D)	CM = ($C_{m_{cg}}$)	CROLL = (C_ℓ)	CN = ($C_{n_{cg}}$)	CY = (C_y)

CONTROLS

DE = (δ_e)	STAB = (s)	DSPL = (δ_{SP_L})	DFLAP = (δ_{FLAP})	DSIG = ($\delta\sigma$)	DCOL = (δ_{COL})
DAIL = (δ_a)	DR = (δ_R)	DSPR = (δ_{SP_R})	DW = (δ_W)	FSIG = (F_σ)	FCOL = (F_{COL})
			FW = (F_W)	DTH = (δ_{TH})	DP = (δ_p)
				FTH = (F_{TH})	FP = (F_p)

THRUST

TG1 =	MDOT1 =	LT =	XT =		
TG2 =	MDOT2 =	MT =	YT =		
TG3 =	MDOT3 =	NT =	ZT =		
TG4 =	MDOT4 =				
TG = (T_G)	MDOT = ($\dot{m}_a$)	CJ = (C_J)	SIGMA = (σ)		

INERTIAL POSITION

SX =	SY =	h =			

ANGLE

ALB = (α)	THETA = (θ)	GAMMA = (γ_I)	GAMMAP = (γ_{AP})		
BETD = (β)	PHI = (ϕ)	PSI = (Ψ)	PSIGT = (Ψ_{GT})		

RATES AND ACCELERATIONS (Angular Terms Have The Units Of Degrees)

P =	PS = (P_S)	U =	UA = (U_A)	U_w = (Uw)	VT = (V_T)
Q =	QS = (Q_S)	V =	VA = (V_A)	V_w = (Vw)	VE = (V_E)
R =	RS = (R_S)	W =	WA = (V_A)	W_w = (Ww)	VG = (V_G)
ALD = ($\dot{\alpha}$)	PHIDOT = ($\dot{\phi}$)	PDOT = ($\dot{P}$)	UDOT = ($\dot{U}$)	SXD = ($S\dot{x}$)	AX = (a_x)
BETD = ($\dot{\beta}$)	THETDOT = ($\dot{\theta}$)	QDOT = ($\dot{Q}$)	VDOT = ($\dot{V}$)	SYD = ($S\dot{y}$)	AY = (a_y)
GAMDOT = ($\dot{\gamma}_I$)	PSIDOT = ($\dot{\Psi}$)	RDOT = ($\dot{R}$)	WDOT = ($\dot{W}$)	HD = ($\dot{h}$)	AZ = (a_z)

FIGURE 44: CURRENT STATUS HOLD PRINT

FIGURE 45: CONTROL SYSTEM PERFORMANCE DATA

DATE = FCS NO. = RUN NO. =

Initial Condition:

W =	Altitude (h) =	Ground Track (Ψ_{GT}) =
cg =	Lateral Disp. (S_Y) =	Shear Velocity (u_{SHEAR}) =
V_T =	Thrust Command (T_G) =	Shear Angle (Ψ_{SHEAR}) =
γ =	Vector Angle ( ) =	Turbulence (σ_{TURB}) Intensity =

Pilot Work Load: σ ( ) = RMS ( )

Total		Tracking	
$\sigma\delta_{COL}$ =	$\sigma\delta_{TH}$ =	$\sigma\delta_{COL}$ =	$\sigma\delta_{TH}$ =
$\sigma\delta_W$ =	$\sigma\delta_\sigma$ =	$\sigma\delta_W$ =	$\sigma\delta_\sigma$ =
$\sigma\delta_P$ =		$\sigma\delta_P$ =	

Control Surface Activity: σ ( ) = RMS ( )

$\sigma\delta_{DLC}$ =	σT_G =	$\sigma\delta_a$ =	$\sigma\delta_R$ =
$\sigma\delta_e$ =	$\sigma\sigma$ =	$\sigma\delta_{SP}$ =	

Tracking Performance: σ ( ) = RMS ( )

Glide Slope Error ($\sigma\epsilon_{GS}$) = Airspeed Error ($\sigma\epsilon_{V_T}$) =

Ground Track Error ($\sigma\epsilon_{GT}$) =

Touchdown Data:

S_X =	S_y =	Ψ_{GT} =	V_G =
V_T =	$\dot{h}$ =	$S_y^{\cdot}$ =	

Maximums:

Total			Below 300 Ft.		
α_{MAX} =	$\dot{P}_{MAX}$ =	δe_{MAX} =	α_{MAX} =	$\dot{P}_{MAX}$ =	δe_{MAX} =
β_{MAX} =	$\dot{Q}_{MAX}$ =	δa_{MAX} =	β_{MAX} =	$\dot{Q}_{MAX}$ =	δa_{MAX} =
ϕ_{MAX} =	$\dot{R}_{MAX}$ =	δSP_{RMAX} =	ϕ_{MAX} =	$\dot{R}_{MAX}$ =	δSP_{RMAX} =
P_{MAX} =	$A_{Y_{MAX}}$ =	δSP_{LMAX} =	P_{MAX} =	$A_{Y_{MAX}}$ =	δSP_{LMAX} =
Q_{MAX} =	$A_{Z_{MAX}}$ =	δR_{MAX} =	Q_{MAX} =	$A_{Z_{MAX}}$ =	σ_{MAX} =
R_{MAX} =		σ_{MAX} =	R_{MAX} =		σ_{MIN} =
		σ_{MIN} =			

FIGURE 46: CONTROL SYSTEM DESCRIPTION

CONTROL LAW GAINS

Longitudinal (FCS No.)			Lateral/Directional (FCS No.)		
K_1 =	K_{11} =	G_1 =	K_1 =	K_{11} =	G_1 =
K_2 =	K_{12} =	G_2 =	K_2 =	K_{12} =	G_2 =
K_3 =	K_{13} =	G_3 =	K_3 =	K_{13} =	G_3 =
K_4 =	K_{14} =	G_4 =	K_4 =	K_{14} =	G_4 =
K_5 =	K_{15} =	G_5 =	K_5 =	K_{15} =	G_5 =
K_6 =	K_{16} =	G_6 =	K_6 =	K_{16} =	G_6 =
K_7 =	K_{17} =		K_7 =	K_{17} =	
K_8 =	K_{18} =		K_8 =	K_{18} =	
K_9 =	K_{19} =		K_9 =	K_{19} =	
K_{10} =	K_{20} =		K_{10} =	K_{20} =	

CONTROL SYSTEM STATUS

Control Surface	Status*	Electrical Authority	Mechanical Authority	Rate Limit
Stabilizer	nxxxxxxxx			
Elevator				
Left Wing Spoiler				
Right Wing Spoiler				
Aileron				
Rudder				
Thrust Vector				
Angle				

*n = number of operating channels

*x = switch status: i.e., 1: closed, 0: open

SECTION III.2

AERODYNAMIC PROPERTIES

III.2.1 General

The external aerodynamic loads are simulated by continuously solving the six aerodynamic force and moment equations. These equations are expressed in non-dimensional form and are defined for a stability axes system. The effects of altitude, airplane attitude, rotational rates, control deflections, and the engine's flow field on the aerodynamic loads are accounted for separately in each equation. Figure 47 summarizes the input and output properties of the aerodynamic module.

The following expressions relate the aerodynamic, non-dimensional coefficients to the aerodynamic forces and moments, which appear in the equations of motion.

$$X_{SA} = -.5\,\rho\, V_T^2\, S_w\, C_D \qquad \text{slug-ft/sec}^2$$

$$Y_{SA} = .5\,\rho\, V_T^2\, S_w\, C_y \qquad \text{slug-ft/sec}^2$$

$$Z_{SA} = -.5\,\rho\, V_T^2\, S_w\, C_L \qquad \text{slug-ft/sec}^2$$

$$L_{SA} = .5\,\rho\, V_T^2\, S_w\, b_w\, C_\ell \qquad \text{slug-ft}^2/\text{sec}^2$$

$$M_{SA} = .5\,\rho\, V_T^2\, S_w\, \bar{c}_w\, C_{m_{cg}} \qquad \text{slug-ft}^2/\text{sec}^2$$

$$N_{SA} = .5\,\rho\, V_T^2\, S_w\, b_w\, C_{n_{cg}} \qquad \text{slug-ft}^2/\text{sec}^2$$

Section III.2.2 describes the aerodynamic module which was used for the conceptual control law phase. These data are based on a series of low-speed wind tunnel tests (Ref. 2 and 13) of STOL configurations, which are similar to the 953-801. References 3 and 4 have been used to correct for configurational differences between the wind tunnel model and the -801. The lift, drag, and pitching moment characteristics of the drooped, BLC aileron are based on Reference 5. The influence of ground proximity on the lift, drag, and pitching moment characteristics are based on the methods presented by References 6 and 7.

The digital computer program described by Reference 8 was used to calculate the lateral-directional dynamic stability derivatives.

Section III.2.3 describes the aerodynamic module which was used for the mechanization and the validation phases. The mathematical model was modified to simplify the incorporation of STOL TAI wind tunnel data.

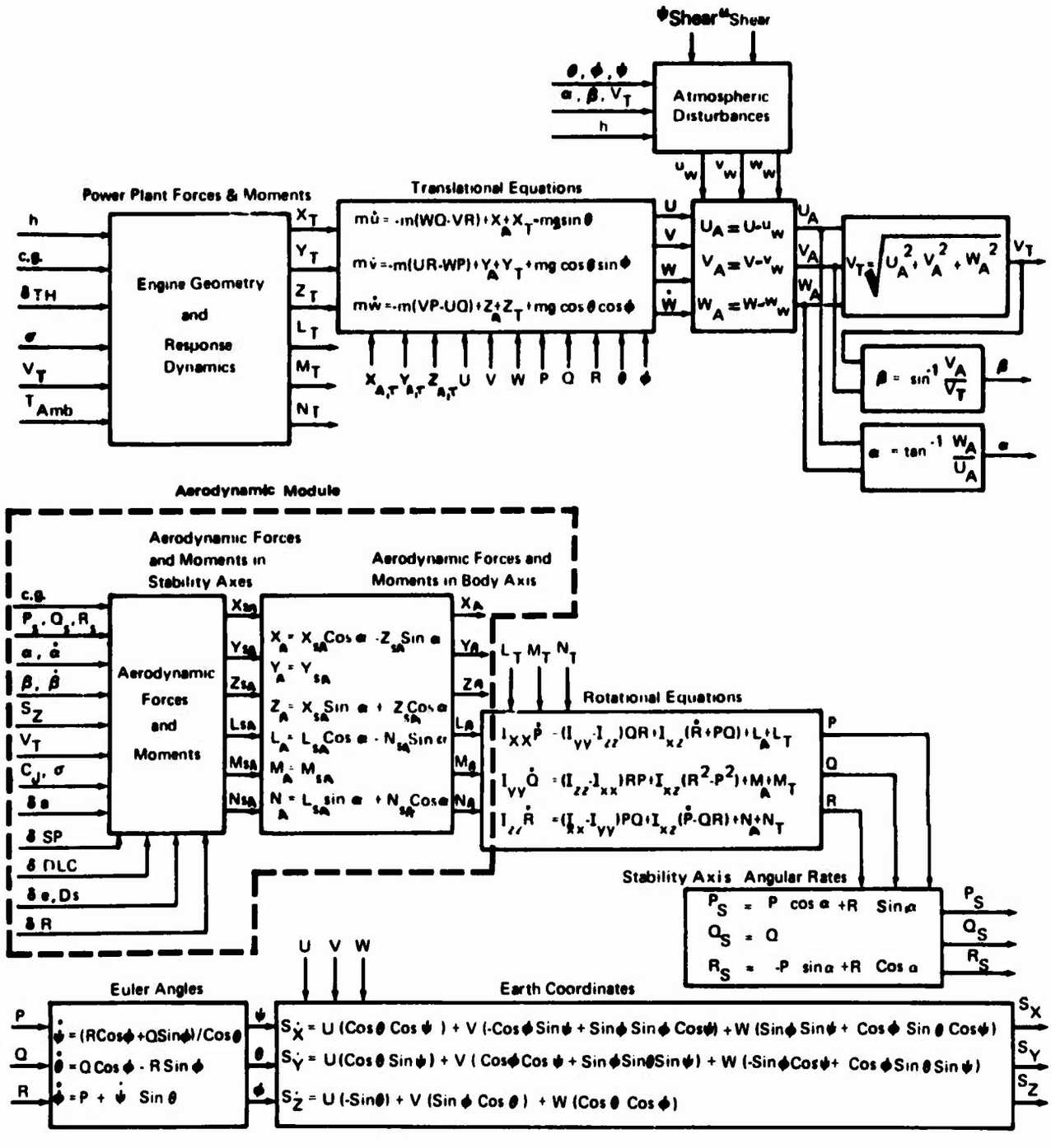

Figure 47: Equation of Motion : Aerodynamic Module

For the mechanization phase, the induced aerodynamic terms (e.g., $\Delta C_{L_{WBC_J \neq 0}}$) were set equal to zero for increments (or one for ratios) since these data were not available when the aerodynamic model was updated. For the validation phase, the simulation included all induced aerodynamic terms presented in this section.

III.2.2 Aerodynamic Module: Conceptual Control Law Phase

III.2.2.1 Lift Equation

The dimensionless aerodynamic lift force of the airplane is separated into its important contributing elements in the equation below.

$$C_L = C_{L_{BASIC}} + C_{L_{\hat{\dot{\alpha}}}} \frac{\dot{\alpha}\bar{c}}{2V_T} + C_{L_{\hat{q}}} \frac{q\bar{c}}{2V_T} + \Delta C_{L_{TAIL}} + \Delta C_{L_{SIDESLIP}} + \Delta C_{L_{LAT}}$$

where:

$C_{L_{BASIC}}$ = Basic lift coefficient for airplane in steady "1g" flight with the stabilizer and elevator set for zero deflection. $C_{L_{BASIC}}$ if a function of α_B and h; $C_{L_{BASIC}}$ is presented by Figure 48.

$C_{L_{\hat{\dot{\alpha}}}} \frac{\dot{\alpha}\bar{c}}{2V_T}$ = Variation in $C_{L_{BASIC}}$ due to rate of change of angle of attack; $C_{L_{\hat{\dot{\alpha}}}} = -8.18$ 1/RAD.

$C_{L_{\hat{q}}} \frac{q\bar{c}}{2V_T}$ = Variation in $C_{L_{BASIC}}$ due to airplane pitch rate; $C_{L_{\hat{q}}} = 7.54$ 1/RAD.

$\Delta C_{L_{TAIL}}$ = Change in $C_{L_{BASIC}}$ due to changes in stabilizer and elevator angles from $\delta = 0°$ and $\delta_e = 0°$.

$$\Delta C_{L_{TAIL}} = \frac{S_H}{S_w} \left[(C_{L_{TAIL}})_{\substack{\delta=0 \\ \delta_e=0}} - (C_{L_{TAIL}})_{\substack{\delta\neq 0 \\ \delta_e=0}} + (\Delta C_{L_{TAIL}})_{\delta_e} \right]$$

where

$\frac{S_H}{Sw}$ = ratio of horizontal tail area to wing area.

$(C_{L_{TAIL}})_{\delta_e=0}$ = horizontal tail lift coefficient with $\delta_e = 0°$; $(C_{L_{TAIL}})_{\delta_e=0}$ is defined by Figure 49.

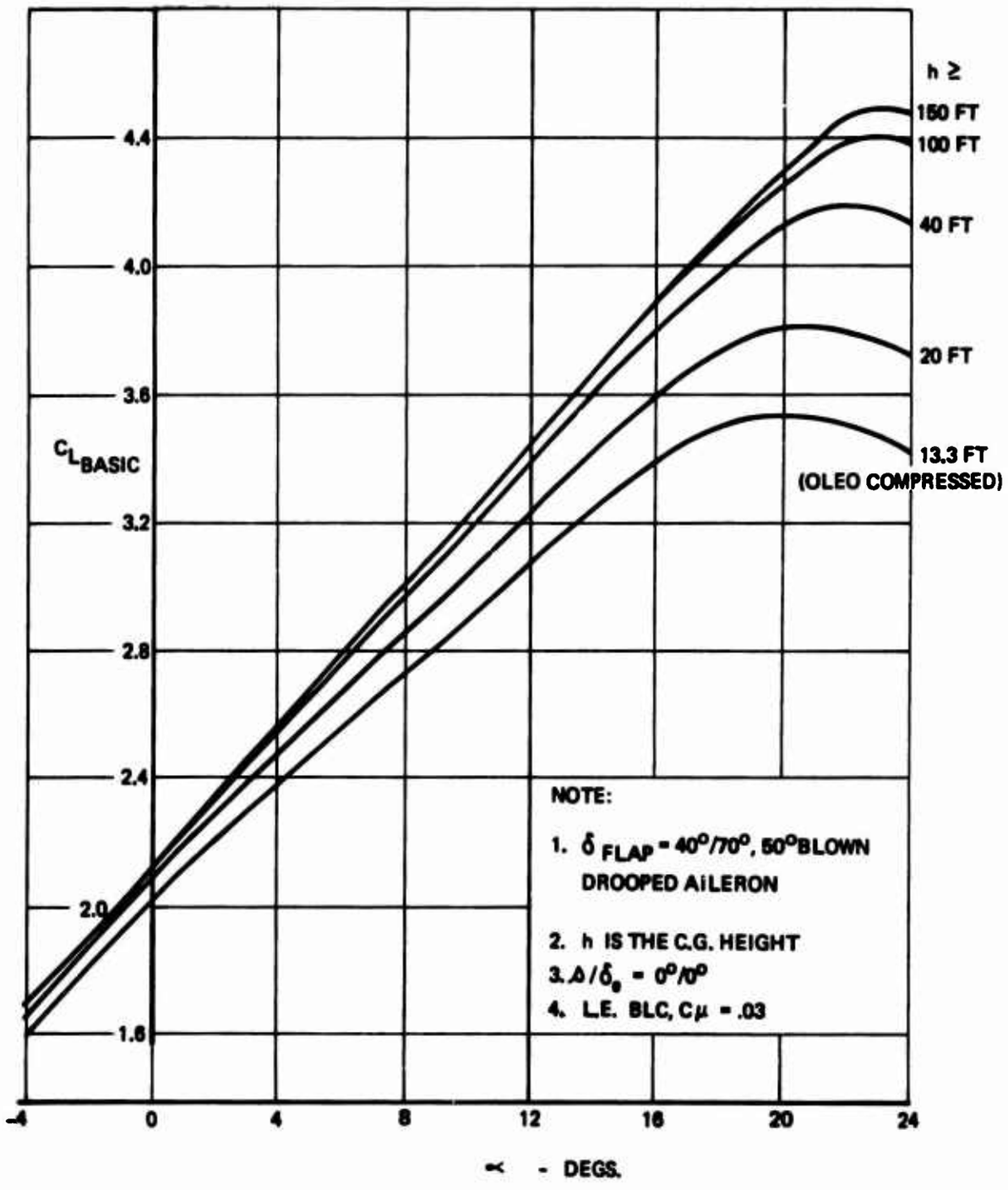

Figure 48: Lift Coefficient: Effect of α on $C_{L_{Basic}}$

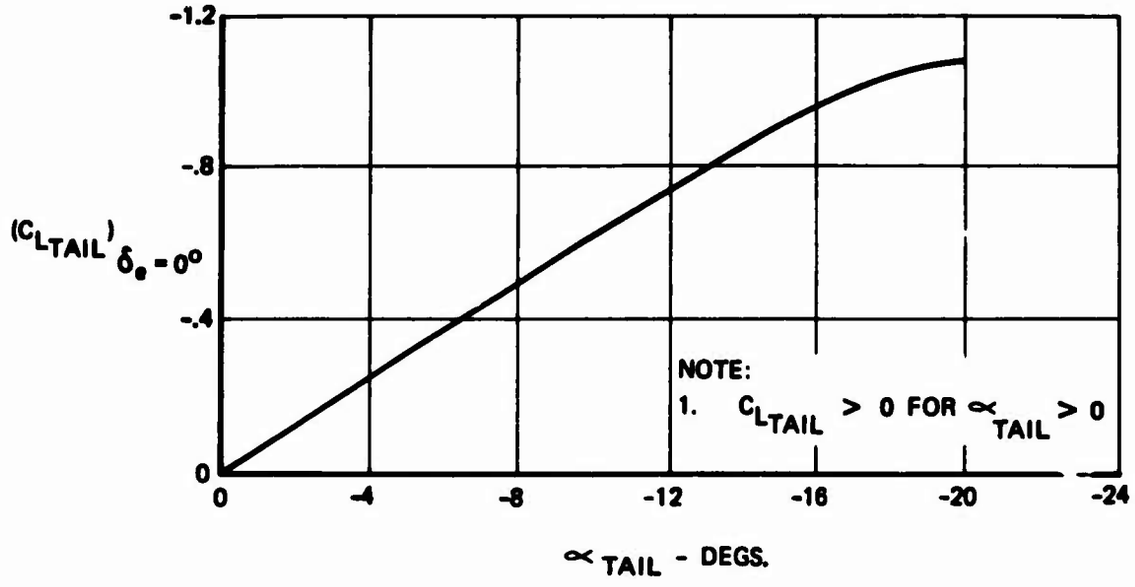

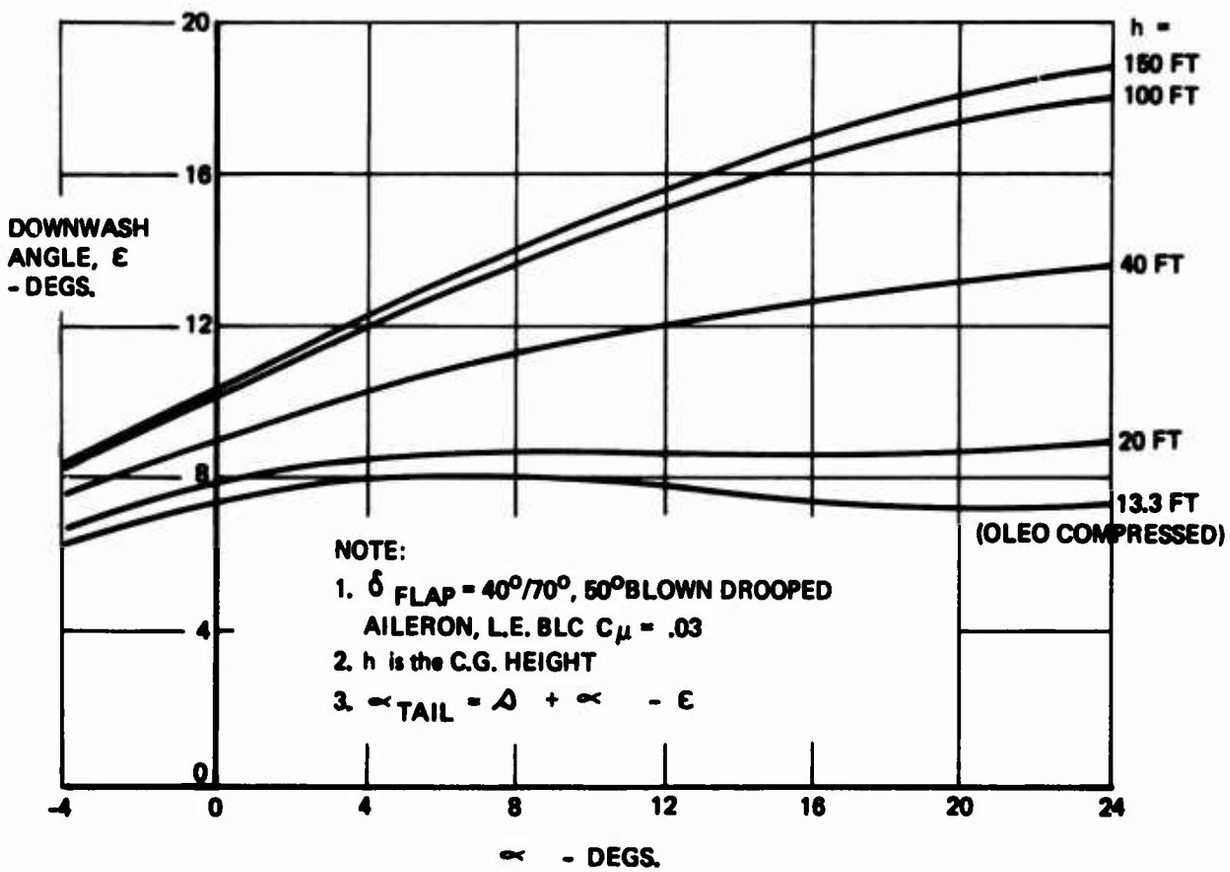

Figure 49: Horizontal Tail Lift ($\delta_e = 0^o$) and Downwash

$(\Delta C_{L_{TAIL}})_{\delta_e}$ = Change in horizontal tail lift due to elevator deflection. $(\Delta C_{L_{TAIL}})_{\delta_e}$ is a function of horizontal load, $|C_{L_{TAIL}}|_{\delta_e=0°}$ and δ_e as defined by Figure 50.

$\Delta C_{L_{SIDESLIP}}$ = Change in $C_{L_{BASIC}}$ due to flying at an angle of sideslip. $C_{L_{SIDESLIP}}$ is presented as a function of β by Figure 51.

$\Delta C_{L_{LAT}}$ = Change in $C_{L_{BASIC}}$ due to lateral control deflection. $C_{L_{LAT}}$ is a function of α and the control deflection angle; $\Delta C_{L_{LAT}}$ is presented by Figure 52.

III.2.2.2 Drag Equation

The dimensionless aerodynamic drag force is separated into its important contributing elements in the equation below.

$$C_D = C_{D_{BASIC}} + \Delta C_{D_{SIDESLIP}} + \Delta C_{D_{LAT}} + \Delta C_{D_{RUD}} + \Delta C_{D_{ELEV}}$$

where:

$C_{D_{BASIC}}$ = Basic drag coefficient of the airplane in the landing configuration and with all control devices faired. $C_{D_{BASIC}}$ is presented by Figure 53 as a function of α and h.

$\Delta C_{D_{SIDESLIP}}$ = Change in $C_{D_{BASIC}}$ due to flying at an angle of sideslip. $\Delta C_{D_{SIDESLIP}}$ is presented by Figure 51 as a function of β.

$\Delta C_{D_{LAT}}$ = Increment in $C_{D_{BASIC}}$ due to lateral control deflection. $\Delta C_{D_{LAT}}$ is a function of α and the lateral control deflection angle, and it is presented by Figure 54.

$\Delta C_{D_{RUD}}$ = Change in $C_{D_{BASIC}}$ due to rudder deflection. $\Delta C_{D_{RUD}}$ is plotted as a function of β and δ_R by Figure 55.

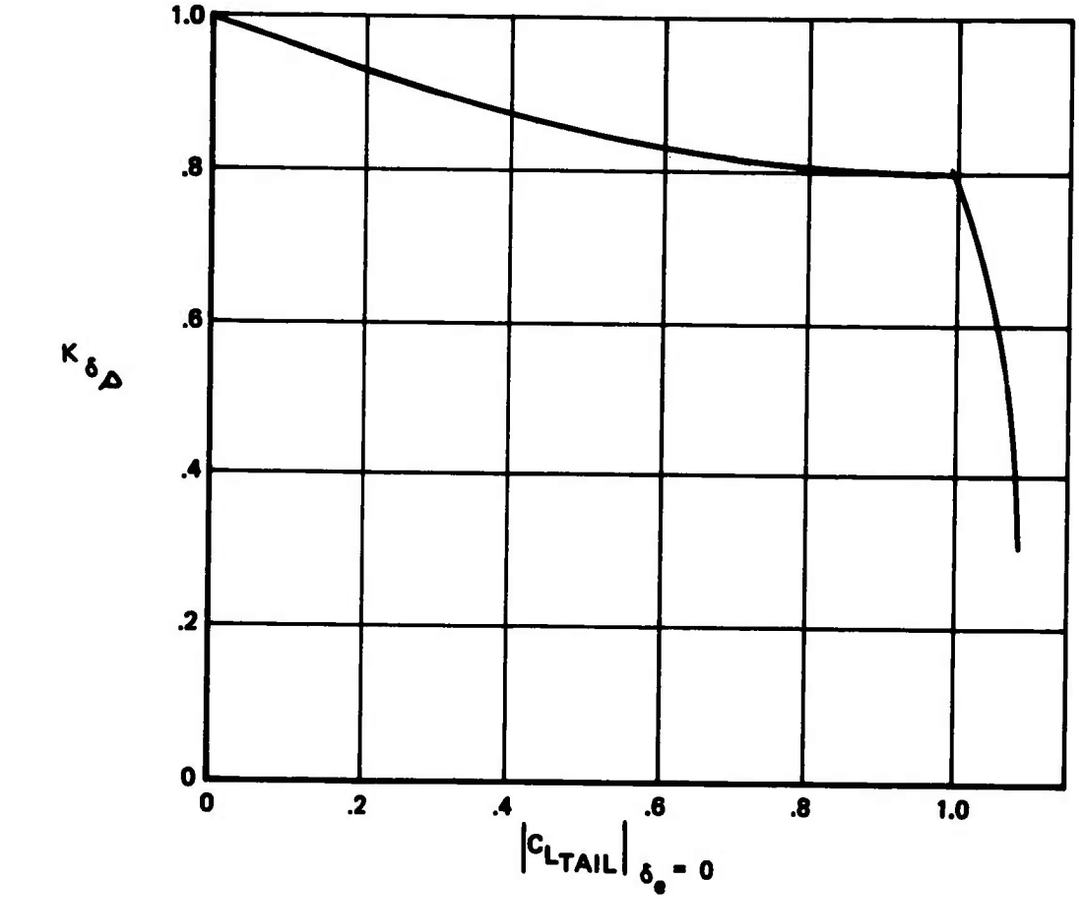

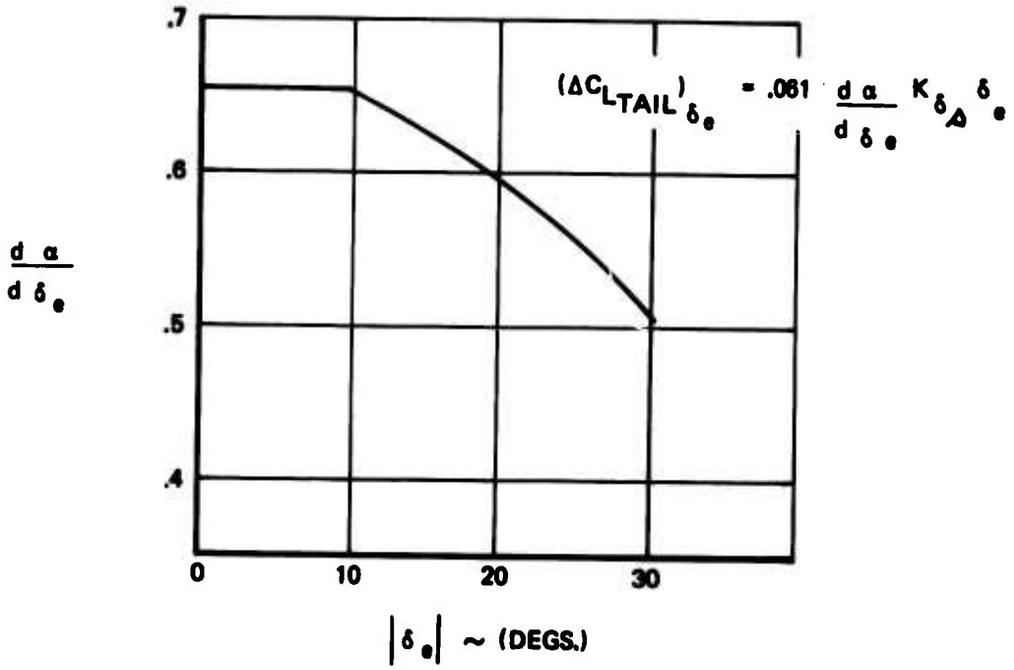

Figure 50: Change in Horizontal Tail Lift Due to Elevator Deflection

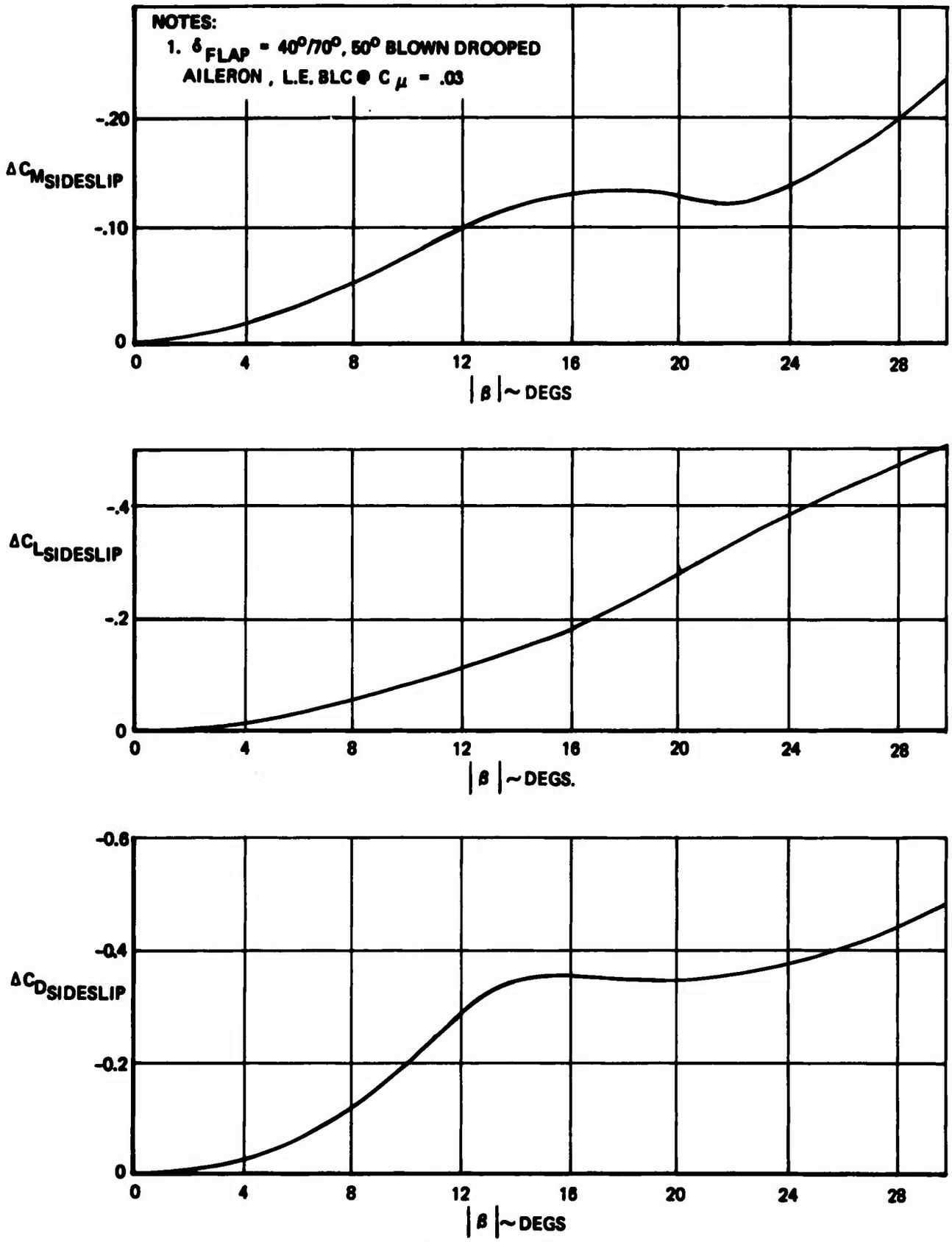

Figure 51: Change in the Lift, Drag, and Pitching Moment Coefficients Due to Sideslip

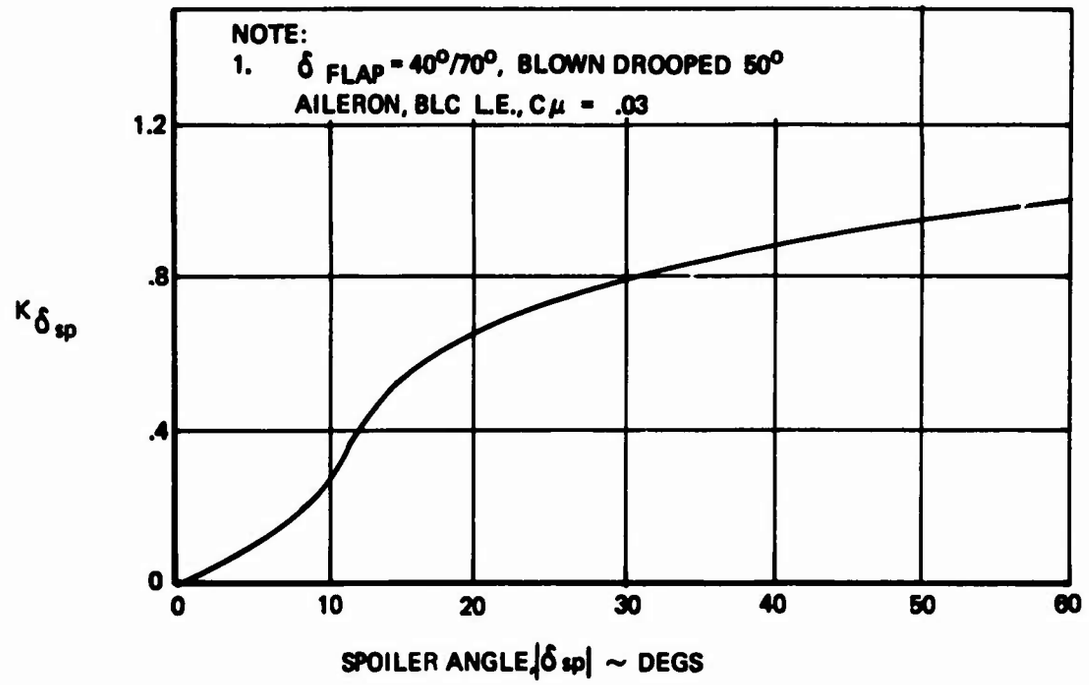

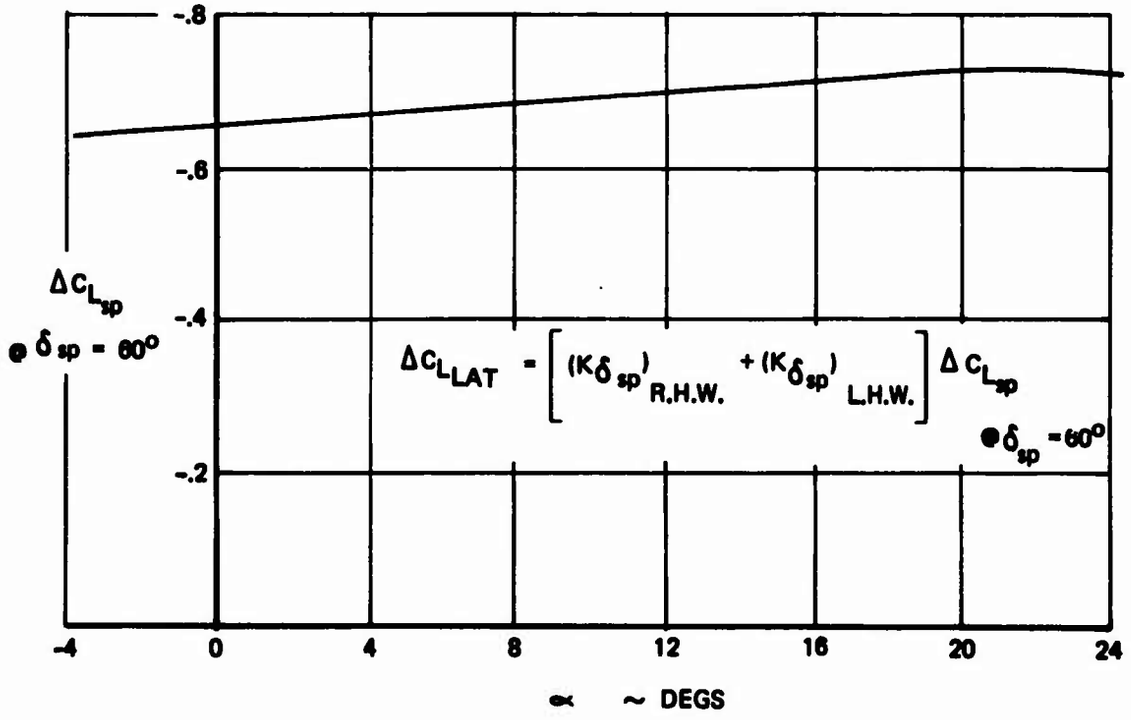

Figure 52: Lift Coefficient : Effect of Lateral Control

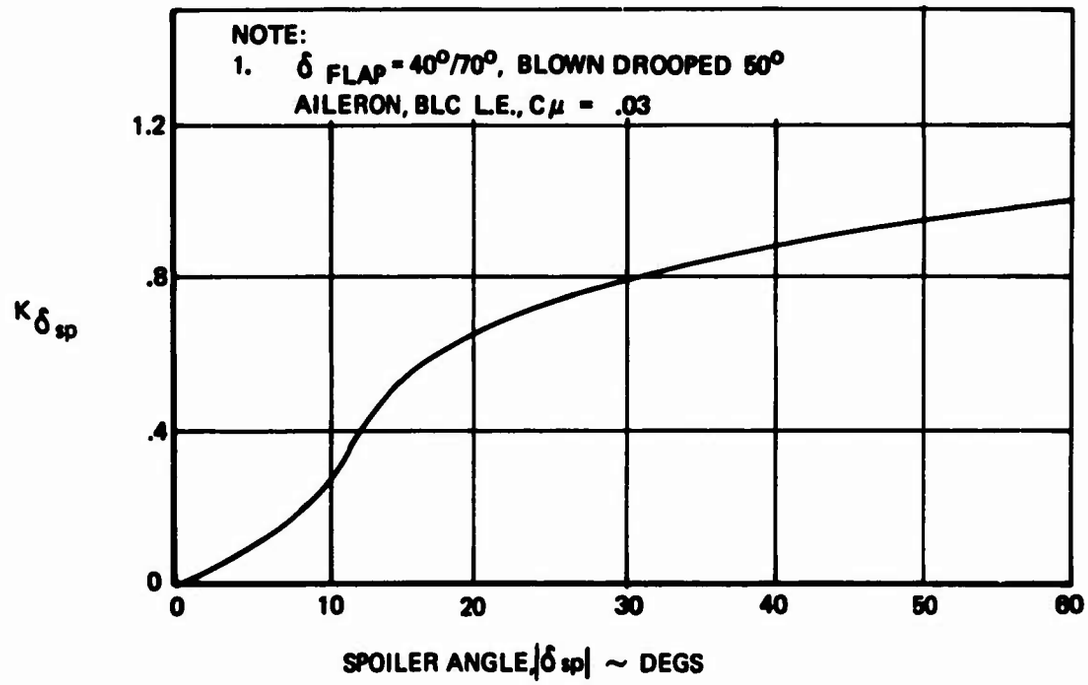

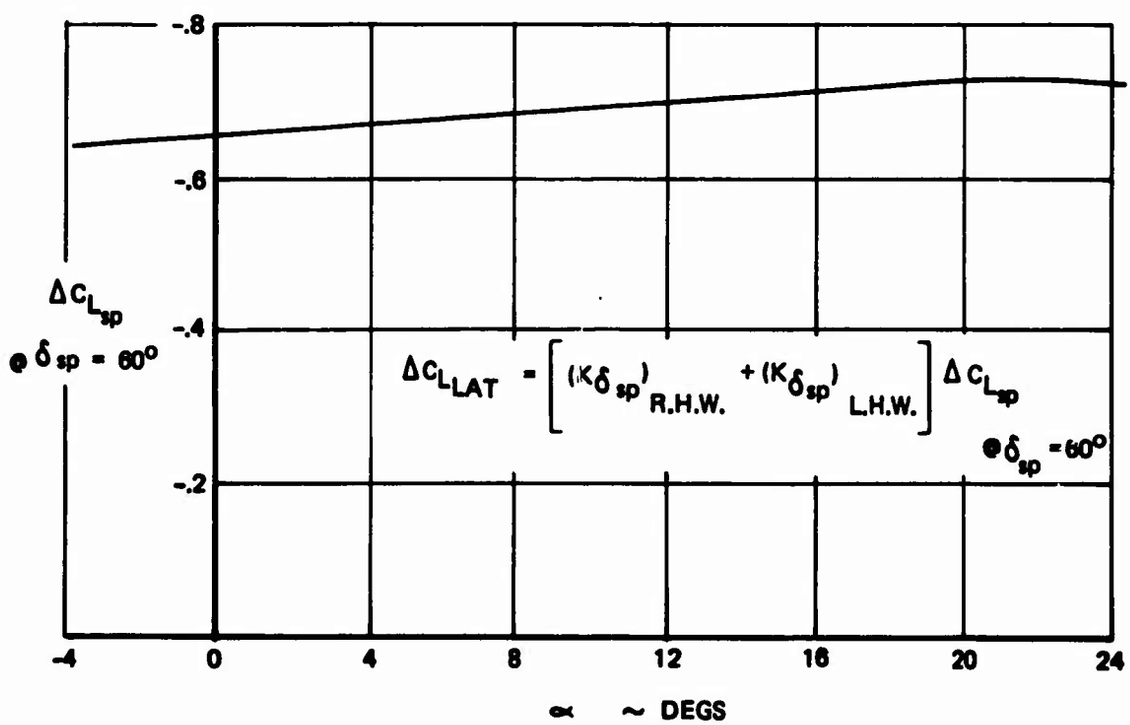

Figure 52: Lift Coefficient : Effect of Lateral Control

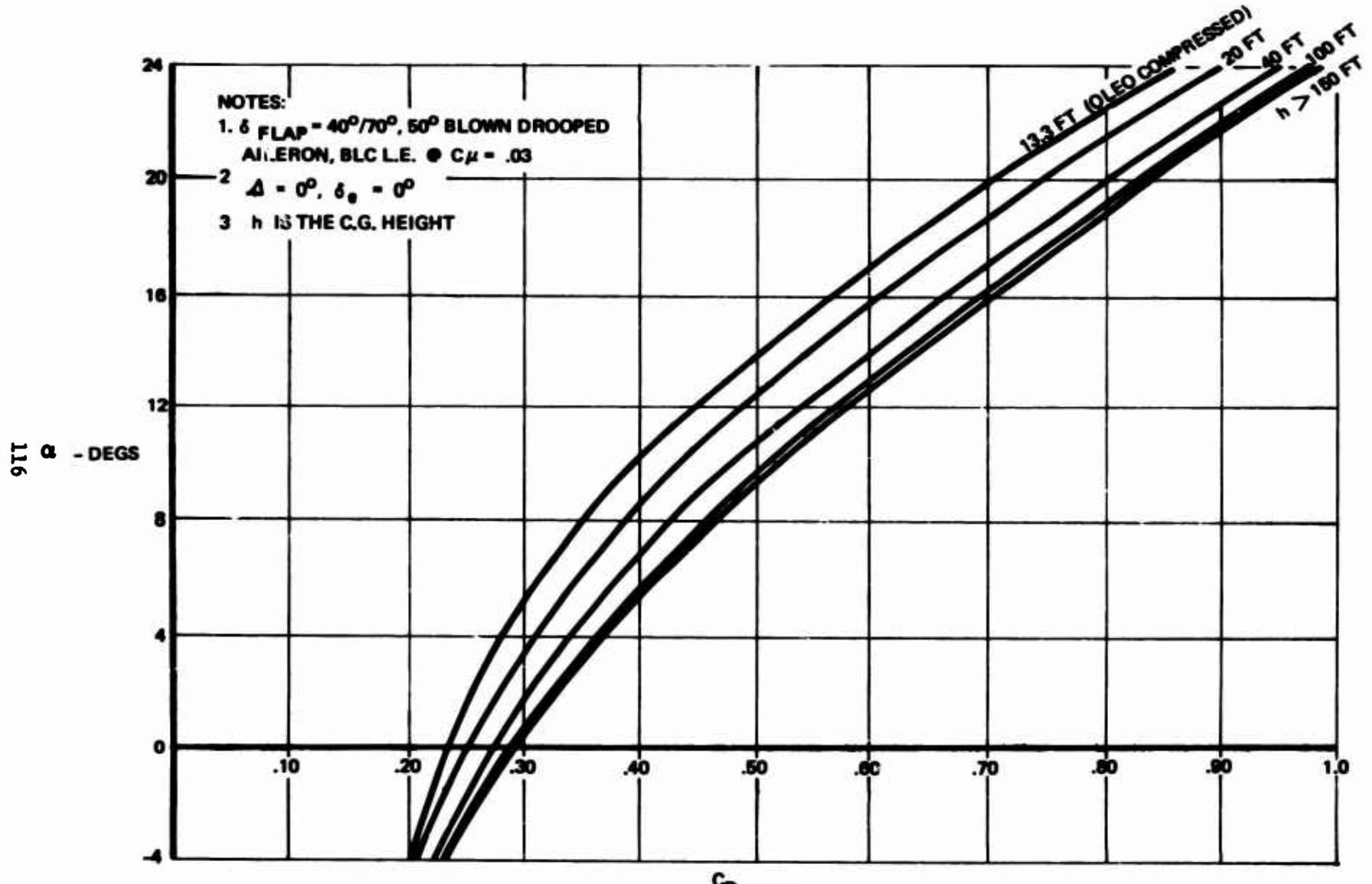

Figure 53: Drag Coefficient : Effect of α On $C_{D_{Basic}}$

NOTE:

1. δ FLAPS = 40°/70°, 50° BLOWN DROOPED AILERON, L.E. BLC C_μ = .03

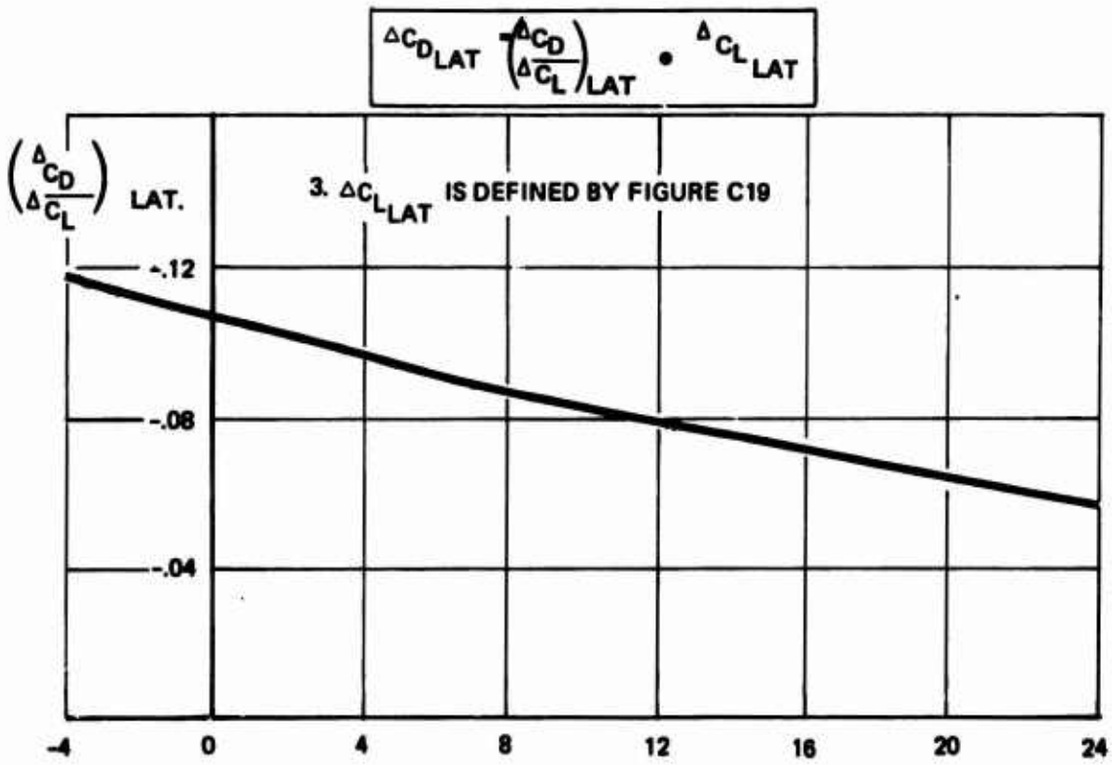

Figure 54: Change in Drag Due to Lateral Control

NOTES:

1. FLAP = 40°/70°, 50°BLOWN DROOPED
   AILERON, L.E. BLC Cμ= .03

2. $\Delta C_{D_{RUDDER}}$ = 0 FOR δ_R = 0

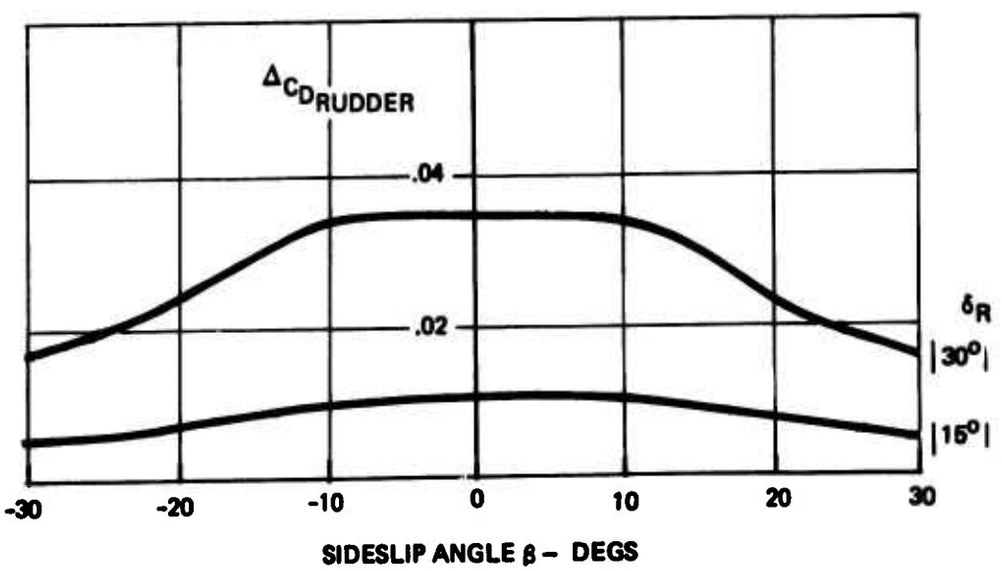

Figure 55: Drag Coefficient Effect of Rudder

$\Delta C_{D_{ELEV}}$ = Change in $C_{D_{BASIC}}$ due to elevator deflection.

$\Delta C_{D_{ELEV}}$ is a function of $(C_{L_{TAIL}})_{\delta_e = 0}$ and δ_e

as shown by Figure 56.

III.2.2.3 Pitching Moment Equation

The dimensionless aerodynamic pitching moment about the center of gravity is separated into its important contributing elements in the equation below.

$$C_{m_{cg}} = C_{m_{.25_{BASIC}}} + C_L(cg-.25) + C_{m_{\hat{\dot{\alpha}}}} \frac{\dot{\alpha}\bar{c}}{2V_T} + C_{m_{\hat{q}}} \frac{q\bar{c}}{2V_T} + \Delta C_{m_{TAIL}} + \Delta C_{m_{SIDESLIP}} + \Delta C_{m_{LAT}}$$

where:

$C_{m_{.25_{BASIC}}}$ = Basic pitching moment coefficient for the airplane in steady "1g" flight with the stabilizer and elevator set for zero deflection and the center of gravity at .25 $\bar{c}_w$. $C_{m_{.25_{BASIC}}}$ is presented by Figure 57 as a function of α and h for $\beta = 0^o$.

$C_L(cg-.25)$ = The increment in pitching moment due to movement of the c.g. from the reference location ($.25\bar{c}_w$). C_L is the total lift coefficient previously defined in Section III.2.2.1.

$C_{m_{\hat{\dot{\alpha}}}} \frac{\dot{\alpha}\bar{c}}{2V_T}$ = Variation in $C_{m_{.25_{BASIC}}}$ due to rate of change of the angle of attack; $C_{m_{\hat{\dot{\alpha}}}} = -6.06$ 1/RAD.

$C_{m_{\hat{q}}} \frac{q\bar{c}}{2V_T}$ = Variation in $C_{m_{.25_{BASIC}}}$ due to airplane pitch rate; $C_{m_{\hat{q}}} = -32.94$ 1/RAD.

$\Delta C_{D_{ELEV}} = 0$ FOR $\delta_E = 0$

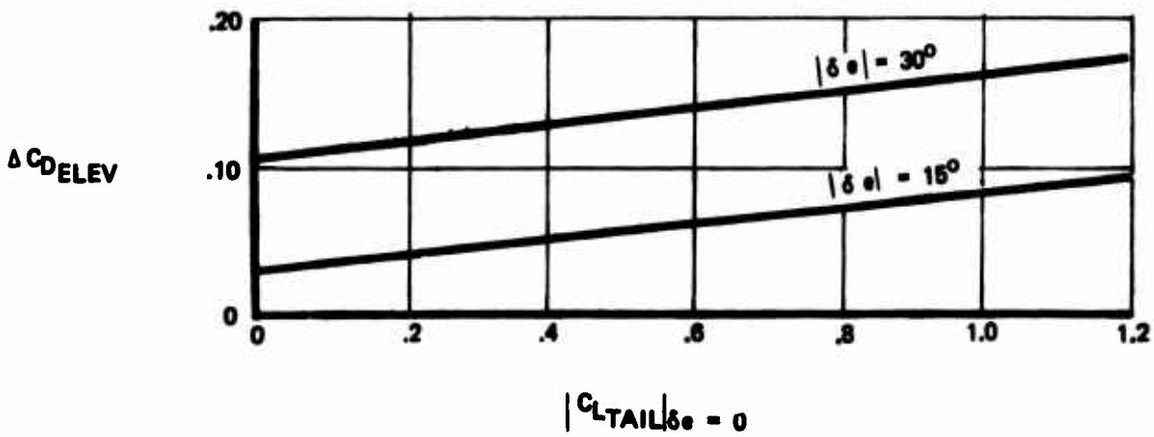

Figure 56: Drag Coefficient Effect of Elevator

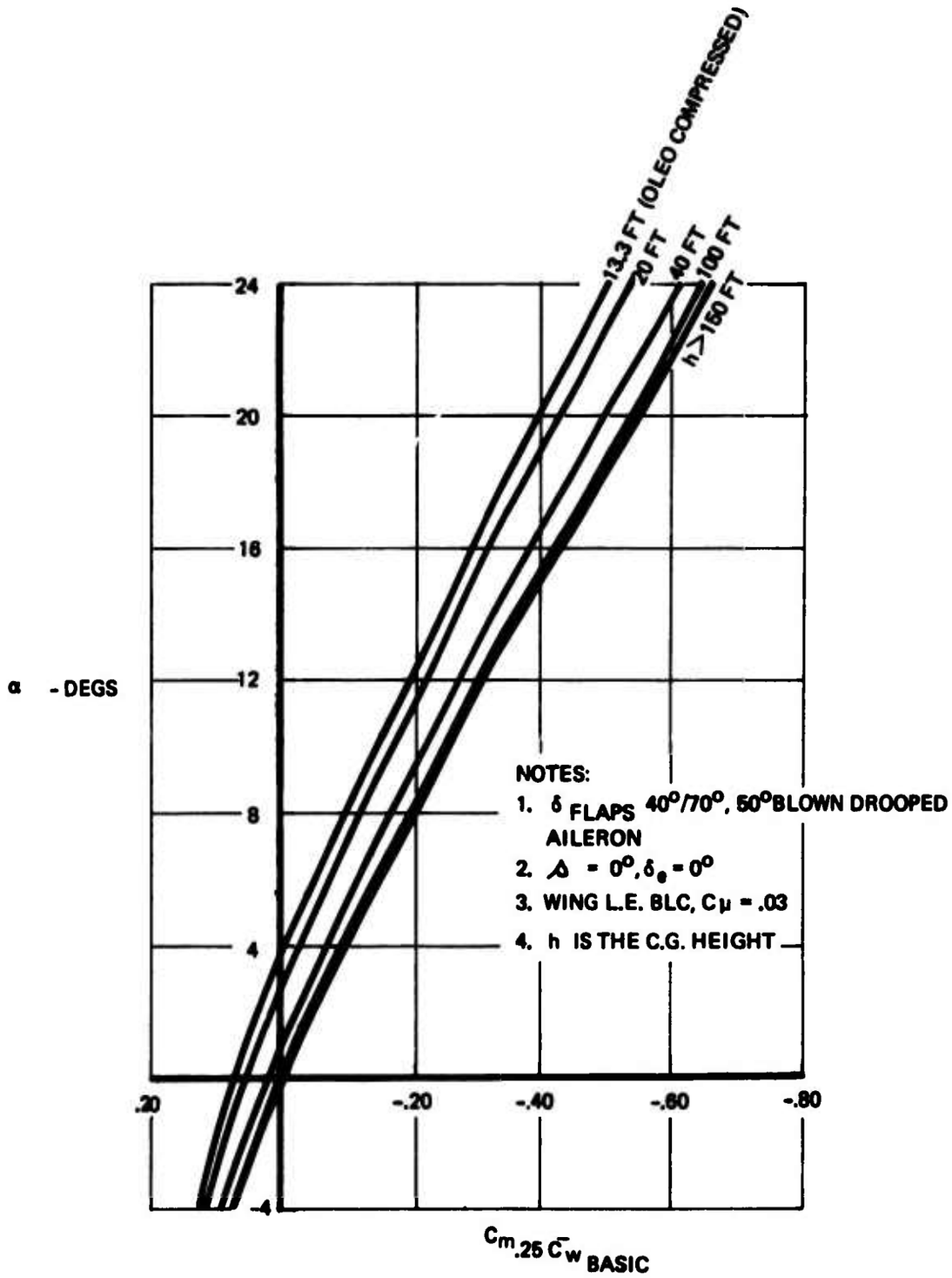

Figure 57: Pitching Moment Coefficient : Effect of α on $C_{m_{.25\,\bar{C}_W}}$ Basic

$\Delta C_{m_{TAIL}}$ = Change in $C_{m_{.25_{BASIC}}}$ due to changes in stabilizer and elevator angles from $\alpha = 0^{\circ}$ and $\delta_e = 0^{\circ}$.

$$\Delta C_{m_{TAIL}} = -\frac{\ell_H}{\bar{c}_w} \Delta C_{L_{TAIL}}$$

$\Delta C_{L_{TAIL}}$ is defined in Section III.2.2.1.

$\Delta C_{m_{SIDESLIP}}$ = Changes in $C_{m_{.25_{BASIC}}}$ due to flying at an angle of sideslip $\Delta C_{m_{SIDESLIP}}$ is presented by Figure 51 as a function of β.

$\Delta C_{m_{LAT}}$ = Changes in $C_{m_{.25_{BASIC}}}$ due to lateral control deflection. $\Delta C_{m_{LAT}}$ is dependent on α and the control deflection angle, and it is defined by Figure 58.

III.2.2.4 Yawing Moment Equation

The dimensionless aerodynamic yawing moment about the center of gravity is separated into its important contributing components in the equation below.

$$C_{n_{cg}} = K_{\beta_1} C_{n_\beta} \beta + C_{n_{\dot{\beta}}} \frac{\dot{\beta} b_w}{2V_T} + C_{n_{\hat{r}}} \frac{r_s b_w}{2V_T} + C_{n_{\hat{p}}} \frac{p_s b_w}{2V_T} +$$

$$\Delta C_{n_{LAT}} + \Delta C_{n_{RUD}} + C_y \, (cg-.25) \frac{\bar{c}_w}{b_w}$$

NOTES:

1. δ_{FLAPS} = 40°/70°, 50° BLOWN DROOPED
   AILERON, L.E. BLC $C\mu$ = .03

2. $$\Delta C_{m_{LAT}} = \left(\frac{\Delta C_m}{\Delta C_L}\right)_{LAT} \Delta C_{L_{LAT}}$$

3. $\Delta C_{L_{LAT}}$ IS DEFINED BY FIGURE C19

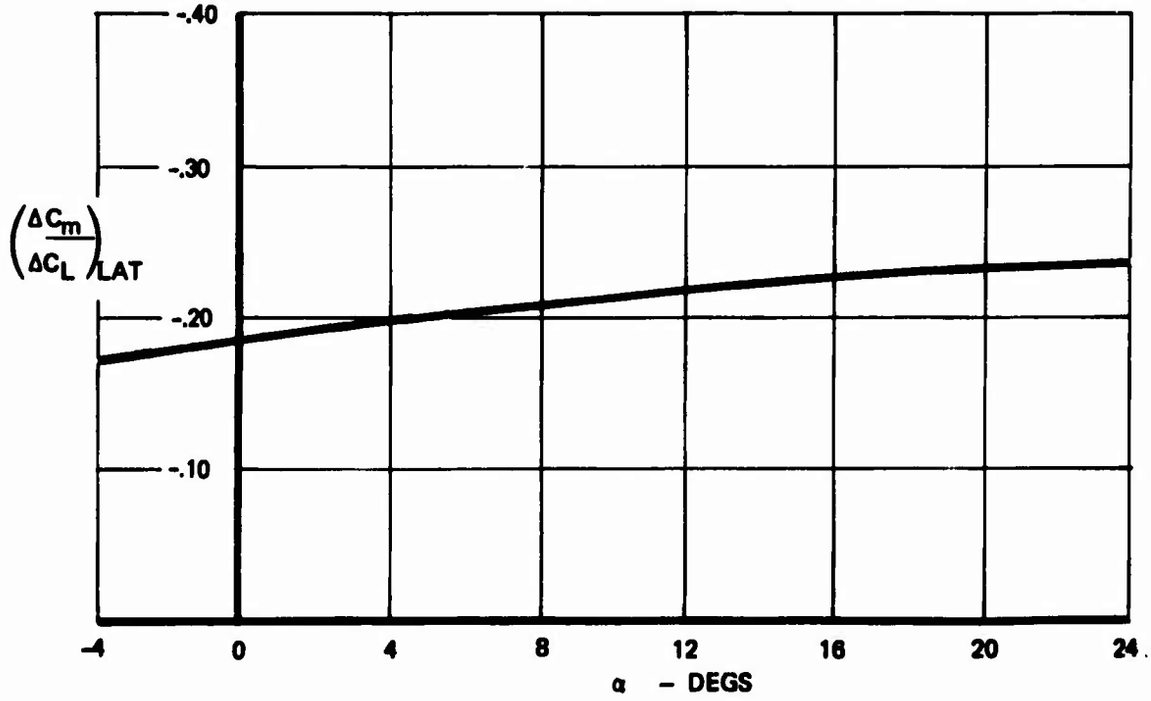

Figure 58: Change in Pitching Moment Due to Lateral Control

where:

$K_{\beta_1} C_{n_\beta}$ = the yawing moment coefficient due to sideslip about the reference center of gravity (cg @ .25c). C_{n_β} is the linear slope through $\beta = 0^o$, and is presented by Figure 59 as a function of α. K_{β_1} is a factor which accounts for the nonlinear variation of C_n with β. K_{β_1} is also presented by Figure 59.

$C_{n_{\hat{\dot{\beta}}}} \frac{\dot{\beta} b_w}{2V_T}$ = Variation in yawing moment due to rate of change sideslip angle. $C_{n_{\hat{\dot{\beta}}}}$ is presented as a function of α by Figure 60.

$C_{n_{\hat{r}}} \frac{r_s b_w}{2V_T}$ = Variation in yawing moment due to airplane yaw rate. $C_{n_{\hat{r}}}$ is presented as a function of α by Figure 60.

$C_{n_{\hat{p}}} \frac{p_s b_w}{2V_T}$ = Variation in yawing moment due to airplane roll rate. $C_{n_{\hat{p}}}$ is defined as a function of α by Figure 60.

$\Delta C_{n_{LAT}}$ = Change in yawing moment due to lateral control deflection. $\Delta C_{n_{LAT}}$ is related to $\Delta C_{\ell_{LAT}}$ by:

$\Delta C_{n_{LAT}} = \frac{\Delta C_n}{\Delta C_{\ell_{LAT}}} \Delta C_{\ell_{LAT}}$ where $\Delta C_{\ell_{LAT}}$ is defined in in Section III.2.2.5, and $\frac{\Delta C_n}{\Delta C_{LAT}}$ is defined by Figure 61.

$\Delta C_{n_{RUD}}$ = Change in yawing moment due to rudder deflection. $\Delta C_{n_{RUD}}$ is dependent on the rudder deflection angle and β as defined by Figure 62.

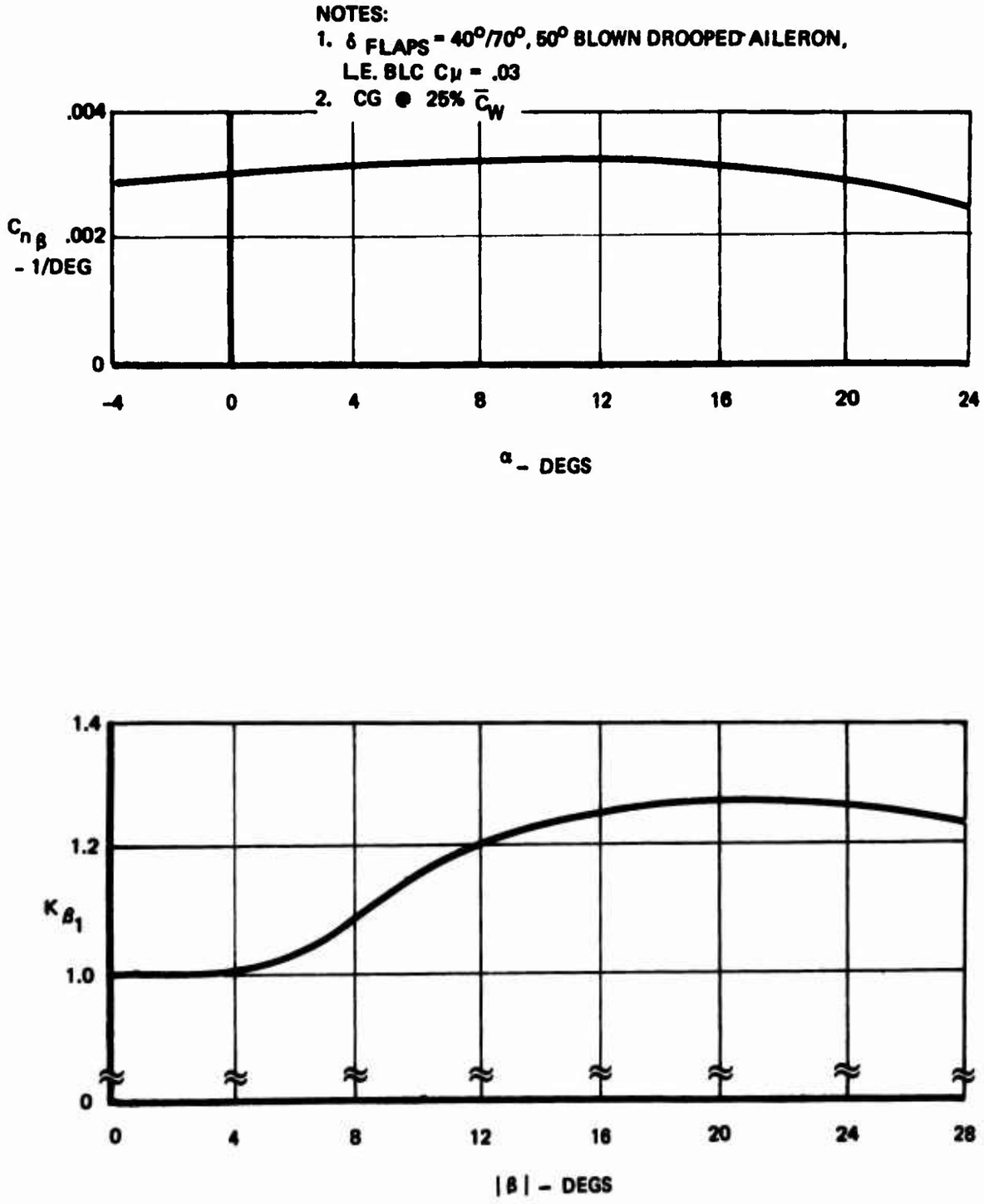

Figure 59: Yawing Moment Coefficient Effect of Sideslip

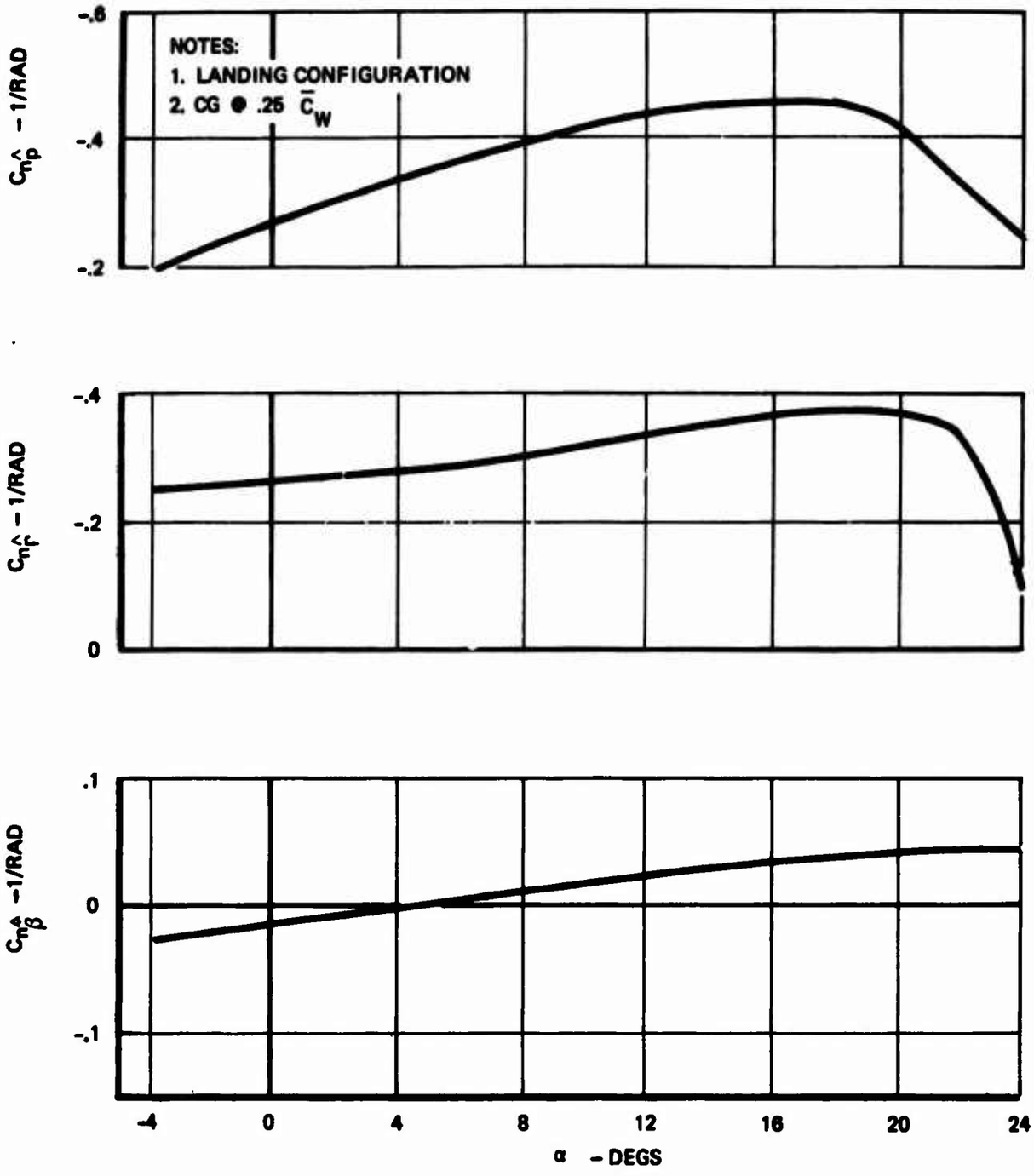

Figure 60: Yawing Moment Coefficient Effect of $\hat{p}$, $\hat{r}$. $\hat{\beta}$

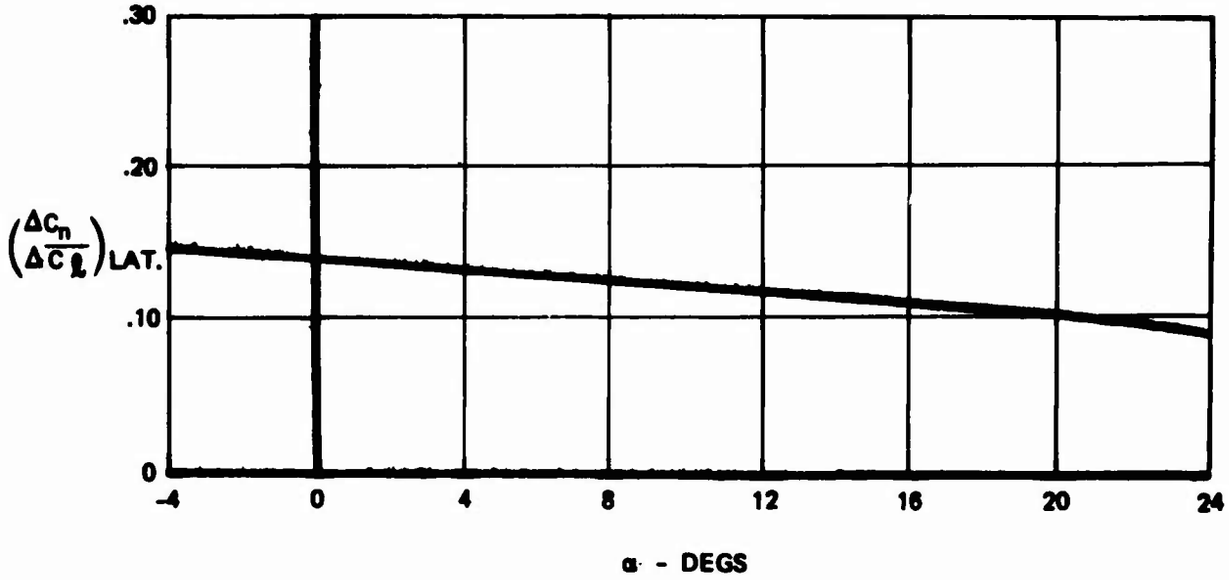

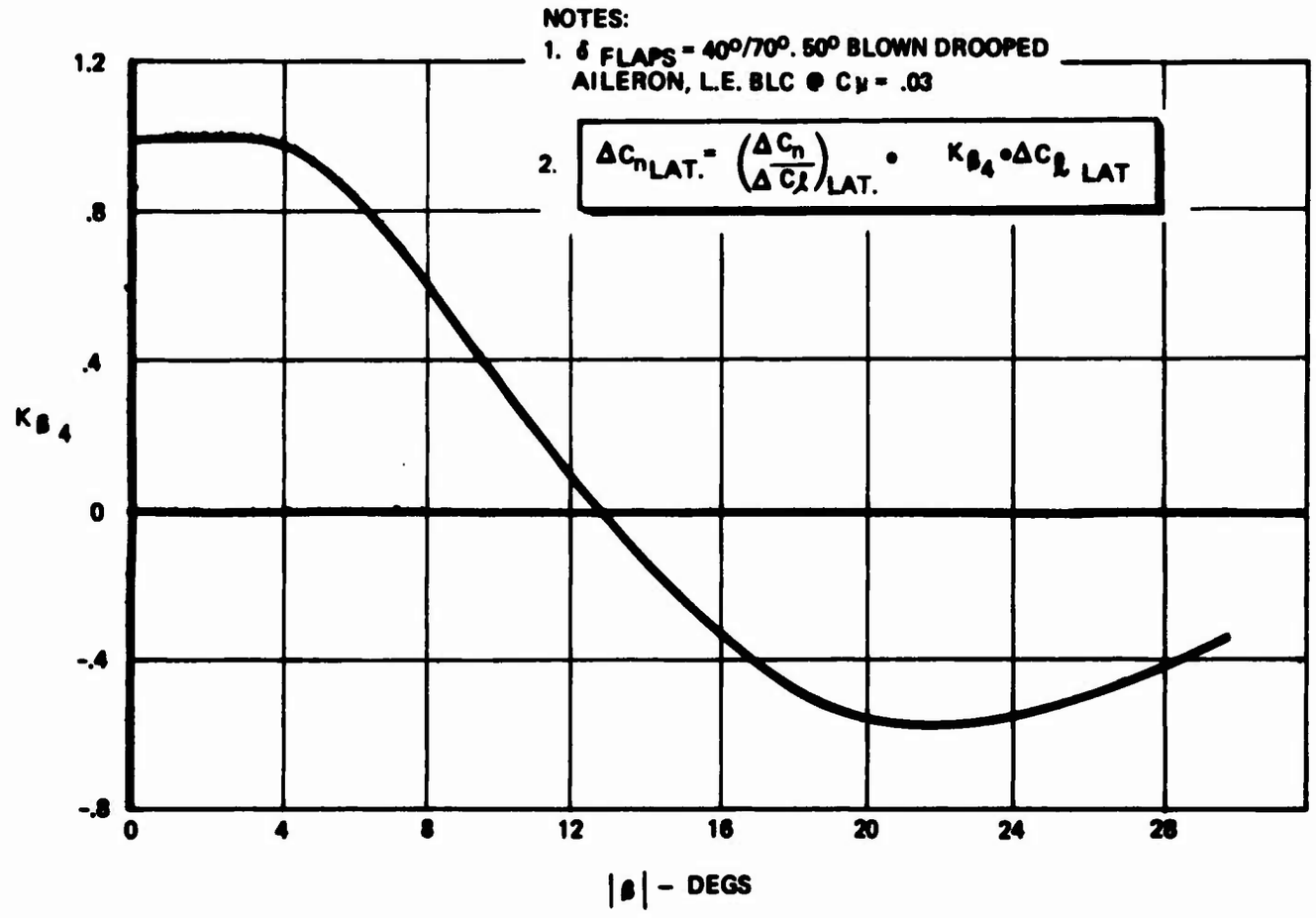

Figure 61: Yawing Moment Coefficient Effect of Lateral Control

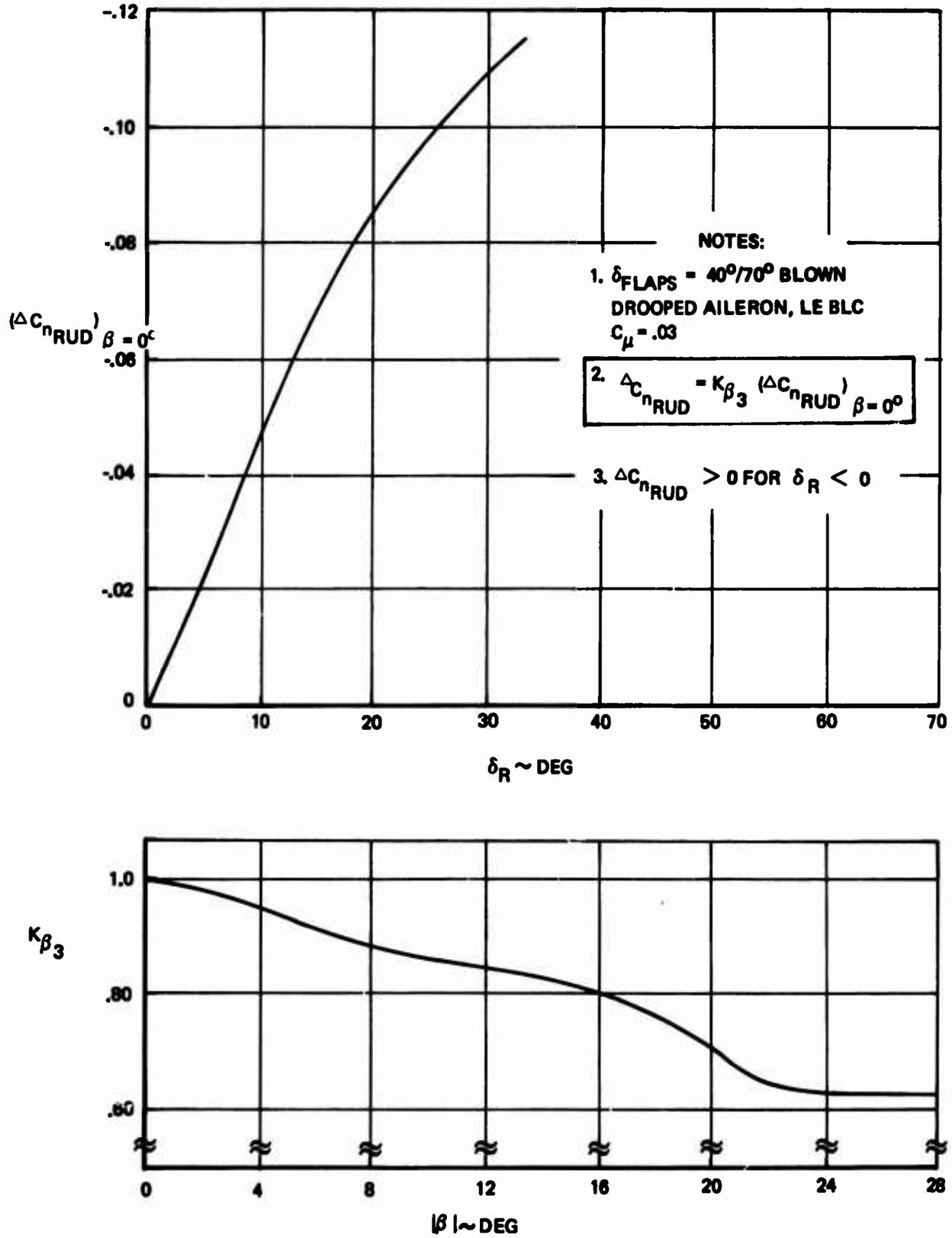

Figure 62: Yawing Moment Coefficient Effect of Rudder Deflection

$C_Y(cg-.25)\frac{\bar{c}_w}{b_w}$ = The change in yawing moment due to center of gravity variations from the reference c.g. C_Y is defined in Section III.2.2.6.

III.2.2.5 Rolling Moment Equation

The dimensionless aerodynamic rolling moment is separated into its important contributing components by the equation given below.

$$C_\ell = K_{\beta_2} C_{\ell_\beta} \beta + C_{\ell_{\hat{\dot{\beta}}}} \frac{\dot{\beta} b_w}{2V_T} + C_{\ell_{\hat{r}}} \frac{r_s b_w}{2V_T} + C_{\ell_{\hat{p}}} \frac{p_s b_w}{2V_T} + \Delta C_{\ell_{LAT}} + \Delta C_{\ell_{RUD}}$$

where:

$K_{\beta_2} C_{\ell_\beta} \beta$ = The rolling moment coefficient due to sideslip. C_{ℓ_β} is the linear slope through $\beta = 0^o$, and K_{β_2} accounts for the nonlinear variation of C_ℓ with β. Both factors are presented by Figure 63.

$C_{\ell_{\hat{\dot{\beta}}}} \frac{\dot{\beta} b_w}{2V_T}$ = Variation in rolling moment due to rate of change of sideslip angle. $C_{\ell_{\hat{\dot{\beta}}}}$ is presented as a function of α by Figure 64.

$C_{\ell_{\hat{r}}} \frac{r_s b_w}{2V_T}$ = Variation in rolling moment due to airplane yaw rate. $C_{\ell_{\hat{r}}}$ is presented as a function of α by Figure 64.

$C_{\ell_{\hat{p}}} \frac{p_s b_w}{2V_T}$ = Variation in rolling moment due to airplane roll rate. $C_{\ell_{\hat{p}}}$ is defined as a function of α by Figure 64.

$\Delta C_{\ell_{LAT}}$ = Change in rolling moment due to lateral control deflection. $\Delta C_{\ell_{LAT}}$ is a function of α and the control deflection angle, and it is defined by Figure 65.

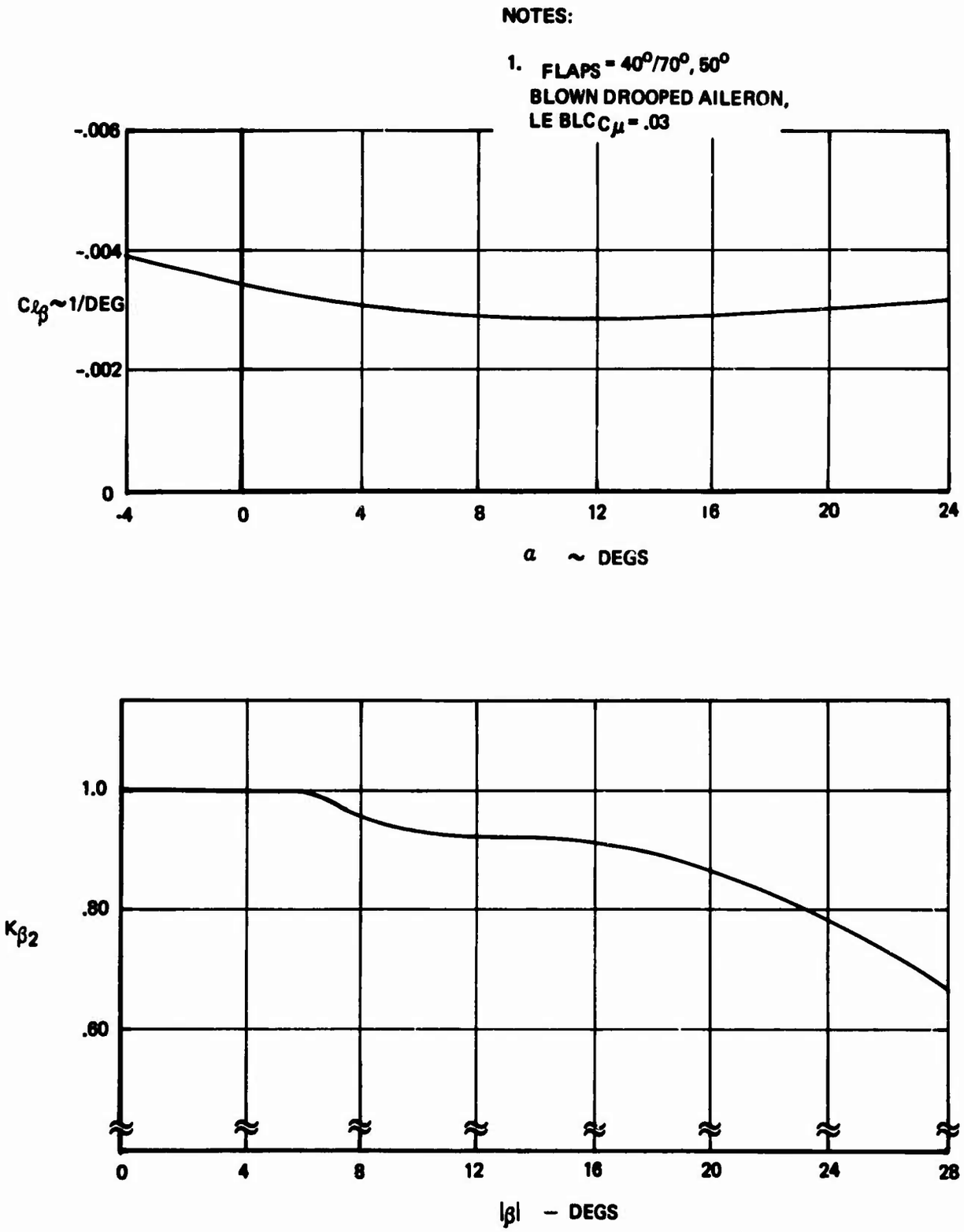

Figure 63: Rolling Moment Coefficient:Effect of Sideslip

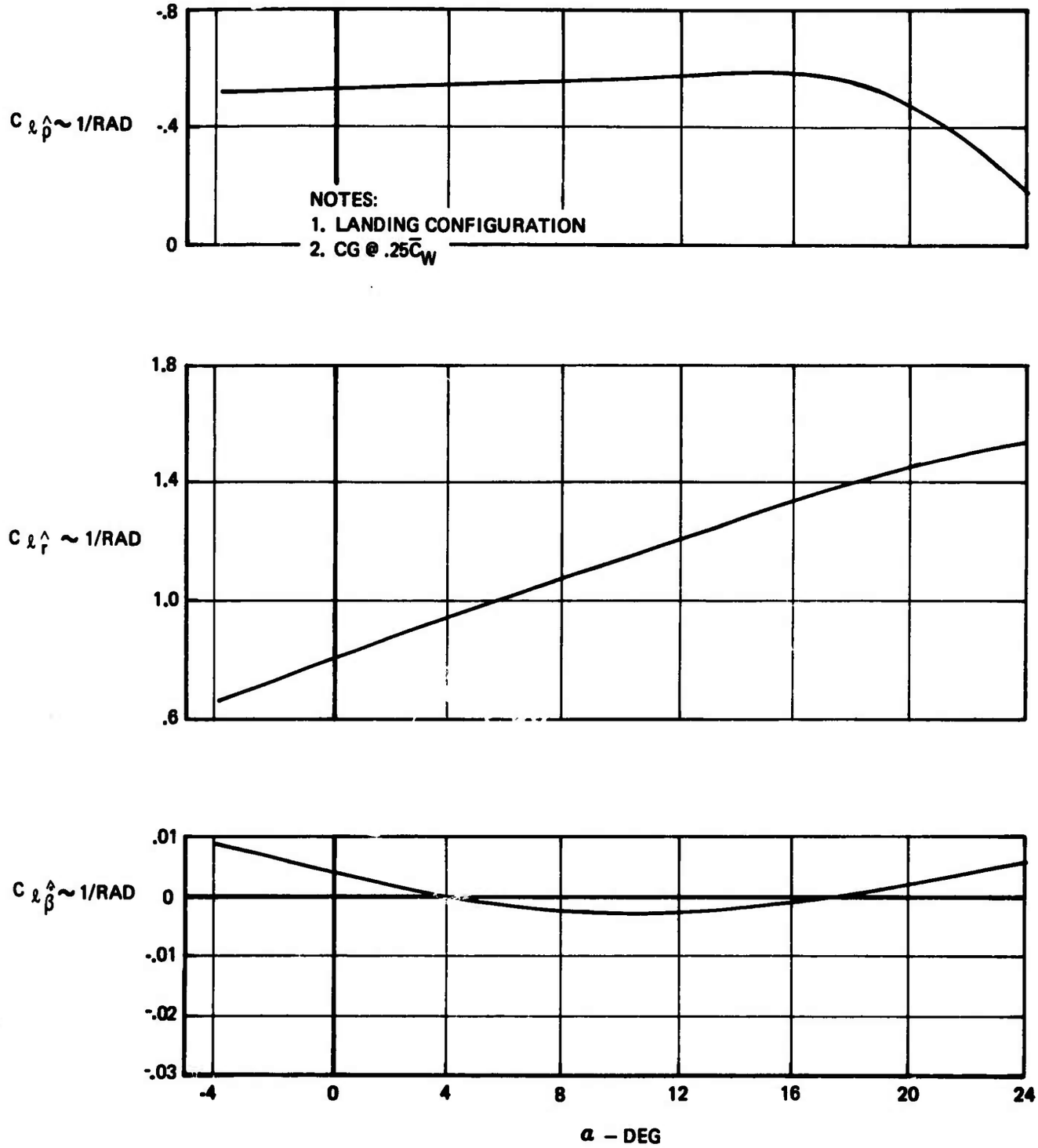

Figure 64: Rolling Moment Coefficient:Effect of $\hat{p}$ $\hat{r}$ & $\hat{\beta}$

1. FLAP = 40°/70°, BLOWN DROOPED 50°
   AILERON, LE BLC, $C\mu = .03$

2. $\Delta C_{\ell_{LAT}} = [(K_{\delta_{SP}})_{RHW} - (K_{\delta_{SP}})_{LHW}]\Delta C_{\ell_{SP}} @ \delta_{SP} = 60^{o} + .00107\,\delta a$

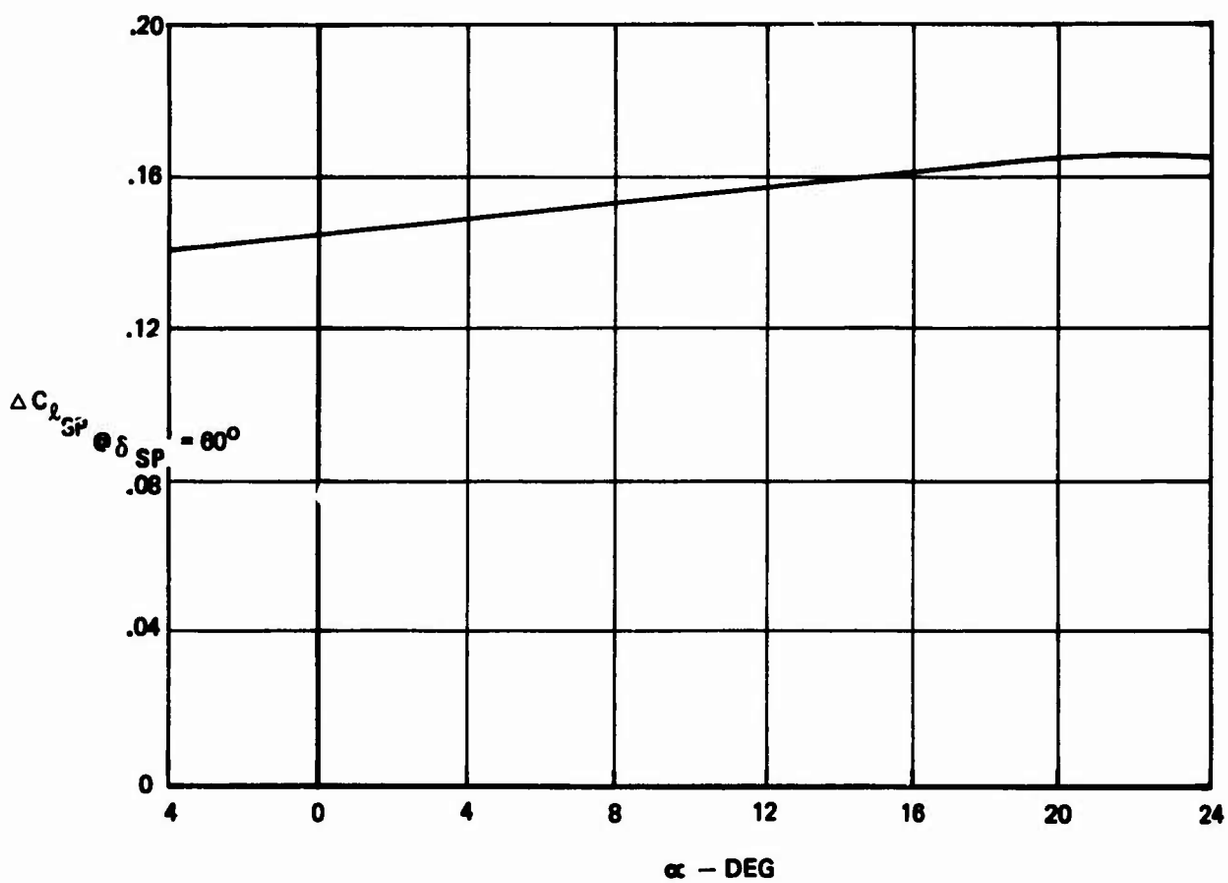

Figure 65: Rolling Moment Coefficient: Effect of Lateral Control

$\Delta C_{\ell_{RUD}}$ = Change in rolling moment due to rudder deflection. $\Delta C_{\ell_{RUD}}$ is dependent on α, β, and the rudder deflection angle as defined by Figure 66.

III.2.2.6 Side Force Equation

The dimensionless aerodynamic side force is separated into its important contributing components by the equation given below.

$$C_y = C_{y_\beta}\,\beta + C_{y_{\hat{\dot{\beta}}}}\frac{\dot{\beta} b_w}{2V_T} + C_{y_{\hat{r}}}\frac{r_s b_w}{2V_T} + C_{y_\beta}\frac{p_s b_w}{2V_T} + \Delta C_{y_{RUD}}$$

where:

$C_{y_\beta}\,\beta$ = The side force coefficient due to sideslip. C_{y_β} is presented as a function of α by Figure 67.

$C_{y_{\hat{\dot{\beta}}}}\frac{\dot{\beta} b_w}{2V_T}$ = Variation in side force due to rate of change of sideslip angle, $C_{y_{\hat{\dot{\beta}}}}$ is a function of α and, it is presented by Figure 68.

$C_{y_{\hat{r}}}\frac{r_s b_w}{2V_T}$ = Variation in side force due to airplane yaw rate. $C_{y_{\hat{r}}}$ varies with α as illustrated by Figure 68.

$C_{y_{\hat{p}}}\frac{p_s b_w}{2V_T}$ = Variation in side force due to airplane roll rate. $C_{y_{\hat{p}}}$ is defined as a function of α by Figure 68.

$\Delta C_{y_{RUD}}$ = Change in side force due to rudder deflection. $\Delta C_{y_{RUD}}$ is dependent on the rudder deflection angle and β as defined by Figure 69.

III.2.3 Aerodynamic Module: Mechanization and Validation Phases

III.2.3.1 Lift Equation

The dimensionless aerodynamic lift force of the airplane is separated into its important contributing elements in the equation below.

$$C_L = C_{L_{WB}} + C_{L_{TAIL}} + \frac{\bar{c}_w}{2V_T}\left(C_{L_{\hat{\dot{\alpha}}}}\dot{\alpha} + C_{L_{\hat{q}}}\,q\right) + \Delta C_{L_{SIDESLIP}} + \Delta C_{L_{LAT}}$$

NOTES: 1. $\Delta C_{\ell_{RUD}} = K_{\beta_3} \quad K_{a_1} (\Delta C_{\ell_{RUD}})^{\beta=0^o}_{a=0^o}$

2. $\delta_{FLAP} = 40^o/70^o$, 50^o BLOWN DROOPED AILERON, LE BLC $C_\mu = .03$

3. $(\Delta C_{\ell_{RUD}})^{\beta=0^o}_{a=0^o} < 0$ FOR $\delta_R < 0$

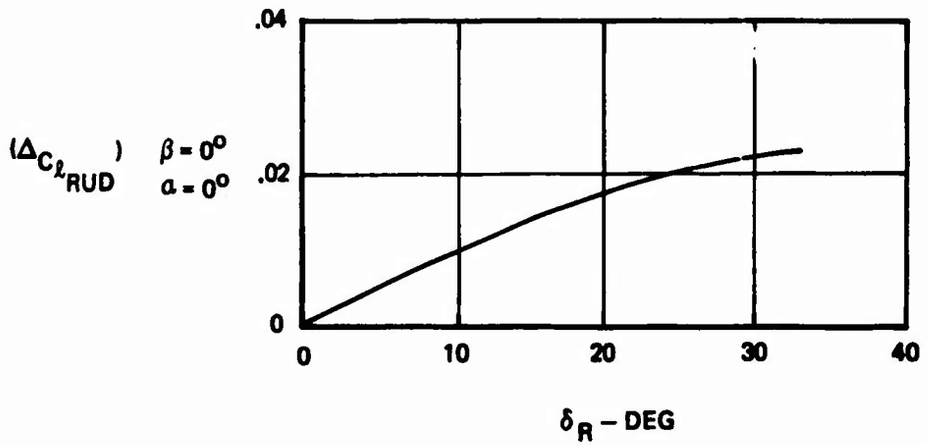

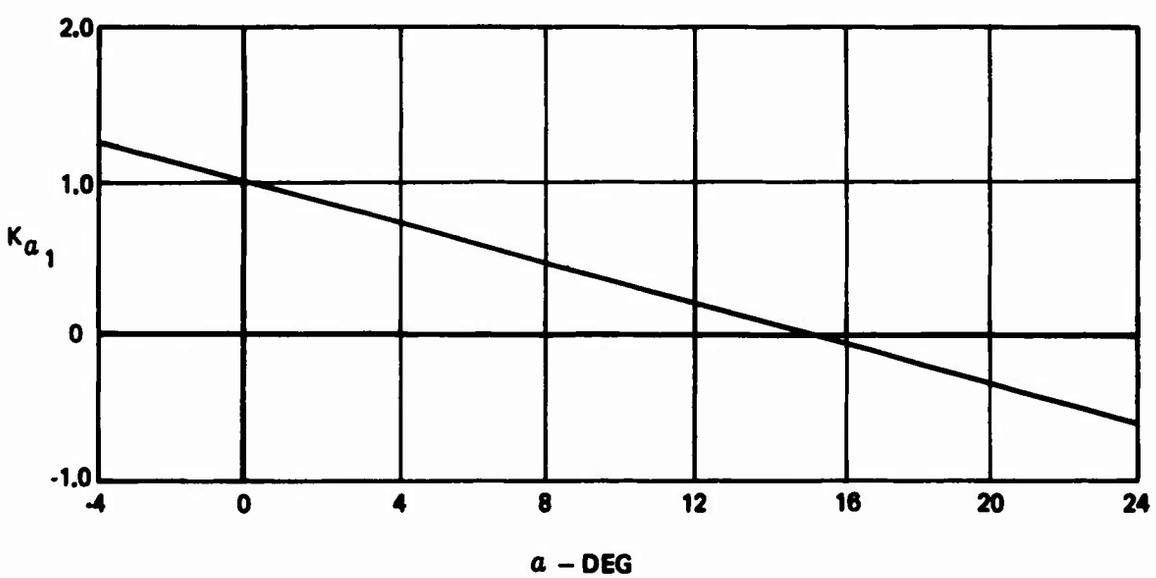

Figure 66: Rolling Moment Coefficient:Effect of Rudder Deflection

NOTES:

1. $\delta_{FLAPS} = 40^{o}/70^{o}, 50^{o}$ BLOWN DROOPED AILERON, LE BLC $C_{\mu} = .03$

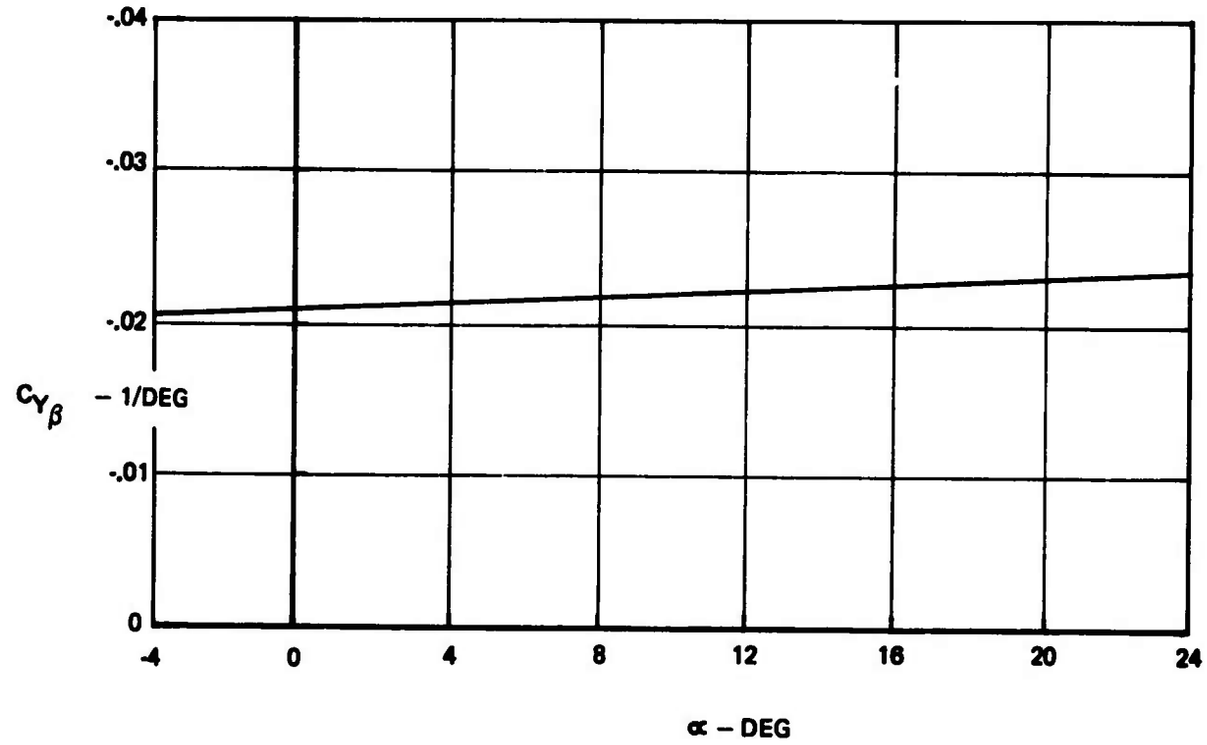

Figure 67: Side Force Coefficient:Effect of Sideslip

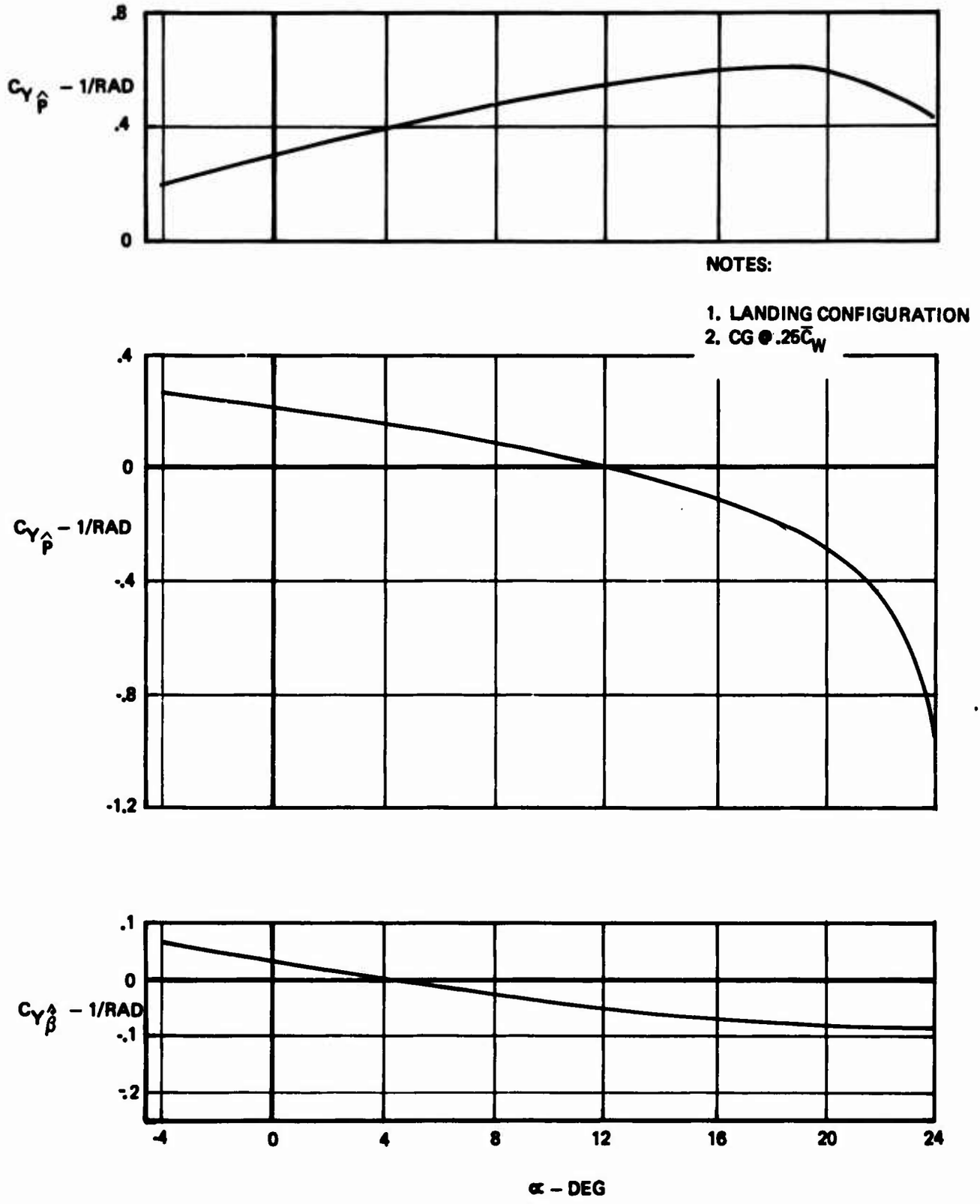

Figure 68: Side Force Coefficient:Effect of $\hat{p}$ $\hat{r}$ & $\hat{\beta}$

NOTES:

1. $\delta_{FLAPS} = 40^o/70^o, 50^o$ BLOWN DROOPED AILERON, LE BLC $C_\mu = .03$
2. $\Delta C_{Y_{RUD}} = K_{\beta_3} (\Delta C_{Y_{RUD}})_{\beta = 0^o}$
3. $\Delta C_{Y_{RUD}} < 0$ FOR $\delta_R < 0$

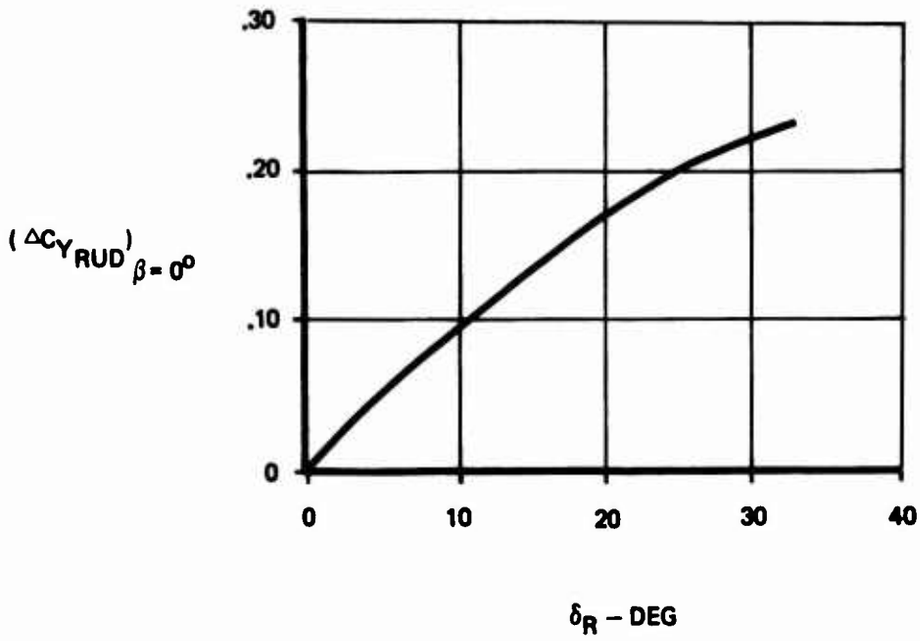

Figure 69: Side Force Coefficient:Effect of Rudder Deflection

1. Wing-body Lift

$$C_{L_{WB}} = C_{L_{WB_{C_{J=0}}}} + \Delta C_{L_{WB_{C_{J=0}}}} + \Delta C_{L_{WB_{GE}}}$$
$$\qquad\qquad\qquad\quad FA \qquad\qquad\quad FA$$

(a) $C_{L_{WB_{C_{J=0}}}} = f(\alpha)$ (Figure 70)
$\qquad\qquad\quad FA$

(b) $\Delta C_{L_{WB_{C_{J\neq 0}}}} = f(\alpha, C_J, \sigma)$ (Figure 71)
$\qquad\qquad\quad FA$

(c) $\Delta C_{L_{WB_{GE}}} = (\Delta C_{L_{WB_{C_{J=0}}}} + \Delta C_{L_{WB_{C_{J\neq 0}}}}) . F_{G_1}$
$\qquad\qquad\qquad\qquad\qquad\quad GE \qquad\qquad\quad GE$

i) $\Delta C_{L_{WB_{C_{J=0}}}} = f(\alpha)$ (Figure 72)
$\qquad\qquad\quad GE$

ii) $\Delta C_{L_{WB_{C_{J\neq 0}}}} = f(\alpha, C_J, \sigma)$ (Figure 73)
$\qquad\qquad\quad GE$

iii) $F_{G_1} = f(h_{MG})$ (Figure 72)

2. Horizontal Tail Lift

$$C_{L_{TAIL}} = \left(\frac{S_H}{S_W}\right)\left[C_{L_{TAIL\ \delta_e=0}} + \Delta C_{L_{TAIL\ \delta_e}}\right]$$

(a) $(C_{L_{TAIL\ \delta_e=0}}) = f(\alpha_{TAIL})$ (Figure 74)

where $\alpha_{TAIL} = \alpha - \varepsilon + \delta$

and $\varepsilon = \varepsilon_{C_{J=0}} + \Delta\varepsilon_{C_{J\neq 0}} + \Delta\varepsilon_{GE}$
$\qquad\qquad\quad FA \qquad\qquad\quad FA$

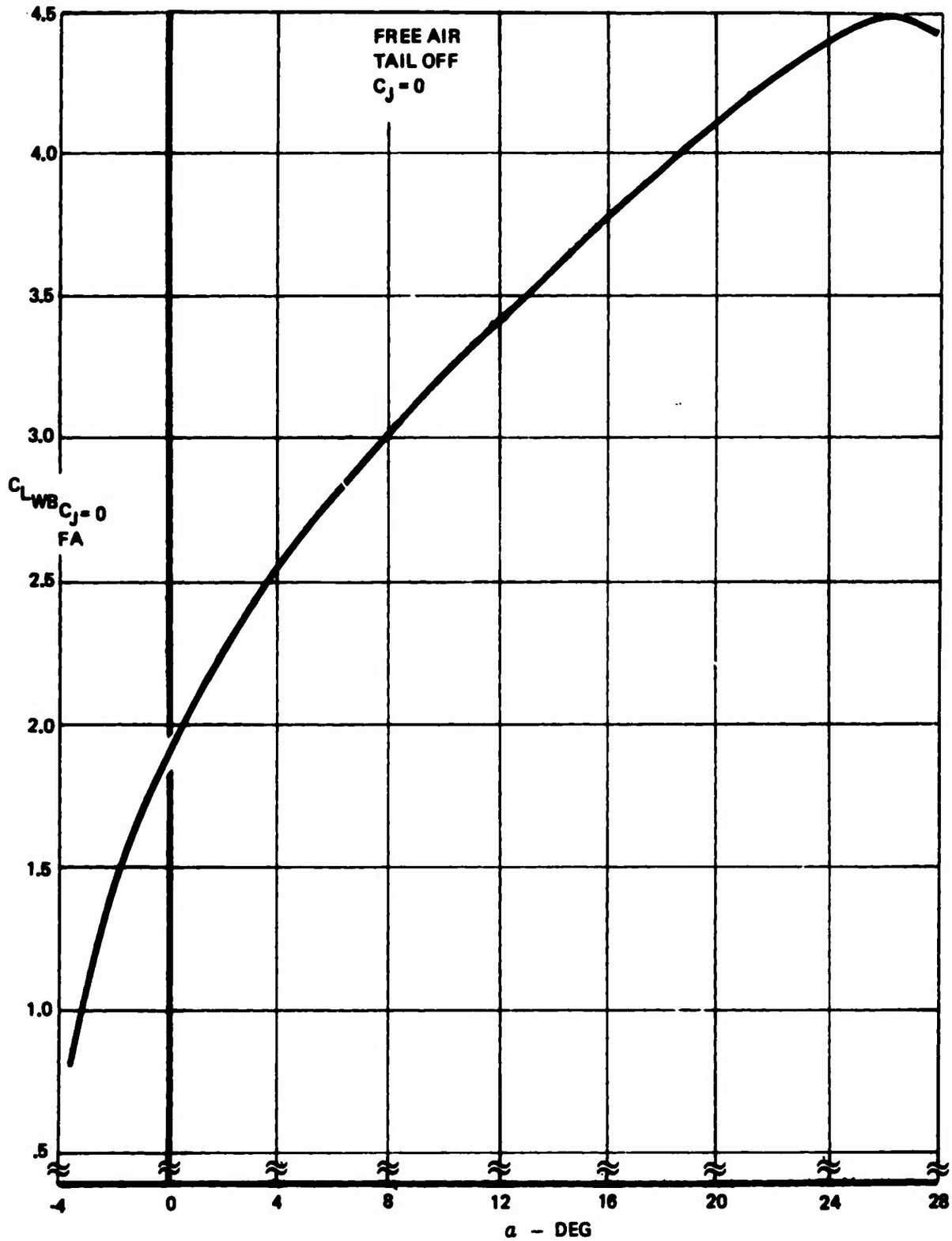

Figure 70: Wing Body Lift – Free Air – $C_J = 0$

$$\Delta C_{L_{WB_{C_J \& 0}}} = \left\{ \frac{\Delta C_{L_{WB_{C_J}=0}}}{\sqrt{C_J}} \right\} \sqrt{C_J}$$

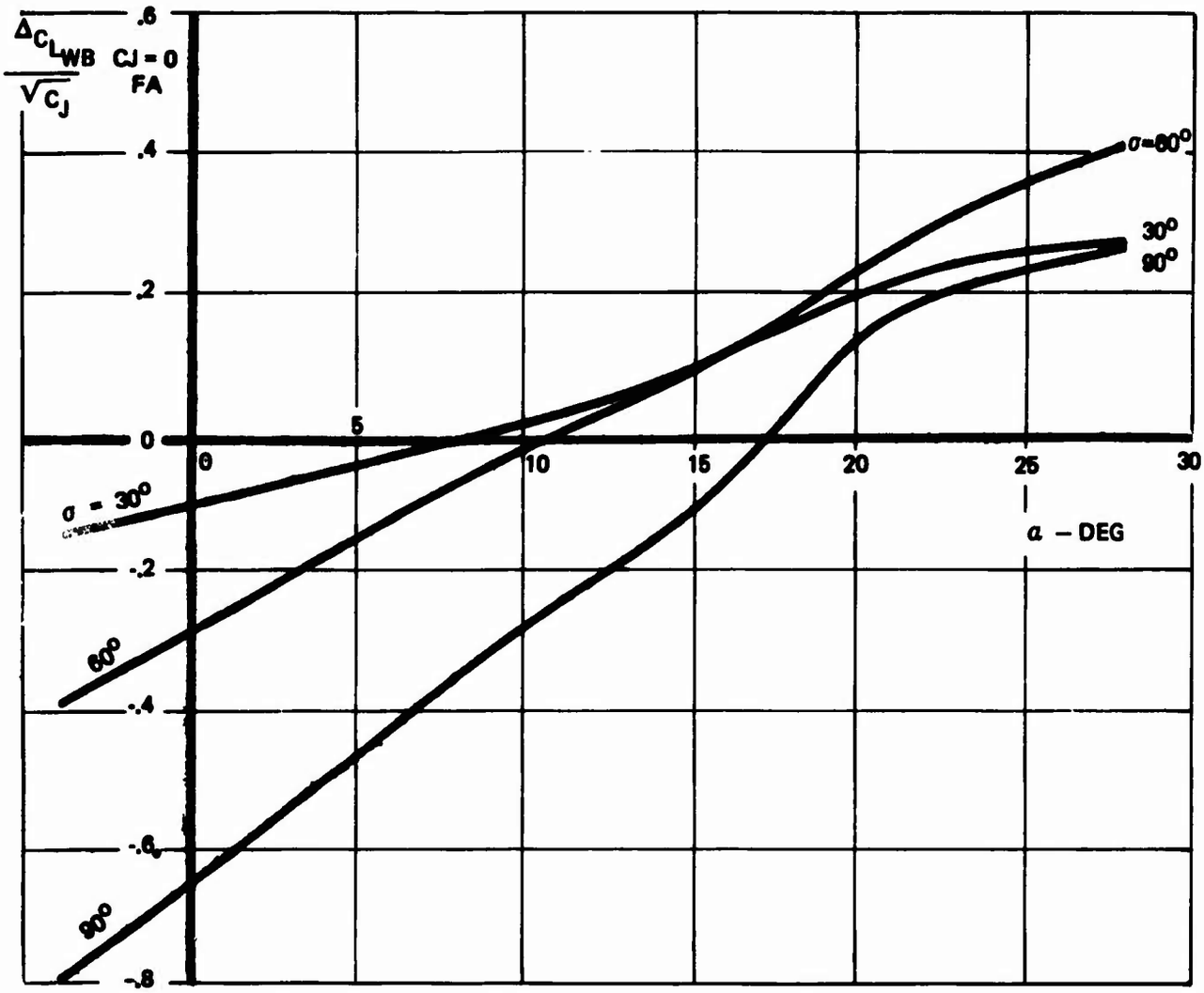

Figure 71: Effect of Power on Lift (Free Air) $\delta_F = 35^o$ – Tail Off

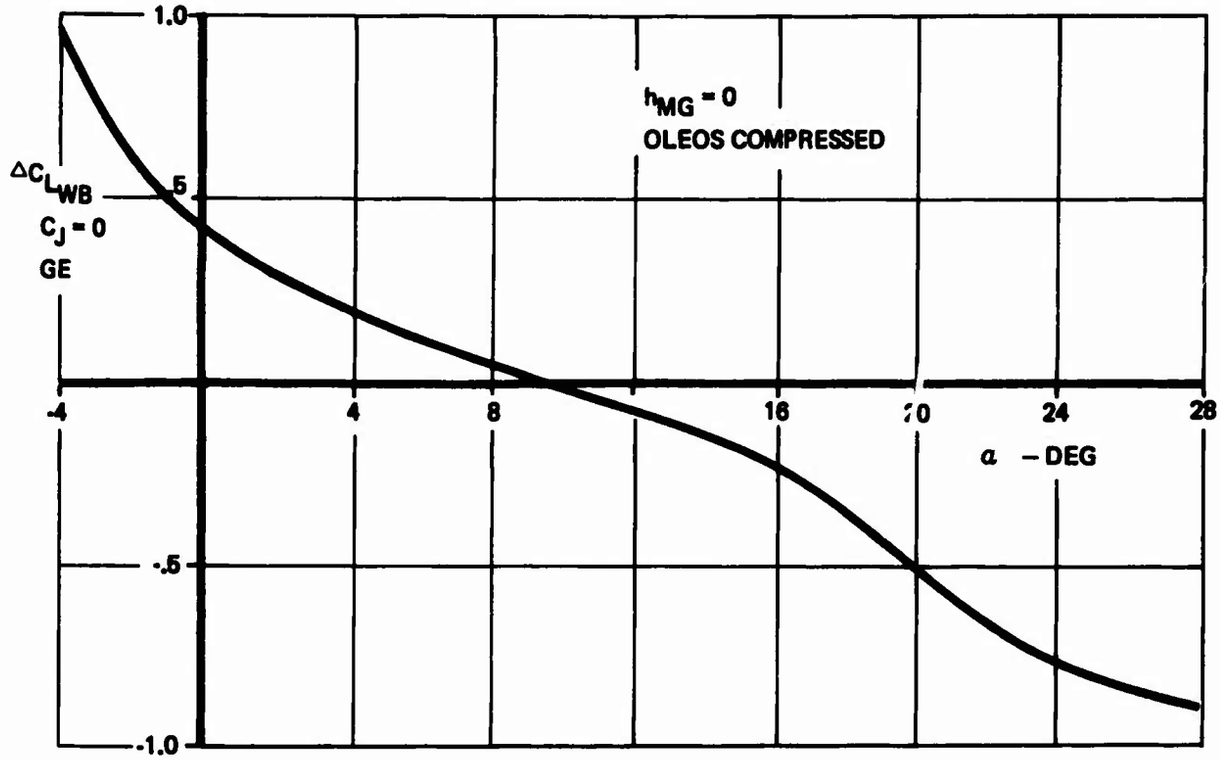

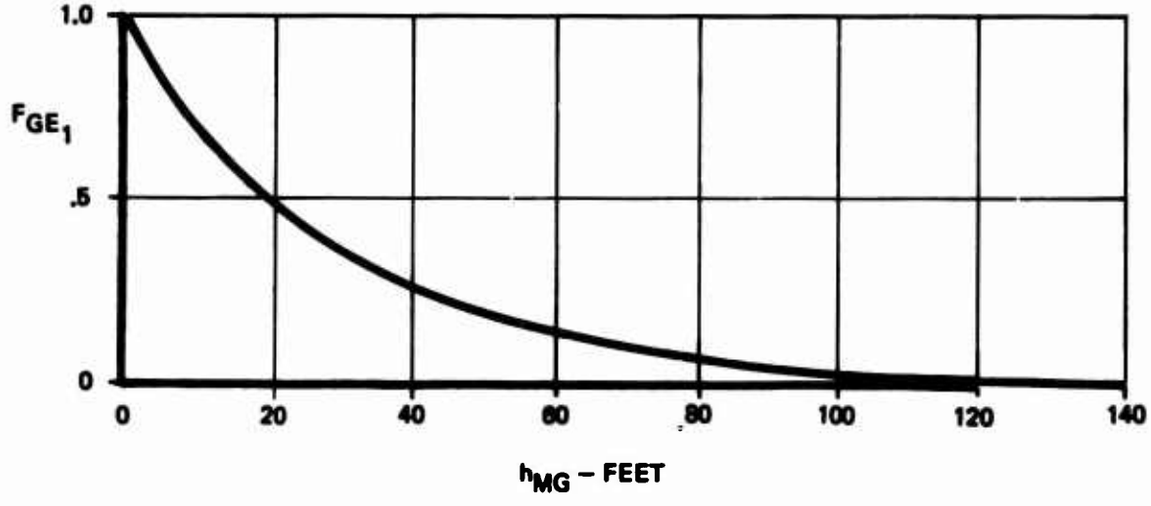

Figure 72: Change in Wing Body Lift Due to Ground Effect ~ $C_J = 0$

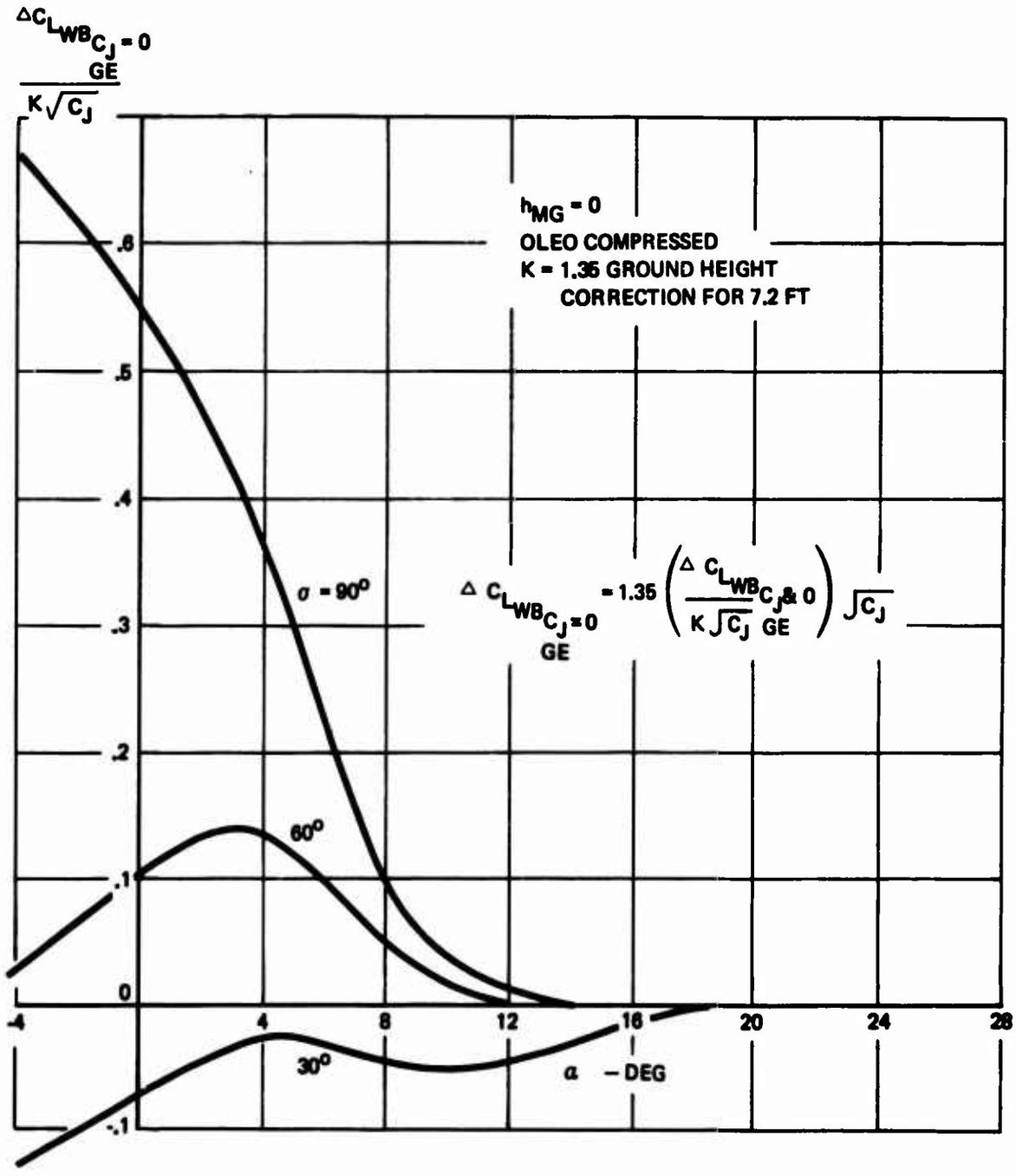

Figure 73: Effect of Power on Lift in Ground Effect ~ $\delta_F = 35^o$, Tail Off

NOTE: $C_{L_{TAIL}} > 0$ FOR $\alpha_{TAIL} > 0$
(REVERSE SIGN OF $(C_{L_{TAIL}})_{\delta_e = 0}$ FOR $\alpha_{TAIL} > 0^o$)

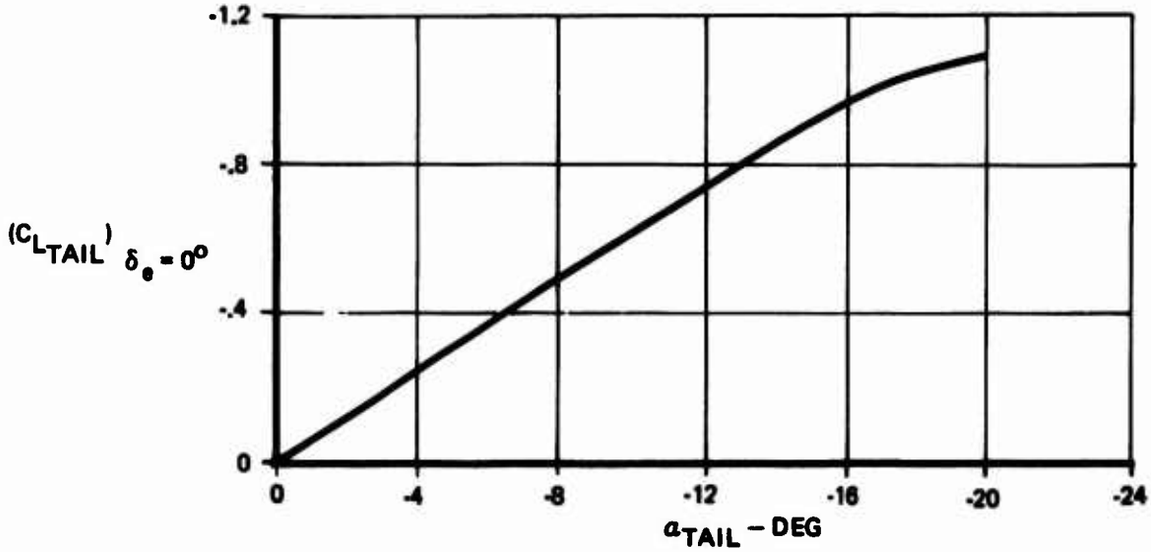

Figure 74: Horizontal Tail Lift With $\delta_e = 0^o$

i) $\varepsilon_{C_{J=0}}$ = f (α) (Figure 75)
FA

ii) $\Delta\varepsilon_{C_{J\neq0}}$ = f (α, C_J, σ) (Figure 76)
FA

iii) $\Delta\varepsilon_{GE} = (\Delta\varepsilon_{C_{J=0}} + \Delta\varepsilon_{C_{J\neq0}})\ F_{GE_2}$
GE GE

where

$\Delta\varepsilon_{C_{J=0}}$ = f (α) (Figure 77)
GE

$\Delta\varepsilon_{C_{J\neq0}}$ = f (α, C_J, σ) (Figure 78)
GE

F_{GE_2} = f (h_{MG}) (Figure 77)

(b) $(\Delta C_{L_{TAIL}})_{\delta e} = .061 \left(\frac{\partial \alpha_T}{\partial \delta_e}\right) K_\delta\ \delta_e$

i) $\frac{\partial \alpha_T}{\partial \delta_e}$ = f (δe) (Figure 79)

ii) K_δ = f $(C_{L_{TAIL}})_{\delta e=0}$ (Figure 79)

3. Lift Due To $\dot{\alpha}$ and q

(a) $C_{L_{\dot{\alpha}}}$ = -8.18 1/RAD

(b) $C_{L_{\hat{q}}}$ = 7.54 1/RAD

4. Lift Due To Sideslip

$\Delta C_{L_{SIDESLIP}}$ = f (β) (Figure 80)

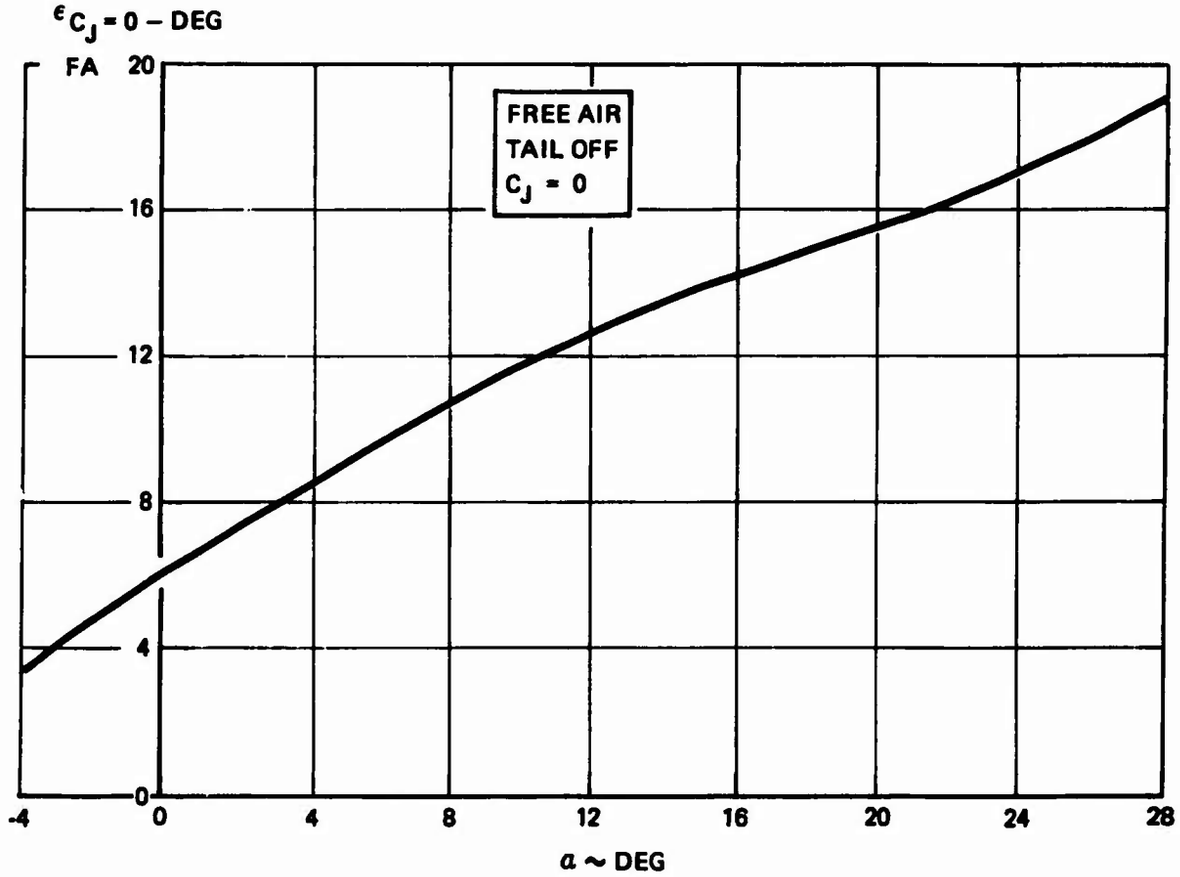

Figure 75: Free Air Downwash $C_J = 0$

$$\Delta\epsilon_{C_J \neq 0} = \left(\frac{\Delta\epsilon_{C_J \neq 0}}{\sqrt{C_J}}\right)\sqrt{C_J}$$
FA

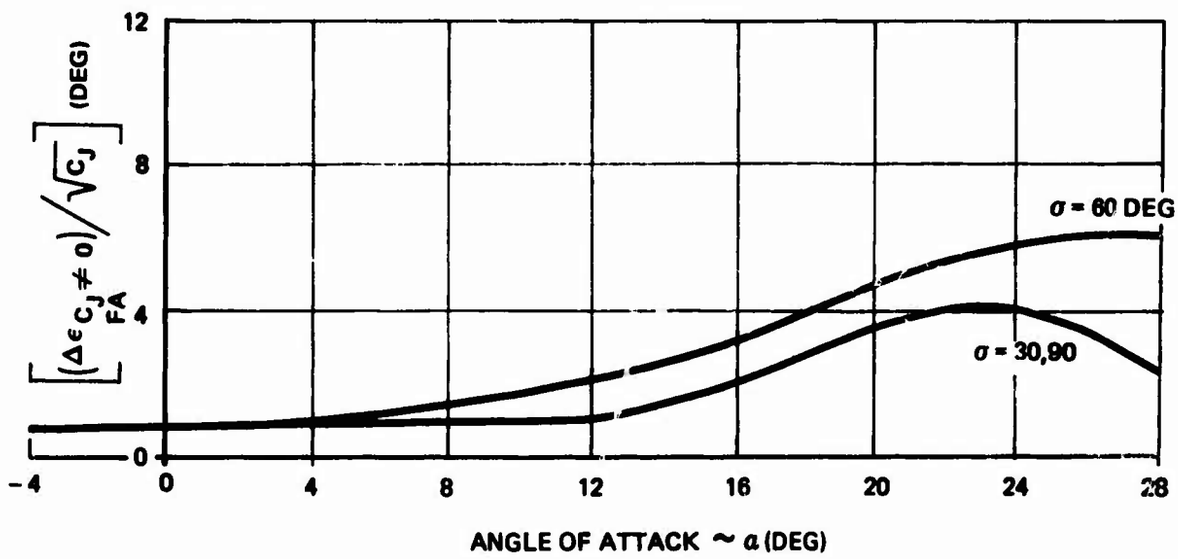

Figure 76: Thrust Effect on Downwash , $\delta_F = 35^0$

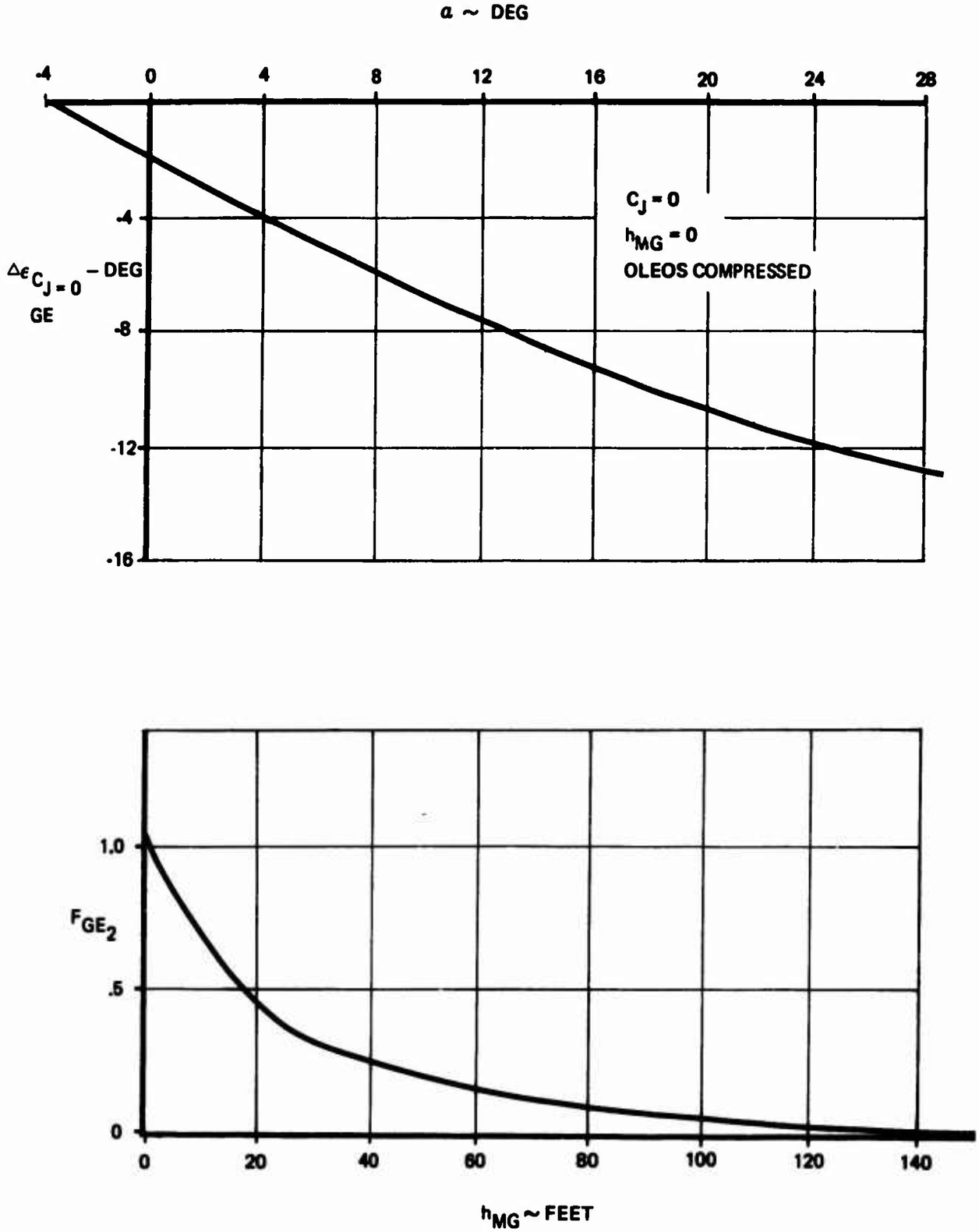

Figure 77: Change in Downwash Due to Ground Effect $C_J = 0$

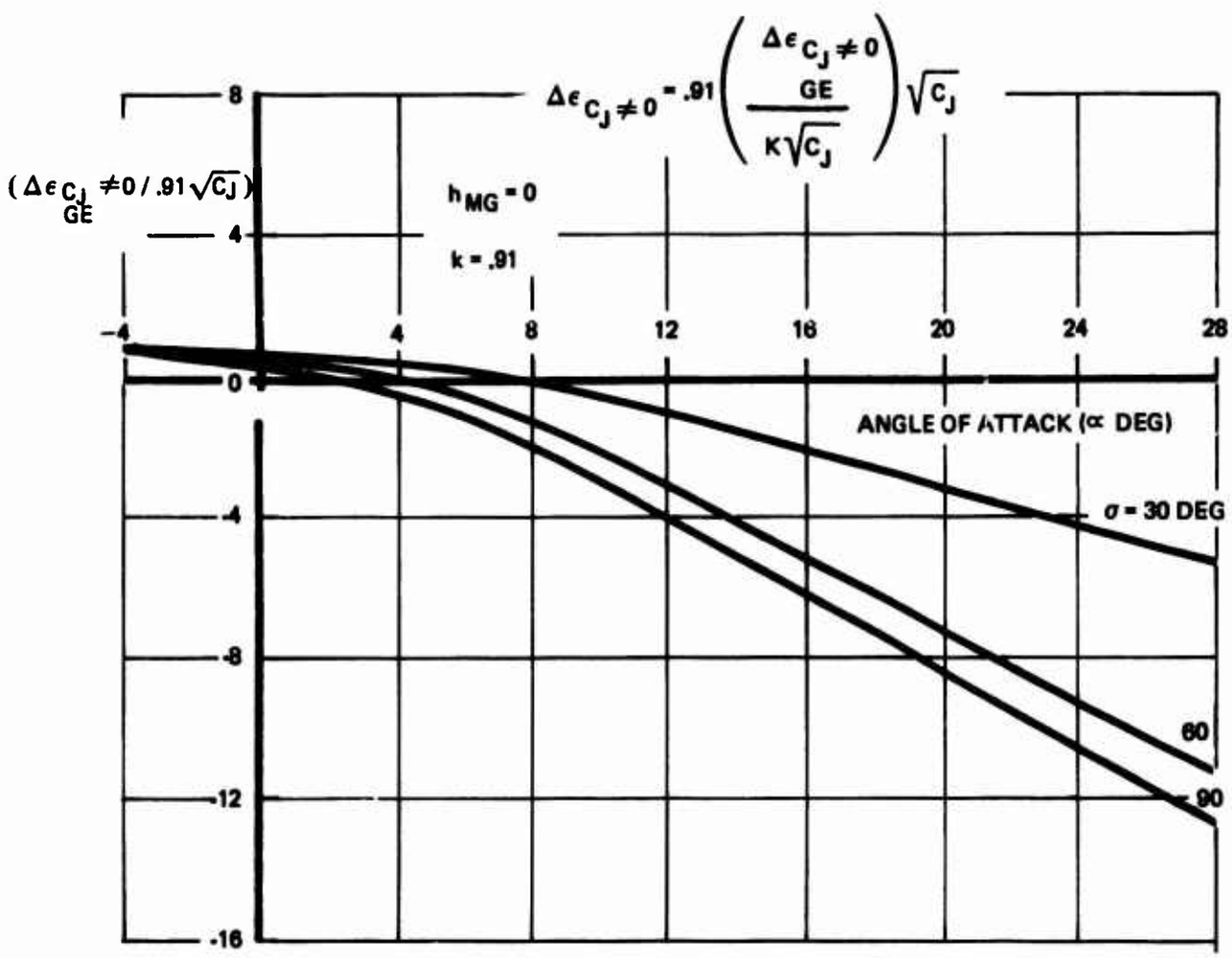

Figure 78: Ground Effect on Downwash, $\delta_F = 35^o$

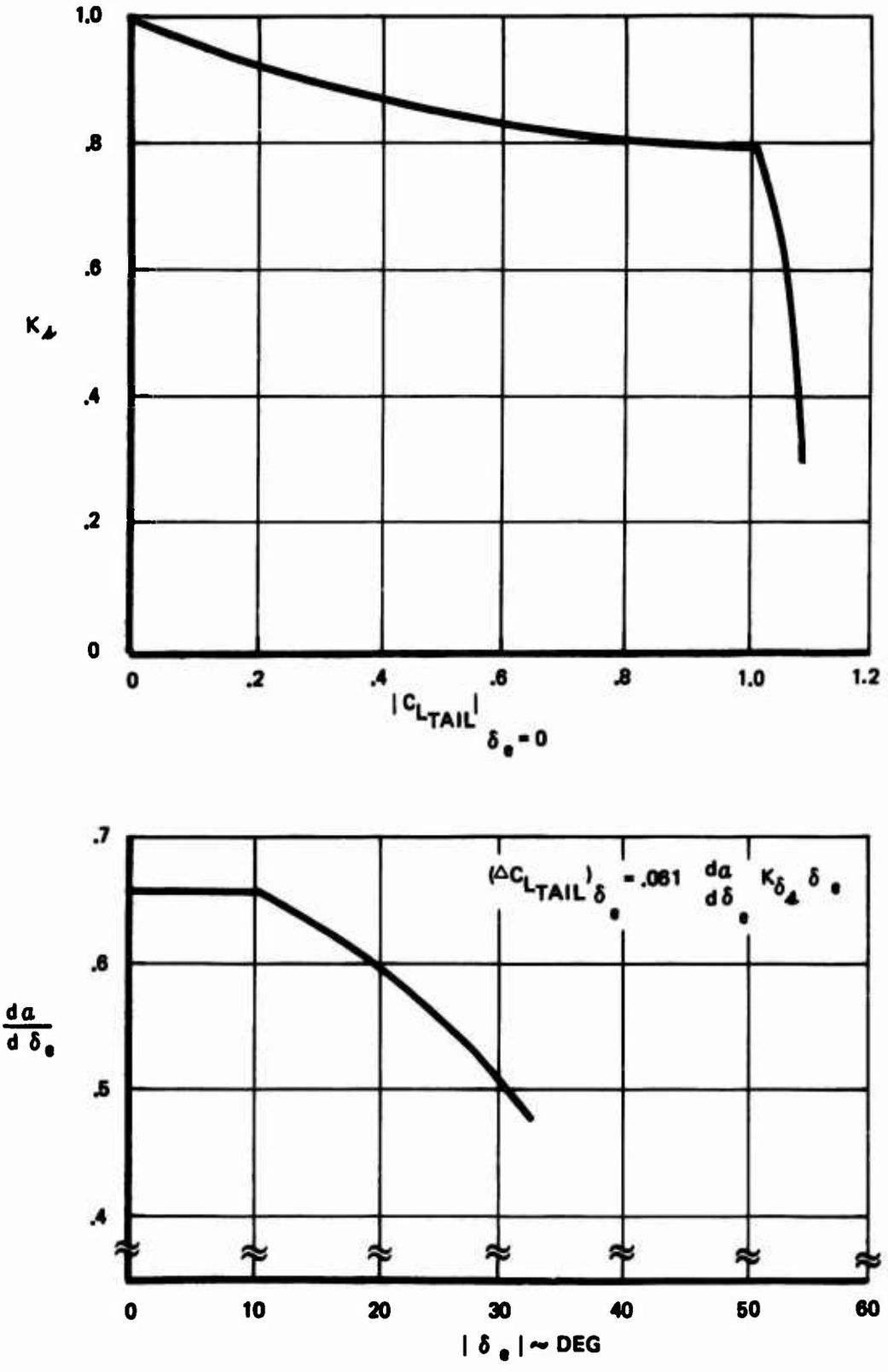

Figure 79: Change in Horizontal Tail Lift Due to Elevator Deflection

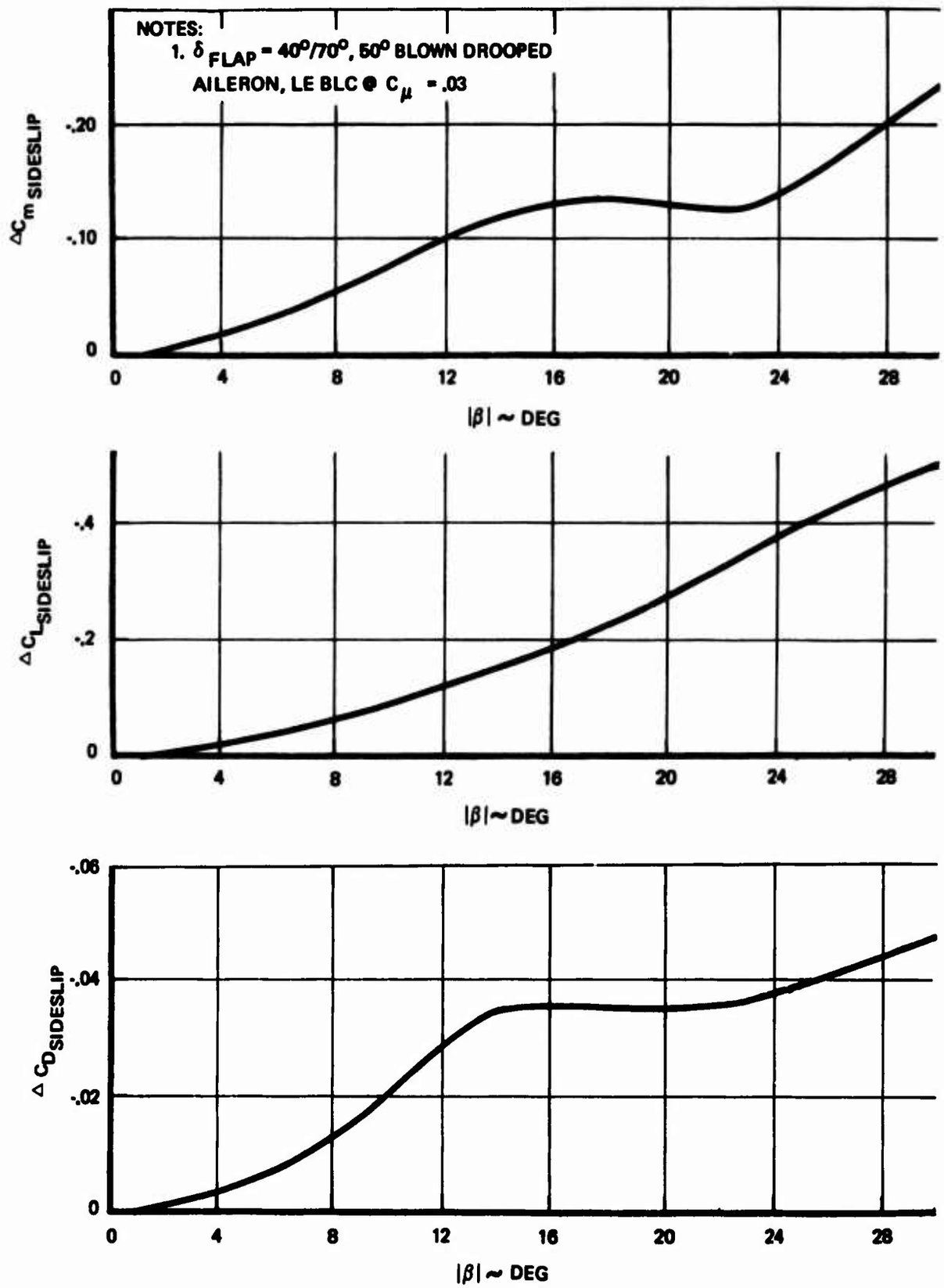

Figure 80: Change in the Lift, Drag, and Pitching Moment Coefficients Due to Sideslip

5. Lift Due to Lateral Control

$$\Delta C_{L_{LAT}} = \left[(K_{\delta_{SP\ RHW}}) + K_{\delta_{SP\ LHW}} \right] \Delta C_{L_{SP_{@\delta_{SP=60^\circ}}}}$$

where

$$(K_{\delta_{SP\ RHW}}) = f(\delta_{SP}) \quad \text{(Figure 81)}$$

$$\Delta C_{L_{SP_{@\delta_{SP=60^\circ}}}} = f(\alpha) \quad \text{(Figure 81)}$$

III.2.3.2 Drag Equation

The dimensionless aerodynamic drag force is separated into its important contributing elements in the equation below.

$$C_D = C_{D_{WB}} + \Delta C_{D_{SIDESLIP}} + \Delta C_{D_{LAT}} + \Delta C_{D_{RUD}} + \Delta C_{D_{ELEV}}$$

1. Wing-body Drag

$$C_{D_{WB}} = C_{D_{WB_{C_{J=0}}}} + \Delta C_{D_{WB_{C_{J\neq 0}}}} + \Delta C_{D_{WB_{GE}}}$$

(a) $C_{D_{WB_{C_{J=0}}}} = f(\alpha)$ (Figure 82)

(b) $\Delta C_{D_{WB_{C_{J\neq 0}}}} = f(\alpha, C_J, \sigma)$ (Figure 83)

(c) $\Delta C_{D_{WB}} = (\Delta C_{D_{C_{J=0}}} + \Delta C_{D_{C_{J\neq 0}}}) F_{GE_3}$

NOTE:

1. $\delta_{FLAP} = 40^{o}/70^{o}$, BLOWN DROOPED 50^{o}
   AILERON, BLC LE $C_{\mu} = .03$

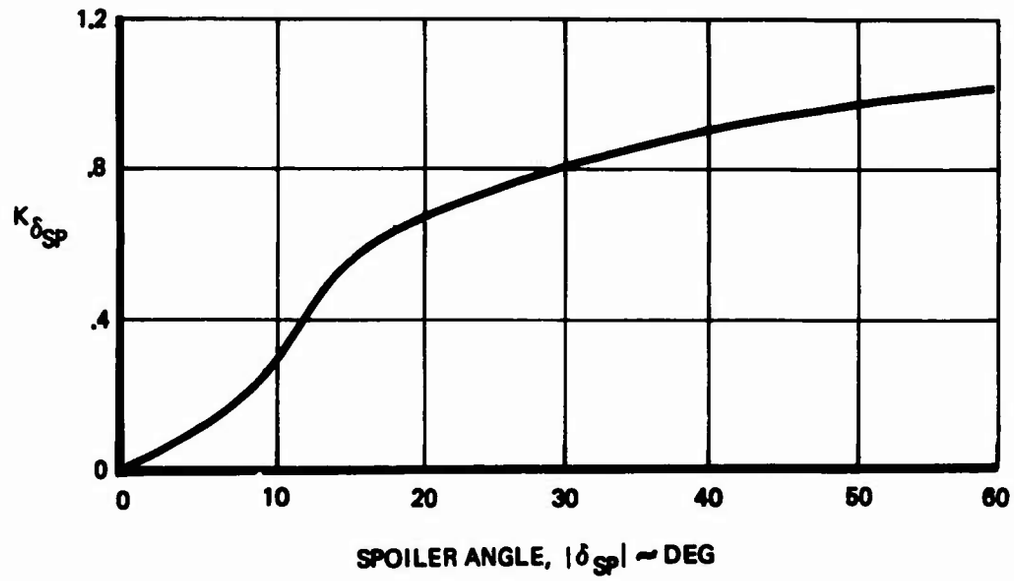

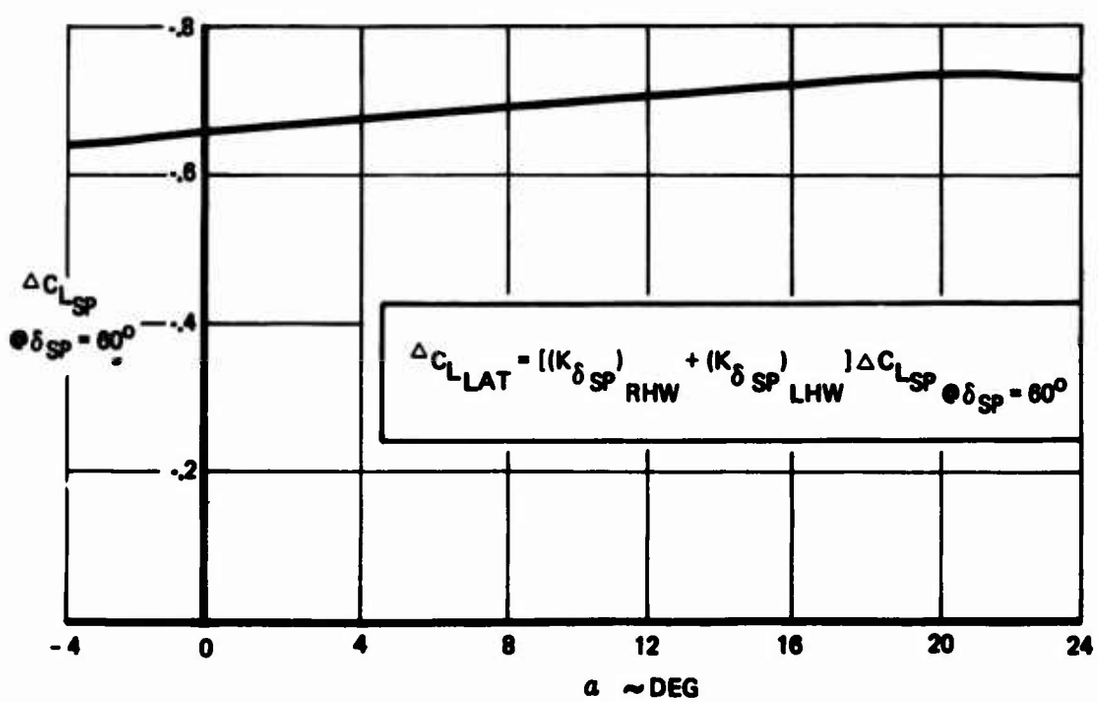

Figure 81: Lift Coefficient Effect of Lateral Control

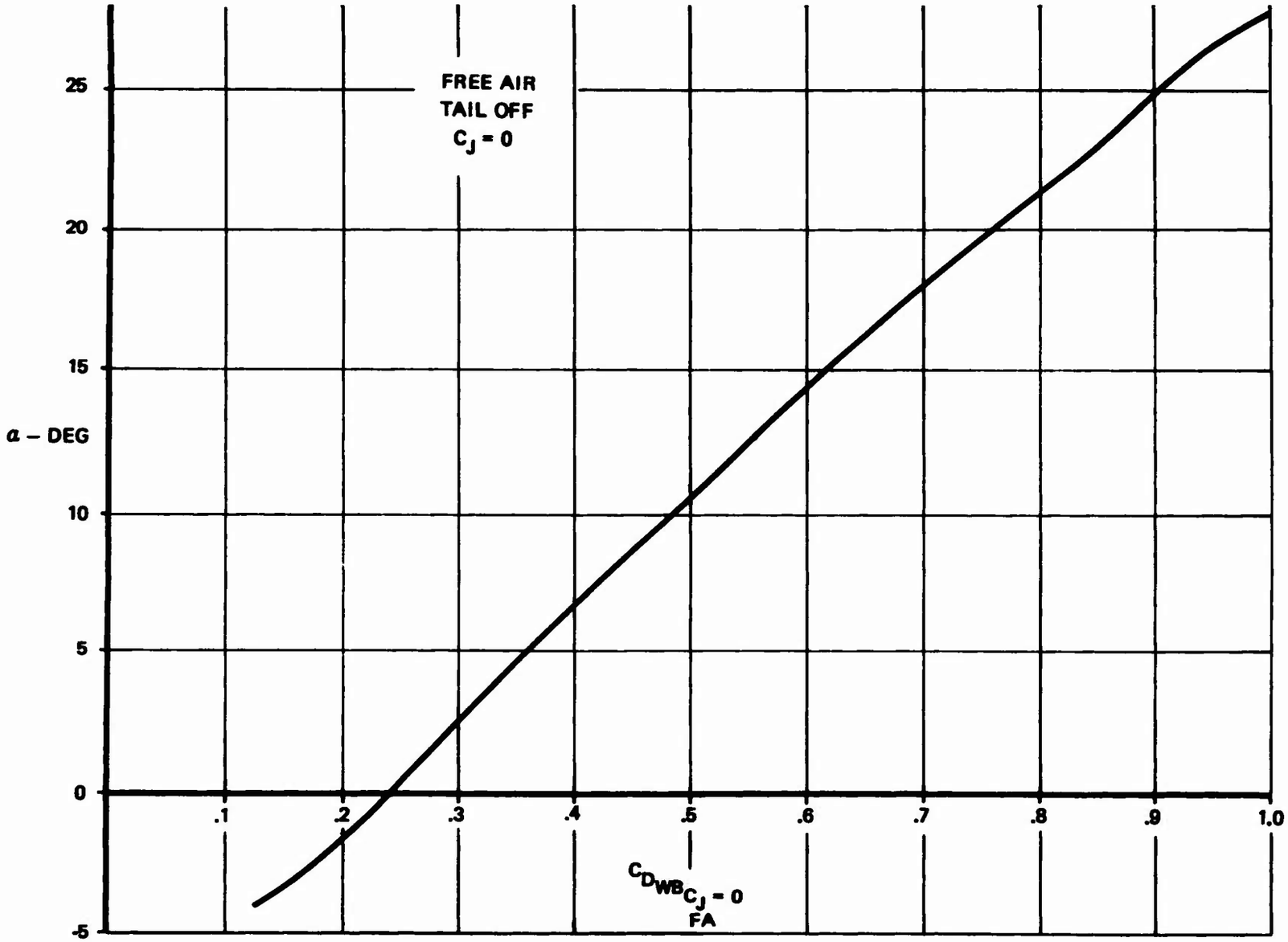

Figure 82: Wing Body Drag Free Air, $C_J = 0$

$$\Delta C_{D_{WB_{C_J \neq 0}}} = \left[\frac{\Delta C_{D_{WB_{C_J \neq 0}}}}{\sqrt{C_J}} \right] \sqrt{C_J}$$

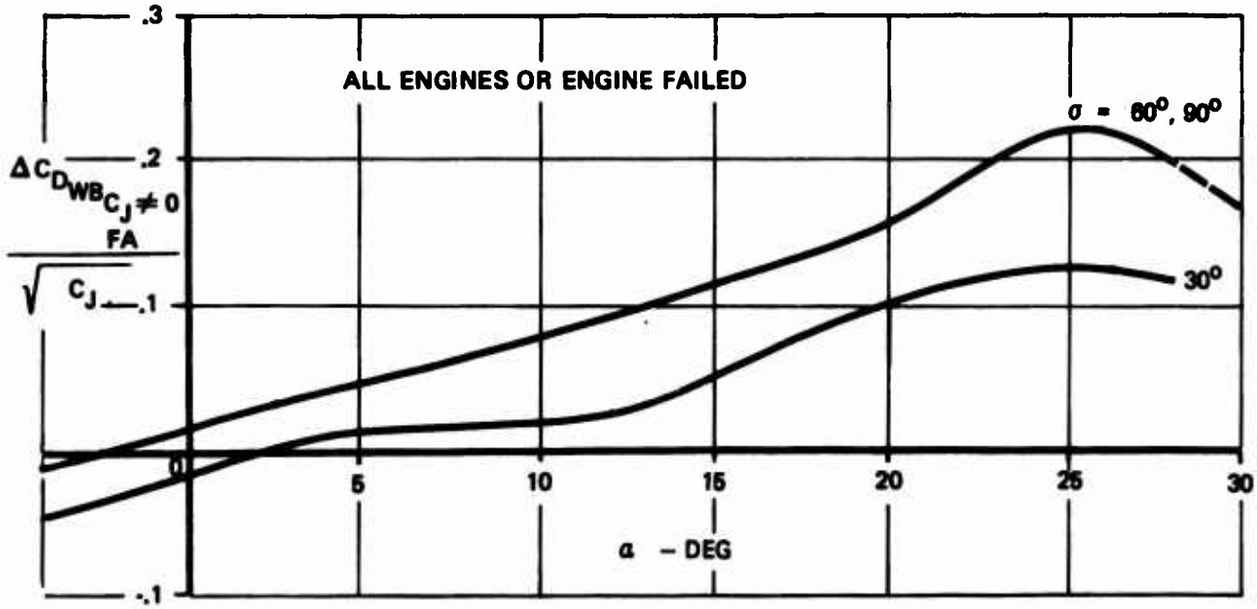

Figure 83: Effect of Power On Drag Free Air $\delta_F = 35^o$ – Tail Off

i) $\Delta C_{D_{\substack{C_J=0 \\ GE}}} = f(\alpha)$ (Figure 84)

ii) $\Delta C_{D_{\substack{C_J\neq 0 \\ GE}}} = f(\alpha, C_J, \sigma)$ (Figure 85)

iii) $F_{GE_3} = f(h_{MG})$ (Figure 84)

2. Drag Due to Sideslip

$$\Delta C_{D_{SIDESLIP}} = f(\beta)$$ (Figure 80)

3. Drag Due to Lateral Control

$$\Delta C_{D_{LAT}} = \left(\frac{\Delta C_D}{\Delta C_L}\right)_{LAT} \cdot \Delta C_{L_{LAT}}$$ (Figure 86)

(a) $\left(\frac{\Delta C_D}{\Delta C_L}\right)_{LAT} = f(\alpha)$

(b) $\Delta C_{L_{LAT}}$ is defined by Figure C48.

4. Drag Due to Directional Control

$$\Delta C_{D_{RUD}} = f(\beta, \delta_R)$$ (Figure 87)

5. Drag Due to Longitudinal Control

$$\Delta C_{D_{ELEV}} = f(C_{L_{TAIL_{\delta_e=0}}}, \delta_e)$$ (Figure 88)

III.2.3.3 Pitching Moment Equation

The dimensionless aerodynamic pitching moment about the center of gravity is separated into its important contributing elements in the equation below.

$$C_{m_{cg}} = C_{m_{WB_{.25\bar{c}}}} + C_{m_{TAIL}} + C_L\,(cg-.25) + \frac{\bar{c}}{2V_T}\,(C_{m_{\hat{\dot{\alpha}}}}\,\dot{\alpha} + C_{m_{\hat{q}}}\,q) +$$

$$\Delta C_{m_{SIDESLIP}} + \Delta C_{m_{LAT}}$$

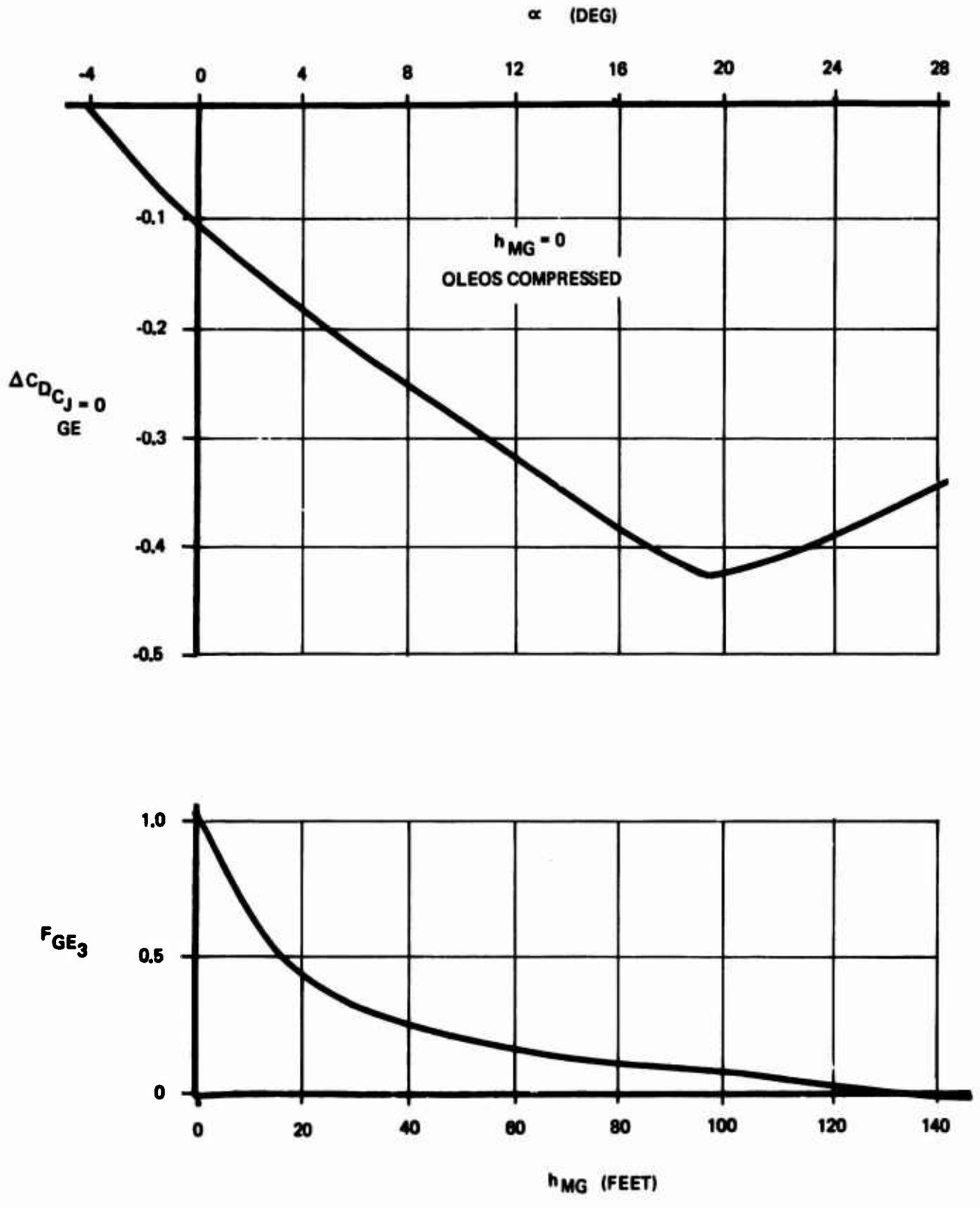

Figure 84: Change in Wing Body Drag Due to Ground Effect, $C_J = 0$

$$\Delta C_{D_{C_J \neq 0}} = \left(\frac{\Delta C_{D_{C_J \neq 0}}}{\sqrt{C_J}} \right) \sqrt{C_J}$$

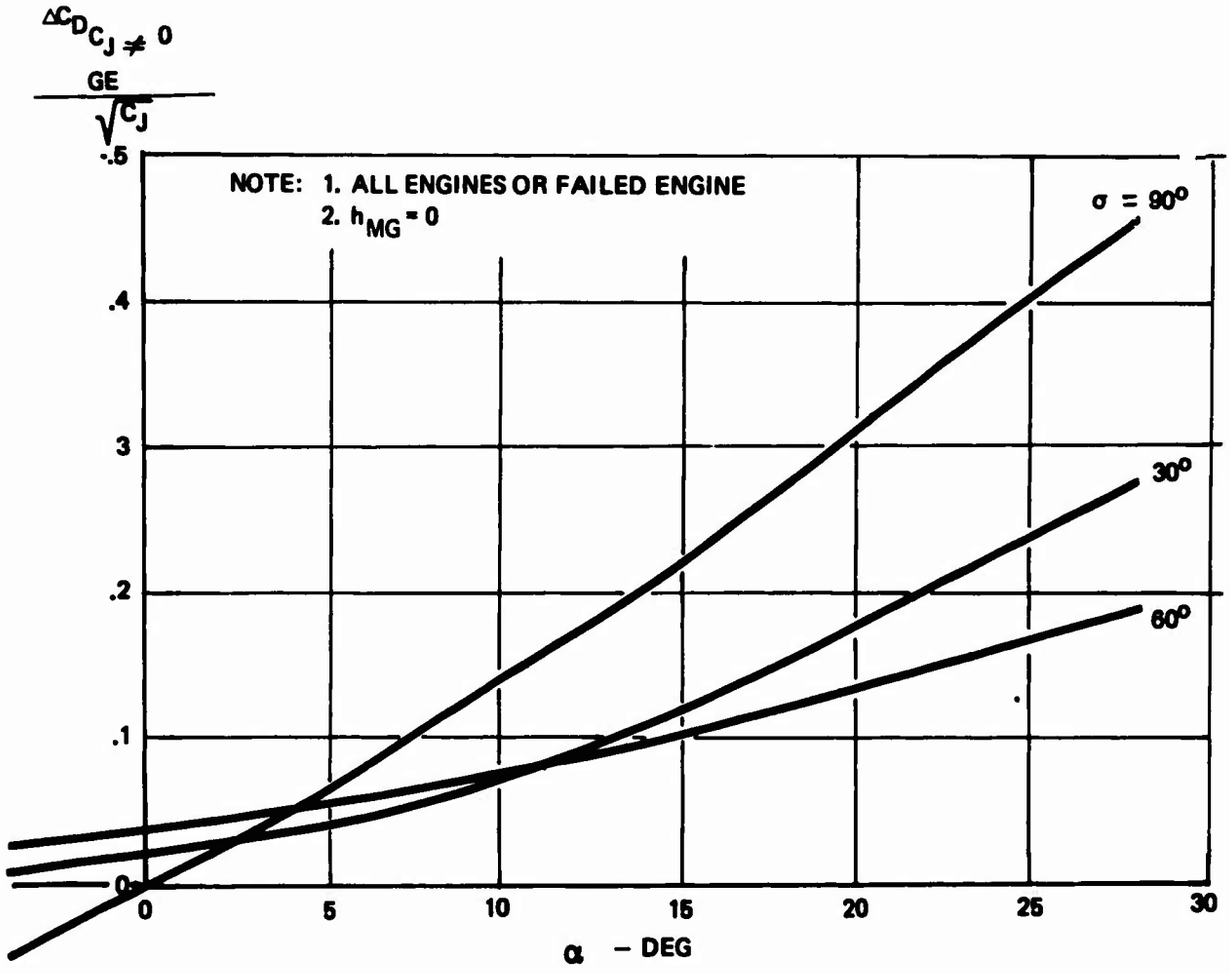

Figure 85: Effect of Power on Drag: In Ground Effect, $\delta_F = 35^o$, Tail Off

NOTES:

1. $\delta_{FLAPS} = 40^{o}/70^{o}, 50^{o}$ BLOWN DROOPED AILERON, LE BLC $C_{\mu} = .03$
2. $\Delta C_{D_{LAT}} = \left(\frac{\Delta C_D}{\Delta C_L}\right)_{LAT} \Delta C_{L_{LAT}}$
3. $\Delta C_{L_{LAT}}$ IS DEFINED BY FIGURE 81

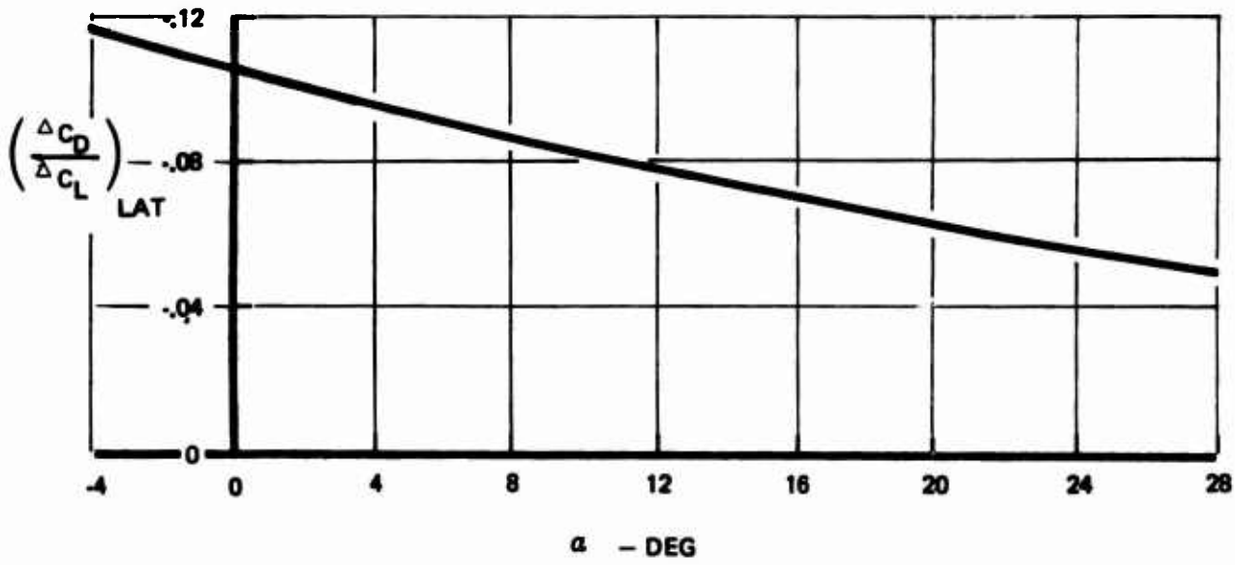

Figure 86: Change in Drag Due to Lateral Control

NOTE:

1. $\delta_{FLAPS} = 40^{o}/70^{o}$, BLOWN DROOPED 50^{o} AILERON, LE BLC $C_{\mu} = .03$

2. $\Delta C_{D_{RUDDER}} = 0$ FOR $\delta_R = 0^{o}$

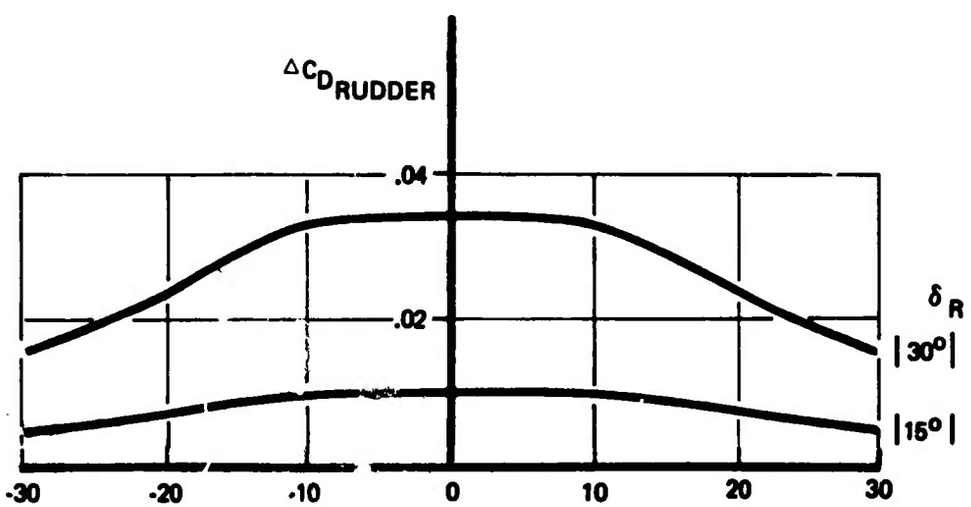

Figure 87: Drag Coefficient: Effect of Rudder

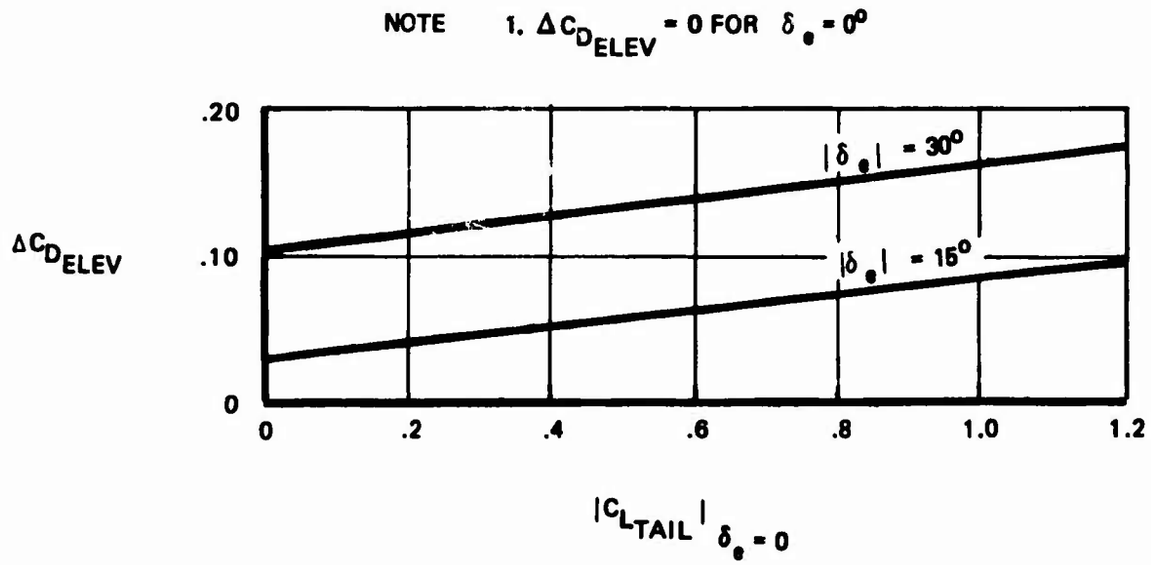

Figure 88: Drag Coefficient: Effect of Elevator

1. Wing-Body Pitching Moment

$$C_{m_{WB_{.25\bar{c}}}} = C_{m_{WB_{C_J=0}}}{}_{FA} + \Delta C_{m_{WB_{C_J\neq 0}}}{}_{FA} + \Delta C_{m_{WB_{GE}}}$$

(a) $C_{m_{WB_{C_J=0}}}{}_{FA} = f(\alpha)$ (Figure 89)

(b) $\Delta C_{m_{WB_{C_J\neq 0}}}{}_{FA} = f(\alpha, C_J, \sigma)$ (Figure 90)

(c) $\Delta C_{m_{WB_{GE}}} = (\Delta C_{m_{WB_{C_J=0}}}{}_{GE} + \Delta C_{m_{WB_{C_J\neq 0}}}{}_{GE}) F_{GE_4}$

i) $\Delta C_{m_{WB_{C_J=0}}}{}_{GE} = f(\alpha)$ (Figure 91)

ii) $\Delta C_{m_{WB_{C_J\neq 0}}}{}_{GE} = f(\alpha, C_J, \sigma)$ (Figure 92)

iii) $F_{GE_4} = f(h_{MG})$ (Figure 91)

2. Horizontal Tail Pitching Moment

$C_{m_{TAIL}} = -\left(\frac{\ell_H}{\bar{c}_w}\right) C_{L_{TAIL}}$; $C_{L_{TAIL}}$ is defined in Section III.2.3.1.

3. Pitching Moment Due to $\dot{\alpha}$ and q

(a) $C_{m_{\hat{\dot{\alpha}}}} = -6.06$ 1/RAD

(b) $C_{m_{\hat{q}}} = -32.94$ 1/RAD

4. Pitching Moment Due to Sideslip

$\Delta C_{m_{SIDESLIP}} = f(\beta)$ (Figure 80)

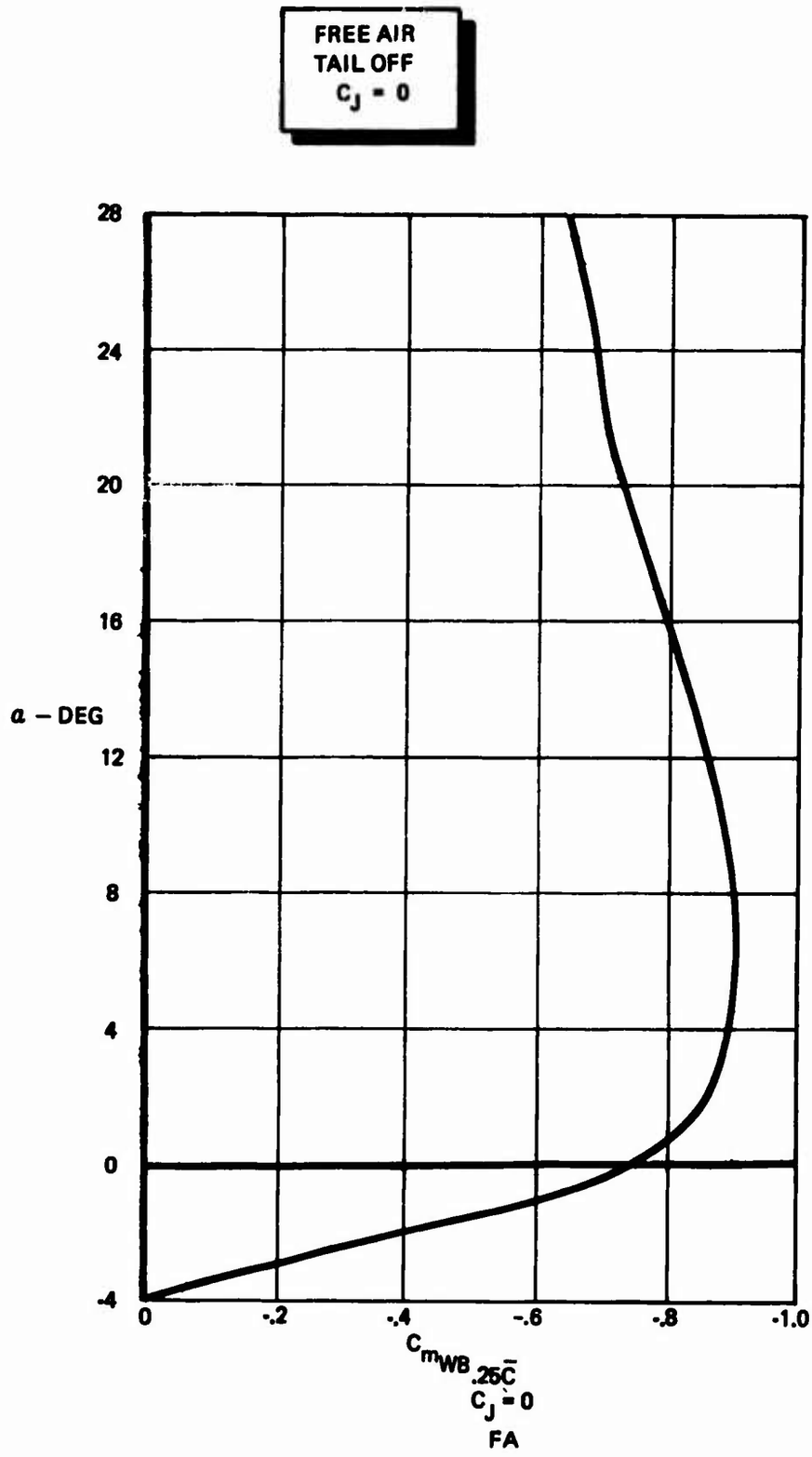

Figure 89: Wing Body Pitching Moment : Free Air, $C_J = 0$

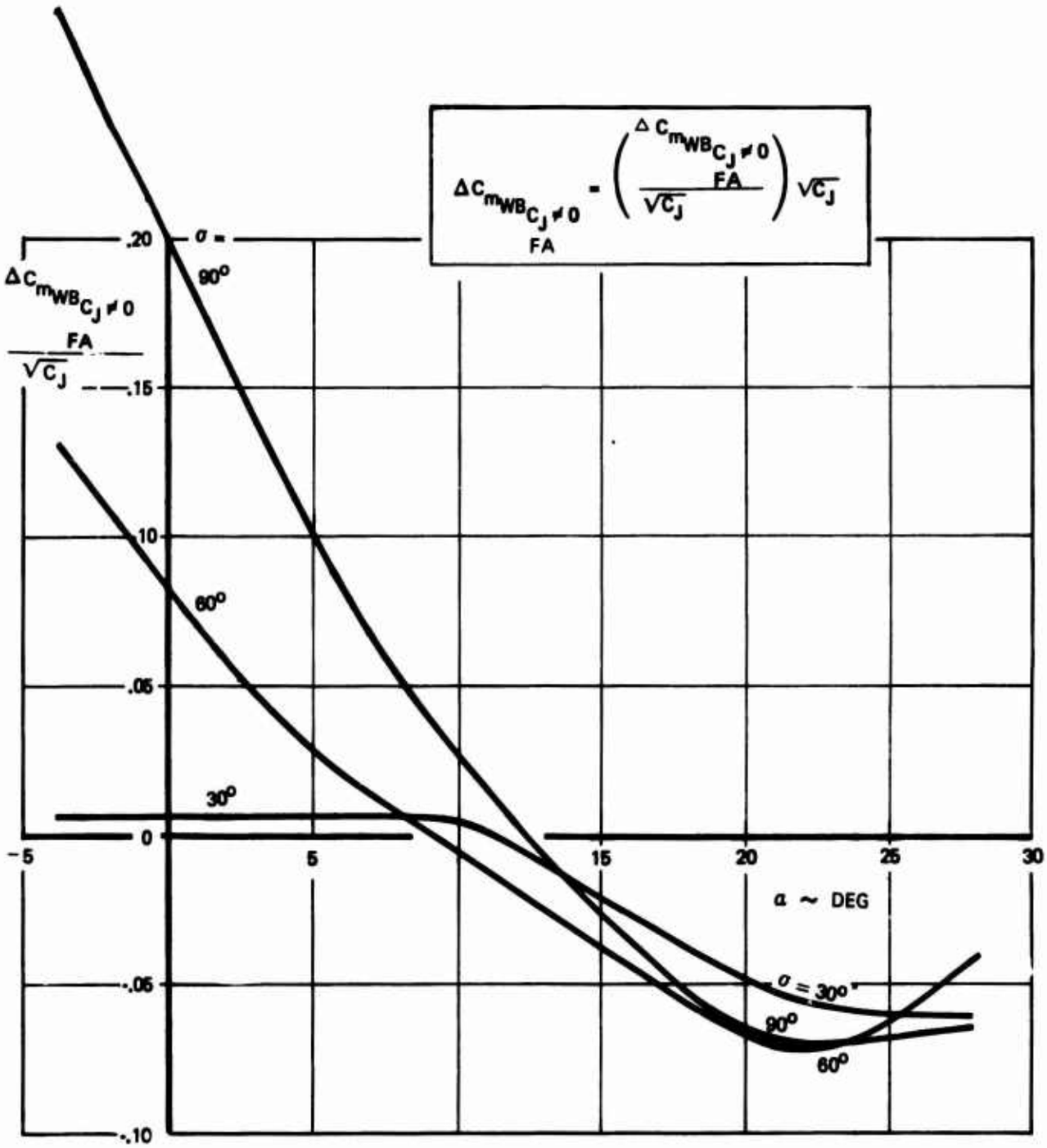

Figure 90: Effect of Thrust on Pitching Moment : Free Air, $\delta_F = 35^0$, Tail Off

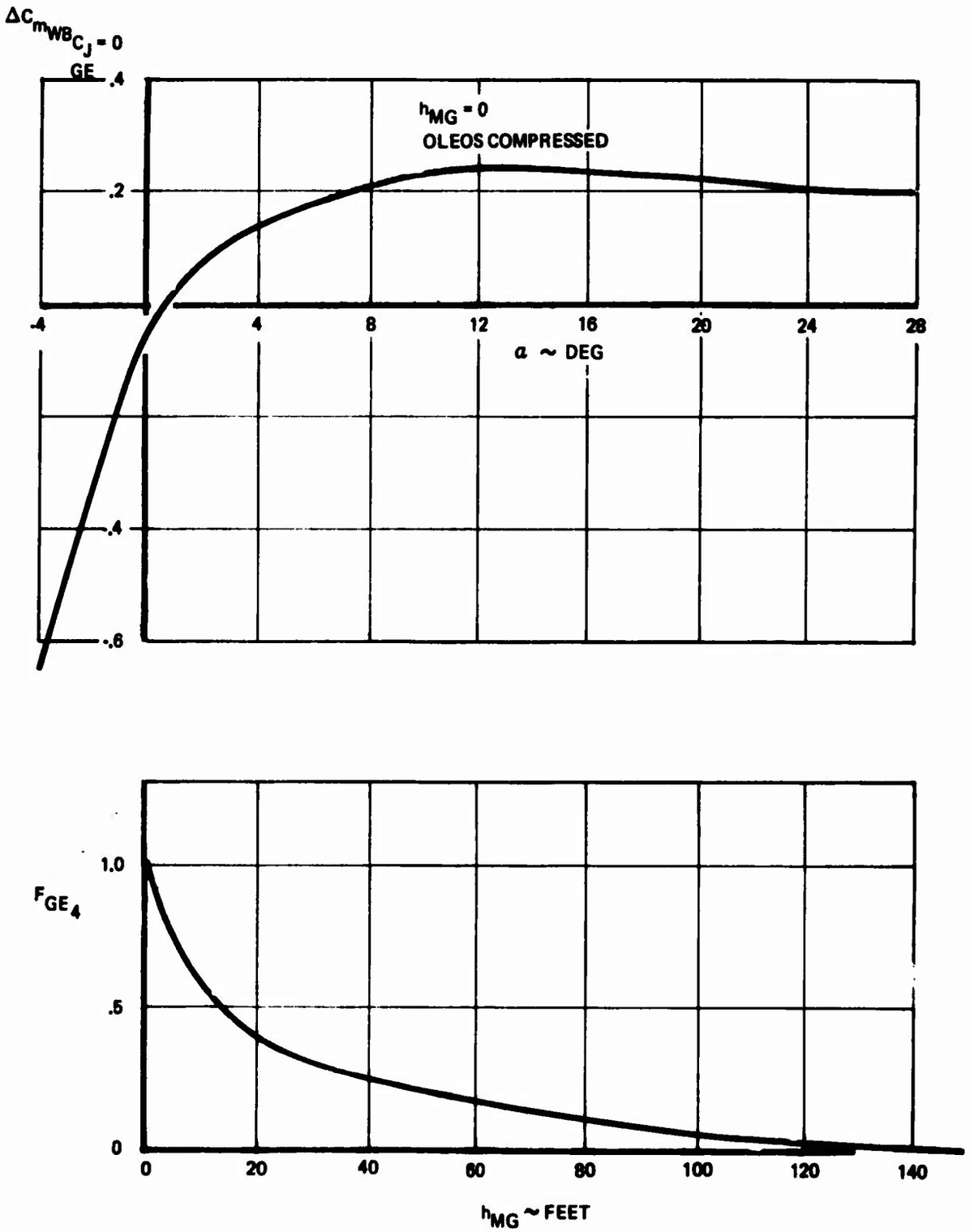

Figure 91: Change in Wing Body Pitching Moment Due to Ground Effect : $C_J = 0$

$h_{MG} = 0$

OLEO COMPRESSED

K = 1.47 CORRECTION FACTOR FOR 7.2 FEET

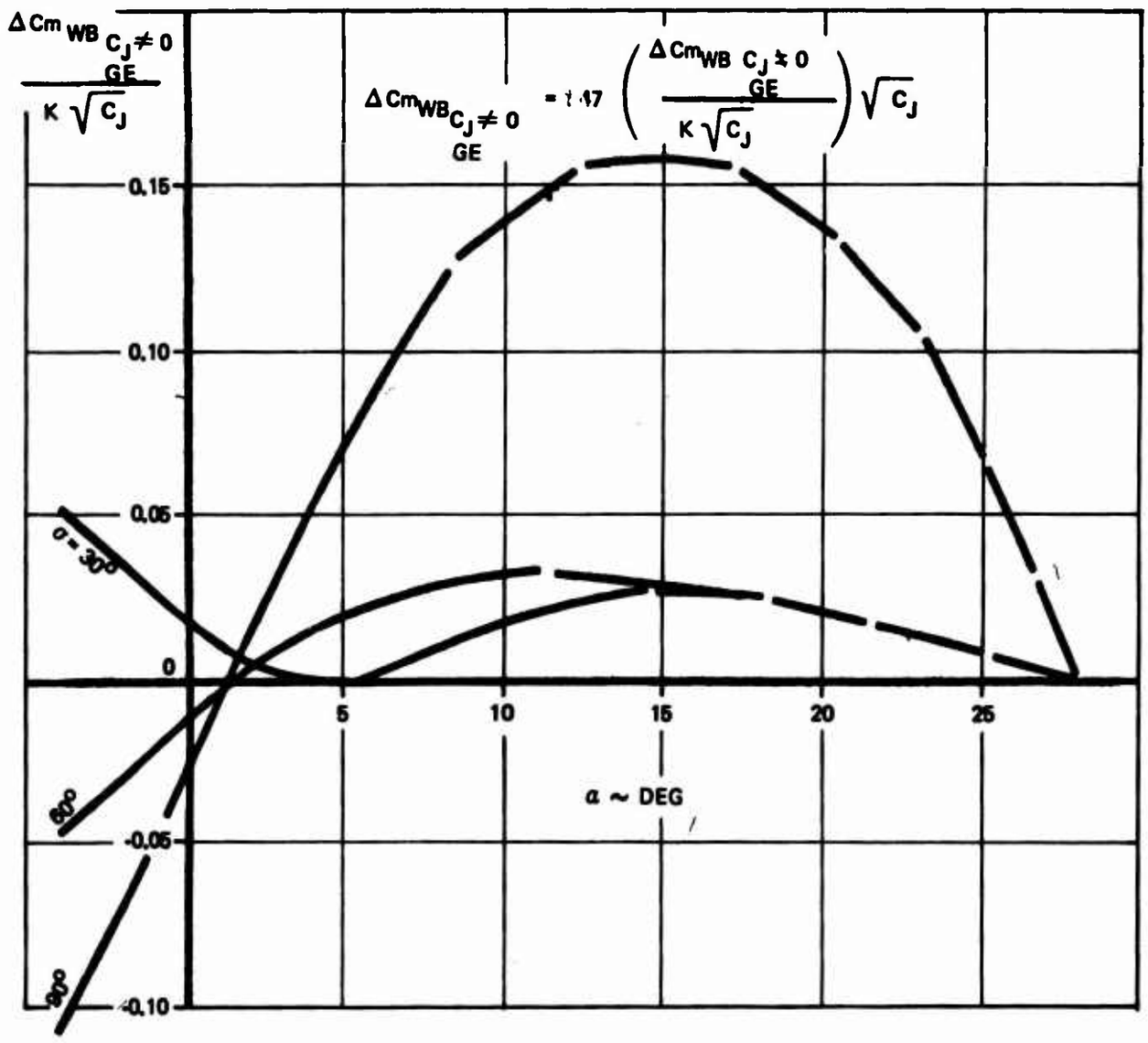

Figure 92: Effect of Power on Pitching Moment in Ground Effect : $\delta_f = 35^o$, Tail Off

5. Pitching Moment due to Lateral Control

$$\Delta C_{m_{LAT}} = \left(\frac{\Delta C_m}{\Delta C_L}\right)_{LAT} \cdot \Delta C_{L_{LAT}}$$

(Figure 93)

(a) $\left(\frac{\Delta C_m}{\Delta C_L}\right)_{LAT} = f(\alpha)$

(b) $\Delta C_{L_{LAT}}$ is defined by Figure 81.

III.2.3.4 Yawing Moment Equation

The dimensionless aerodynamic yawing moment about the center of gravity is separated into its important contributing components in the equation below.

$$C_{n_{CG}} = \Delta C_{n_{SIDESLIP}} + \frac{b_w}{2V_T}\left(C_{n_{\hat{\beta}}}\dot{\beta} + C_{n_{\hat{r}}} r_s + C_{n_{\hat{p}}} p_s\right) + \Delta C_{n_{LAT}} + \Delta C_{n_{QUAD}}$$

$$+ C_y\,(cg-.25)\,\frac{\bar{c}w}{bw}$$

1. Yawing Moment Due to Sideslip

$$\Delta C_{n_{SIDESLIP}} = \left[K_{\beta_1} C_{n_{\beta_{\substack{C_J=0\\FA}}}} \left(\frac{C_{n_{\beta_{GE}}}}{C_{n_{\beta_{FA}}}}\right)\right]\beta$$

(a) $K_{\beta_1} = f(\beta)$ (Figure 94)

(b) $C_{n_{\beta_{\substack{C_J=0\\FA}}}} = f(\alpha)$ (Figure 94)

(c) $\left(\frac{C_{n_{\beta_{GE}}}}{C_{n_{\beta_{FA}}}}\right) = f(h_{MG})$ (Figure 95)

2. Yawing Moment Due to $\dot{\beta}$, r_s, and p_s

(a) $C_{n_{\hat{\beta}}} = f(\alpha)$ (Figure 96)

(b) $C_{n_{\hat{r}}} = f(\alpha)$ (Figure 96)

(c) $C_{n_{\hat{p}}} = f(\alpha)$ (Figure 96)

NOTES:

1. δ_{FLAP} = 40°/70°, 50° BLOWN
   DROOPED AILERON, L.E. BLC $C\mu$ = .03
2. $$\Delta C_{m_{LAT}} = \left(\frac{\Delta C_m}{\Delta C_L}\right)_{LAT} \Delta C_{L_{LAT}}.$$
3. $\Delta C_{L_{LAT}}$ IS DEFINED BY Fig. 81

$\left(\frac{\Delta C_m}{\Delta C_L}\right)_{LAT.}$

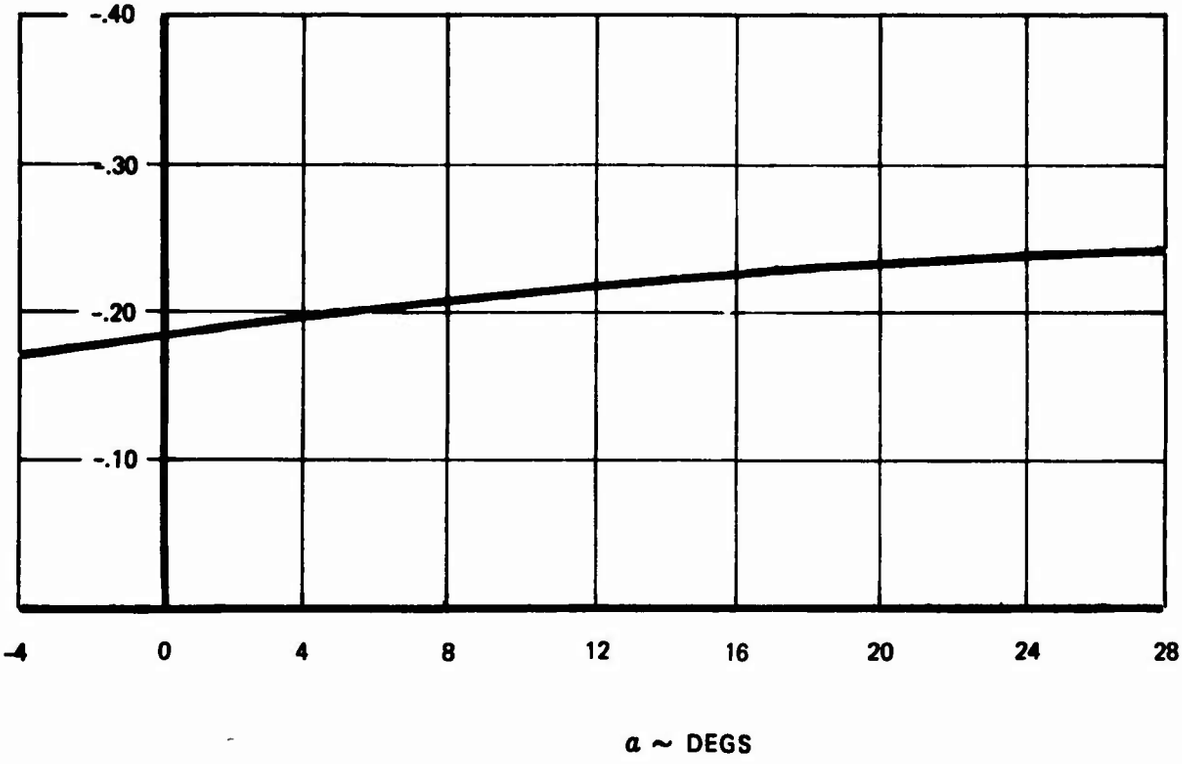

Figure 93: Change In Pitching Moment Due To Lateral Control

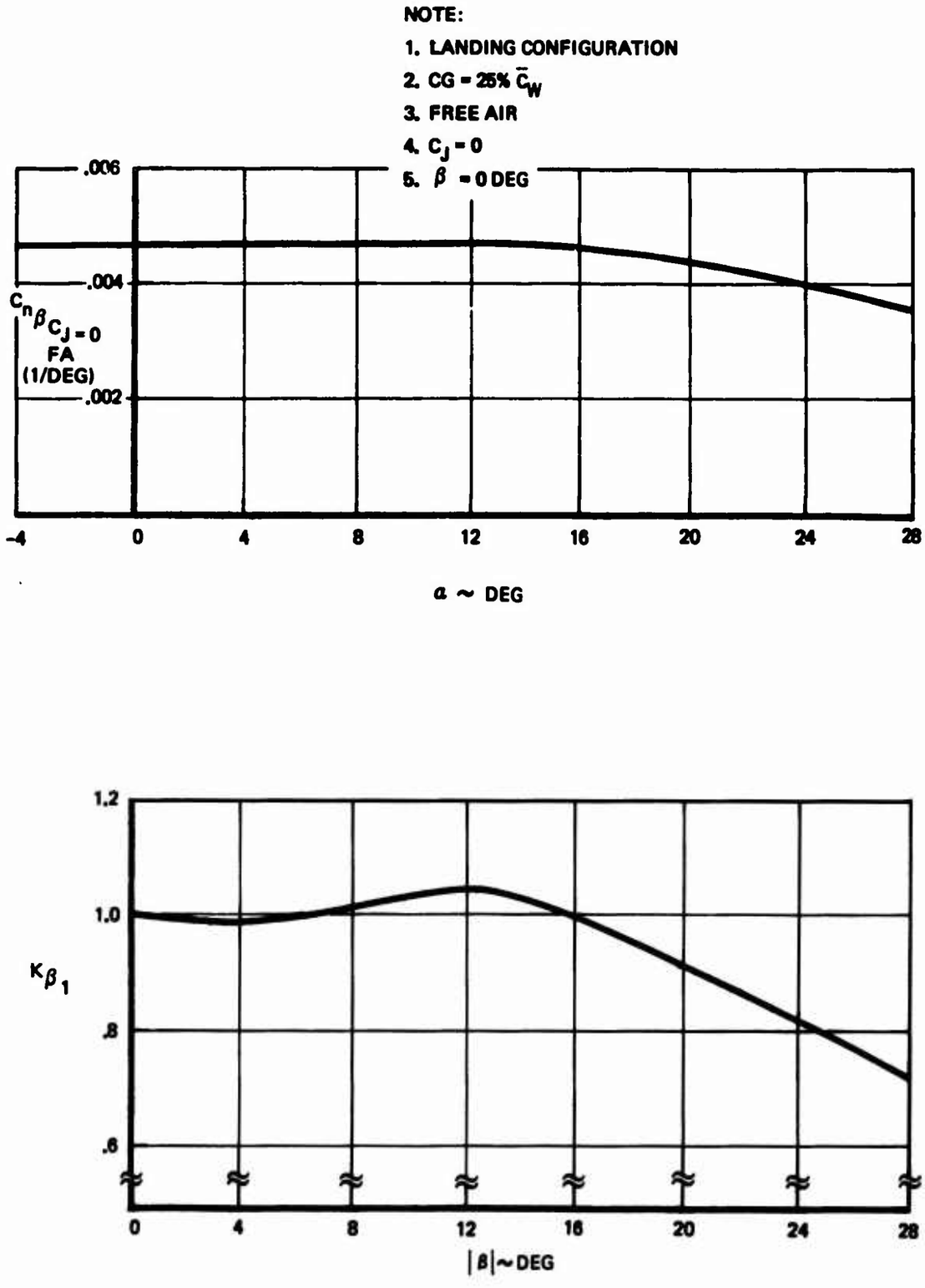

Figure 94: Yawing Moment Due to Sideslip : Free Air, $C_J = 0$

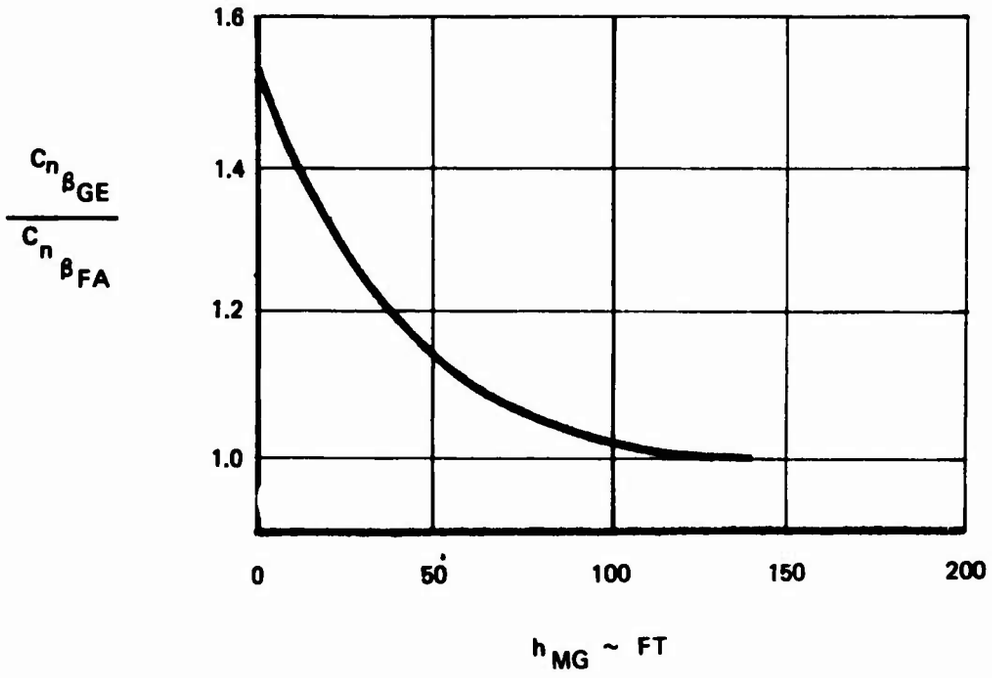

Figure 95: Effect of Ground Proximity on Yawing Moment Due to Sideslip

NOTE:

1. LANDING CONFIGURATION
2. C. G. = 25% MAC

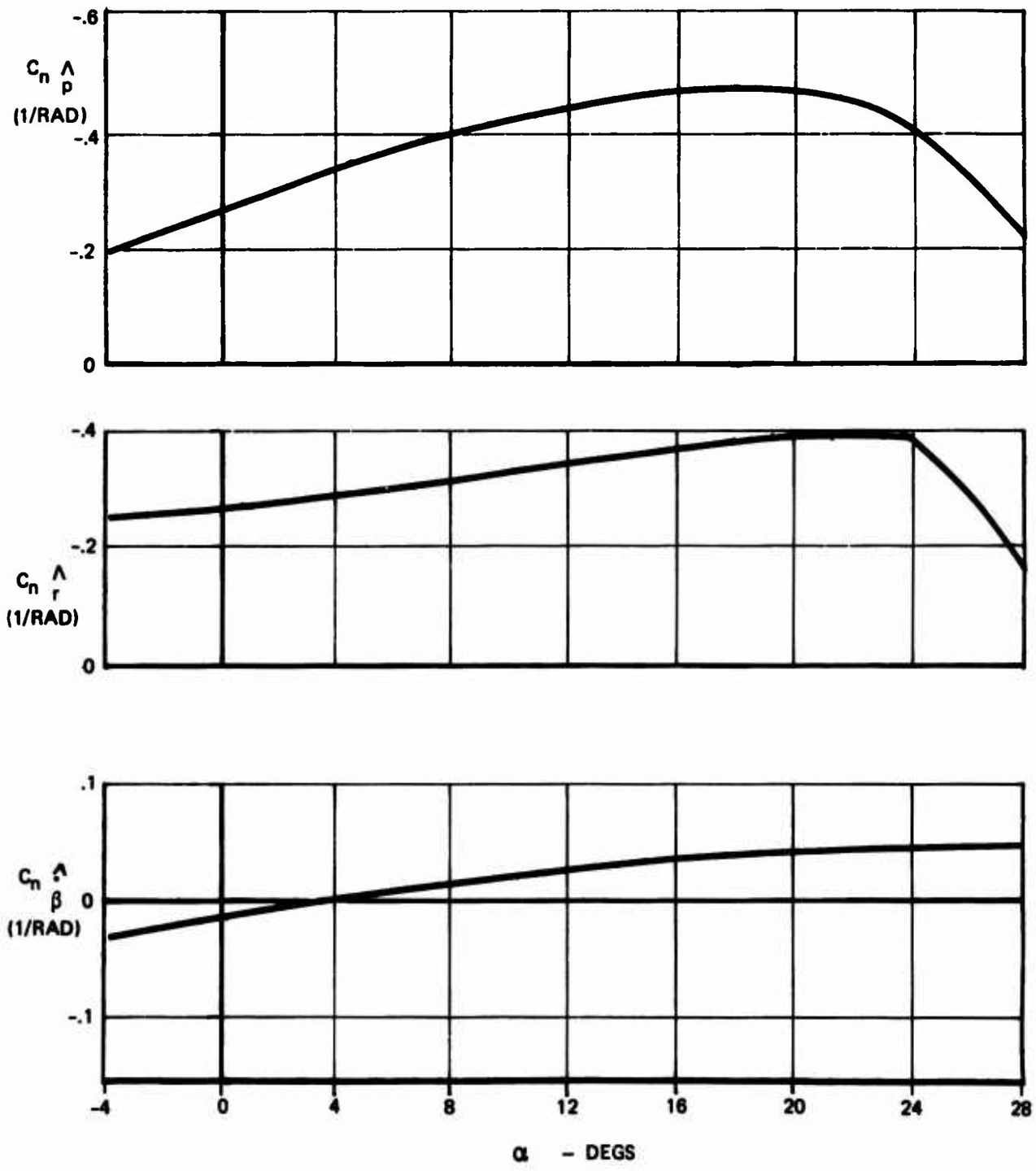

Figure 96: Yawing Moment Due to $\hat{p}$, $\hat{r}$, AND $\Delta\beta$

3. Yawing Moment Due To Lateral Control

(a) $K_{\beta_4} = f(\beta)$ (Figure 97)

(b) $(\Delta C_n/\Delta C_l)_{LAT} = f(\alpha)$ (Figure 97)

(c) $\Delta C_{l_{LAT}}$ is defined by Section III.2.3.5

4. Yawing Moment Due To Directional Control

$$\Delta C_{n_{RUD}} = K_{\beta_3}(\Delta C_{n_{RUD}})_{\beta=0}$$

(a) $K_{\beta_3} = f(\beta)$ (Figure 98)

(b) $(\Delta C_{n_{RUD}})_{\beta=0} = f(\delta_R)$ (Figure 98)

III.2.3.5 Rolling Moment Equation

The dimensionless aerodynamic rolling moment is separated into its important contributing components by the equation below.

$$C_l = \Delta C_{l_{SIDESLIP}} + \frac{b_w}{2V_T}\left(C_{l_{\hat{\beta}}}\dot{\beta} + C_{l_{\hat{p}}} r_s + C_{l_{\hat{p}}} p_s\right) + \Delta C_{l_{LAT}} + \Delta C_{l_{RUD}}$$

1. Rolling Moment Due To Sideslip

$$\Delta C_{l_{SIDESLIP}} = \left[K_{\beta_2} C_{l_{\beta_{C_J=0}}}\left(\frac{C_{l_{\beta_{C_J\neq 0}}}^{FA}}{C_{l_{\beta_{C_J=0}}}}\right)\right]\beta$$

(a) $K_{\beta_2} = f(\beta)$ (Figure 99)

(b) $C_{l_{\beta_{C_J=0}}} = f(\alpha)$ (Figure 99)

(c) $\left(\frac{C_{l_{\beta_{C_J\neq 0}}}^{FA}}{C_{l_{\beta_{C_J=0}}}}\right) = f(\alpha, C_J)$ (Figure 100)

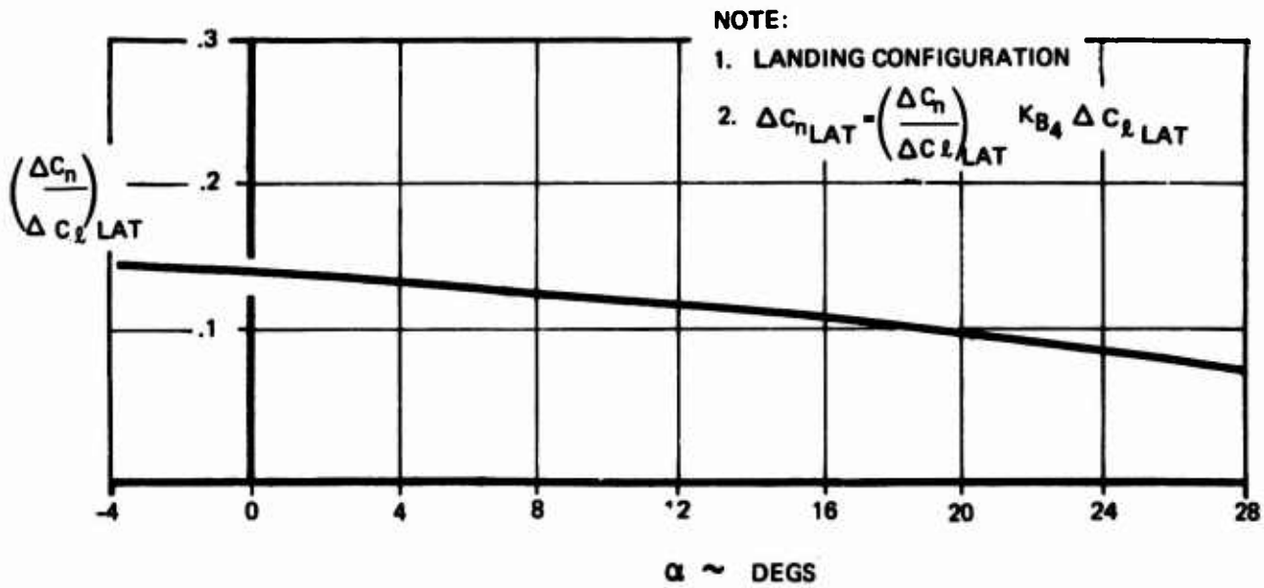

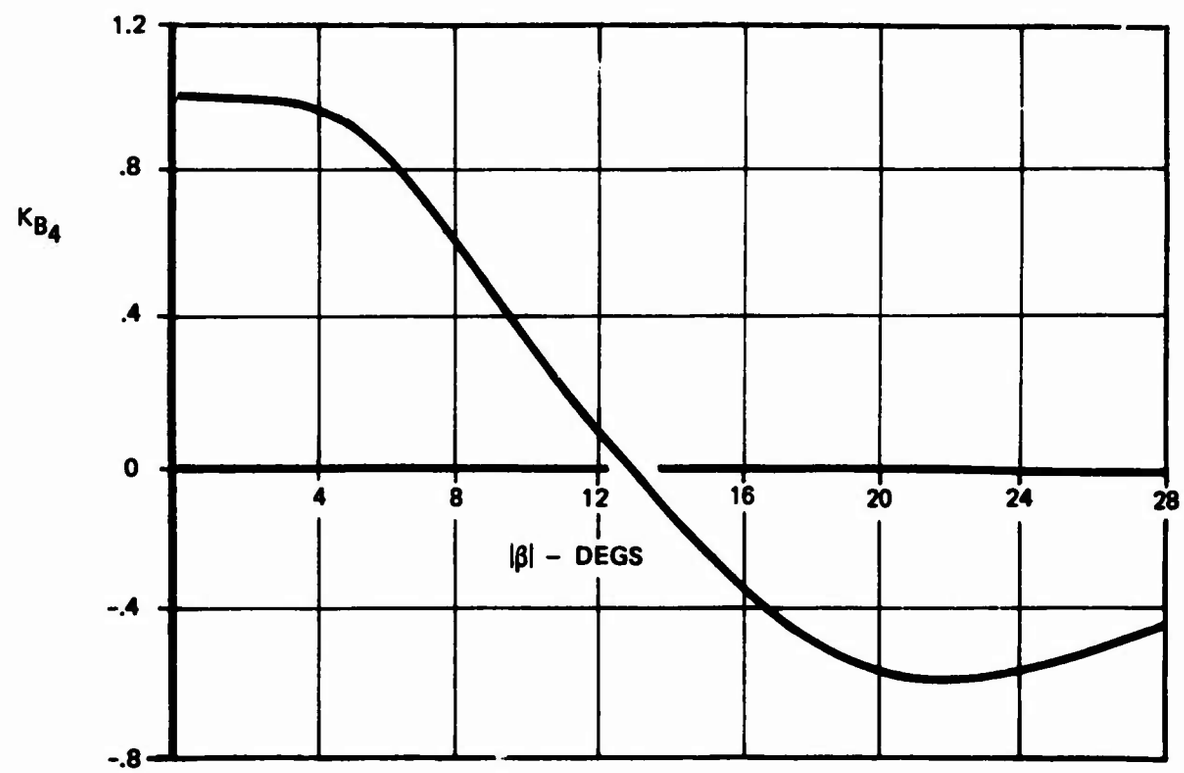

Figure 97: Yawing Moment Due to Lateral Control

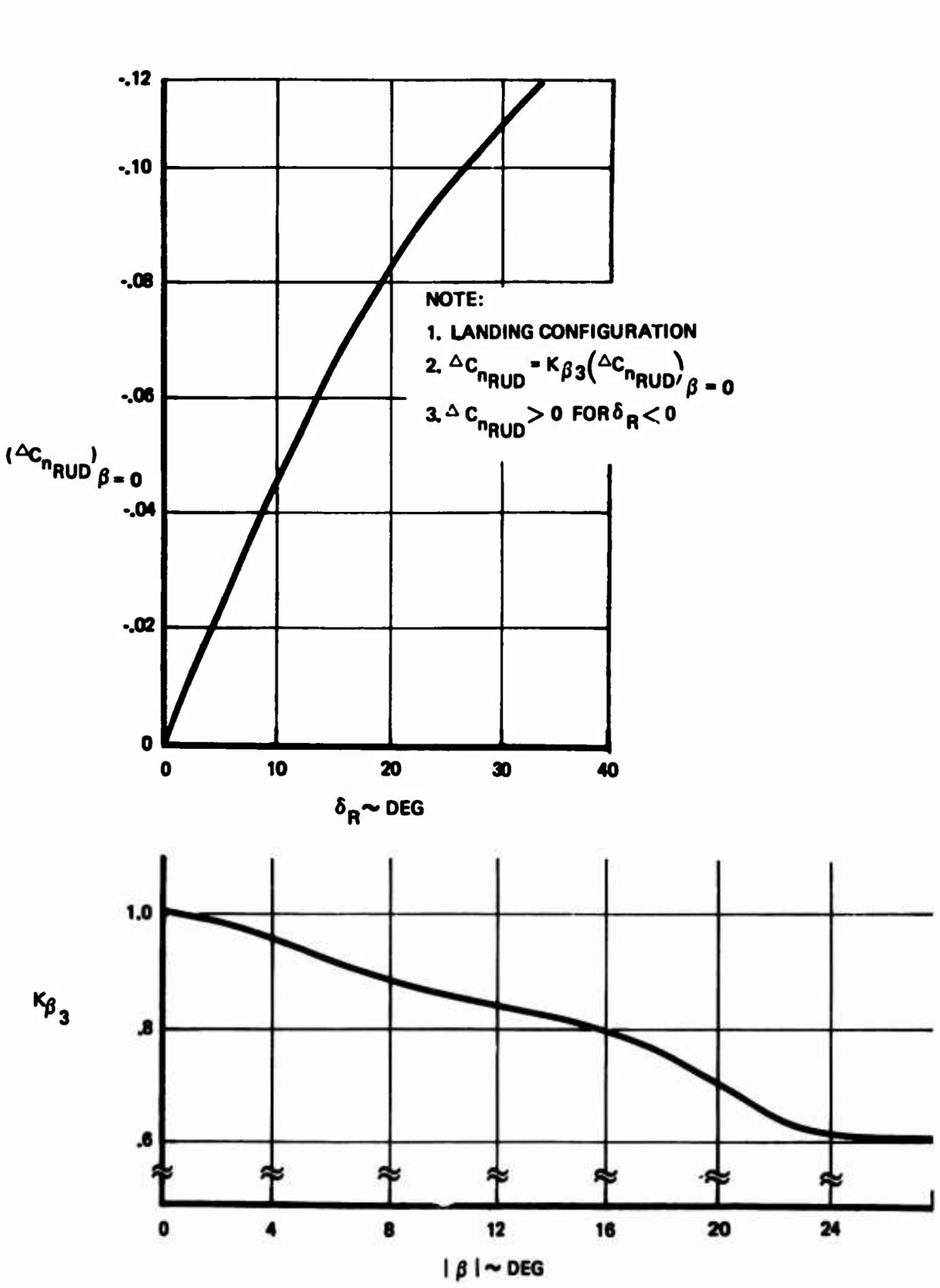

Figure 98: Yawing Moment Due to Directional Control

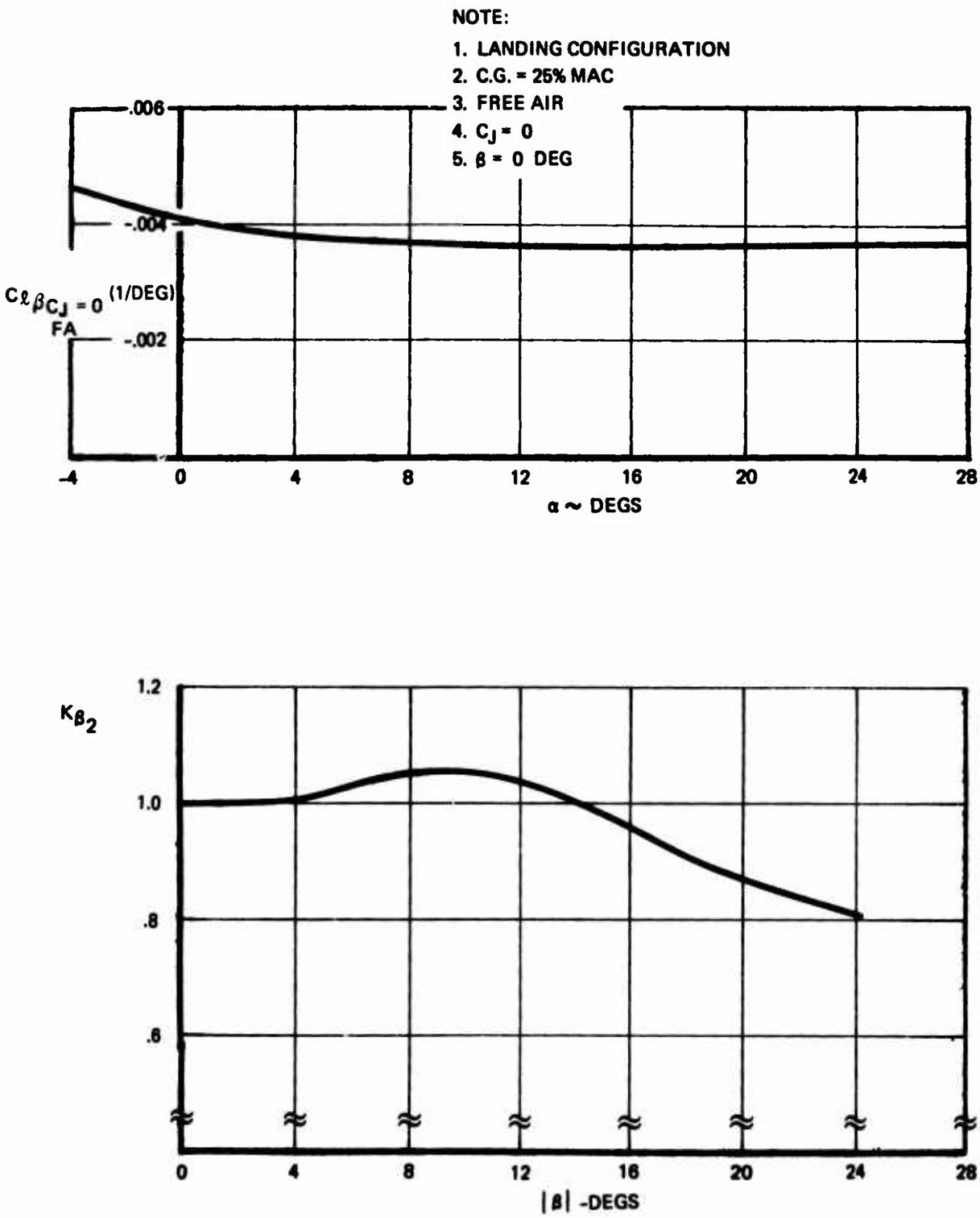

Figure 99: Rolling Moment Due to Sideslip: Free Air, $C_J = 0$

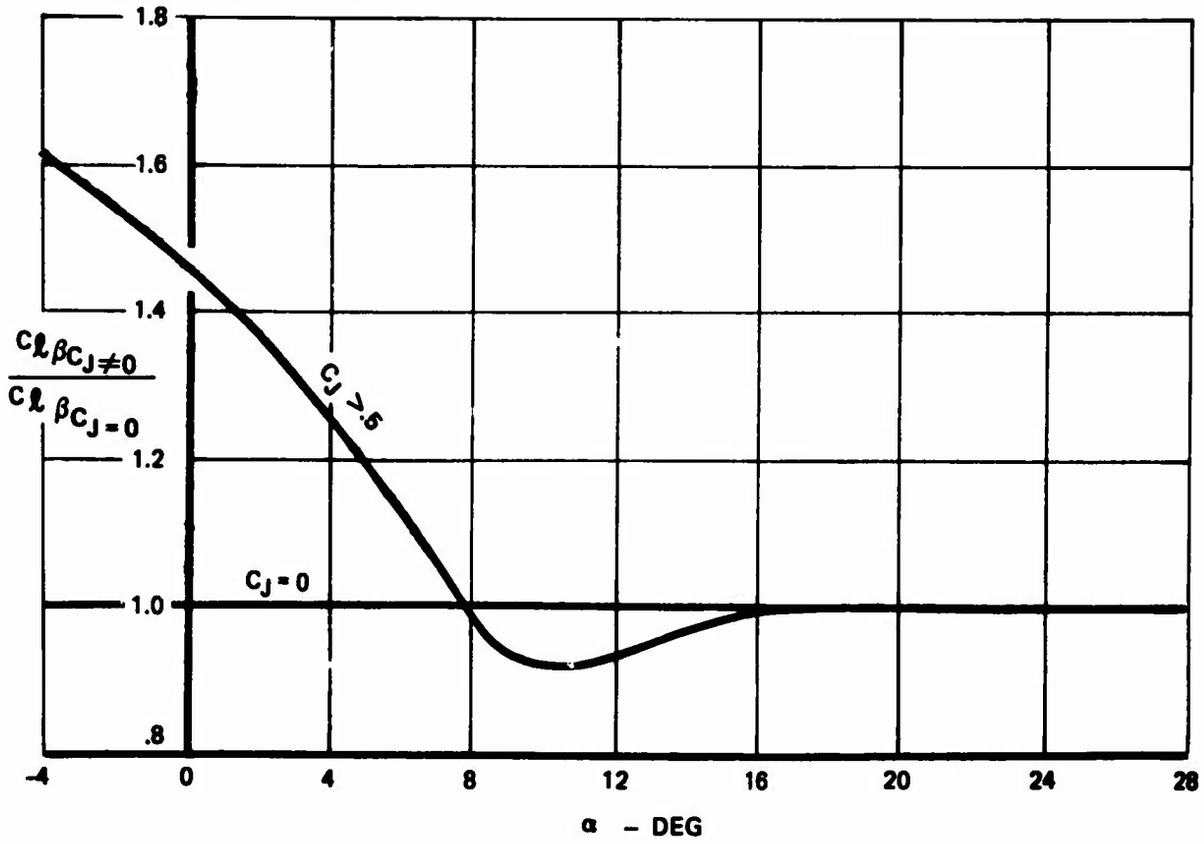

Figure 100: Effect of Thrust on Rolling Moment Due to Sideslip

2. Rolling Moment Due To $\dot{\beta}$, r_s and p_s

(a) $C_{l_{\dot{\beta}}} = f(\alpha)$ (Figure 101)

(b) $C_{l_{\hat{r}}} = f(\alpha)$ (Figure 101)

(c) $C_{l_{\hat{p}}} = f(\alpha)$ (Figure 101)

3. Rolling Moment Due To Lateral Control

$$\Delta C_{l_{LAT}} = \left[(K_{\delta_{SP}})_{RHW} - (K_{\delta_{SP}})_{LHW}\right] \Delta C_{l_{SP_{@\delta_{SP}=60^\circ}}} + .00135\,\delta_a$$

(a) $(K_{\delta_{SP}})_{\substack{RHW \\ LHW}}$ is defined by Figure 81

(b) $\Delta C_{l_{SP_{@\delta_{SP}=60^\circ}}} = f(\alpha)$ (Figure 102)

4. Rolling Moment Due To Directional Control

$$\Delta C_{l_{RUD}} = K_{\beta_3} K_{\alpha_1} (\Delta C_{l_{RUD}})_{\alpha=0}$$

(a) K_{β_3} is defined by Figure 98

(b) $K_{\alpha_1} = f(\alpha)$ (Figure 103)

(c) $(\Delta C_{l_{RUD}})_{\substack{\alpha=0 \\ \beta=0}} = f(\delta_R)$ (Figure 103)

III.2.2.6 Side Force Equation

The dimensionless aerodynamic side force is separated into its important contributing components by the equation given below.

$$C_y = \Delta C_{y_{SIDESLIP}} + \frac{b_w}{2V_T}\left(C_{y_{\dot{\beta}}}\dot{\beta} + C_{y_{\hat{p}}} r_s + C_{y_\beta} p_s\right) + \Delta C_{y_{RUD}}$$

1. Side Force Due To Sideslip

$$\Delta C_{y_{SIDESLIP}} = \left[C_{y_{\beta_{\substack{C_J=0 \\ FA}}}} \left(\frac{C_{y_{\beta_{C_J\neq 0}}}}{C_{y_{\beta_{C_J=0}}}}\right)\left(\frac{C_{y_{\beta_{GE}}}}{C_{y_{\beta_{FA}}}}\right)\right]\beta$$

(a) $C_{y_{\beta_{\substack{C_J=0 \\ FA}}}} = -.019$ 1/DEG

(b) $\left(\frac{C_{y_{\beta_{C_J\neq 0}}}}{C_{y_{\beta_{C_J=0}}}}\right) = f(C_J)$ (Figure 104)

NOTE:

1. LANDING CONFIGURATION
2. C.G. = 25% MAC

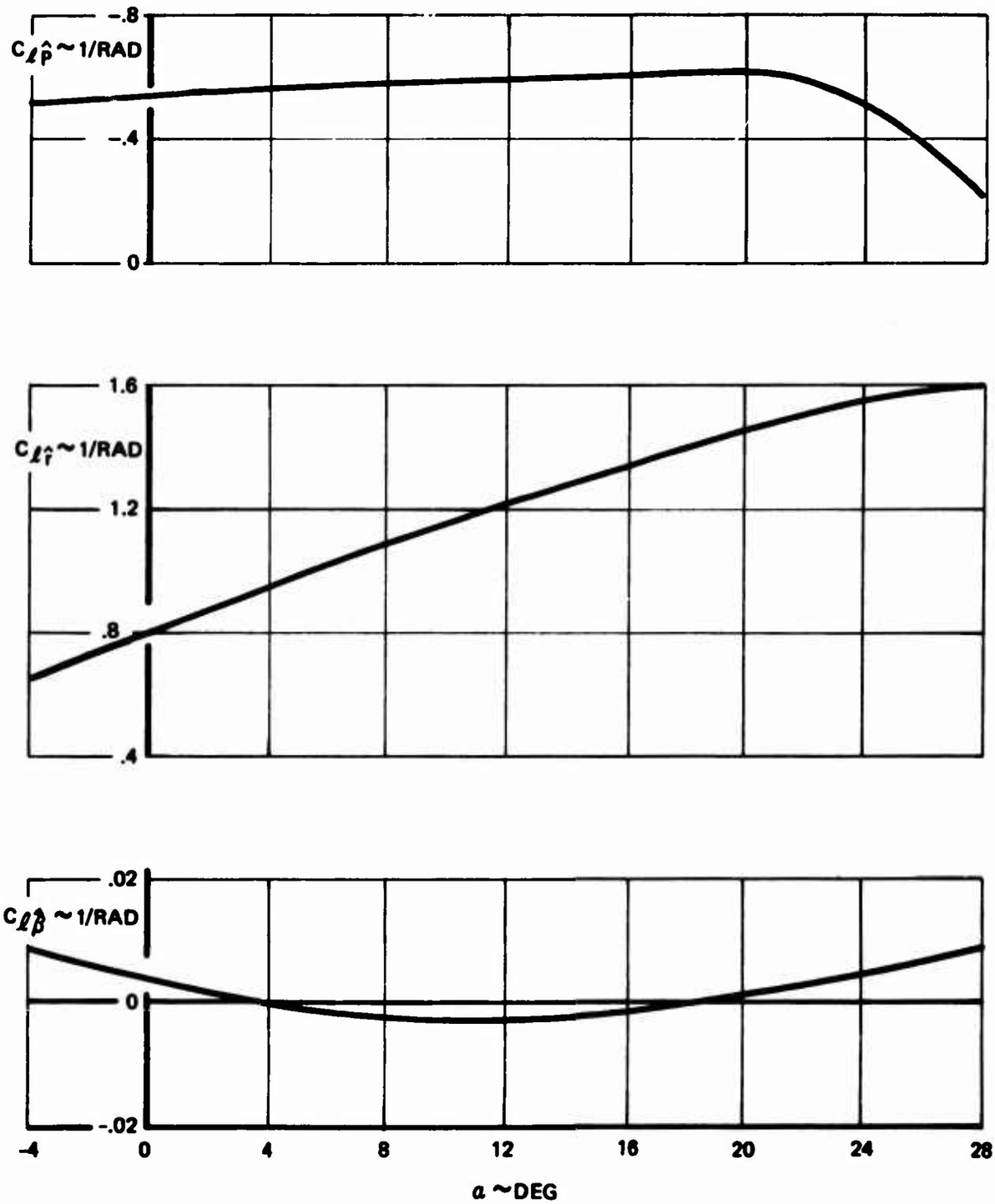

Figure 101: Rolling Moment Due to $\hat{p}$, $\hat{r}$ AND $\hat{\beta}$

NOTE:

1. LANDING CONFIGURATION

2. $\Delta C_{\ell_{LAT}} = \left[(K_{\delta SP})_{RHW} - (K_{\delta SP})_{LHW}\right] \Delta C_{\ell_{SP_{\delta SP = 60^o}}} + .00135\,\delta_a$

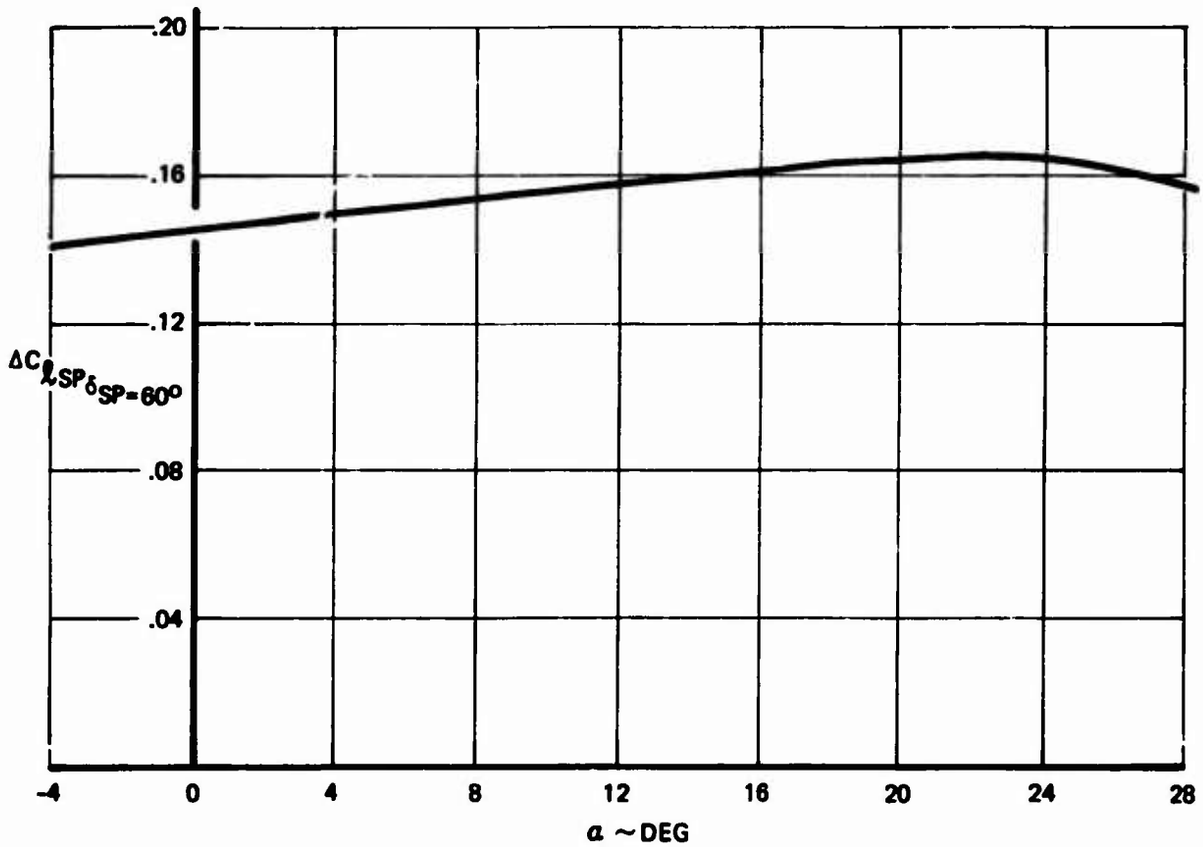

Figure 102: Rolling Moment Due to Lateral Control

NOTE:

1. LANDING CONFIGURATION
2. $\Delta C_{\ell\,RUD} = K_{\beta 3} K_{\alpha_1} (\Delta C_{\ell\,RUD})_{\substack{\alpha=0 \\ \beta=0}}$
3. $(\Delta C_{\ell_{RUD}})_{\substack{\alpha=0 \\ \beta=0}} < 0$ FOR $\delta_R < 0$

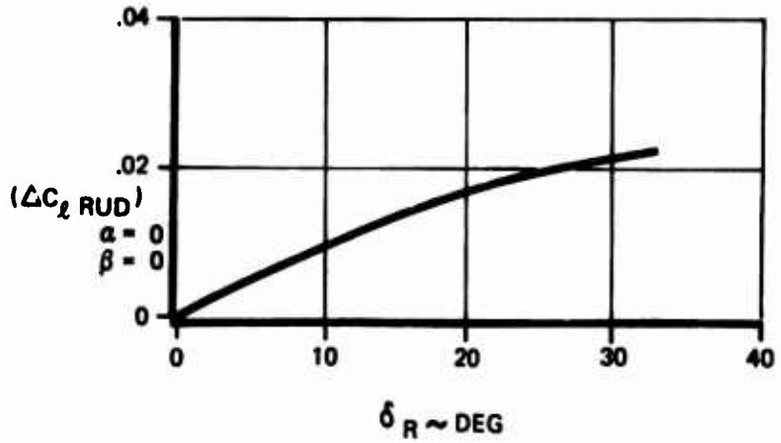

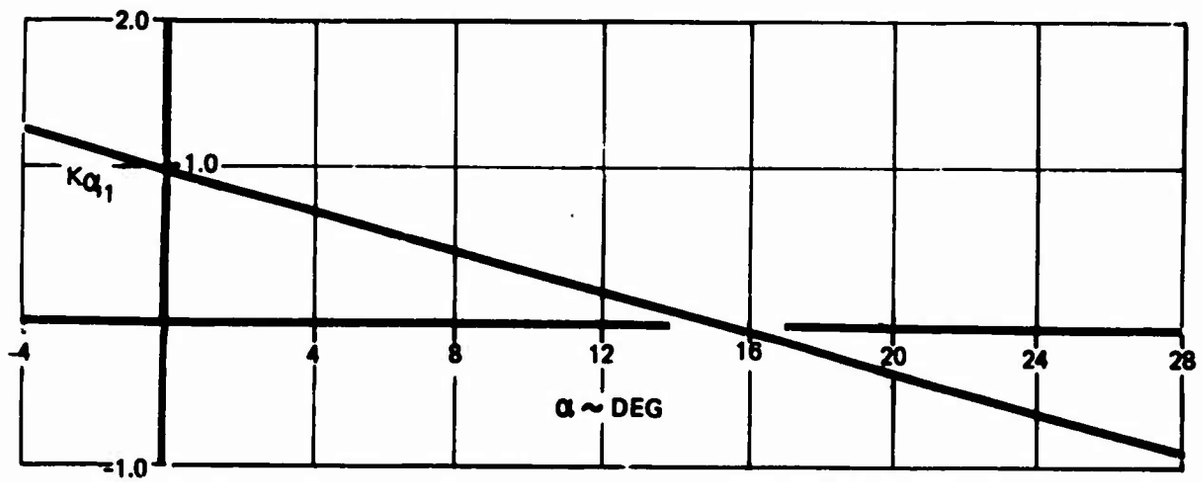

Figure 103: Rolling Moment Due to Directional Control

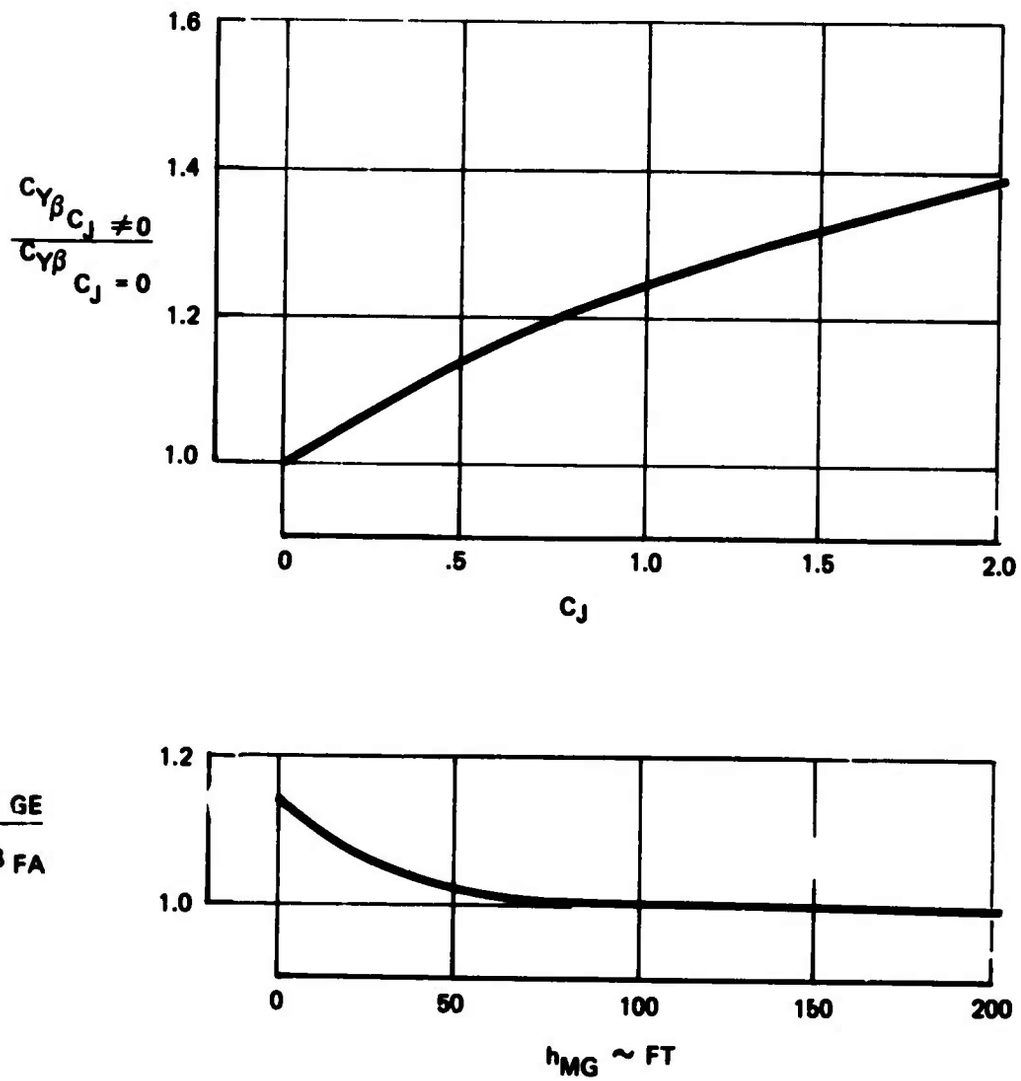

Figure 104: Effect of Thrust and Ground Proximity on Side Force Due to Sideslip

(c) $\left(\frac{C_{Y_{\beta_{GE}}}}{C_{Y_{\beta_{OA}}}}\right) = f(h_{MQ})$ (Figure 104)

2. Side Force Due To $\dot{\beta}$, r_s, p_s

(a) $C_{Y_{\dot{\beta}}} = f(\alpha)$ (Figure 105)

(b) $C_{Y_{p_f}} = f(\alpha)$ (Figure 105)

(c) $C_{Y_{\beta}} = f(\alpha)$ (Figure 105)

3. Side Force Due To Directional Control

$$\Delta C_{Y_{RUD}} = K_{\beta_3} (\Delta C_{Y_{RUD}})_{\beta=0}$$

(a) K_{β_3} is defined by Figure 98

(b) $(\Delta C_{Y_{RUD}})_{\beta=0} = f(\delta_R)$ (Figure 106)

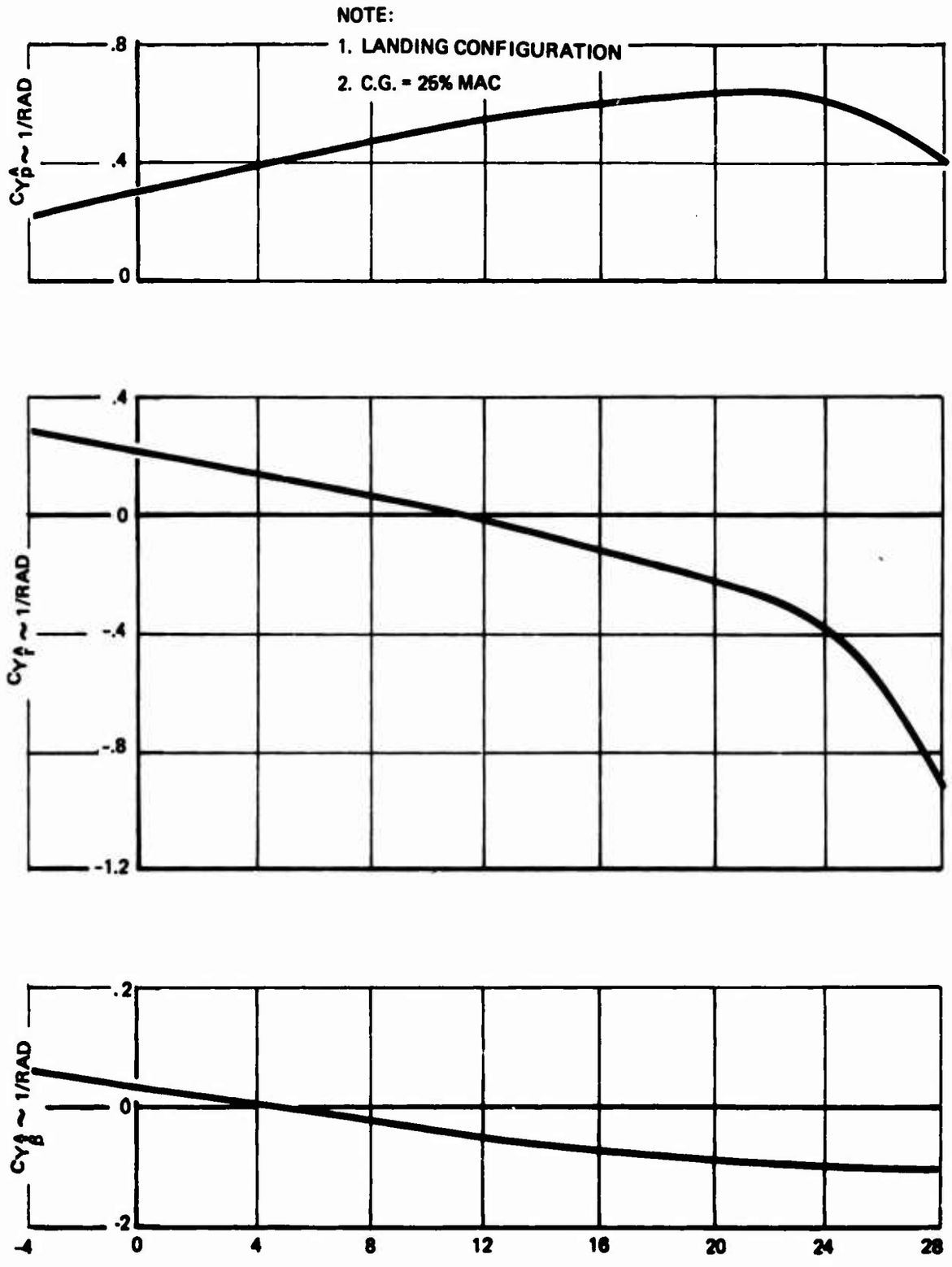

Figure 105: Side Force Due to $\hat{p}, \hat{r}$, and $\hat{\dot{\beta}}$

NOTE:

1. LANDING CONFIGURATION
2. $\Delta C_{Y_{RUD}} = K_{\beta 3} \left(\Delta C_{Y_{RUD}}\right)_{\beta = 0}$
3. $\Delta C_{Y_{RUD}} < 0$ FOR $\delta_R < 0$

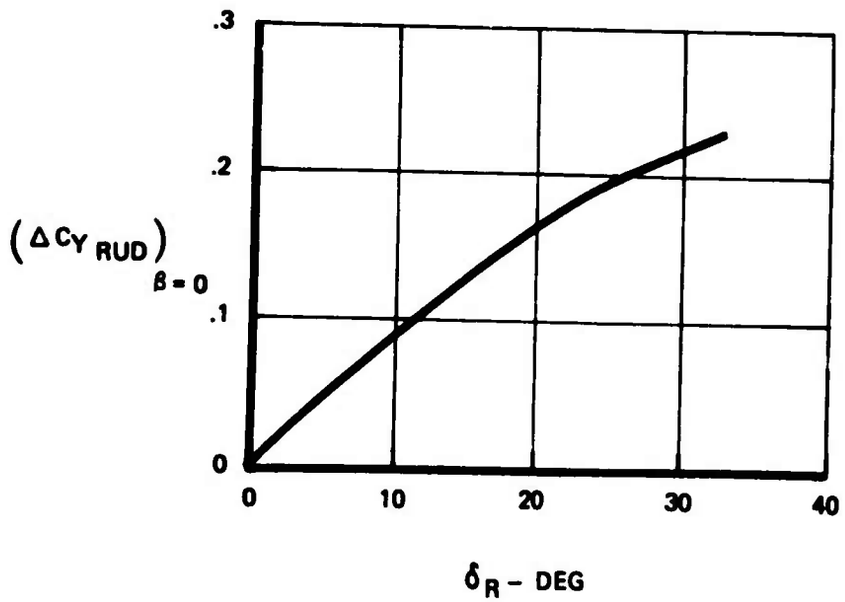

Figure 106: Side Force Due to Directional Control

SECTION III.3

PROPULSION SYSTEM

The powered-lift concept, which Boeing investigated for the STOL TAI program, utilizes a vectored thrust engine. The propulsion system is used for lift augmentation, and it is incorporated into the flight control system. Thus, it is necessary to simulate inlet and nozzle forces separately and to account for the engine response. The propulsion system simulation is illustrated by the block diagram presented by Figure 107.

Simulated gross thrust and inlet air mass flow rate are functions of power lever setting and altitude. When the engine nozzle is aligned with the engine centerline, the commanded gross thrust and air mass flow rate are defined by the following equations:

$$\left(T_{G_{\sigma=0}}\right)_c = \left(\frac{T_G}{\delta_{AMB}}\right)\delta_{AMB}$$

$$\dot{m}_{a_c} = \left(\frac{\dot{m}_a}{\delta_{AMB}}\right)\delta_{AMB}$$

where, (T_G/δ_{AMB}) and $(\dot{m}_a/\delta_{AMB})$ are a function of engine power lever angle as defined by Figures 108 and 109, respectively. The variations of the ambient pressure ratio, δ_{AMB}, with altitude is presented by Figure 110.

When the nozzle is vectored, the commanded gross thrust level changes from the aligned nozzle value. The nozzle turning efficiency (η_σ) is defined by Figure 111, and the commanded gross thrust becomes:

$$T_{G_c} = (T_{G_{\sigma=0}})\eta_\sigma$$

The engine response for acceleration and deceleration is assumed to be represented by a time-lagged, rate limited, second order system. Limits for $\partial T_G/\partial t$ and $\partial \dot{m}_a/\partial t$ are defined as a function of corrected air flow rate by Figure 112. In calculating corrected air flow rate for determining the rate limits, the current value of $\dot{m}_a$ must be used.

The body axes propulsion force and moment equations are defined as follows:

$$X_T = \sum_{i=1}^{4}\left(T_{G_i}\cos\sigma_i - V_T\cos\alpha_B\cos\beta\dot{m}_{a_i}\right)$$

$$Y_T = 0$$

$$Z_T = -\sum_{i=1}^{4}\left(T_{G_i}\sin\sigma_i + V_T\sin\alpha_B\cos\beta\dot{m}_{a_i}\right)$$

$$L_T = \sum_{i=1}^{4} (T_{Gi} \sin\sigma_i + V_T \sin\alpha_B \cos\beta \dot{m}_{ai}) Y_{ei}$$

$$M_T = \sum_{i=1}^{4} \{T_{Gi} \sin\sigma_i [X_{ei} + \bar{c}_W (cg - .25)] + V_T \sin\alpha_B \cos\beta \dot{m}_{ai} [X_{Ri} + \bar{c}_W (cg - .25)] + T_{Gi} \cos\sigma_i Z_{ei} - V_T \cos\alpha_B \cos\beta \dot{m}_{ai} Z_{Ri}\}$$

$$N_T = \sum_{i=1}^{4} (T_{Gi} \cos\sigma_i - V_T \cos\alpha_B \cos\beta \dot{m}_{ai}) Y_{ei}$$

Note: Each of the four engines is simulated separately since engine failure transients and recoveries are of paramount interest.

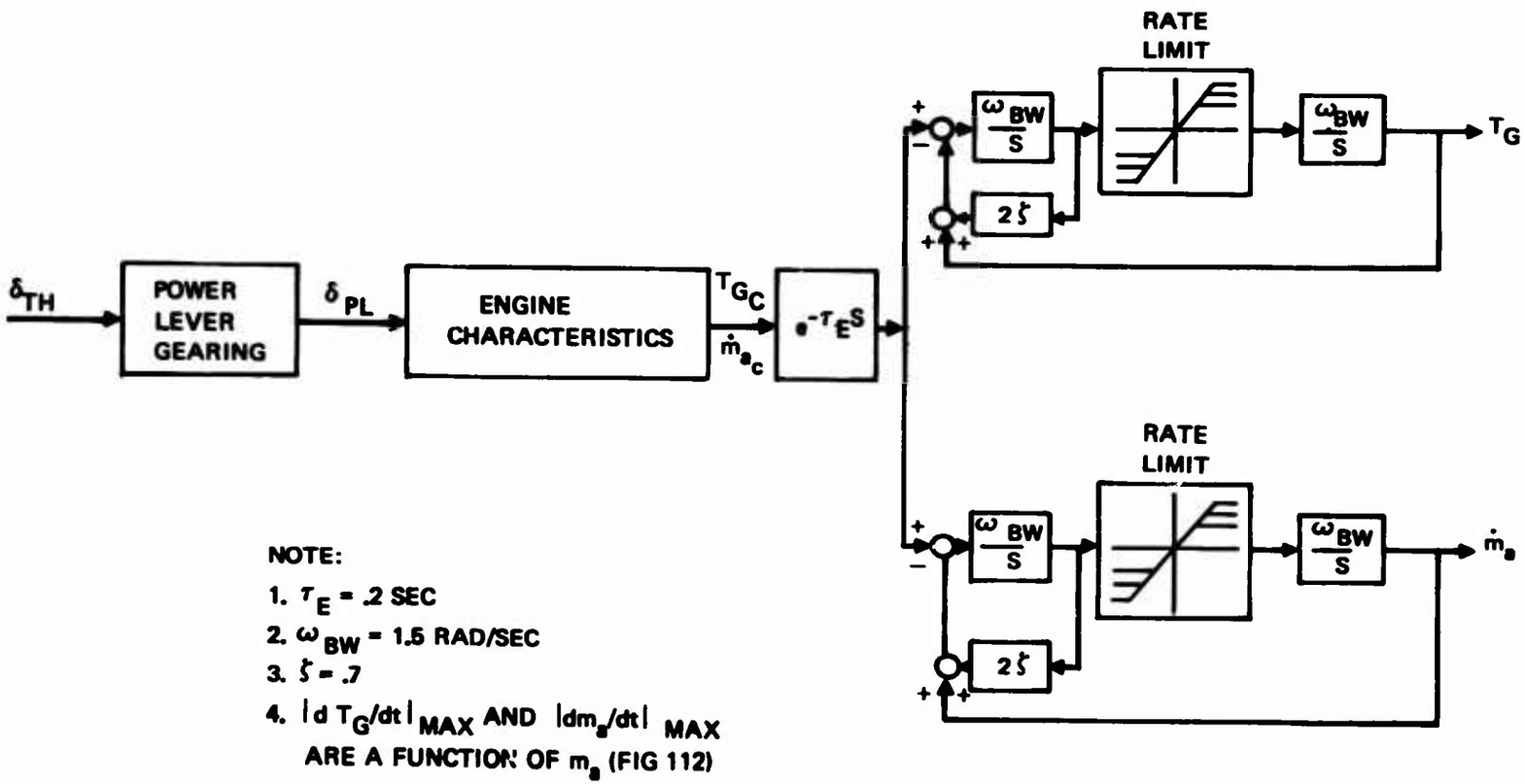

Figure 107: Block Diagram of Propulsion System Simulation

NOTES:

1. STATIC RATED THRUST = 17,200 LB
2. SCALED JT9D
3. 100% RAM RECOVERY
4. NO BLEED OR HOSEPOWER EXTRACTION
5. T_{AMB} = 59°F
6. $M_{\infty} < .15$

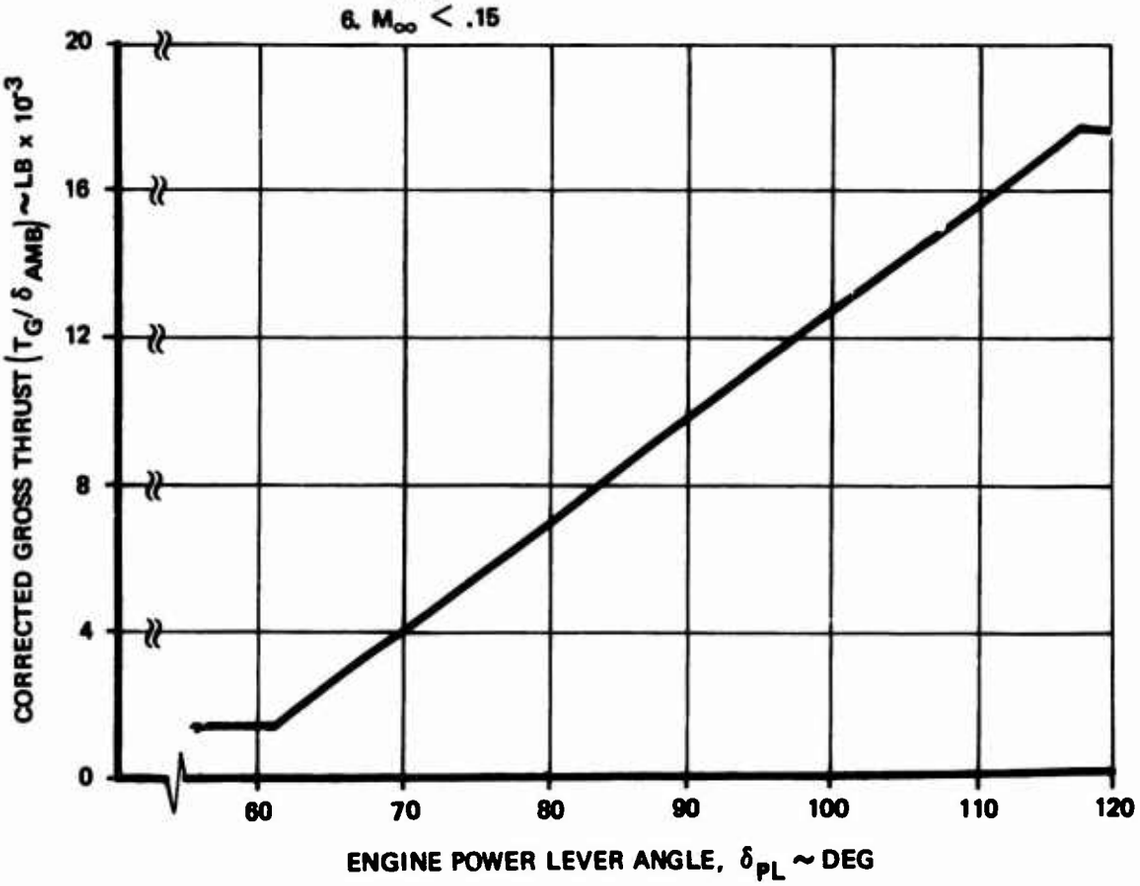

Figure 108: Corrected Gross Thrust

NOTES:

1. STATIC RATED THRUST = 17,200 LB
2. SCALED JT9D
3. 100% RAM RECOVERY
4. NO BLEED OR HORSEPOWER EXTRACTION
5. $T_{AMB} = 59^{o}F$
6. $M_{oo} < .15$

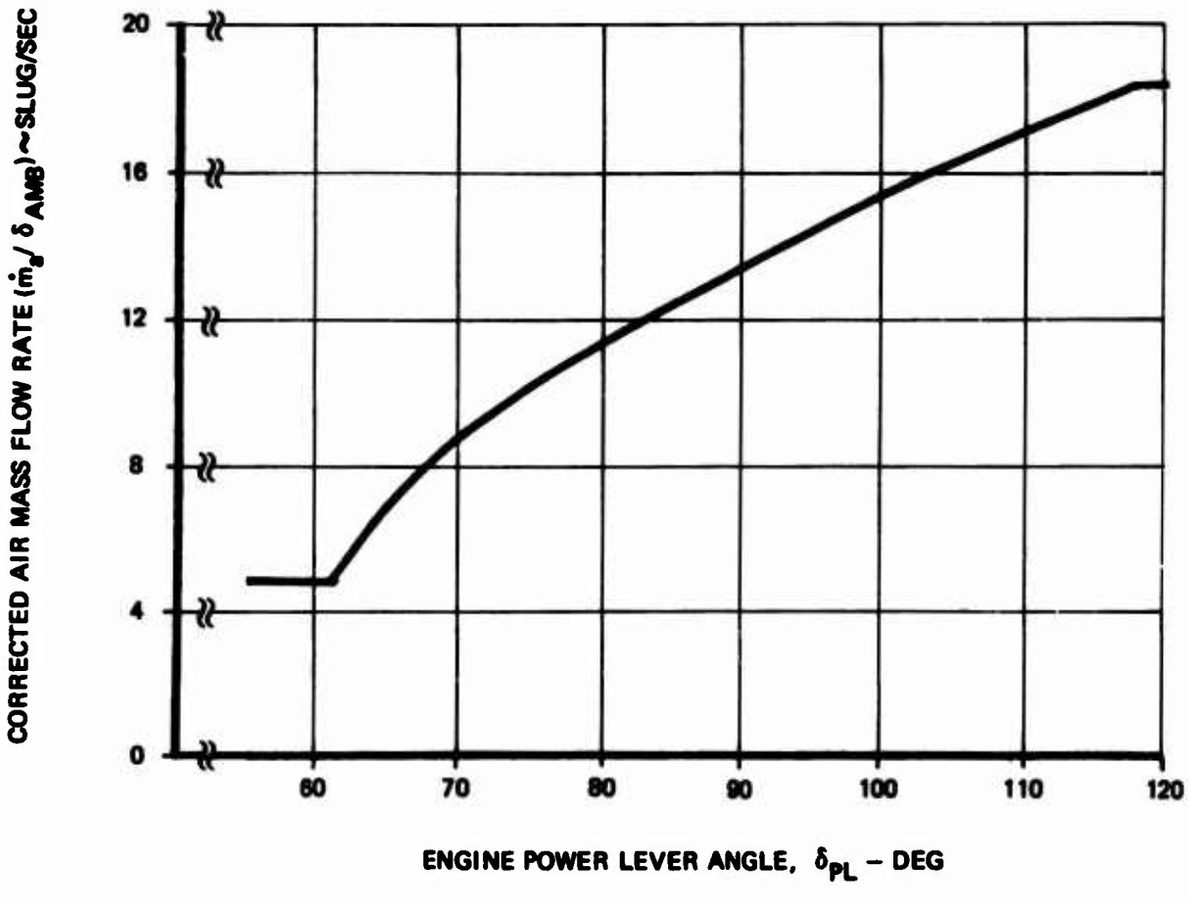

Figure 109: Corrected Air Mass Flow Rate

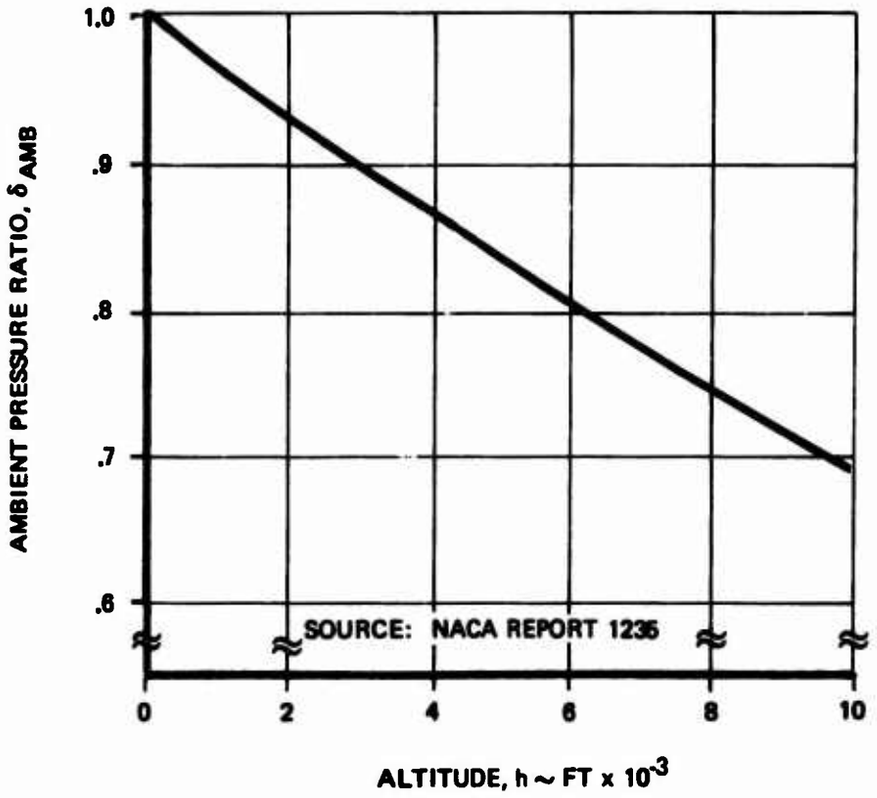

Figure 110: Ambient Pressure Ratio

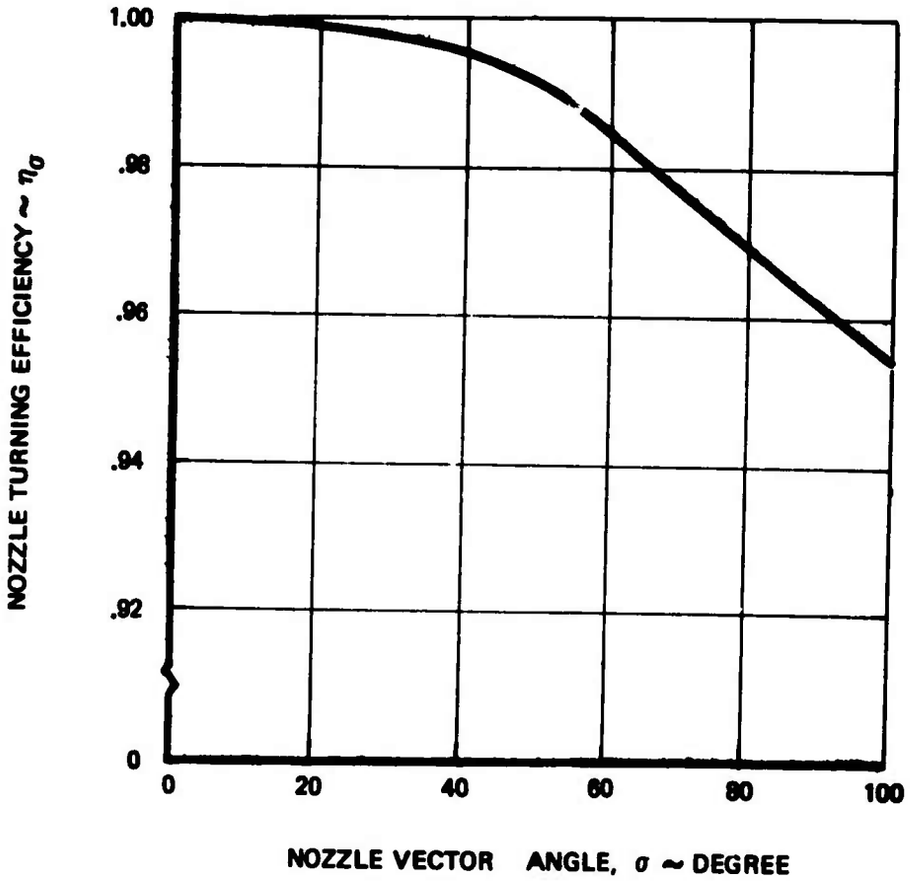

Figure 111: Nozzle Turning Efficiency

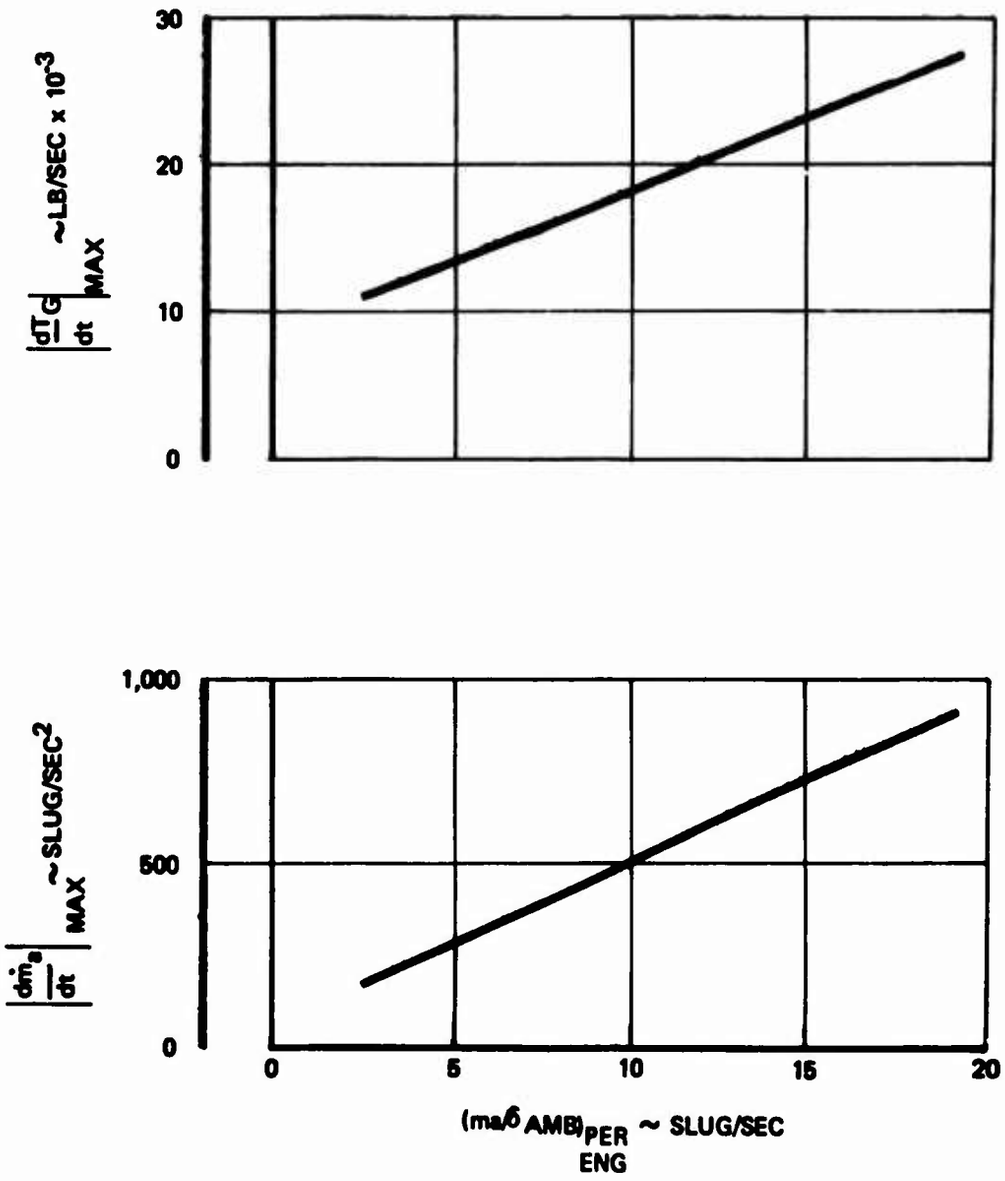

Figure 112: Gross Thrust and Air Mass Flow Rate of Change Limits

SECTION III.4

FLIGHT CONTROL SYSTEM

III.4.1 General

The flight control system (FCS) is the heart of the STOL TAI simulation program. A major portion of the STOL TAI simulation schedule is devoted to control system mechanization and control law investigations.

Control mechanization accounts for the physical properties of the flight control system. Non linearities such as friction, control dead zones, actuator rate and control surface saturation, and non-linear gains in mixers and/or ratio changers are included in the FCS math model. Friction, dead zones, and gain variations are critical for precision control tasks since these parameters can affect the system's stability. Actuator rate and control surface saturation are important for evaluating post failure flying qualities, stability, and the effect of turbulence. The control law defines the relationship of feedback and pilot generated signals to the force/moment producers. The control law determines the interaction between pilot workload, task performance, control authority, and FCS complexity.

The FCS mathematical model is based on the following assumptions:

(1) Control surfaces are fully powered.

(2) For mechanical control systems, control forces comprise friction and spring forces.

(3) Control forces for fly-by-wire systems result from electrically generated breakout forces and force gradients.

(4) Controller position does not change with trim setting.

III.4.2 Control System Description

A description of all control systems, which have been evaluated on the simulator, are described in this section. Descriptions of control laws for the Control Law Development, Control System Mechanization, and Control System Validation phases may be found in subsection III.4.2.1, III.4.2.2, and III.4.2.3, respectively. The control system descriptions include the following details:

(1) Generalized longitudinal and lateral/directional block diagrams

(2) Control law gains for each control law

(3) Surface rate and position limits

(4) Surface gearing characteristics

(5) Signal path characteristics.

The following convention is used to identify each control law:

ABXX

A = { M: Unaugmented control system
S: Stability augmentation control system
D: Automatic control system
F: Fly-By-Wire System (lateral-directional only)

B = { P: Longitudinal control system
R: Lateral/directional control system

XX = Control system number

Thus, "SP02" is the second, longitudinal, stability augmentation system.

All of the candidate control systems will contain standard elements that are described below:

(1) Control gearing and/or saturation

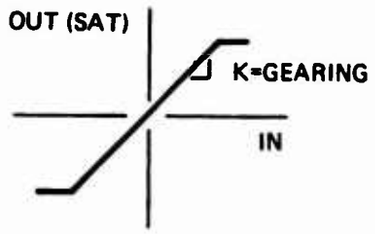

This element can be described in any quadrant by specifying the slope of the gearing (positive or negative) and can be limited to any quadrant by placing constraints on the input/output relationship.

(2) Control deadzone

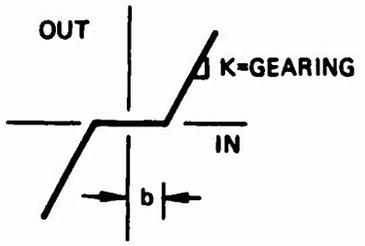

$$\delta_{OUT} = \begin{cases} 0 & , |\delta_{IN}| \leq |b| \\ (\delta_{IN} - b)K & , \delta_{IN} > b \\ (\delta_{IN} + b)K & , \delta_{IN} < -b \end{cases}$$

(3) Backlash

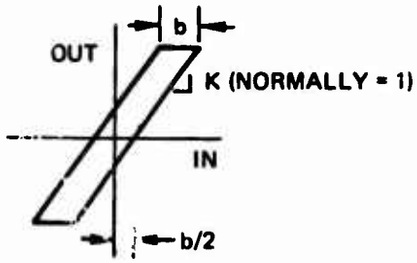

III.4.2.1 Control Law Development Phase

This section defines the control systems which were tested during the control law development phase. This description includes control law block diagrams, tables of control law gains, a specification of control surface deflection and rate limits, control gearing characteristics, and controller force properties (see Figures 113 through 119 and Tables XV through XVII).

III.4.2.2 Control System Mechanization Phase

This section defines the control system configurations applicable to the mechanization evaluation. Several control gearing definitions utilized in the initial control evaluation are still applicable. These are:

(a) Longitudinal control mechanization (Figure 115)

(b) Directional control mechanization (Figure 117)

(c) Propulsion system mechanization (Figure 118)

(d) Controller forces (Figure 119)

New control characteristics are shown in Figures 120 through 123 and Tables XVIII and XIX.

Mechanization details and failure state logic for the control systems described in this section are defined in Section III.4.3.

III.4.2.3 Control System Validation Phase

One longitudinal and two lateral-directional control systems were evaluated during this phase of the program. Block diagrams for CP21, CR20, and CR21 are presented by Figures C91 through C93. Control surface gearing, surface deflection and rate limits, and controller forces for these control systems are specified in Section III.4.2.2. Mechanization details of these systems including failure state logic are described in Section III.4.3.

III.4.3 Control System Mechanization

III.4.3.1 Math Model

The generalized control system actuator model, including signal path integration, is illustrated by Figure 127. This block diagram is

representative of the elevator, nozzle angle, left and right spoilers, aileron, and rudder systems.

This math model was formulated to accurately simulate flight control system mechanization details with a minimum burden on computer frame time and core storage. Features of this model are highlighted as follows:

(1) Multiple electrical and mechanical signal paths.

(2) Unique signal non-linearities such as mechanical signal backlash, dead zones, control gearing, signal saturation, and failure induced non-linearities.

(3) Rate limited actuators with control surface saturation.

(4) Signal path logic for normal operation and failure states.

Specific mechanization details such as control surface gearing, actuator rate limits, and surface position limits for each of the simulated flight control systems may be found in Section III.4.2.

III.4.3.2 Signal Path and Failure State Logic*

The actuation system shown in Figure 127 can be used to simulate either a multi-channel (force or position summed signal path) or a multi-surface (position summed) system. Either electrical or mechanical control can be selected by actuating the appropriate switches as shown in Table XXIII.

Non-linear functions are included in the simulation to describe control cable and linkage friction, linkage deadzone, command signal saturation, actuator rate saturation and actuator displacement saturation. Saturation levels, friction and backlash can be adjusted to values which describe system constraints.

Failure modes can be simulated in one or more channels or surfaces by actuating the appropriate switches (see Table XXIII) and by setting the appropriate bias, bang-bang, or deadzone level for hardover command, open feedback or force summed system failure, respectively. The specific number of channels (n) that apply to electrical or mechanical position summed systems can be determined from Tables XX through XXII for each surface actuation system. The unique design of the vector angle actuation system results in failure modes applicable only to this control as discussed in Table XXIII.

III.4.3.3 Lateral Axis Signal Path Definition

The lateral axis utilizes two separate control surfaces to generate rolling moments. The intergration of the ailerons and spoilers

* Signal path and failure state logic were not included for the conceptual control law phase.

involved unique problems caused by:

(a) The non-linear characteristic of rolling moment to spoiler deflection.

(b) The doubling of spoiler effectiveness when combined with spoiler direct lift control deflections.

(c) The yaw and lift coupling caused by spoilers are such that it is desirable to provide roll control for small demands without using the spoilers.

These considerations have led to the lateral signal path shown in Figure 128. Specific non-linear characteristics and system gains are included in Section III.4.2.

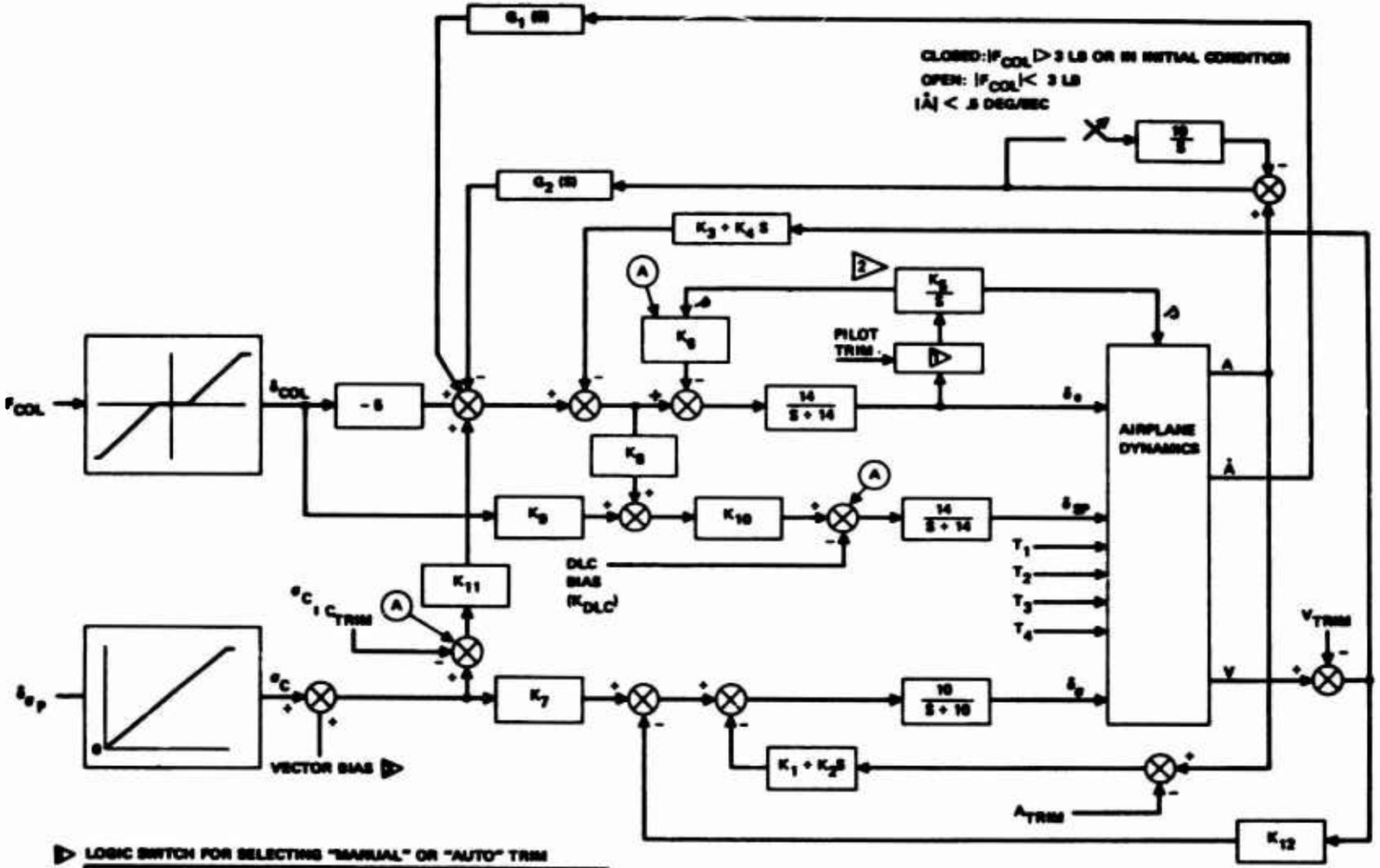

▷ LOGIC SWITCH FOR SELECTING "MANUAL" OR "AUTO" TRIM

MODE	INPUT	SIGNAL DEADZONE
"MANUAL"	PILOT TRIM (+ 1, 0, OR -1)	NONE
"AUTO"	δ_e	± 2 DEG

▷ INITIAL CONDITION FOR TRIM INTEGRATOR $\frac{K_5}{S}$ (0) = T_{TRIM}

▷ THE VECTOR BIAS IS REQUIRED TO REFLECT NORMAL SENSITIVITY SINCE EXISTING COCKPIT CONTROL DISPLACEMENT LIMIT OF 0 ⟷ 20 DEGREES IS UNNECESSARILY RESTRICTIVE

Figure 113: TAI Conceptual Longitudinal Control Laws — General Case

Table XV: TAI Longitudinal Gains

SYSTEM	DEFINE A = ( )	$G_{\delta C/A}$ G_1 (S)	$G_{\delta C/A}$ G_2 (S)	$K_{\delta\sigma/A}$ (K_1)	$K_{\delta\sigma/\dot{A}}$ (K_2)	$K_{\delta C/V}$ (K_3)	$K_{\delta C/\dot{V}}$ (K_4)	$K_{\delta ST}$ (K_5)	$K_{\delta ST}$ (K_6)	$K_{\delta\sigma}$ (K_7)	$K_{\delta SP/\delta C}$ (K_8)	$K_{\delta SP/\delta C}$ (K_9)	$K_{\delta SP/\delta C}$ (K_{10})	$K_{\delta C/\sigma\sigma}$ (K_{11})	$K_{\delta\sigma/V}$ (K_{12})
MP01	–	0	0	0	0	0	0	1.0	0	1.0	0	0	①	0	0
MP02	–	0	0	0	0	0	0	1.0	0	1.0	1.0*	0	.62	0	0
MP03	–	0	0	0	0	0	0	1.0	0	1.0	1.0*	0	.62	-.15	0
SP01	θ	.6	0	0	0	0	0	1.0	0	1.0	1.0*	0	.62	0	0
SP02	θ	.6	0	2.0	0	0	0	1.0	0	1.0	1.0*	0	.62	0	-1.0
SP03	θ	1.0	0	2.5	-.65	0	0	1.0	0	1.0	1.0*	0	.62	0	0
DP02	θ	0	0	2.5	-.65	-.04	.22	.5	1.5	1.0	1.0*	0	.62	0	-.5
DP03	θ	0.7	0	2.5	-.67	-.035	.20	.5	1.5	1.0	0	0	.62	0	-.7
DP05	γ	$\frac{7(S+.5)}{S+2.5}$	0	3.0	4.4	0	0	.5	1.5	1.0	1.0*	0	.62	0	-1.3
AP01	γ	0	-.5	3.0	4.4	-.04	-.34	.5	1.5	1.0	1.0*	0	.62	0	-1.3
AP02	γ	$\frac{7(S+.5)}{S+2.5}$	0	3.0	4.4	-.04	-.34	.5	1.5	1.0	1.0*	0	.62	0	-1.3
AP03 ③	θ	.6	-2.0	2.0	0	0	0	1.0	0	1.0	1.0*	0	.62	0	-1.0
AP05 ②	γ	$\frac{7(S+.5)}{S+2.5}$	-1.0	3.0	4.4	0	0	.5	1.5	1.0	1.0*	0	.62	0	-1.3

*OUTPUT LIMITED AT (+22.6; -17.8)

① REMOVE 11 DEG DLC BIAS

② "γ" HOLD LOGIC

CLOSED: $|F_{COL}| > 3$ LB

OPEN: $|F_{COL}| < 3$ LB AND $|\dot{\gamma}| < .5$ DEG/SEC

③ "θ" HOLD LOGIC CLOSED: $|\delta|_{COL} > .6$ INCH

OPEN: $|\delta|$ COL $< .6$ INCH AND

$|\dot{\theta}| < .5$ DEG/SEC

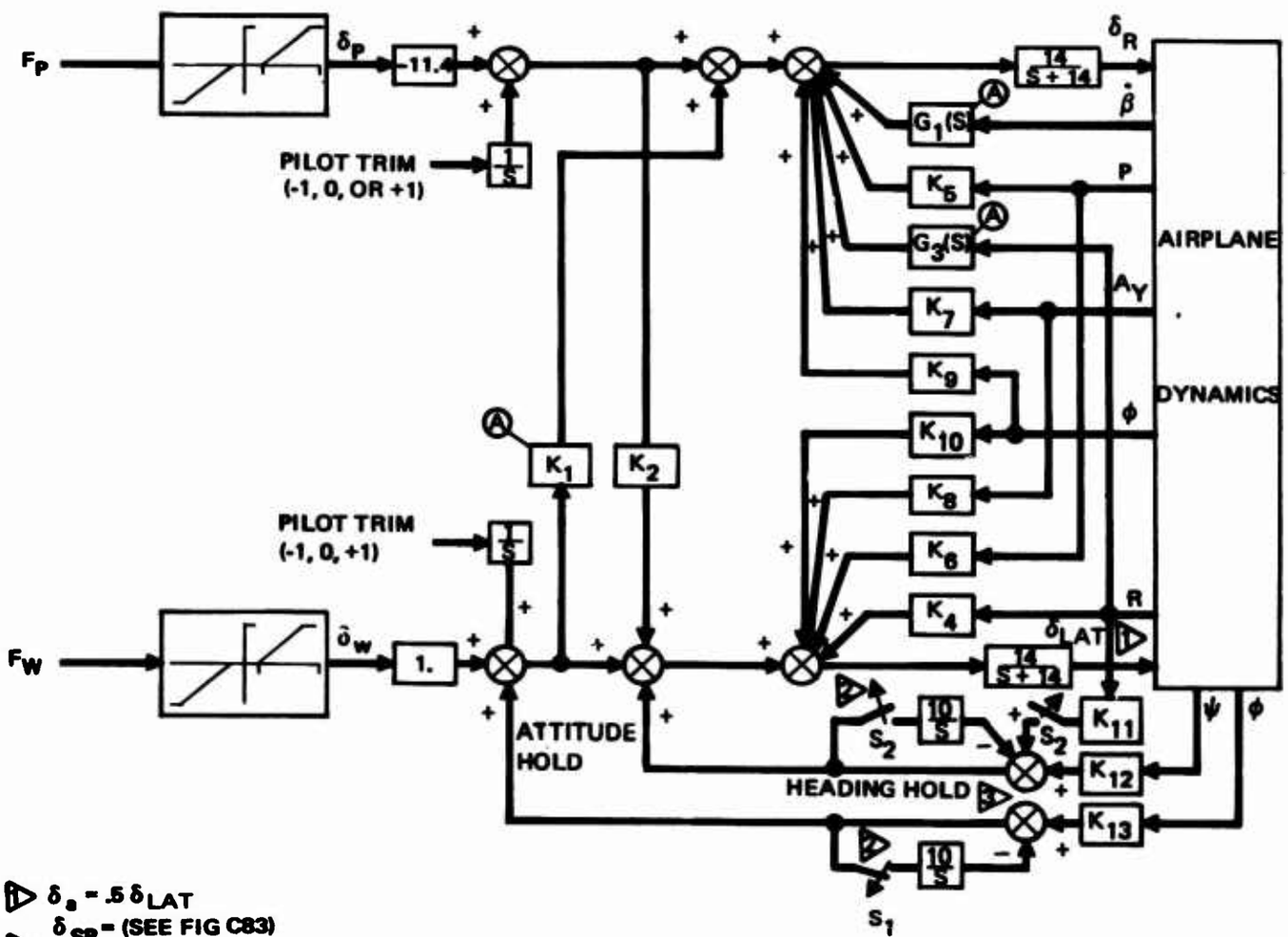

1 $\delta_e = .5\,\delta_{LAT}$
δ_{SP} = (SEE FIG C83)

2 SWITCHES S_1 AND S_2 ARE CLOSED IN THE INITIAL CONDITION MODE

3 SWITCH LOGIC DEFINED BY TABLE XVI

Figure 114: TAI Conceptual Lateral/Directional Control Laws

Table XVI: TAI Lateral-Directional Gains

SYSTEM	$K_{\delta R/\delta W}$ (K_1)	$K_{\delta R/\delta R}$ (K_2)	$K_{\delta R/r}$ $G_3(S)$	$K_{\delta A/r}$ (K_4)	$K_{\delta R/P}$ (K_5)	$K_{\delta A/P}$ (K_6)	$K_{\delta R/Ay}$ (K_7)	$K_{\delta A/Ay}$ (K_8)	$K_{\delta R/\phi}$ (K_9)	$K_{\delta A/\phi}$ (K_{10})	$K_{\delta R/\dot{\beta}}$ $G_1(S)$	K_R (K_{11})	$K_{\psi H}$ (K_{12})	$K_{\phi H}$ (K_{13})
MRO821	0	0	0	0	0	0	0	0	0	0	0	0	0	0
SRO821	-1.0	0	0	-.90	0	-.37	0	0	0	0	0	0	0	0
SR10	.5	0	1.98	-.79	-.29	.12	0	0	-.51	0	0	0	0	0
SR11	0	0	-.21	-.74	-1.38	.11	0	0	0	0	0	0	0	0
DR141	0	.09	.44	-1.05	-.99	-.09	6.31	-1.73	-.26	-.03	0	0	0	0
DR142	0	.09	.43	-1.15	-1.04	-.84	6.31	-1.73	-.26	-.02	0	0	0	0
AR141 (1)	0	.09	.44	-1.05	-.99	-.09	6.31	-1.73	-.26	-.03	0	-1.0	-.12	-.5
AR142 (1)	0	.09	.43	-1.15	-1.04	-.84	6.31	-1.73	-.26	-.02	0	-4.0	-.70	-1.0
AR21 (2)	0	.09	.43	-1.15	-1.04	-.84	6.31	-1.73	-.26	-.02	0	-4.0	-.70	-1.0

HEADING AND ATTITUDE HOLD LOGIC (OPENS SYNCHRONIZER SWITCH FOR INDICATED CONDITION)

(1) **HEADING HOLD** — **BANK ANGLE HOLD**

$|FW| < 2$ LB AND $|FW| < 3$ LB

$|\phi| \leq 10$ DEG AND $|\phi| > 15$ DEG

$|FP| < 10$ LB

(2) **HEADING HOLD** — **BANK ANGLE HOLD**

$|FW| < 2$ LB AND $|FW| < 3$ LB

$|\phi| \leq 3$ DEG AND $|\phi| > 10$ DEG

$|FP| < 7$ LB

TABLE XVII

SURFACE DEFLECTION AND
RATE LIMITS

1. Control Deflection Limits:

a) δ_e: $-30° \leq \delta_e \leq 30°$

b) $\mathcal{A}$: $-10° \leq \mathcal{A} \leq 10°$

c) σ : $0° \leq \sigma \leq 100°$

d) δ_{SP}: $0° \leq \delta_{SP} \leq 60°$

e) δ_a: $-30° \leq \delta_a \leq 30°$

f) δ_R: $-33° \leq \delta_R \leq 33°$

2. Control Actuation Rate Limits

a) $|\dot{\delta}_e|_{MAX}$ = 50 deg/sec

b) $|\dot{\mathcal{A}}|_{MAX}$ = 5 deg/sec

c) $|\dot{\sigma}|_{MAX}$ = 40 deg/sec

d) $|\dot{\delta}_{SP}|_{MAX}$ = 100 deg/sec

e) $|\dot{\delta}_a|_{MAX}$ = 50 deg/sec

f) $|\dot{\delta}_R|_{MAX}$ = 55 deg/sec

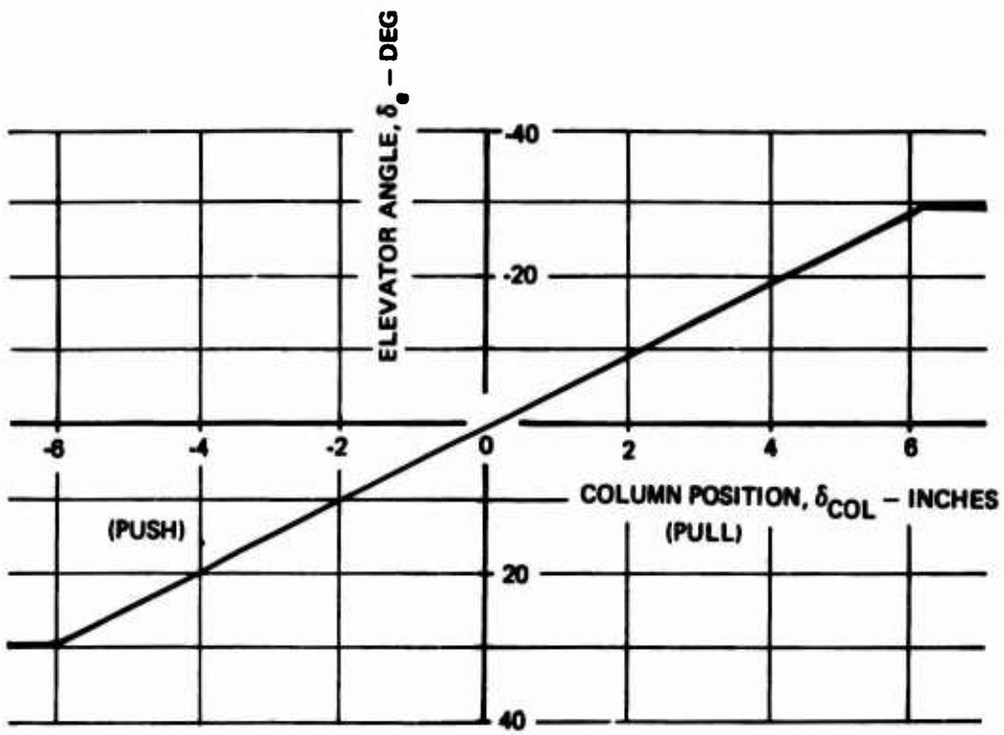

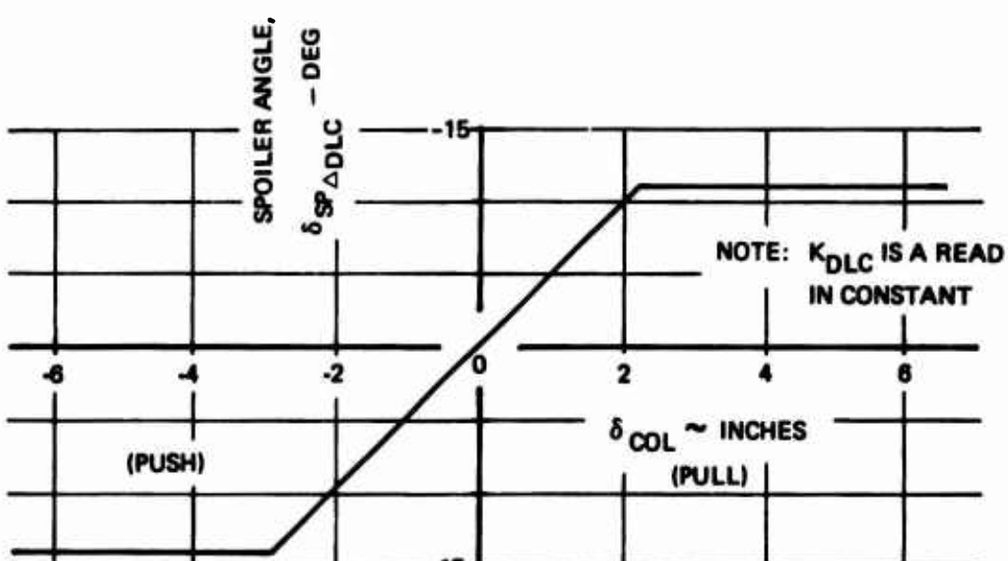

$$\delta_{SP_{RHW_{DLC}}} = \delta_{SP_{LHW_{DLC}}} = K_{DLC} + \delta_{SP_{\Delta DLC}}$$

$$K_{DLC} = 11.0$$

Figure 115: Longitudinal Control Mechanization

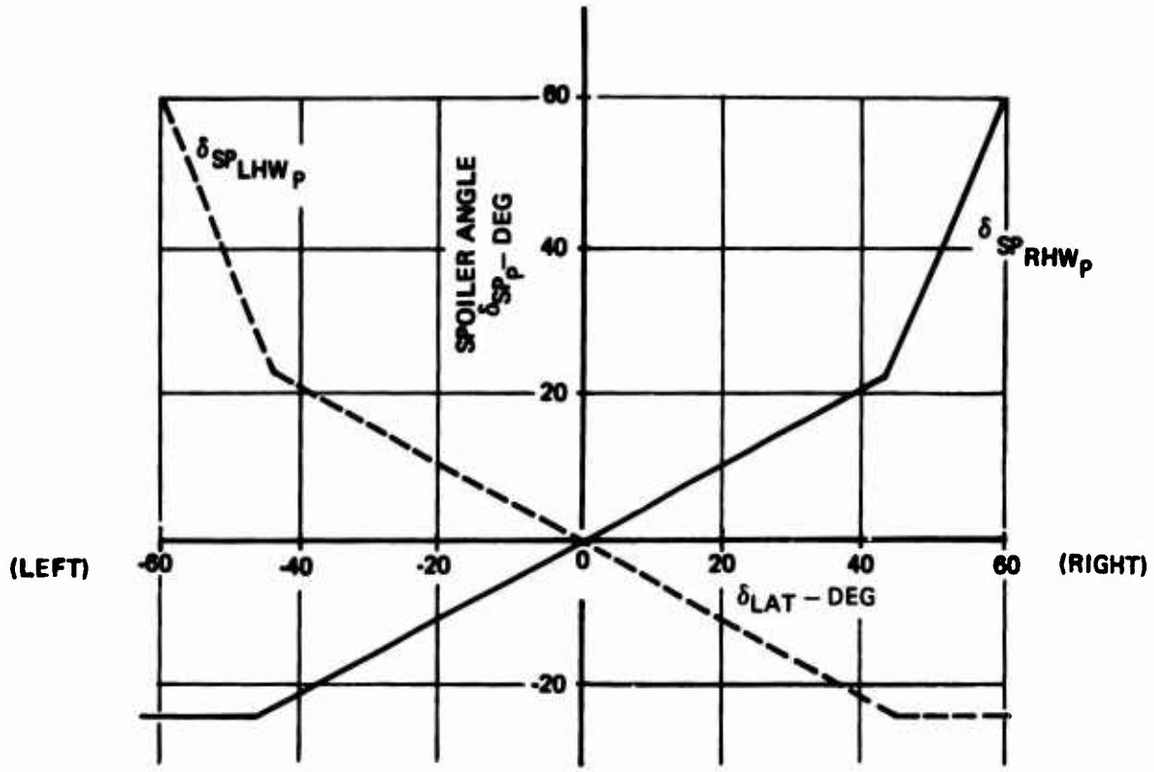

$$\delta_{SP_{RHW}} = \delta_{SP_{RHW_{DLC}}} + \delta_{SP_{RHW_P}}$$

$$\delta_{SP_{LHW}} = \delta_{SP_{LHW_{DLC}}} + \delta_{SP_{LHW_P}}$$

SPOILER DEFLECTION LIMITS

$$0 < \delta_{SP} < 60$$

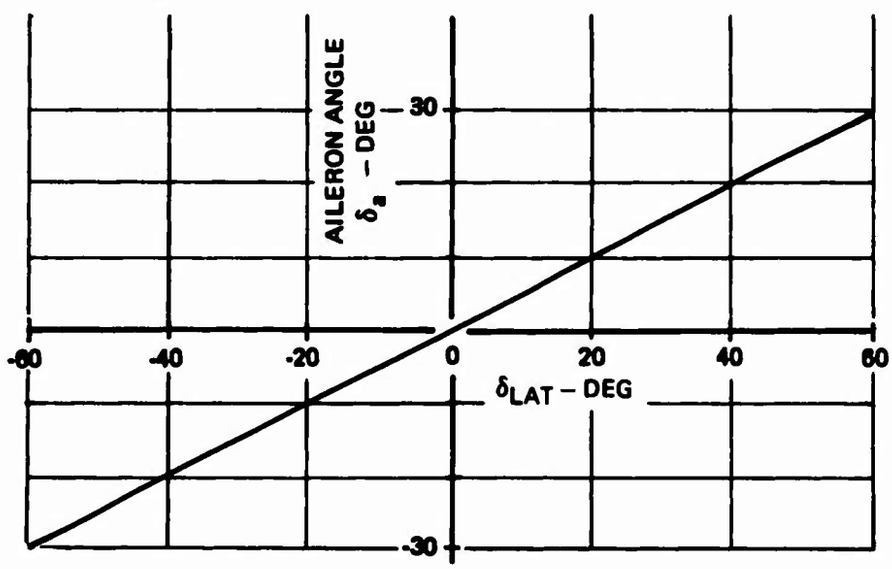

Figure 116: Lateral Control Feed Forward Gains

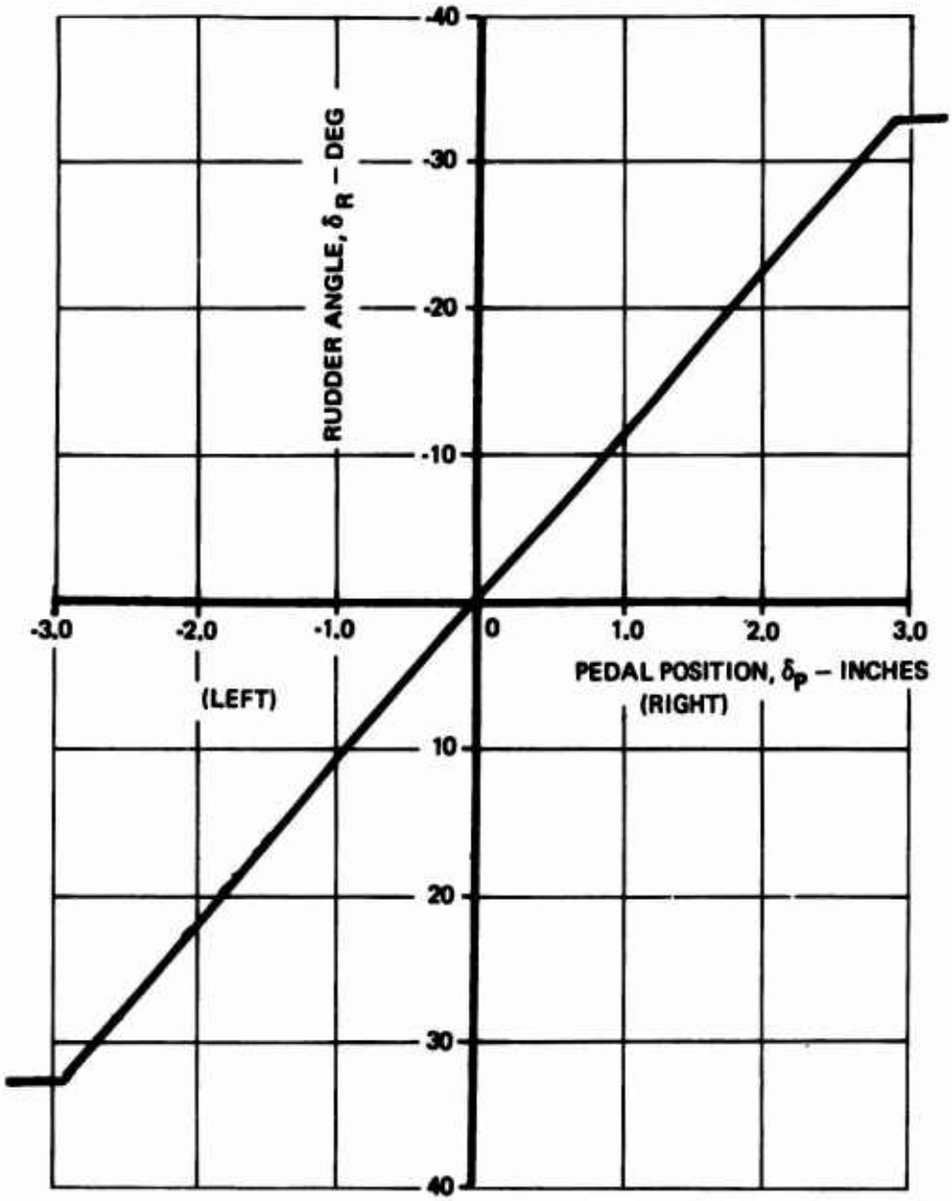

Figure 117: Directional Control Mechanization

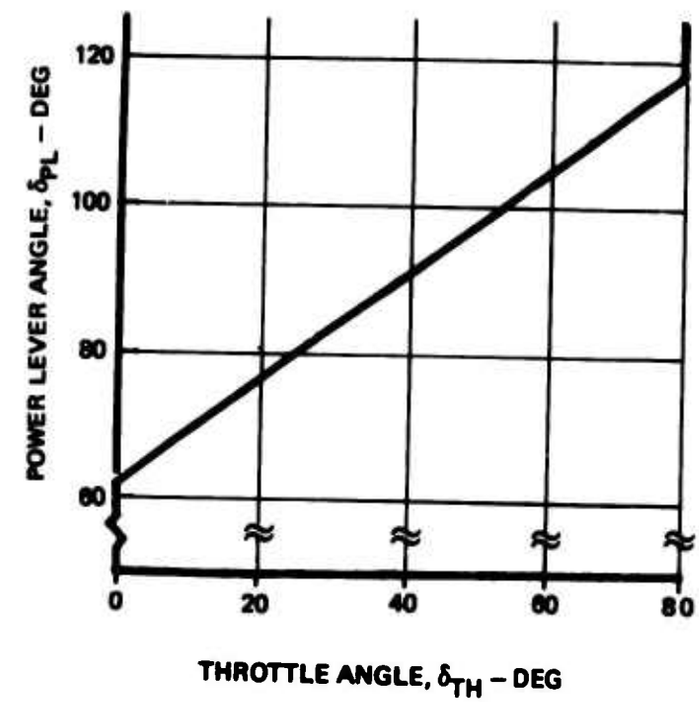

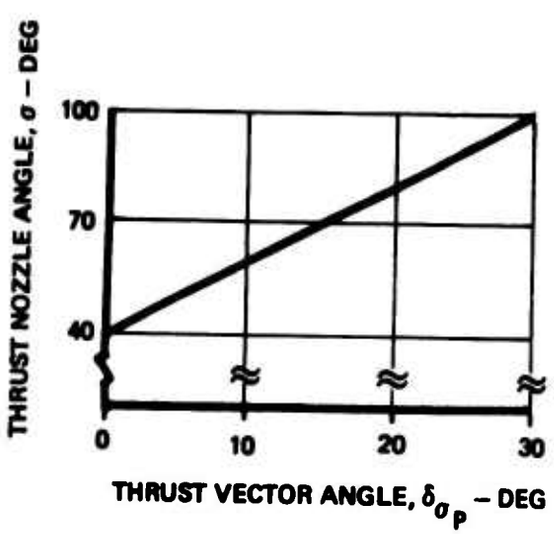

Figure 118: Propulsion System Mechanization

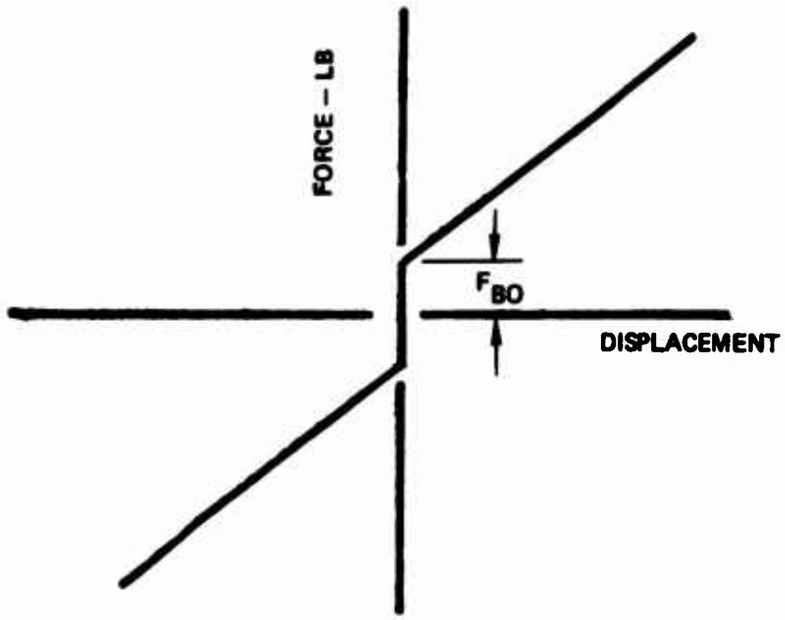

CONTROLLER	F_{BO}	K	$\|F_{MAX}\|$
COLUMN	3 LB	3 LB/IN.	21 LB
THRUST VECTOR	1.0 LB	–	–
THROTTLE	1.0 LB	–	–
WHEEL	2.0 LB	.25 LB/DEG	17 LB
PEDALS	7.0 LB	20 LB/IN.	63 LB

Figure 119: Controller Forces

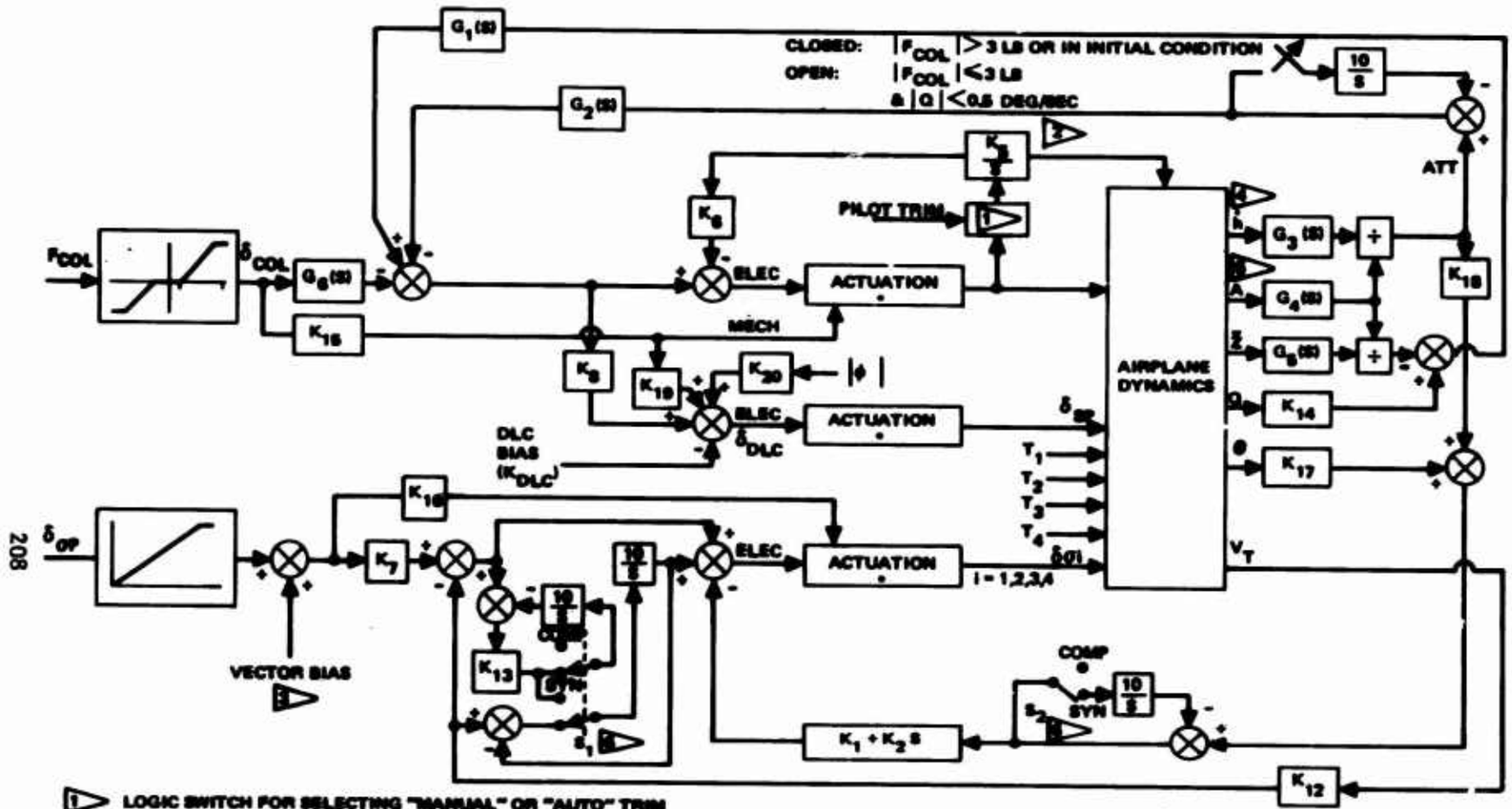

1 LOGIC SWITCH FOR SELECTING "MANUAL" OR "AUTO" TRIM

MODE	INPUT	SIGNAL DEAD ZONE
"MANUAL"	PILOT TRIM (+1, 0, OR -1)	NONE
"AUTO"	δ_e	±2 DEG

2 INITIAL CONDITON FOR TRIM INTEGRATOR $\Delta(\delta e) = \delta_{TRIM}$

3 THE VECTOR BIAS IS REQUIRED TO REFLECT NORMAL SENSITIVITY SINCE EXISTING COCKPIT CONTROL DISPLACEMENT LIMIT OF 0 + 30 DEGREES IS UNNECESSARILY RESTRICTIVE

4 $\dot{h}$ IS A BLEND OF $\dot{h}_{BARO}$ AND $\dot{\bar{z}}$ $\left[\dot{h} = \frac{\dot{h}_{BARO} - T\dot{\bar{z}}}{(TS+1)}\right]$, WHERE $\bar{z} = z_z + \delta$

5 A IS EITHER V_{GROUND} OR V_{TAS}

6 SWITCH S_1/S_2 SHOWN IN SYNCHRONIZED MODE

• SEE PREPARED ACTUATION BLOCK DIAGRAM, FIGURE 127

Figure 120: TAI Longitudinal Control Laws : Mechanization Phase

Table XVIII: TAI Longitudinal Control Laws — Mechanization Phase

SYSTEM	δ [illegible] $G_1(S)$	δ [illegible] $G_2(S)$	[illegible] $G_3(S)$	[illegible] $G_4(S)$	AZ [illegible] $G_5(S)$	δ_{C_0} $G_6(S)$	δ [illegible] K_1	δ [illegible] K_2	δ [illegible] K_5	δ [illegible] K_6	δ [illegible] K_7	δ [illegible] K_8	δ [illegible] K_{12}	δ [illegible] K_{13}	δ [illegible] K_{14}	δ [illegible] K_{15}	δ [illegible] K_{16}	δ [illegible] K_{17}	LOGIC K_{18}	δ [illegible] K_{19}	δ [illegible] K_{20}	[illegible] "X"	ATTITUDE HOLD LOGIC
[illegible] 2	0	0	0	0	0	0	0	0	1.0	0	0	0	0	0	0	-6.0	1.0	0	0	.02	0	-	NO
[illegible]	.5	0	0	0	0	0	0	0	1.0	0	0	.02	0	0	1.0	-6.0	1.0	1.0	0	.02	0	-	NO
[illegible]	.5	0	0	0	0	5	2.0	0	1.0	0	1.0	.02	-1.0	0	1.0	0	0	1.0	0	0	-2	-	NO
[illegible]	1.0	0	0	0	0	0	2.5	-.05	1.0	0	0	.02	0	0	1.0	-6.0	1.0	1.0	0	.02	0	-	NO
[illegible]	2.0	0	0	0	0	5	2	0	1.0	0	1.0	1.24	-1.0	0	1.0	0	0	1.0	0	0	-2	-	NO
[illegible]	2.0	0	0	0	0	5	2	0	1.0	0	2.0	1.24	-3.0	.01	1.0	0	0	1.0	0	0	-2	-	NO
[illegible]	[illegible]	0	1;τ=2	[illegible]	1.0	5	3.0	4.4	.5	0	1.0	.02	-1.3	0	0	0	0	0	1.0	0	-2	V_G	NO
[illegible]	-	0	1;τ=2	[illegible]	1.0	5	3.0	4.4	.5	0	1.0	.02	-1.3	0	0	0	0	0	1.0	0	-2	V_T	
[illegible]	1.0	0	1;τ=2	[illegible]	1.0	0	3.0	2.0	.5	0	1.3	1.5	-1.5	0	0	0	0	0	1.0	0	-2	V_G	NO
[illegible]	.5	0	0	0	0	1.5	2.0	0	0	0	0	.5	-1.0	0	1.0	-8.5	1.0	1.0	0	.02	-2	-	NO
[illegible]	.5	-8.0	0	0	0	1.5	2.0	0	0	0	0	.5	-1.0	0	1.0	-8.5	1.0	1.0	0	.02	-2	-	YES

NOTES:

1. K_8 AND K_{19} OUTPUTS ARE LIMITED AT +14; -11
2. SWITCHES S_1 & S_2 SHOULD TRANSFER TO COMPUTE DURING FIRST COMPUTATION INTERVAL OF THE SIMULATION RUN
3. INITIAL TRIM VALUE IS THE STABILIZER POSITION DURING "AIRPLANE TRIM" COMPUTATION

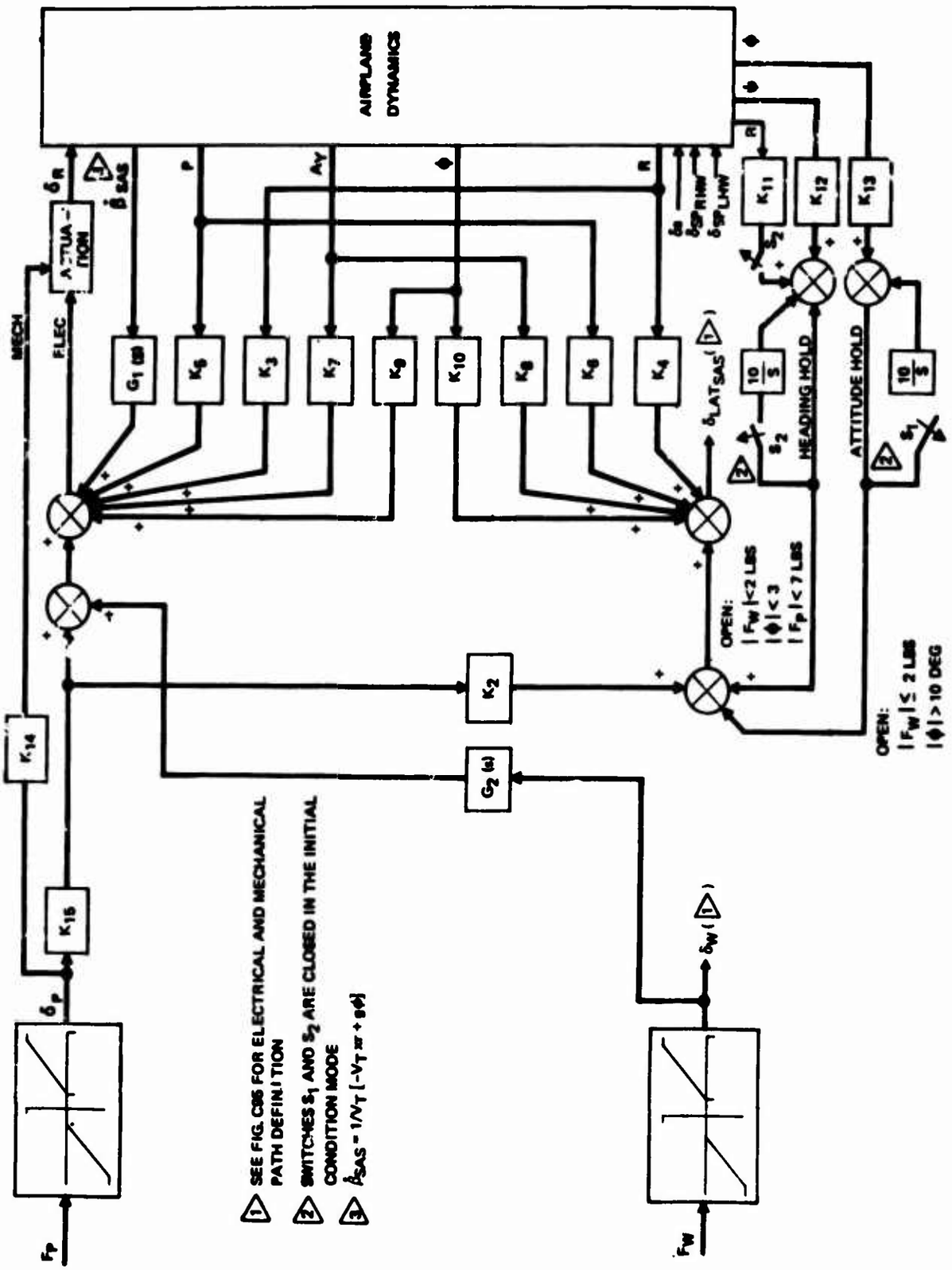

Figure 121: TAI Lateral/Directional Control Laws: Mechanization Phase

Table XIX: Lateral/Directional Control Law Gains

SYSTEM	$\delta_{R/\dot{\theta}_{SAS}}$ $G_1(S)$	δ_{R/δ_W} $G_2(S)$	δ_{P^c/δ_P} K_2	$\delta_{R/R}$ K_3	$\delta_{P^c/R}$ K_4	$\delta_{R/P}$ K_5	$\delta_{P^c/P}$ K_6	δ_{R/A_Y} K_7	δ_{P^c/A_Y} K_8	$\delta_{R/\phi}$ K_9	$\delta_{P^c/\phi}$ K_{10}	K_R K_{11}	K_{ϕ_H} K_{12}	K_{ϕ_H} K_{13}	δ_{R_M/δ_P} K_{14}	$\delta_{R\ C\delta_P}$ K_{15}	δ_{A/δ_W} K_{16}	δ_{P^cm/δ_W} K_{17}	δ_{SP/δ_W} K_{18}
MRO821	0	0	0	0	0	0	0	0	0	0	0	0	0	0	-11.4	0	0	1.0	0
SR20	-1.5	-.25	0	0	-1.35	0	0	0	0	0	0	0	0	0	-11.4	0	0	1.0	1.0
SR21	$\frac{-3.0}{.88+1}$	-.20	0	0	-1.35	0	-4.00	0	0	0	0	0	0	0	-11.4	0	0.5	1.0	1.5
CR20	$\frac{-3.0}{.88+1}$	$\frac{-.25}{.839+1}$	0	0	-1.35	0	-4.0	0	0	0	0	0	0	0	-11.4	0	1.0	.5	1.5
CR21	0	0	0	.42	-2.93	-1.66	-1.93	6.19	-5.75	-.27	-0.89	0	0	0	-11.4	0	.5	.5	1.0
FR20	$\frac{-3.0}{.88+1}$	$\frac{-.25}{.839+1}$	0	0	-1.35	0	-4.00	0	0	0	0	0	0	0	0	-11.4	1.5	0	1.5
FR21	0	0	0	.42	-2.93	-1.66	-1.93	6.19	-5.75	-.27	-0.89	0	0	0	0	-11.4	1.0	0	1.0
AR20	$\frac{-3.0}{.88+1}$	$\frac{-.25}{.839+1}$	0	0	-1.35	0	-4.0	0	0	0	0	-8.0	-2.0	-2.0	-11.4	0	1.0	.5	1.5

NOTES:

1. THE AILERON TRIM SIGNAL SHALL BE LIMITED AT $\pm 20^0$. THE TRIM GAIN (K_{AT}) SHALL BE REDUCED BY ½ FOR AIL. MECH. PATH FAILURES.
2. THE SPOILER TRIM PATH SHALL INCORPORATE A $\pm 2^0$ DEADZONE. THE TRIM GAIN (K_{ST}) SHALL BE REDUCED BY 1/3 FOR ALL SPOILER FAILURES.
3. THE RUDDER TRIM GAIN (K_{RT}) SHALL BE REDUCED 1/3 FOR ALL MECHANICAL PATH FAILURES.

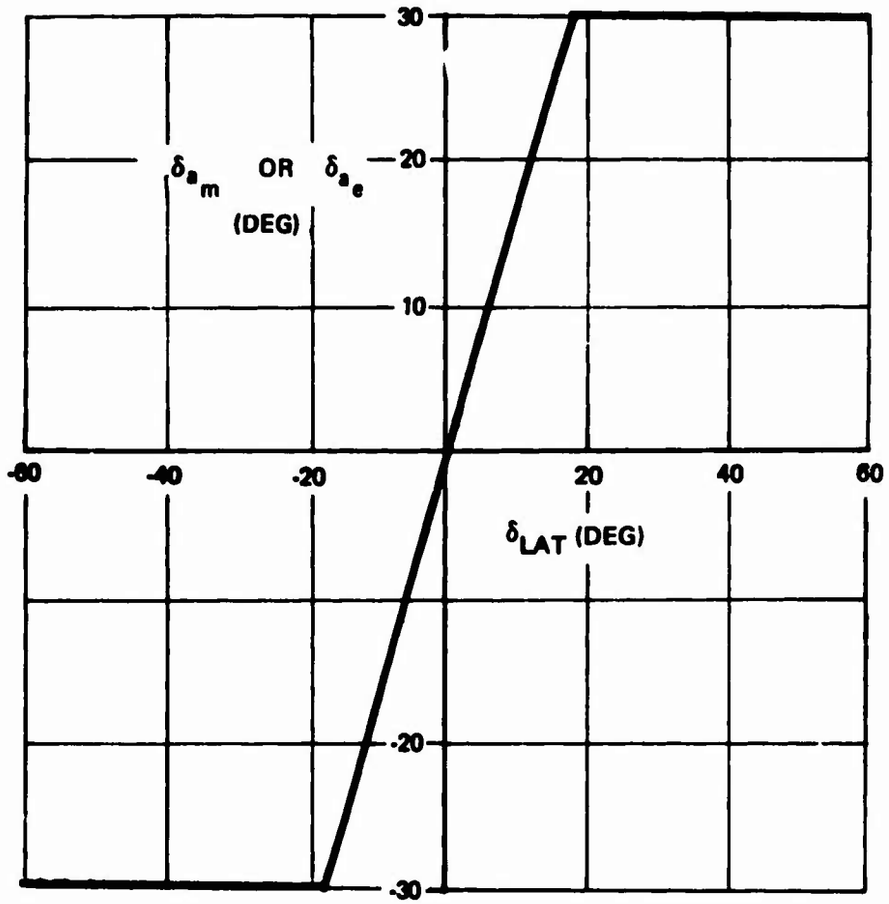

Figure 122: Aileron Control Gearing

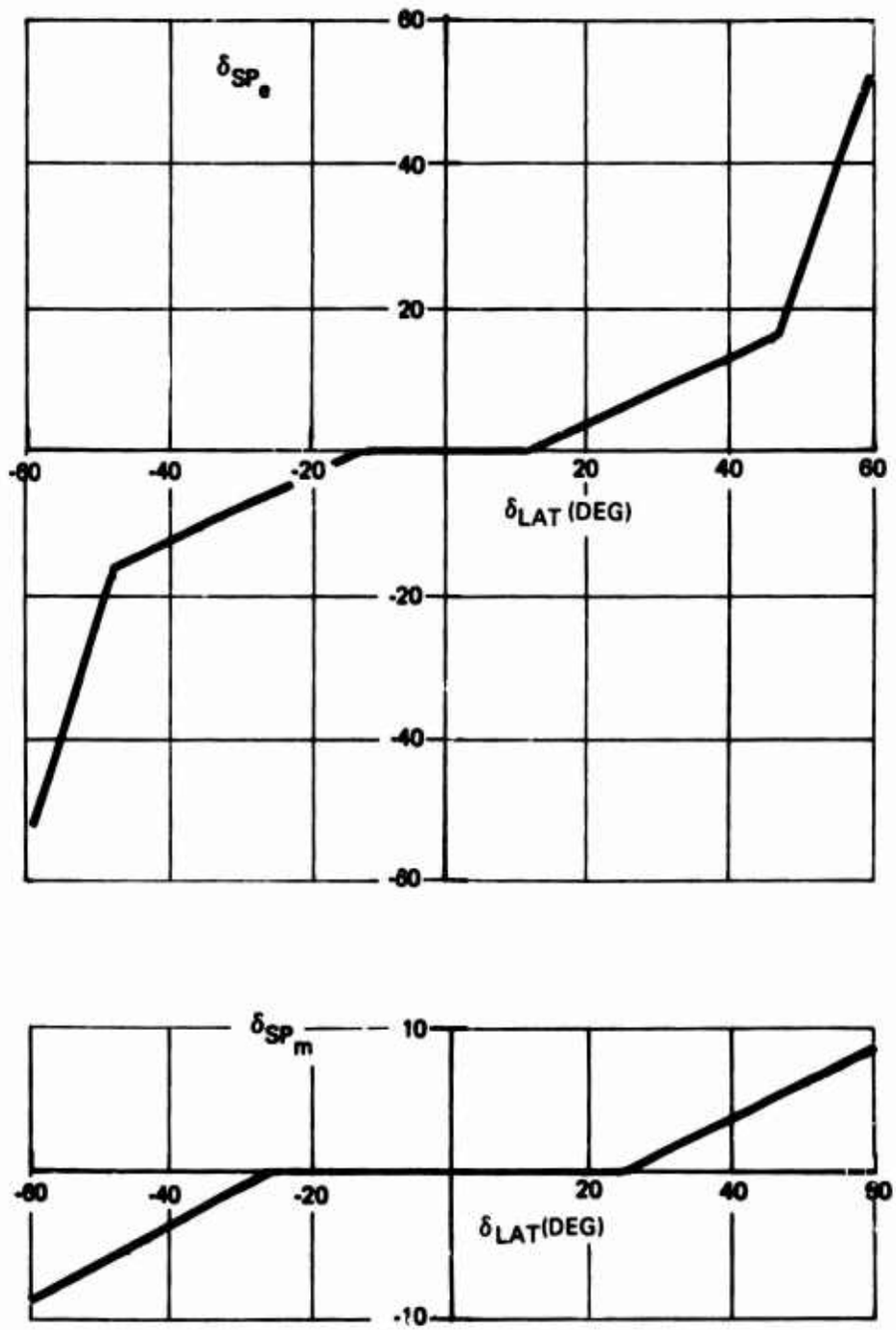

Figure 123: Spoiler Control Gearing

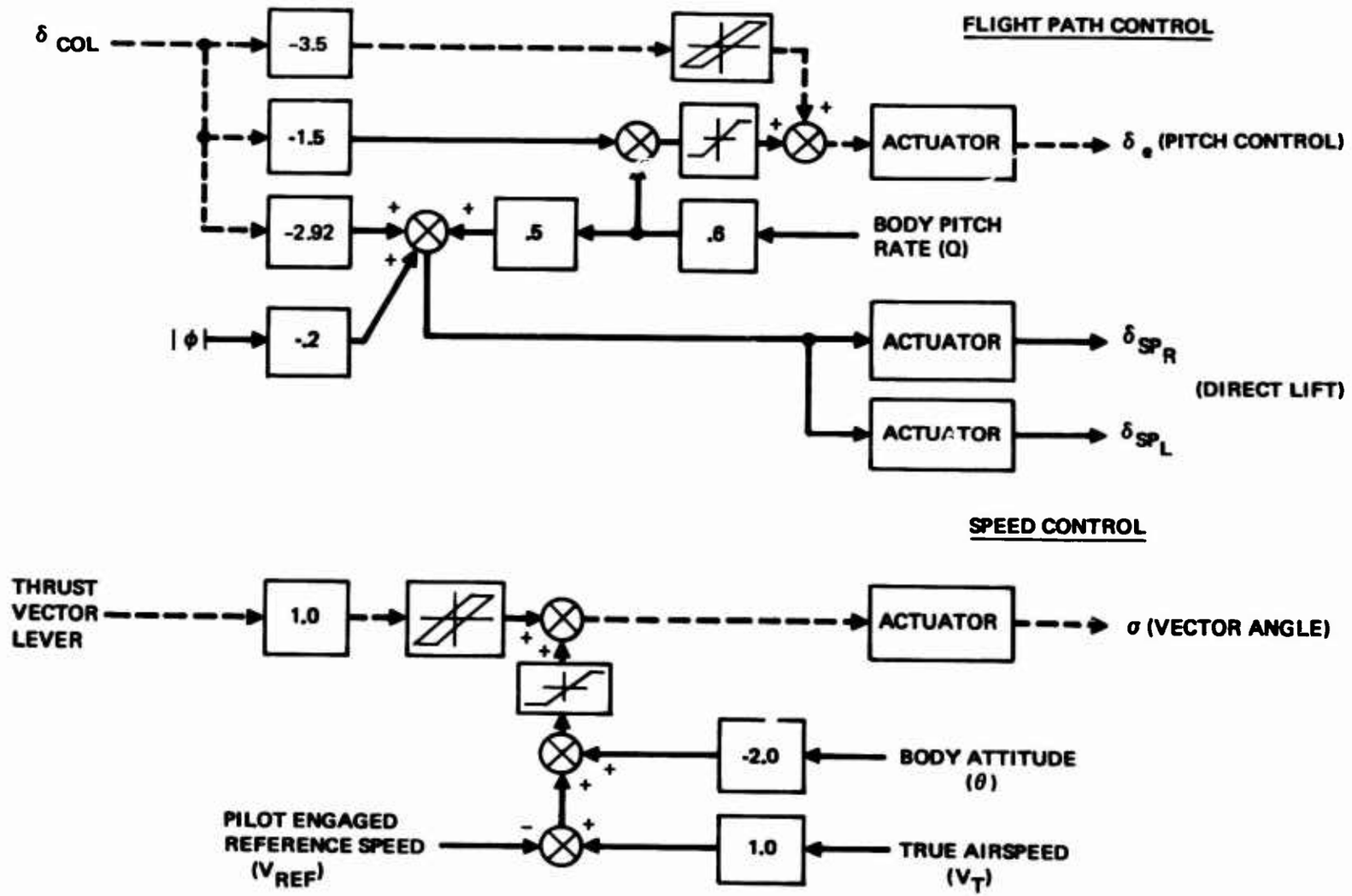

Figure 124: Longitudinal System: CP 21

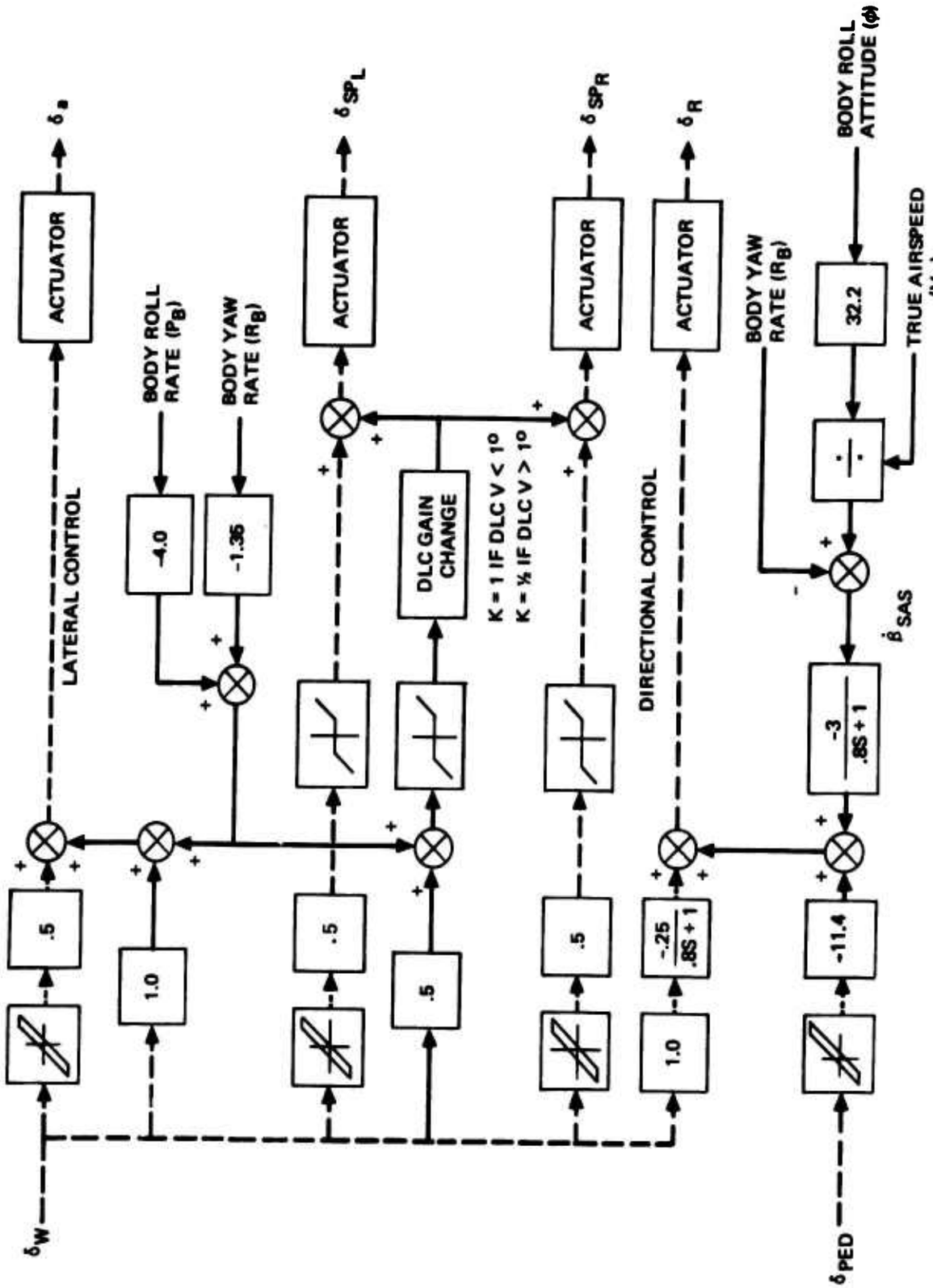

Figure 125: Lateral/Directional System: CR 20

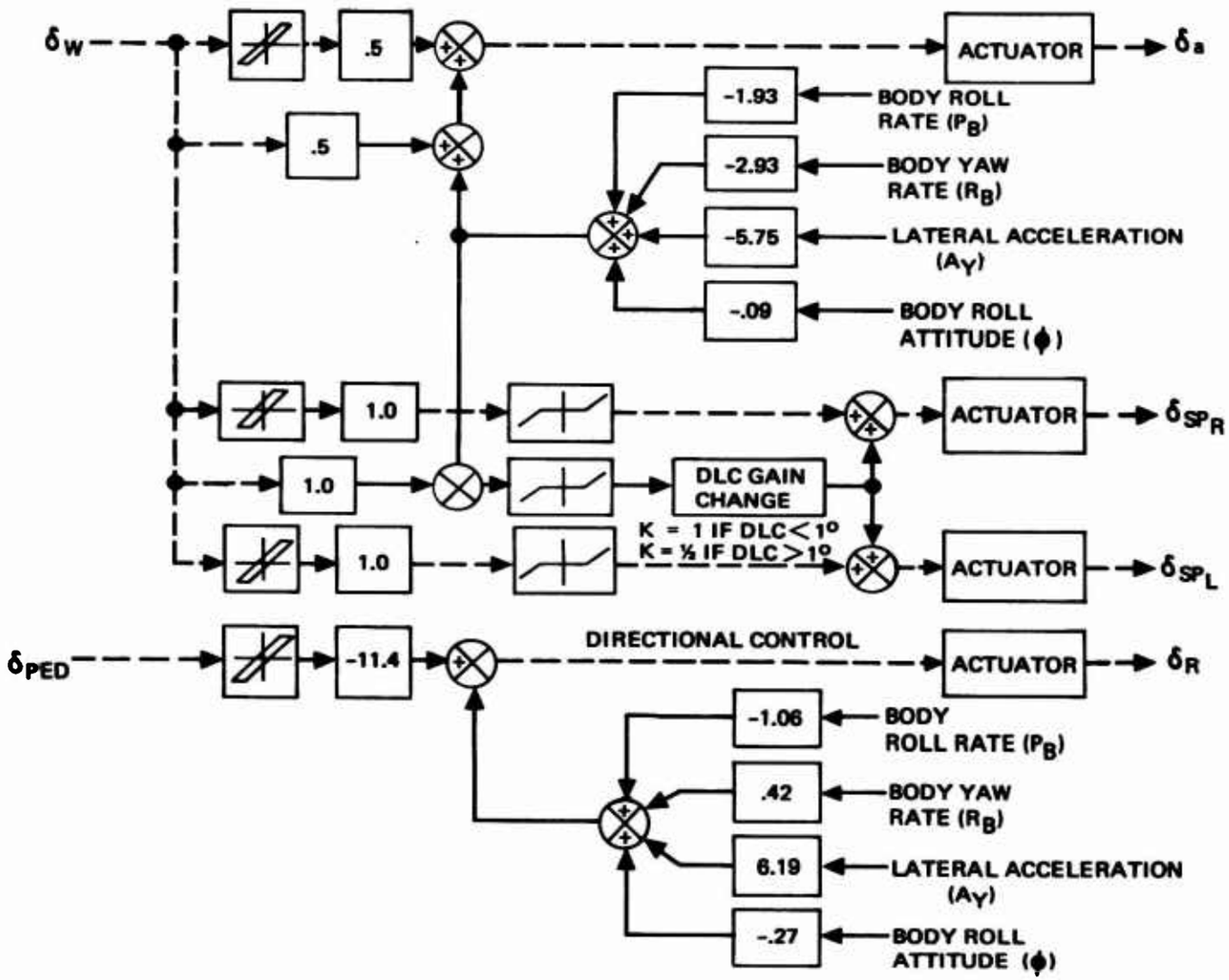

Figure 126: Decoupled Lateral/Directional Control System: CR 21

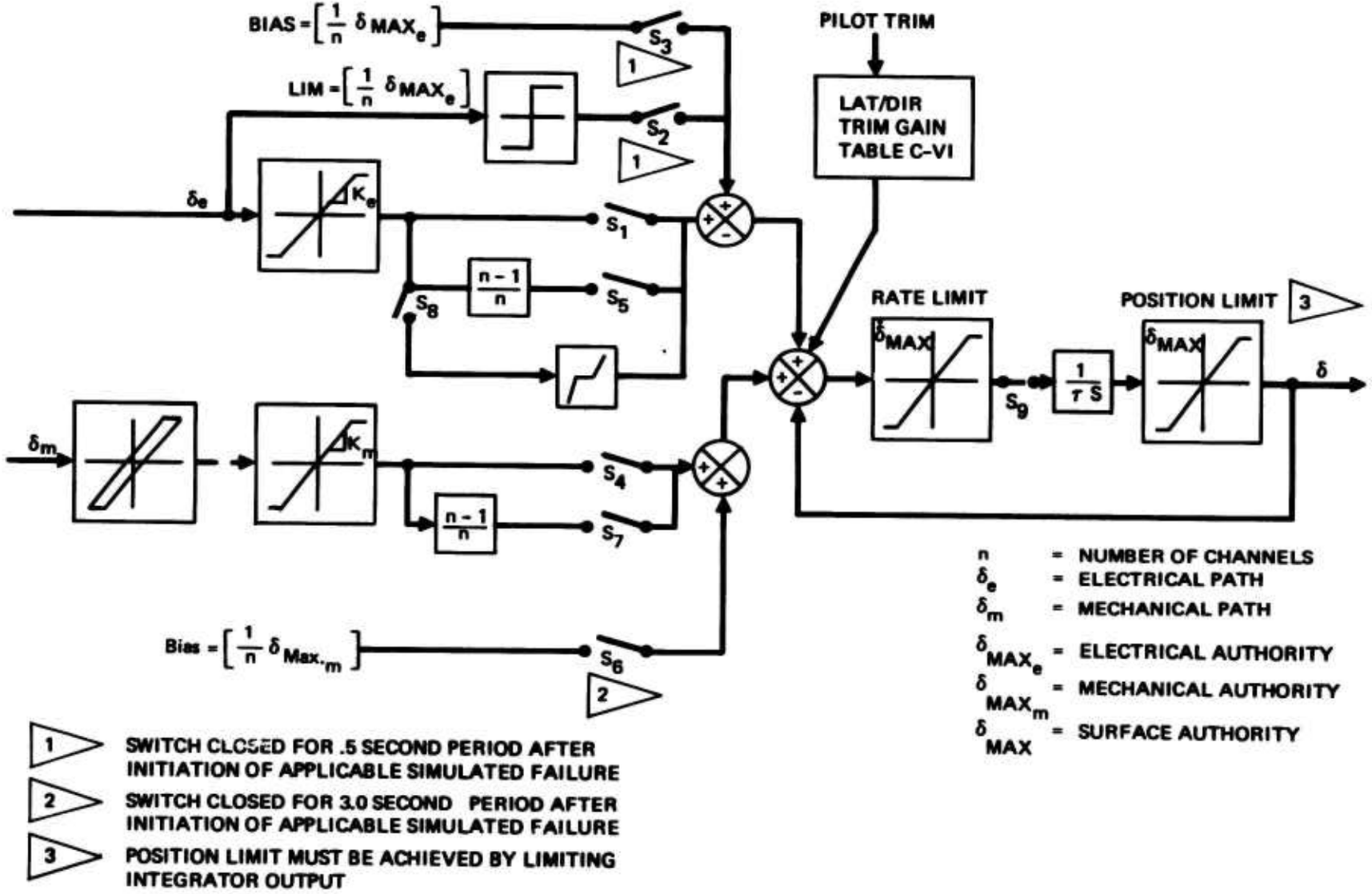

Figure 127: Generalized Actuator Model

Table XX: TAI Longitudinal System Actuation

SYSTEM DESIG-NATION	ELEVATOR											VECTOR ANGLE						
	AUTHORITY LIMITS			ACT. DYNAM.		SIGN. NON-LIN.		EFFECTIVE CHANNELS(n)				AUTHORITY LIMITS			ACT. DYNAM.		SIG. NON-LIN.	
	δ_{MAX}	δ_{MAX_M}	δ_{MAX_e}	$\dot{\delta}_{MAX}$	τ	E_{DZ}	M_{HYS}	1	2	3	4	δ_{MAX}	δ_{MAX_M}	δ_{MAX_e}	$\dot{\delta}_{MAX}$	τ	E_{DZ}	M_{HYS}
MP02	±30°	±30°	0	50°/sec	.0715	.3deg	.4deg	-	4	-	4	0-100°	0-100°	0	40°/sec	.100	-	1.0deg
SP01	±30°	±30°	±5°	50°/sec	.0715	.3deg	.4deg	3	4	3	4	0-100°	0-100°	±20°	40°/sec	.100	-	1.0deg
SP02R	±30°	(5)	±30°	50°/sec	.0715	.3deg	.4deg	3	4	3	-	0-100°	(5)	0-100°	40°/sec	.100	-	1.0deg
SP03	±30°	±30°	±5°	50°/sec	.0715	.3deg	.4deg	3	4	3	4	0-100°	0-100°	±20°	40°/sec	.100	-	1.0deg
SP04R	±30°	(5)	±30°	50°/sec	.0715	.3deg	.4deg	3	4	3	-	0-100°	(5)	0-100°	40°/sec	.100	-	1.0deg
SP05R	±30°	(5)	±30°	50°/sec	.0715	.3deg	.4deg	3	4	3	4	0-100°	(5)	0-100°	40°/sec	.100	-	1.0deg
DP05R	±30°	(5)	±30°	50°/sec	.0715	.3deg	.4deg	3	4	3	-	0-100°	(5)	0-100°	40°/sec	.100	-	1.0deg
DP07R	±30°	(5)	±30°	50°/sec	.0715	.3deg	.4deg	3	4	3	-	0-100°	(5)	0-100°	40°/sec	.100	-	1.0deg
CP21	±30°	±30°	±5°	50°/sec	.0715	.3deg	.4deg	3	4	3	4	0-100°	0-100°	±20°	40°/sec	.100	-	1.0deg

1 ACTIVE ELEC. PATH FAILURES

2 ACTIVE MECH. PATH FAILURES

3 PASSIVE ELEC. PATH FAILURES

4 PASSIVE MECH. PATH FAILURES

5 SYSTEM REVERTS TO MECH. CONTROL AFTER COMPLETE LOSS OF ELEC. PATH.

6 VECTOR ANGLE CONTROL FAILURES WILL CONSIST OF LOSS OF SIGNAL PATH (e.g. S1 OR S4 OF FIG.127 OPENED) OR PASSIVE ACTUATION (S9 of FIG.127 OPENED).

Table XXI: TAI Lateral System Actuation

SYSTEM DESIG-NATION	AILERON											SPOILERS									
	AUTHORITY LIMITS			ACT. DYNAM.		SIG. NON-LIN.		EFFECTIVE CHANNELS(a)				AUTHORITY LIMITS			ACT. DYNAM		SIG. NON-LIN.		EFFECTIVE CHANNELS(a)			
	ζ_{MAX}	ζ_{MAX_M}	ζ_{MAX_e}	$\dot{\zeta}_{MAX}$	τ	K_{DZ}	K_{NYS}	△	△	△	△	ζ_{MAX}	ζ_{MAX_M}	ζ_{MAX_e}	$\dot{\zeta}_{MAX}$	τ	K_{DZ}	K_{NYS}	△	△	△	△
MR0821	±30°	±30°	0	50°/sec	.0715	.3deg	.4deg	-	2	-	2	0-60°	(5)△	(6)△	100°/sec	.0715	.5deg	.7deg	3	1	3	1
SR20	±30°	±30°	±30°	50°/sec	.0715	.3deg	.4deg	3	2	3	2	0-60°	(5)△	(6)△	100°/sec	.0715	.5deg	.7deg	3	1	3	1
SR21	±30°	±30°	±30°	50°/sec	.0715	.3deg	.4deg	3	2	3	2	0-60°	(5)△	(6)△	100°/sec	.0715	.5deg	.7deg	3	1	3	1
CR20	±30°	±30°	±30°	50°/sec	.0715	.3deg	.4deg	3	2	3	2	0-60°	(5)△	(6)△	100°/sec	.0715	.5deg	.7deg	3	1	3	1
CR21	±30°	±30°	±30°	50°/sec	.0715	.3deg	.4deg	3	2	3	2	0-60°	(5)△	(6)△	100°/sec	.0715	.5deg	.7deg	3	1	3	1
FR20R	±30°	(5)△	±30°	50°/sec	.0715	.3deg	.4deg	3	2	3	2	0-60°	(5)△	(6)△	100°/sec	.0715	.5deg	.7deg	3	1	3	1
FR21R	±30°	(5)△	±30°	50°/sec	.0715	.3deg	.4deg	3	2	3	2	0-60°	(5)△	(6)△	100°/sec	.0715	.5deg	.7deg	3	1	3	1
AR20	±30°	±30°	±30°	50°/sec	.0715	.3deg	.4deg	3	2	3	2	0-60°	(5)△	(6)△	100°/sec	.0715	.5deg	.7deg	3	1	3	1

△ ACTIVE ELECTRICAL PATH FAILURES

△ ACTIVE MECHANICAL PATH FAILURES

△ PASSIVE ELECTRICAL PATH FAILURES

△ PASSIVE MECHANICAL PATH FAILURES

△ SYSTEM REVERTS TO FULL MECHANICAL CONTROL AFTER COMPLETE LOSS OF ELECTRICAL PATH

(5) ζ_{MAX_M} = 0 to 8.85 DEG (SEE FIGURE 123)

(6) ζ_{MAX_e} = 0 to 51.4 DEG (SEE FIGURE 123)

Table XXII: TAI Directional System Actuation

SYSTEM DESIGNATION	RUDDER										
	AUTHORITY LIMITS			ACT. DYNAM.		SIG.NON-LIN.		EFFECTIVE CHANNELS(n)			
	δ_{MAX}	δ_{MAX_M}	δ_{MAX_c}	$\dot{\delta}_{MAX}$	τ	K_{DZ}	M_{HYS}	⚠1	⚠2	⚠3	⚠4
MR0821	±33°	±33°	0	55°/sec	.0715	.6deg	.4deg	3	3	3	3
MR20	±33°	±33°	±15°	55°/sec	.0715	.6deg	.4deg	3	3	3	3
MR21	±33°	±33°	±15°	55°/sec	.0715	.6deg	.4deg	3	3	3	3
CR20	±33°	±33°	±15°	55°/sec	.0715	.6deg	.4deg	3	3	3	3
CR21	±33°	±33°	±15°	55°/sec	.0715	.6deg	.4deg	3	3	3	3
FR20R	±33°	⚠5	±33°	55°/sec	.0715	.6deg	.4deg	3	3	3	3
FR21R	±33°	⚠5	±33°	55°/sec	.0715	.6deg	.4deg	3	3	3	3
AR20	±33°	±33°	±15°	55°/sec	.0715	.6deg	.4deg	3	3	3	3

⚠1 ACTIVE ELECTRICAL PATH FAILURES

⚠2 ACTIVE MECHANICAL PATH FAILURES

⚠3 PASSIVE ELECTRICAL PATH FAILURES

⚠4 PASSIVE MECHANICAL PATH FAILURES

⚠5 SYSTEM REVERTS TO FULL MECHANICAL CONTROL AFTER COMPLETE LOSS OF ELECTRICAL PATH

Table XXIII: Major Failure Modes

TYPE OF CONTROL MECHANIZATION	ELECTRICAL PATHS						MECHANICAL PATH	
	HARDOVER		LOSS FEEDBACK		PASSIVE		HARDOVER	LOSS FED. (PASSIVE)
	Σ	VOTED	Σ	VOTED	Σ	VOTED	Σ	
MECH.	-	-	-	-	-	-	S_6, S_7	S_7
SAS	S_3, S_5	-	S_2, S_5	-	S_5	-	S_6, S_7	S_7
CAS	S_3, S_5	S_8	S_2, S_5	S_8*	S_5	S_8	S_6, S_7	S_7
FBW	S_3, S_5	S_8	S_2, S_5	S_8*	S_5	S_8	-	S_7
FBW	S_3, S_5	S_8	S_2, S_5	S_8*	S_5	S_8	S_6, S_7	S_7

NOTES-(FAILURE MODES):

1. THE NORMAL OPERATING MODE HAS SWITCHES S_1 AND S_4 CLOSED AND SWITCHES S_2, S_3, S_5, S_6, S_8 OPEN.
2. FOR ALL ELECTRICAL PATH FAILURES, SWITCH S_1 IS OPENED AND THE SWITCHES INDICATED FOR SPECIFIC FAILURE MODES ARE CLOSED.
3. FOR ALL MECHANICAL PATH FAILURES, SWITCH S_4 IS OPENED AND THE SWITCHES INDICATED FOR SPECIFIC FAILURE MODES ARE CLOSED.
4. THE ELECTRICAL PATH FAILURES ARE DIVIDED INTO TWO CATEGORIES. THE 1ST CATEGORY REPRESENTS SYSTEMS THAT UTILIZE SUMMATION TECHNIQUES TO ACHIEVE REDUNDANCY. THE VOTED SYSTEM REPRESENTS THE UTILIZATION OF A TECHNIQUE THAT SELECTS ONE OF SEVERAL POSSIBLE CONTROL PATHS TO CONTROL THE OUTPUT VARIABLE.
5. VECTOR ANGLE CONTROL FAILURES WILL CONSIST OF LOSS OF SIGNAL PATHS (S_1 OPENED FOR ELECTRICAL PATH FAILURES OR S_2 OPENED FOR MECHANICAL PATH FAILURES) OR LOSS OF ACTUATION WITH RESULTANT LOCKED OUTPUT (S_9 OPENED TO DISABLE ACTUATION MOTION).

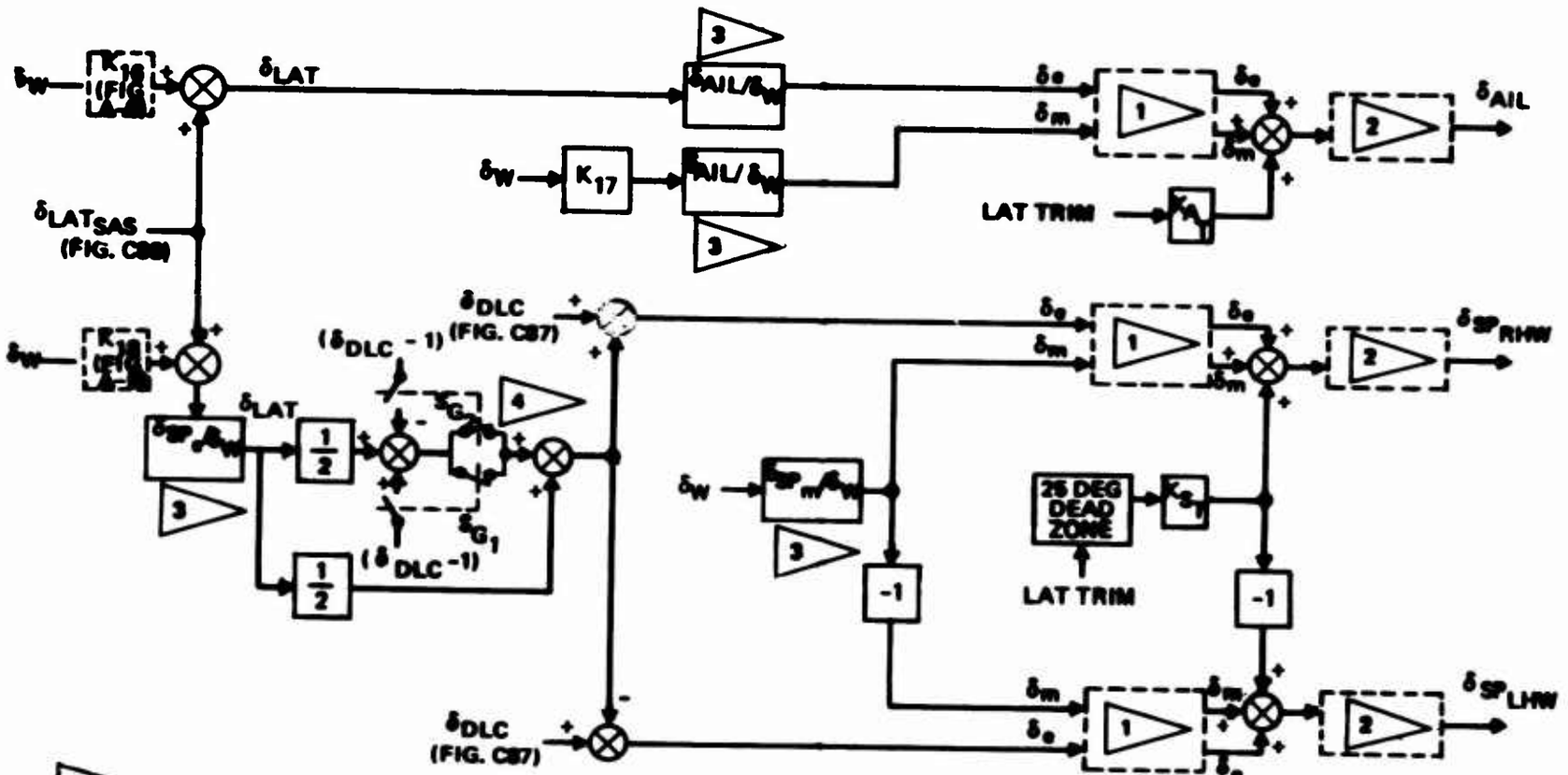

Figure 126: Lateral Signal Path Definition

SECTION III.5

ATMOSPHERIC DISTURBANCES

III.5.1 General

Atmospheric disturbances in the form of turbulence and shears are used to improve the realism of simulated flight conditions. Specifically, the STOL TAI turbulence and shear model is used for the following reasons:

(1) to determine the effect of control systems on reducing touchdown dispersions;

(2) to assess the effects of atmospheric disturbances on flying qualities and controllability;

(3) to ensure that the airplane has sufficient control effectiveness to be manageable during flight in atmospheric disturbances.

The output of the atmospheric disturbance module is three airplane body axes translational velocity components. Figure 129 depicts how these components are incorporated into the simulation. The body axes atmospheric velocity components comprise random turbulence and shear disturbances. Simulation of random turbulence is discussed in Section III.5.2. Section III.5.3 describes the shear model.

III.5.2 Random Turbulence

Random turbulence velocities are generated digitally by using a power spectral density technique which is discussed in Reference 10. The STOL TAI random turbulence mathematical model is based on the following assumptions:

(1) At low altitudes, turbulence is inhomogeneous. The turbulence scale lengths vary with altitude; the following equations define this dependence (Reference 11):

Above $h = 1750$ ft; $L_u = L_v = L_w = 1750$ ft

Below $h = 1750$ ft; $L_u, L_v = 145\, h_{cg}^{.333}$ ft

$L_w = h_{cg}$ ft

(2) Atmospheric turbulence is a stationary process: i.e., its statistical properties are independent of time. Non-stationary effects are not considered since the duration of each simulation run is only a few minutes.

(3) The turbulence field is "frozen" with respect to time (i.e., Taylor's hypothesis). The significance of this assumption is that time and spatial frequencies are related by the airplane's true airspeed (i.e., $\omega = V_T \Omega$).

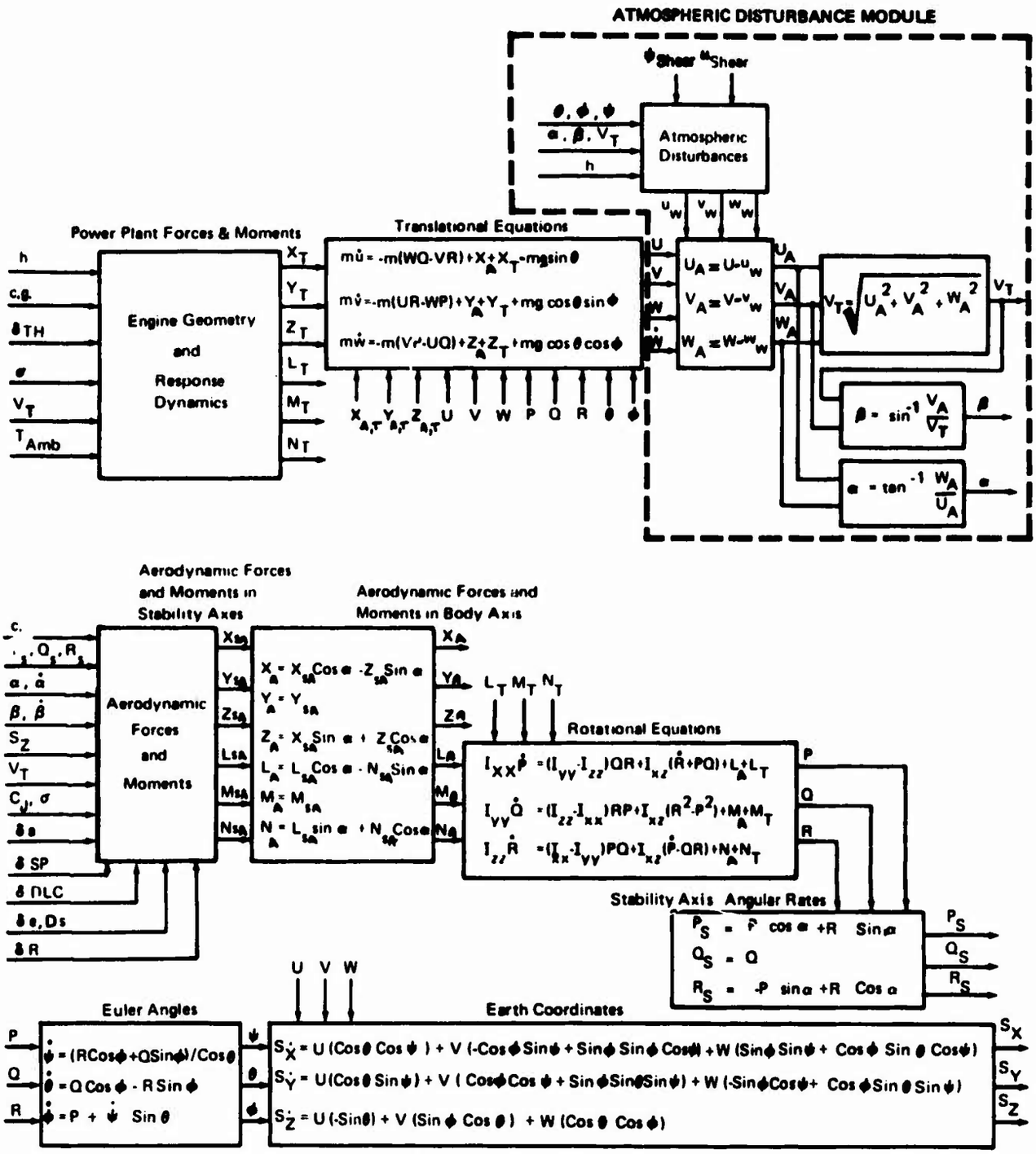

Figure 129: Equations of Motion : Atmospheric Disturbance Module

(4) The statistical characteristics of turbulence are defined for the airplane's body axes system.

(5) The Dryden power spectral density (PSD) form is used due to its mathematical simplicity for real-time digital simulation. The Von Karman PSD form cannot be programmed directly for real time simulation due to its noninteger exponential form. Figure 130 shows that the difference between the two PSD forms is slight for the frequency range of interest. For rigid airplane handling quality and control law studies (i.e., .1 rad/sec<ω<5 rad/sec), the two forms are within two decibels of each other.

(6) Turbulence intensities are isotropic: i.e., $\sigma_u = \sigma_V = \sigma_W$

III.5.2.1 Power Spectral Densities (Dryden)

$$\Phi_u(\omega) = \left(\frac{L_u}{V_T}\right)\left(\frac{2\sigma_u^2}{\pi}\right)\frac{1}{1 + (L_u/V_T)^2\omega^2}$$

$$\Phi_v(\omega) = \left(\frac{L_v}{V_T}\right)\left(\frac{\sigma_v^2}{\pi}\right)\frac{1 + 3(L_v/V_T)^2\omega^2}{\left[1 + (L_v/V_T)^2\omega^2\right]^2}$$

$$\Phi_w(\omega) = \left(\frac{L_w}{V_T}\right)\left(\frac{\sigma_w^2}{\pi}\right)\frac{1 + 3(L_w/V_T)^2\omega^2}{\left[1 + (L_w/V_T)^2\omega^2\right]^2}$$

The above equations are defined such that $\int_0^\infty \Phi(\omega)\,d\omega = \sigma^2$

III.5.2.2 Simulation Procedure

For simulation it is necessary to generate turbulence with the required spectrum, intensity, and scale length for a given flight velocity and altitude. To do this, a wide band noise source, $\Phi_x(\omega)$, is applied to a linear filter of the proper frequency response to obtain $\Phi_y(\omega)$ (see sketch below)

The relation of input to output spectrum is

$$\Phi_y(\omega) = \left|F(s)\right|^2_{s=j\omega}\Phi_x(\omega)$$

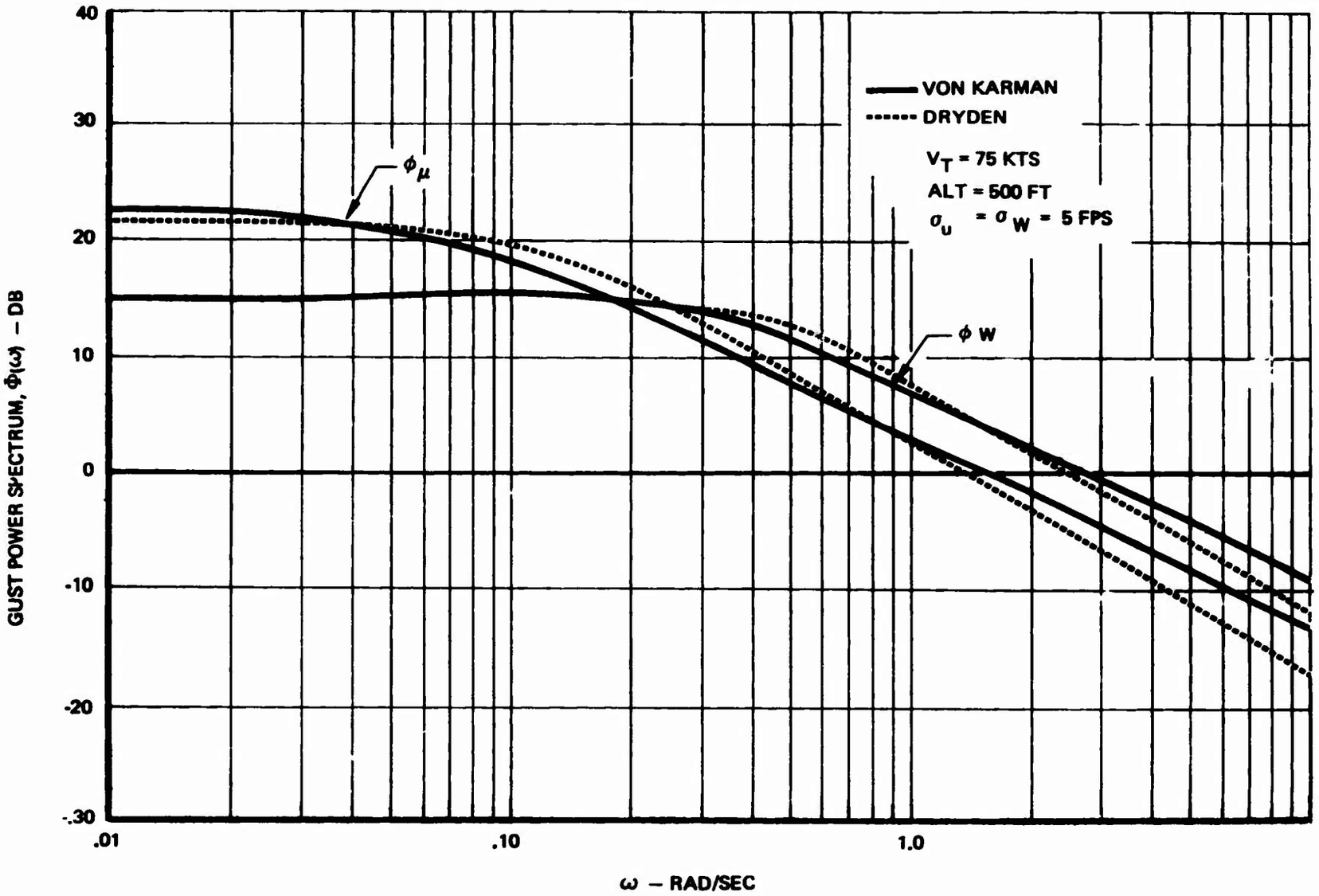

Figure 130: Comparison of Von Karman and Dryden Power Spectrums

If the input power spectrum is white noise (i.e., $\Phi_x(\omega) = 1$), then

$$\Phi_y(\omega) = \left|F(s)\right|^2_{s=j\omega}$$

Thus, the turbulence filters can be defined by using the PSD's defined in Section III.5.2.1 and the expression above.

$$F_u(s) = \frac{\sqrt{K_u}}{s + a_u}$$

$$F_v(s) = \frac{\sqrt{K_v}(s + b_v)}{(s + a_v)^2}$$

$$F_w(s) = \frac{\sqrt{K_w}(s + b_w)^2}{(s + a_w)^3}$$

where,

$$a_u = \frac{V_T}{L_u} \qquad K_u = \frac{2V_T\sigma_u^2}{L_u\pi}$$

$$a_v = \frac{V_T}{L_v} \qquad K_v = \frac{3V_T\sigma_v^2}{L_v\pi} \qquad b_v = \frac{V_T}{\sqrt{3}\,L_v}$$

$$a_w = \frac{V_T}{L_w} \qquad K_w = \frac{3V_T\sigma_w^2}{L_w\pi} \qquad b_w = \frac{V_T}{\sqrt{3}\,L_w}$$

When turbulence is generated by the technique above, the time required to obtain a stationary process is dependent on the turbulence filters' break frequency and on the starting values for the random number generator. The time required to produce a stationary process varies inversely with the size of the break frequency. Since these break frequencies are directly proportional to airspeed, they are quite low (i.e., $\omega < .1$ rad/sec) for STOL landing approach simulations. Figure 131 shows that the starting numbers also have a profound effect on the time required to reach a stationary process. Because it is necessary to have stationary turbulence, three sets (i.e., five numbers per set) of starting numbers that produce a stationary process within twenty-five seconds were determined. Before selecting a set of starting numbers, it was shown that the set worked for each of the three turbulence filters. The three sets of starting numbers were stored in the computer and automatically cycled after each simulation run.

III.5.2 Shear Model

The shear model for the STOL TAI simulation is defined by the following equation:

$$u_{SHEAR} = \left[.348 \ln(h_{cg} + 3) - .383\right] u_{SHEAR\,@\,h_{cg}=50'}$$

This is the model recommended by Reference 12, and it uses a surface roughness height of 3 ft.

The transformation of the shear velocity into body axes wind components and the turbulence model are detailed by Figure 132.

NOTE: 1. Dryden Spectra
2. V_g = 83 Kts
3. Alt = 1,000 Ft
4. σ_{V_g} = 5 fps

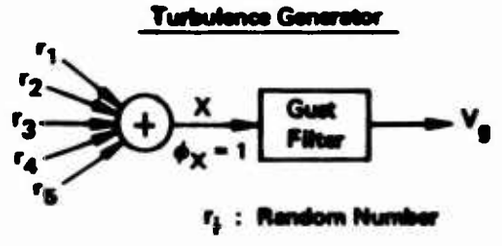

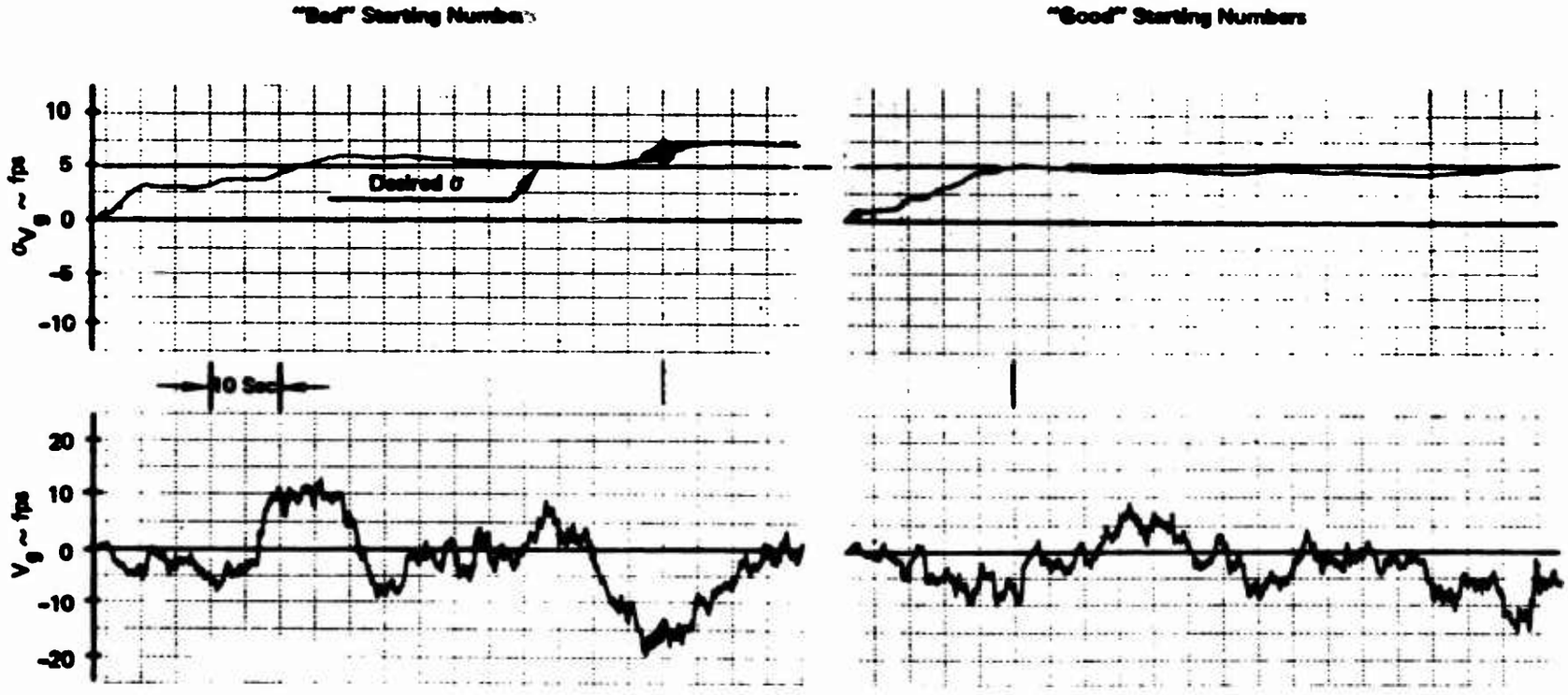

Figure 131: Effect of Starting Numbers on Turbulence

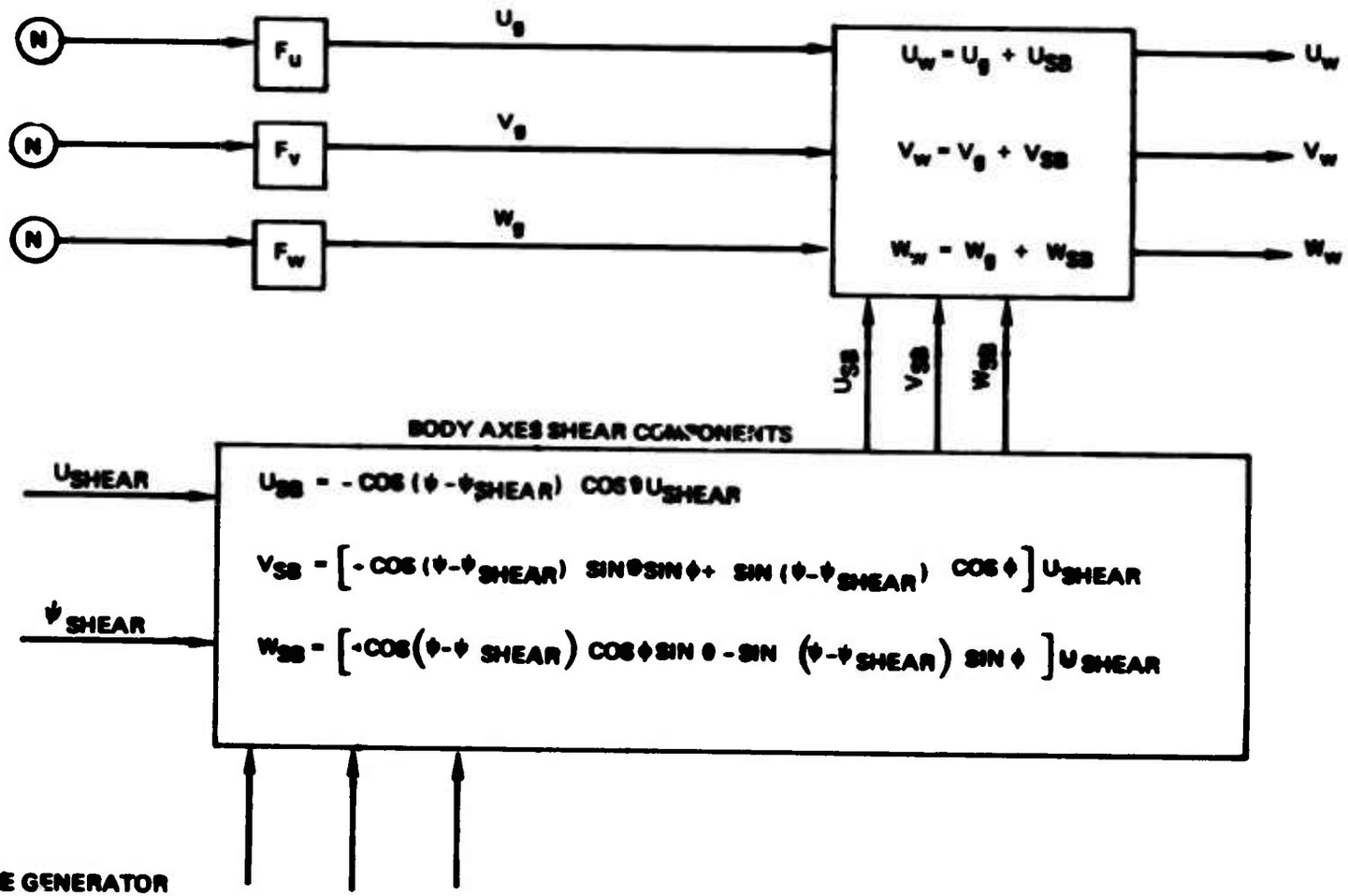

N : WHITE NOISE GENERATOR

$F_{(\,)}$: TURBULENCE FILTER

Figure 132: Atmospheric Disturbance Simulation

REFERENCES

1. Kennedy, J. B., Neville, A. M., Basic Statistical Methods for Engineers and Scientists, International Textbook Company, July, 1964.

2. Zierten, T. A., Vincent, J. H., A High Lift and Stability and Control Analysis of a Typical High-Wing STOL Transport Configuration: Based on UWAL 1012, Boeing Document D162-10384-1, December 1970.

3. Eldridge, A. H., Grow, T. L., Kirk, P. S., Approximate Calculation Procedures for Airplane Aerodynamic Characteristics, Boeing Document D6A12022-1, July 1970.

4. USAF Stability and Control Handbook (DATCOM), Douglas Aircraft Company, 1960.

5. Owen, R. B., A Correlation of Blown Flap Test Data with Design Charts for Estimating Blown Flap Lift and C_μ Required, Boeing Document D6-8111, March 1962.

6. Ishimitsu, K. K., Effect of Ground Proximity on the Downwash at the Horizontal Tail Location, Boeing Research Note RN-2, July 1963.

7. daCosta, A. V., A Theoretical Analysis of the Takeoff Problem, Including 1) Flare Analysis 2) Ground Effect 3) Parametric Analysis, Boeing Document D6-4243, Not Released.

8. Moore, W. J., Felix, V. M., Methods for Calculating the Nine Lateral-Directional Dynamic Stability Derivatives, Boeing Technical Note D6-30639TN, November 1969.

9. Anon, Military Specification - Flying Qualities of Piloted V/STOL Aircraft, MIL-F-83300, December 1970.

10. Neuman, F., Foster, J. D., Investigation of a Digital Automatic Aircraft Landing System in Turbulence, NASA TN D-6066, October 1970.

11. Anon, Military Specification - Flying Qualities of Piloted Airplanes, MIL-F-8785B, August 1969.

12. Anon, A Proposed Model of Low Altitude Atmosphere Turbulence for Use in V/STOL Aircraft Handling Quality Studies, Boeing Document D6-10738.

13. Monk, J. R., Aerodynamic Test Summary of BVWT 097, May 1972.